EXAMINATION OF LONG-TERM SOIL DEVELOPMENT AND PHOSPHORUS DYNAMICS IN A HYPERMARITIME CHRONOSEQUENCE, CALVERT ISLAND, BRITISH COLUMBIA, CANADA

by

Lee-Ann Nelson

BSc., University of Northern British Columbia, 2013

THESIS SUBMITTED IN PARTIAL FULFILLMENT OF
THE REQUIREMENTS FOR THE DEGREE OF
MASTER OF SCIENCE
IN
NATURAL RESOURCES AND ENVIRONMENTAL STUDIES

UNIVERSITY OF NORTHERN BRITISH COLUMBIA

April 2018

ABSTRACT

This thesis examines soil development, phosphorus (P) dynamics and ecosystem succession in an aeolian sand dune chronosequence spanning 10,760 years on Calvert Island, in hypermaritime coastal British Columbia, Canada. After 100 years of soil development, thick forest floors have developed (~28 cm), and after ~3,500 years mature Podzols have formed with cemented placic and ortstein horizons. With increasing soil age, mineral soil total P declines linearly and organic P forms become increasingly dominant, with glycerophosphates dominating organic horizons, and inositol hexakisphosphates and DNA dominating mineral horizons on the older sites. After 7,000 years, ecosystem retrogression – a long-term decline in biomass – is suggested by reduced tree basal area and a shift towards shrubby, more stress-tolerant species such as *Pinus contorta* var *contorta* and *Tsuga mertensiana*. Retrogression in the Calvert Island chronosequence is most likely caused by formation of cemented horizons and declining soil P reserves, though further investigation is needed.

TABLE OF CONTENTS

LIST OF TABLES

LIST OF FIGURES

ACKNOWLEDGEMENTS

I would like to thank Eric Peterson and Christina Munck for the financial and logistical support through the Hakai Institute in association with the Coastal Sandy Ecosystems Group; without your support this project would not have been possible. The support staff at the Hakai Institute made planning and performing this research significantly easier than it would have been otherwise. I took great comfort that I also had an experienced summer student, Lori Johnson, that assisted me on all my field work, despite the heavy loads we had to carry each day.

It was my dream to have Paul Sanborn as my supervisor after taking his soil classification class; I am very thankful that I had the opportunity to learn under someone so experienced and down-to-earth, and to attend his trip to the Yukon where was able to cross the geology and soil tour off my bucket list. Paul gathered a great group of scientists together for my committee who made sure that I did the best that I could do. I am very glad that Barbara Cade-Menun was my co-supervisor because she constantly pushed me to become a better writer and scientist whether it was by e-mail, on the phone or in-person in England and Swift Current. I am grateful that Barbara spent many hours working at the Saskatchewan Structural Sciences Centre at the University of Saskatoon because without her effort and time, I would still be manipulating base line corrections! Both Paul and Barbara spent an invaluable amount of time working with me to make this the best project that it could be, and they took extra time out of their days if I needed more guidance. Though I have yet to meet Ian Walker, I liked him from the first time we talked on the phone because he was straight to the point and encouraging. Since Ian is not a soil or phosphorus scientist he added a unique dimension to my thesis that was critical and was able to provide feedback on areas that others did not identify.

I would also like to thank Dr. Corey Liu from the Stanford Magnetic Resonance Laboratory at Stanford University who prioritized the analysis of my samples even while his laboratory was being shut-down, and to Clive Dawson from the BC Ministry of Environment Analytical Chemistry Laboratory who worked with me to analyse the large number of samples with appropriate analyses. I am also very thankful for the help from Christina Neudorf, Olav Lian and Jordan Eamer for answering all my geomorphology and landscape evolution questions throughout this process. Thanks for Derek Heathfield who helped me get Lidar elevations and to Nancy Alexander who helped with mapping.

I could not have done this without the support of my family and friends who read my drafts or listened to my ramblings. Thank you to my mother, Mary Bauman, who was my mentor during this process and who read and re-read my sections over and over. Thank you to my in-laws, Tim, Twyla and Piper, who provided me a place to stay and support while I was at UNBC. I would also like to thank my dog, Karlee, since she provided unconditional love through this and forced me to have a more balanced life. Last, but not least, I am extremely thankful to Garrett, my hubby, who supported me through this thesis and encouraged me when I needed it. I would not have finished this thesis without your support.

1 INTRODUCTION

Knowledge of coastal ecosystems is becoming increasingly important to sustainably manage these areas with the increased demands for food, fiber and recreational uses, as well as to deal with climate change (Banner et al., 2005; Oliver et al., 2017). There has been extensive forestry research on the North Coast Timber Supply Area of British Columbia (BC), within the Coastal Western Hemlock (CWH) zone very wet, hypermaritime variant (CWHvh2), because this area became of interest economically for timber and fibre production (Banner et al., 2005). However, there is little knowledge about pedogenesis, including the time required to develop low-productivity forests, and nutrient-limited soils (Banner et al., 1993; Banner et al., 2005).

The Hakai Institute has increased the ease and accessibility of coastal research within British Columbia (BC) by providing research grants, accommodations and amenities for scientists to conduct research related to oceanic and terrestrial ecosystems. The knowledge gained through the Hakai Institute is continually improving the current understanding of past climates and landscape evolution; extent of previous human occupation; oceanographic ecosystems and nutrient cycling, as well as terrestrial ecosystem functioning and succession (eg., McLaren et al., 2014; 2015; Hoffman et al., 2016a, b; Eamer et al., 2017a, b, c; Oliver et al., 2017).

The specific influence of the five soil forming factors; time, parent material, topography, climate and biology can be examined using a controlled sequence where the factor of interest is the only factor that is altered while all other factors are kept relatively constant (Jenny, 1941). For instance, a climosequence, a series of soils that have the same age, parent material, topography and biology but vary in climate, can be used to examine

how differences in climate affect the paths of pedogenesis. Similarly, a soil chronosequence is a series of soils that only differ in their ages while all other factors are kept relatively constant (eg., biology, topography, climate, parent material; Jenny, 1941). Soil chronosequences can be used to determine the rate of pedogenesis, understand how nutrient reserves change with time and how the ecosystem adapts with these changes (Jenny, 1941). There are limitations to soil chronosequences since most chronosequences span periods that have experienced variations in all soil forming factors, such as climate in the Hawaiian chronosequence (Hotchkiss et al., 2000; Walker et al., 2010). Chronosequences studies provide the only method that can examine the rate of pedogenesis on large time scales, but it is important to acknowledge their limitations of these studies throughout the analysis (Walker et al., 2010). Many global chronosequence studies have identified a decline in above ground biomass with increasing age that is directly related to soil development and declining nutrient reserves, particularly P, which results in ecosystem retrogression (Vitousek and Farrington, 1997; Wardle et al., 2004; Peltzer et al., 2010).

On the coast of British Columbia, there have been three documented soil chronosequences that have examined rates of pedogenesis in the CWH zone: Cox Bay, Naikoon, and Brooks Peninsula (Singleton and Lavkulich, 1987a, b; Maxwell, 1997; Sanborn and Massicotte, 2010). The Cox Bay chronosequence extended only 550 years (Singleton and Lavkulich, 1987a, b), while the Brooks Peninsula spanned > 8,000 years, but the site ages were poorly constrained (Maxwell, 1997). The Naikoon chronosequence was well constrained, with ages determined by optically stimulated luminescence dating (Wolfe et al., 2008); however, limited research has been performed, particularly related to forest productivity and nutrient availability (Sanborn and Massicotte, 2010). This limited body of

existing research suggests the need for more study of the links between pedogenesis, nutrient dynamics and forest productivity within the CWH biogeoclimatic zone.

Within the CWH zone, on Calvert Island, a soil chronosequence spanning ~11,000 years was identified by Ian Walker and Paul Sanborn using ages from distinct sandy landforms determined through optically stimulated luminescence dating techniques (Neudorf et al., 2015). This is the longest documented soil chronosequence on the coast of BC and was used in this study to further understand soil development and ecosystem succession on the coast of BC.

1.1 Objectives and Hypotheses

The aim of this study is to examine soil development and phosphorus (P) transformations with increasing soil age and how these developments may have affected ecosystem succession on the Calvert Island chronosequence, BC. The objectives of this study were threefold:

(1) To determine the changes in general soil chemistry (total carbon (C), nitrogen (N), and phosphorus (P), base cations, aluminum (Al) and iron (Fe)) associated with soil formation and the pathways of pedogenesis;

(2) To examine how soil P forms change during soil development, using P nuclear magnetic resonance (P-NMR) spectroscopy, and related soil chemical analysis; and

(3) To determine if these sandy ecosystems exhibit retrogression during the later stages of soil formation.

The purpose of the first chapter is to introduce the rationale and topics that were examined within this thesis. The second chapter of this study is a literature review on P dynamics and ecosystem changes on long-term chronosequence studies globally, as well as an exploration of current P analysis methods. Chapter Three provides an overview of the regional setting on Calvert Island including site locations, ages, vegetation, climate and geomorphic history.

Within Chapter Four it was hypothesized that with increasing soil age, the pH and base cation status of the soil would decline due to the temperate climate, coarse texture of the soils and the high rainfall (Table 3-2; Singleton and Lavkulich, 1987a, b; Maxwell, 1997; Sanborn and Massicotte, 2010). These chemical changes were hypothesized to be associated with stronger morphological development in the soil profiles with increasing age, resulting in

the formation of Podzolic B horizons and mature Podzols (Singleton and Lavkulich, 1987a, b; Maxwell, 1997; Sanborn and Massicotte, 2010).

The Fifth chapter of this study aimed to examine how P forms changed during soil development; it was hypothesized that organic P would become a more dominant pool of P with age, with deoxyribonucleic acid (DNA) from soil microbes and plant species becoming more dominant in organic horizons and inositol hexakisphosphates (IHP) increasing in dominance within the mineral horizons (Walker and Syers; 1976; McDowell et al., 2007; Turner et al., 2012a; Turner et al., 2014). It was also hypothesized that the P forms found in the litter (L) layer would have similar P forms as the foliage samples.

Chapter Six aimed to gather the conclusions from the previous chapters together to determine if retrogression was occurring on the Calvert Island chronosequence. With increasing age, it was expected that the forests on the intermediate-aged sites would have the maximal above-ground biomass followed by a decline in forest productivity (Wardle et al., 2004; Peltzer et al., 2010; Izquierdo et al., 2013), most likely caused by changes associated with soil development (e.g., cemented horizon development) or declining P reserves (Walker and Syers, 1976; Wardle et al., 2004; Banner et al., 2005; Sanborn et al., 2011). A shift toward shrubbier plants that were adapted to nutrient-poor conditions was also hypothesized (Jenny et al., 1969; Coomes et al., 2005; Eger et al., 2011).

Lastly, chapter Seven is a synthesis and overview of the objectives and hypotheses of this study and explored how the results of this thesis relate to the current knowledge of coastal BC ecosystems and soils.

2 LITERATURE REVIEW

Understanding soil development provides insight into past environments and climates, and can be used to understand ecosystem succession (Wardle et al., 2008; Gaxiola et al., 2010). This information can be used to infer historical land uses or can be applied to other scenarios such as primary and secondary succession. Primary succession refers to the establishment and growth of plant communities on previously unvegetated terrain, whereas secondary succession refers to the establishment and growth of plants following a disturbance (Barnes et al., 1994). To examine soil development with time, soil chronosequences are utilized (Jenny, 1941; Walker et al., 2010). A soil chronosequence is a series of soils that differ in age while other environmental parameters are kept relatively constant including climate, geology, geomorphic history, vegetation, and topography (Jenny, 1941; Walker et al., 2010). Soil chronosequences can answer questions such as how much time is required to develop a certain diagnostic soil horizon, or for the soil to be classified as part of a specific soil taxonomic group. Chronosequences can also be used in conjunction with other studies relating to nutrient cycling, plant diversity, and/or succession.

Long-term trends in the amounts and forms of soil phosphorus (P) during soil development have often been studied via soil chronosequences (Walker and Syers, 1976; Peltzer et al., 2010). Unlike other nutrient elements with important atmospheric reservoirs, such as nitrogen (N) and sulfur (S), P enters unfertilized soil through weathering of soil parent material or underlying bedrock, and/or through transported mineralogical inputs (eg., aeolian dust, or sediment transported by slopes, rivers, glaciers, etc.). With age P becomes depleted in soils, which is caused by uptake of P for plant growth, losses through leaching, and/or losses through erosion (Walker and Syers, 1976). Nitrogen and P are the most

commonly limiting plant nutrients, although these limitations usually occur at different successional stages (Walker and Syers, 1976; Vitousek et al., 2010). Theoretically, a young soil will generally have an adequate supply of P but can be limited by N because most N needs to be fixed biologically (Walker and Adams, 1958). Intermediate-aged soils may be co-limited by both N and P or have an adequate supply of both. Old soils are generally limited by P solely, which has a profound effect on N cycling (Walker, 1962; Walker and Syers, 1976).

To fully explore how P reserves change with time and how the availability of different P forms may affect plant nutrition, a comprehensive understanding of P analysis methods is needed. Methods for P analysis are well-established in soil science research due to the impacts of P on plant growth, food production, and ecosystem succession (Condron et al., 2005; Wardle et al., 2008; Vitousek et al., 2010). Phosphorus analytical methods have evolved considerably during the last 50 years with increasing knowledge about soil P dynamics; however, there is still no direct method for quantifying total organic P (Condron et al., 2005).

Ecosystem retrogression is the pronounced decline in primary productivity caused by impeded soil drainage and/or nutrient limitations, most commonly by P (Vitousek and Farrington, 1997; Wardle et al., 2004; Wardle et al., 2008). Ecosystem retrogression has large implications for soil P forms, plant diversity, litter quality, and plant nutrient acquisition strategies that will be explained further in this chapter (Wardle et al., 2004; Turner et al., 2007; Lambers et al., 2008; Richardson et al., 2008; Peltzer et al., 2010). Understanding ecosystem retrogression is necessary to further current knowledge of ecosystem succession,

because early stages of succession have been studied much more thoroughly than later stages (Vitousek and Farrington, 1997; Wardle et al., 2004; Peltzer et al., 2010).

The objective of this chapter is to provide an overview of i) the most common methods for soil P analysis applied to long-term chronosequence research, ii) a brief introduction to P cycling within soils, iii) the evolution of the Walker and Syers (1976) P model, and iv) the linkage between soil P and ecosystem retrogression.

2.1 Current analytical methods

2.1.1 Total Phosphorus

There are many methods to determine total P, each with benefits and disadvantages. Total P determination requires converting insoluble P forms to soluble forms using methods such as acid digestion or fusion (Kuo, 1996). Fusion is useful for analysis of samples that have components that are insoluble in acid but is more expensive, and time-consuming, and uses a high salt matrix that can interfere with total elemental analysis (Hossner, 1996).

The recommended methods for accurate determination of total P in soils are the Bowman (1988) method using sulfuric acid, hydrogen peroxide and hydrogen fluoride, the Dick and Tabatabai (1977) method using sodium hypobromite and sodium hydroxide, and the Parkinson-Allen (1975) method using sulfuric acid, hydrogen peroxide and lithium sulfate selenate (O'Halloran and Cade-Menun, 2008). However, most recent soil chronosequence studies did not employ the recommended methods for total P determination in soils except for Newman and Hart (2015) who utilized the Parkinson-Allen (1975) method. For example, Turner et al. (2012a), Hayes et al. (2014), and Wardle et al. (2016) used the ignition method by Saunders and Williams (1955) for total P and organic P analysis and the perchloric acid digestion procedure for total P analysis was used by Chen et al.

(2015). Sodium hydroxide (NaOH) fusion was used to determine total P by both Eger et al. (2013) and Coomes et al. (2013).

The Parkinson-Allen (1975) method is well-suited to analysis of many samples when digested on a block heater. The digestion time is longer than the Bowman (1988) and Dick and Tabatabai (1977) methods but is less labour-intensive per sample (O'Halloran and Cade-Menun, 2008).

2.1.2 Organic Phosphorus

Currently, the most common methods of total organic P determination are the Saunders and Williams (1955) ignition method adapted by Walker and Adams (1958; Hayes et al., 2000; Bünemann et al., 2008; Vincent et al., 2010) and the Bowman and Moir (1993) extraction method with NaOH and ethylenediaminetetraacetic acid (EDTA; Turner, 2008; Schneider et al., 2016). The ignition method analyses the P content on an unignited and an ignited sample, both extracted with dilute sulfuric acid (Saunders and Williams, 1955; Walker and Adams, 1958). The difference in P concentration between the ignited and unignited samples is called "organic P" because organic P is converted to inorganic P at high temperatures prior to dissolution. Potential errors when using the ignition method are solubilizing forms of inorganic P after ignition, which overestimates the organic P pool, incomplete combustion which underestimates the organic P pool or inclusion of polyphosphates in the organic fraction during extraction resulting in an overestimation of organic P (Harrap, 1963; Williams et al., 1970; Condron et al., 1990; Condron et al., 2005).

The Bowman and Moir (1993) extractant method is a one-step extraction procedure, so it is much easier than other extraction methods such as Mehta et al. (1954). Cade-Menun and Lavkulich (1997) found that the Bowman and Moir (1993) method and the Saunders and Williams (1955) ignition method had comparable organic P concentrations but both methods

overestimated organic P compared to P nuclear magnetic resonance (P-NMR) spectroscopy. For organic soils, the determination of inorganic P prior to extraction can result in dark extractants that cannot be analysed colorimetrically, limiting the use of the Bowman and Moir (1993) extraction method (Cade-Menun and Lavkulich, 1997). Extraction methods also have risks of incomplete extraction, or hydrolysis of organic P, and overestimation of organic P by inclusion of polyphosphates (Turner et al., 2002; Condron et al., 2005). This has the potential to become a significant error in organic soils, which often have higher polyphosphate concentrations than mineral soils (Makarov et al., 2002; Oberson and Joner, 2005; Bünemann et al., 2008).

2.1.3 Soil Test Phosphorus

Soil test P is a chemically extracted pool of P that is considered to be bioavailable, though this pool does not necessarily represent all of the biologically-available P in soil; rather, the P that is extracted with certain chemical reagents is used to provide an index of P availability (Lindsay, 1979; Beegle, 2005). The concept of soil test P was derived from the need to understand when a nutrient might be limiting, prior to any negative effects on the plant such as reduced crop yield. Soil test P methods were developed for agricultural soils and since have been applied in forest soils (Curran, 1984; Cade-Menun and Lavkulich, 1997; Lanoue, 2003).

In Canada the most common methods for soil test P are Bray-1, Mehlich-3, Olsen, and the modified Kelowna extraction (Bray and Kurtz, 1945; Olsen et al., 1954; Olsen and Sommers, 1982; Mehlich, 1984; Qian et al., 1994; Kuo, 1996; Beegle, 2005). For acid soils, Bray-1 and Mehlich-3 are most common, as the use of dilute strong acid releases aluminum (Al)-bound P and some iron (Fe)-bound P (Kuo, 1996; Beegle, 2005; Ziadi and Tran, 2006). If this method is used on calcareous soils, the calcium carbonates ($CaCO_3$) and calcium (Ca)-

bound P will buffer the acid, preventing total dissolution of P resulting in precipitation of P compounds (Smith et al., 1957; Beegle, 2005). The Olsen method uses sodium bicarbonate to extract P in both acidic and calcareous soils because the bicarbonate ion (HCO_3^-) replaces P in calcareous soils and hydroxide ions (OH^-) replace P in acidic soils (Olsen et al., 1954; Beegle, 2005).

The Bray-1 method uses ammonium fluoride (NH_4F) and dilute HCl to extract available P (Bray and Kurtz, 1945; Kuo, 1996). The fluoride ion (F^-) replaces P on Al complexes to bring P into solution; however, solubilized P can be re-adsorbed by Fe. The Bray-1 method is fast, cost-effective and comparable to the Mehlich-3 method (Tran et al., 1990; Kuo, 1996). The modified Kelowna extraction uses NH_4F like the Bray method but uses concentrated acetic acid rather than a dilute strong acid (Qian et al., 1994). The Mehlich-3 method uses ammonium nitrate, acetic acid, dilute nitric acid and EDTA (Mehlich, 1984; Ziadi and Tran, 2006). In addition to extracting P, the Mehlich-3 method also extracts exchangeable cations, including potassium (K), Ca, magnesium (Mg), sodium (Na), copper (Cu), zinc (Zn), manganese (Mn), boron (B), Al and Fe. The results can be used to infer how P may have been held in the soil. The Mehlich-3 method is considered a universal soil test extractant that is used all over the world (Ziadi and Tran, 2006).

In 1984, Curran evaluated the use of soil test P methods in acidic forest soils within BC and found that unlike agricultural soils, forest soil test P was not correlated to P forms extracted by the modified Chang and Jackson (1957) method (Chang and Juo, 1963). Mehlich-3 (1984) and Bray-1 P (Bray and Kurtz, 1954) concentrations were most strongly correlated to foliar P so Curran (1984) recommended using these two methods for acidic forest soils. Lanoue (2003) evaluated the Bray, Olsen and modified Kelowna extraction

methods in boreal forest soils in natural and reclaimed areas of the Athabasca Oil Sands Region and found that the modified Kelowna method was most suited to these boreal forest soils because it was a widely available method within Alberta, and was useful for forest soils that were acidic and alkaline, unlike the Bray-1 method (Bray and Kurtz, 1945; Tiessen, 2005) and the Olsen method (Olsen et al., 1954; Tiessen, 2005).

Coastal forest soils within British Columbia are predominantly acidic (Banner et al., 1993), so the Mehlich-3, Bray-1 or the modified Kelowna methods could be utilized dependent on the research objective (Bray and Kurtz, 1945; Mehlich, 1984; Qian et al., 1994). The Bray-1 and Mehlich-3 methods are currently the most utilized soil test P methods on long-term chronosequences and/or forestry research sites (e.g. Preston and Trofymow, 2000; Turner, 2008; Vincent et al., 2010; Kranabetter et al., 2013).

2.1.4 Phosphorus NMR

Phosphorus-nuclear magnetic resonance (P-NMR) is expanding our knowledge regarding the forms and functions of organic P in soils (Cade-Menun and Preston, 1996; Condron et al., 2005; Cade-Menun, 2005; Turner et al., 2007). Nuclear magnetic resonance spectroscopy can be used on solid intact samples (solid-state NMR), or on extracts from the samples (liquid-state or solution NMR; Cade-Menun, 2005). Solid state P-NMR produces poorer resolution due to widening of peaks and increased spinning side bands that interfere with data analysis compared to solution P-NMR and is used less frequently for soil P research.

The process of NMR entails the application of a magnetic field to a sample to align the sample's magnetic field and then a pulse of energy is applied that is absorbed by the P nuclei (Cade-Menun, 2005). The amount of energy that the nucleus absorbs, and then reemits once it relaxes, corresponds to the shielding of the nucleus, which in turn corresponds to

specific P compounds, with more shielded or complex P compounds moving upfield, or right, on the spectra (Cade-Menun, 2005). Phosphorus in nature occurs in only one isotopic state, ^{31}P, so P-NMR is a quantitative technique if the P concentration in the NMR tube is measured.

Newman and Tate (1980) were the first to analyse soil extracts for organic P using solution P-NMR. This paper was a milestone in soil P-NMR because it provided the first detailed analysis of the organic P in soil; however, the extraction method used by Newman and Tate (0.5 M NaOH) only extracted 43% of the total P within the sample. Cade-Menun and Preston (1996) revolutionized the P-NMR method by applying the concepts of the Bowman and Moir (1993) extraction method to P-NMR utilizing NaOH and EDTA; the EDTA chelates the cations and releases the P bound up in these forms, increasing the recovery of total P.

A comprehensive review of P-NMR methods used between 2005 and 2013 was performed by Cade-Menun and Liu (2014). The authors acknowledged that choosing an extractant and potential pre- or post-treatment chemicals is important because paramagnetic content (such as Fe and Mn ions), viscosity, and organic matter (OM) content affect the P-NMR spectra, causing changes in line-broadening and in the chemical shifts of peaks for specific P compounds. Phosphonates have a C-P bond that shield the P nuclei less than polyphosphates, so a lower amount of energy is required to resonate the P nuclei in phosphonates resulting in a chemical shift left (downfield) of polyphosphates which are shifted right (upfield; Cade-Menun, 2005). Currently, the most commonly used method is the NaOH+EDTA extraction (Cade-Menun and Preston, 1996) followed by centrifugation or filtering and freeze-drying (Cade-Menun and Liu, 2014).

Phosphorus NMR is gaining popularity for soil P research, because it provides quantitative data on organic P compounds within soil, unlike chemical extractions that represent chemical availability (Newman and Tate, 1980; Condron et al., 2005; Porder and Ramachandran, 2013; Kruse et al., 2015). However, higher pH samples generally have lower recoveries because P bound by Ca and Mg is harder to extract with NaOH-EDTA than P bound to Fe and Al (Turner et al., 2003a; McDowell et al., 2005; Turner and Blackwell, 2013). This method is also time consuming and may be cost prohibitive; however, it provides the most in-depth knowledge about organic P forms (Cade-Menun, 2005; Bünemann et al., 2008). In addition, new forms of P are constantly being discovered, which is advancing this field of research (Turner et al., 2007).

Phosphorus NMR is increasingly being utilized in long-term chronosequence studies to examine the shifts of organic P forms with age on P-depleted soils (e.g., McDowell et al., 2007; Turner et al., 2007; Vincent et al., 2013). This method can add value to the Walker and Syers (1976) model by visually and quantitatively demonstrating increasing proportions of organic and occluded forms of P with age, as well as how these pools are partitioned dependent on specific P compounds (Walker and Syers, 1976; McDowell et al., 2007; Turner et al., 2007; Turner and Laliberté, 2015). Phosphorus NMR is increasing our knowledge about P cycling and dynamics which may aid in future global models of P cycling and understanding soil development with time (Turner et al., 2007; Yang et al., 2013).

2.1.5 Methods for Quantifying Soil Phosphorus

The most common methods to determine P concentration within an extract or digest are colorimetrically or with inductively coupled plasma (ICP) based methods such as ICP-optical emission spectroscopy (ICP-OES; Kuo, 1996; O'Halloran and Cade-Menun, 2008). The acid-molybdate blue method (Murphy and Riley, 1962) is the most commonly utilized

colorimetric method (e.g. Vincent et al., 2010; Turner and Blackwell, 2013; Wang et al., 2014); however, the malachite green method is also used (Motomizu et al., 1983), particularly for samples with very low P concentrations (Ohno and Zibilske, 1991; Bünemann et al., 2008; Hayes et al., 2014; Schneider et al., 2016).

Colorimetric methods only quantify the orthophosphate within solution whereas ICP measures all P in solution, including colloidal P and organic P. Therefore, organic and total P can be quantified using colorimetric methods; whereas ICP can only analyse total P since there is no differentiation between organic and inorganic P forms (Kuo, 1996; Cade-Menun, 2005; Kranabetter et al., 2013; Vincent et al., 2013; Chen et al., 2015).

2.1.6 Quality Control for Phosphorus Determination

Reference materials are necessary to ensure precision and accuracy of elemental analyses in any scientific practice. There are certified reference materials (CRMs) for soil total P analysis such as the National Resource Canada CRM Till-1 through Till-4 and the anion CRMs through RTC Corp (Sigma-Aldrich). Currently there are no CRMs for organic P in soil on the market (O'Halloran and Cade-Menun, 2008), necessitating scientists to create their own in-house reference material, or analyse similar samples that have already undergone analysis. Given that there are CRMs for volatile organic hydrocarbons such as BTEX (Benzene, toluene, ethylbenzene and xylene), it should be possible to create a robust CRM for organic P if there were sufficient demand. Certified reference materials are also available for soil test P including Bray-1, Mehlich-3 and Olsen P through SCP Science.

For P-NMR, the most common way to ensure accurate identification of peaks is to spike a prepared sample with a known P compound with a known chemical shift, such as β-glycerophosphate, and run the sample to show where that peak lines up compared to an already analysed sample (Cade-Menun, 2015). Standard P compounds are generally

purchased from chemical companies such as Sigma-Aldrich, though some researchers have synthesized compounds such as the various configurations of inositol hexakisphosphates (IHP) synthesized by Dr. Cosgrove at the CSIRO in Australia (Doolette et al., 2009; Cade-Menun, 2015). Spiking compounds that have been used include *myo*-IHP, adenosine monophosphate (AMP), α- and β-glycerophosphate, glucose-1-phosphate, glucose-6-phosphate, and phosphocholine (Cade-Menun, 2015).

2.2 Phosphorus Cycling in Soil

Unlike the carbon (C) and N cycles, the P cycle is driven by the need for P using end product inhibition and repression, whereas the C and N cycles are driven by the catabolic need for energy from the oxidation of C compounds (McGill and Cole, 1981). The soil P cycle is controlled by five main pools of P, all of which contain inorganic and organic forms of P: P dissolved within the soil solution; P adsorbed to mineral surfaces; P precipitated within the soil solution; P within microbial biomass; and P contained within non-living OM (Barrow, 1983; Parfitt, 1989; Celi et al., 2001; Celi and Barberis, 2007; Giles and Cade-Menun, 2014; Kruse et al., 2015). Organic P is directly associated with C and hydrogen (H; Walker and Syers, 1976; Cade-Menun, 2005) and includes orthophosphate monoesters (herein referred to as monoesters) that have one C moiety, orthophosphate diesters with two C moieties (herein referred to as diesters), and phosphonates with a direct C-P bond (Cade-Menun, 2005).

The critical pool of P is the soil solution pool that is directly available for sorption, precipitation, biological uptake and incorporation into OM (Kruse et al., 2015). Within soil solution, the concentration of P is low; unlike other nutrients, soil P moves mainly by diffusion, thereby limiting availability (Schachtman et al., 1998; Stevenson and Cole, 1999;

Condron and Tiessen, 2005). Also, plants can only directly use inorganic orthophosphate taken from the soil solution (Schachtman et al., 1998; Stevenson and Cole, 1999).

Adsorption and desorption processes affect the quantity of P within the soil solution, especially in soils with low P concentrations and low pH (Barrow, 1983; Parfitt, 1989; Giesler et al., 2005). Orthophosphate adsorption occurs on Fe, Al and Mn hydroxides and oxides, non-crystalline minerals (e.g., allophane) and edge sites on silicate edges by ligand exchange, or by the formation of ternary complexes, where anions and cations work synergistically to adsorb via cation or anion bridges (McBride, 1994). The first reaction during adsorption is the adsorption of orthophosphate on defect sites (where a hydroxyl group is exposed; Parfitt and Henmi, 1982) by ligand exchange that can form monodentate or bidentate complexes (Parfitt, 1989). The second part of adsorption is a slower reaction involving weaker adsorption of P followed by the disruption of the mineral structure by the precipitation of metal-P, such as Al-P (Parfitt, 1989). Desorption involves the release of P from the mineral, which is enhanced by organic acids and chelating agents that may be exuded from plants or soil microorganisms (Parfitt, 1989; Seeling and Zasoski, 1993; Ryan et al., 2001; Richardson et al., 2009; Richardson and Simpson, 2011).

Orthophosphate adsorption and desorption is controlled by orthophosphate anion concentration, electrolyte concentration, temperature, pH, and length of reaction (Barrow, 1983). Increases in orthophosphate anion concentration, electrolyte concentration, length of reaction, and/or temperature will increase the amount of orthophosphate sorbed onto soil minerals (Barrow, 1978; Barrow et al., 1980; Chien et al., 1982; Barrow, 1983). A decrease in pH generally increases orthophosphate sorption (Sanchez and Uehara, 1980). Once orthophosphate is adsorbed, it will not readily desorb, though the amount that will desorb

will increase with increasing time and temperature (Barrow, 1983). Desorption of P will happen faster if the period of contact with the mineral is shorter (Barrow, 1983). The composition of organic P within a soil is dependent on the orthophosphate sorption capacity of the soil because IHPs, which have a high affinity for sorption with Fe and Al, will increase in concentration within a soil with a high sorption capacity, whereas diesters will dominate in soils with a lower sorption capacity (Magid et al., 1996; Condron et al., 2005; Vincent et al., 2012).

Precipitation and solubilization processes are strongly controlled by the concentrations of P and bonding cations (McBride, 1994). To form precipitates, the ions must be supersaturated; otherwise, the compounds may form in solution (e.g. Al-PO_4-H_2O) but never precipitate (McBride, 1994). Phosphorus tied up in precipitates is more soluble and easier to access than sorbed P (McBride, 1994). At higher pH apatite minerals (Ca-P) will precipitate whereas at low pH Fe, Al or Mn orthophosphate minerals will form. In soils with low P concentrations, sorption is the dominant geological process since it occurs even with low P concentration (McBride, 1994).

Immobilization is uptake of P from the soil solution by plants and microbes, and incorporation into organic forms, complex inorganic forms (e.g. polyphosphate) or stored as orthophosphate in cells (Stevenson and Cole, 1999; Condron et al., 2005). Organic P compounds and complex inorganic P forms can be converted to orthophosphate by mineralization, where the hydrolysis of organic P compounds is initiated by enzymes that may be exuded from plants or soil microorganisms (Smith and Read, 1997; Seeling and Zasoski, 1993; Richardson and Simpson, 2011). The biological cycle (mineralization/immobilization) for P is generally more dominant in the forest floor (L, F, H

horizons), whereas geological cycling (sorption/desorption; precipitation/solubilization) are generally more dominant in the mineral horizons (Wood et al., 1984); however, organically-complexed Al- and Fe-phosphates in the FF are also important (Giesler et al., 2000; 2002).

2.3 Modelling Changes in Soil Phosphorus with Time

2.3.1 Walker and Syers Model Development

The Walker and Syers, (1976) P model is most frequently cited regarding P in long-term chronosequences in many humid and temperate environments. The Walker and Syers model for P was originally developed in the Walker (1965) chapter in *Experimental Pedology* (Fig. 2-1). The purpose of this model was to show how soil P forms change over time with all other soil forming factors kept constant. Numerical scales for X-axes were not specified for any of the P models because these were intended to show only generalized trends in P with age. Actual rates of change would depend on the attributes of the specific soil forming factors in a particular study area. In this original version of the model, soil P was represented as three pools: primary, occluded and organic. Primary mineral P is P found in unweathered minerals, most often in the form of apatite inclusions that could be extracted with 0.5 M sulfuric acid (Syers et al., 1967; Walker and Syers, 1976). Occluded P comprises weathered mineral P or decomposed plant P sequestered in mineral matrices such as between clay sheets, and was determined by calculating the difference between total P, determined by sodium carbonate fusion, and primary and organic P. Organic P is P that is associated with OM, determined using the Saunders and Williams (1955) combustion method (Walker and Syers, 1976).

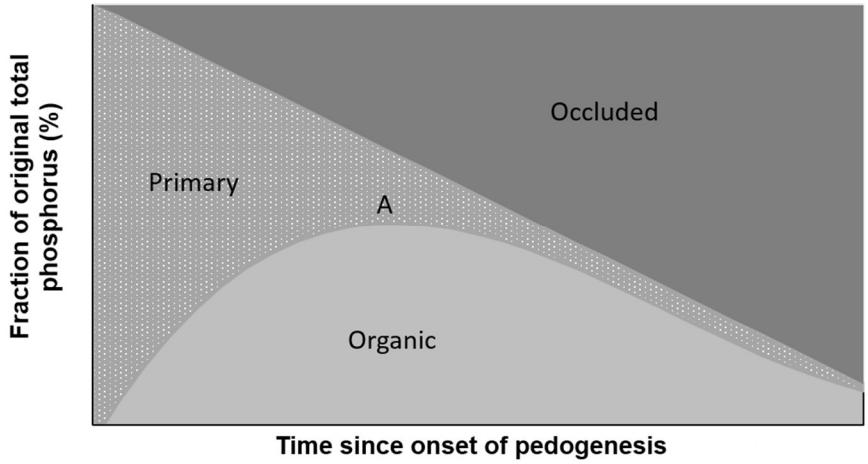

Figure 2-1. Phosphorus transformation model adapted from Walker (1965). This model consists of three main pools of P, primary (mineral P from acid extraction with H_2SO_4), organic P (difference in total P from ignited and un-ignited samples extracted with H_2SO_4) and occluded P (P not extracted with H_2SO_4). The point at A represents the maximum of the organic P curve. The rate of change for each pool of P is dependent on soil forming factors (Jenny, 1941).

In this model, P was assumed to exist solely in the primary mineral form at time zero. The intermediate-aged soil was dominated by almost equal percentages of occluded and organic P, with minimal primary P. In the oldest soil, occluded P was the dominant form, organic P represented a small portion, and primary P was negligible. Primary mineral P is the easiest form for plants to access because it is more soluble than occluded and organic forms and is therefore used quickly (Walker and Syers, 1976; Turner and Condron, 2013).

The initial model was developed by thoroughly examining two maturity sequences of basalt and graywacke, and one chronosequence (Franz Josef) in New Zealand (Walker, 1965). A maturity sequence is a series of soils that illustrate a soil ageing with time though the exact time since formation was not determined, rather the soils were placed in order of increasing maturity (Walker, 1965; Williams and Walker, 1969a). Walker used several precipitation sequences and lithosequences, as well as some research data from cultivated land manipulation in England. The original model had a label denoted “A” on the P transformation graph that indicated the maximum of organic P (Fig. 2-1). The footnote noted

that this model was for humid environments; however, Walker acknowledged that arid chronosequences could also be used but remain skewed to the left of point "A" since these soils have low precipitation and high evapotranspiration leading to slower soil formation processes.

In 1969, Williams and Walker published another P transformation model that included non-occluded P and illustrated a gradual, linear decrease in total P (Fig. 2-2; Williams and Walker, 1969a, b). The y-axis was altered to show P loss with time because Walker (1965) noted that expressing P fractions as a percent of total P did not correctly depict the loss of P over time. Non-occluded P is sorbed to the surfaces of Fe- and Al-hydroxides or tied up in $CaCO_3$ (Williams and Walker, 1969a, b; Walker and Syers, 1976), and was defined as the fraction extracted with NH_4F and NaOH. In the 1969 model, the occluded P fractions consisted of reductant-soluble P, a second NaOH extraction (adapted from Chang and Jackson (1957) and the residual inorganic P.

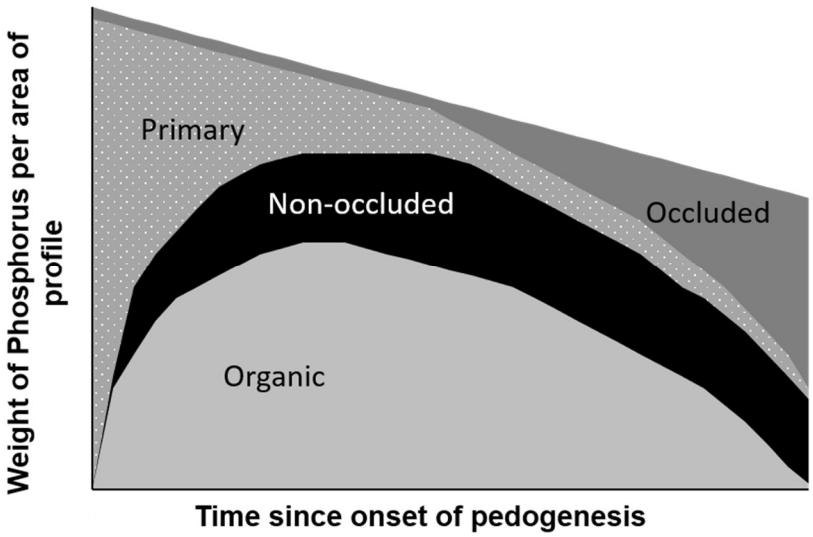

Figure 2-2. Phosphorus transformation model adapted from Williams and Walker (1969b). This model differs from the 1965 Walker model by the addition of the non-occluded pool (determined by ammonium fluoride extraction and sodium hydroxide (Williams and Walker, 1969b)) and the y-axis is the weight of P per area rather than fraction of total P. The rate of change for each pool of P is dependent on soil forming factors (Jenny, 1941).

2.3.2 Walker and Syers Final Model

The final model by Walker and Syers (1976) incorporated adjustments from previous versions (Walker, 1965; Williams and Walker, 1969b; Fig. 2-3). The final model followed the basis of the 1965 model, but included non-occluded P from the 1969 model, expanded the time frame and introduced a final "terminal steady state". A "terminal steady state" is characterized by equilibrium between losses and gains of P, where the losses from the soil profile equal the rejuvenating mineralogical inputs. The final model was created using P fractionation data from four chronosequences (Franz Josef, Manawatu, Reefton and Canterbury), as well as several hydrologic sequences, paleosols and toposequences (Walker and Syers, 1976).

The new model differed by the rate of accumulation of organic P and the length of time that organic P was dominant (Figs. 2-1 to 2-3). The length of time was also extended in the 1976 model, which illustrated the exponential decrease in total P with ageing that was not shown in the 1965 or 1969 models.

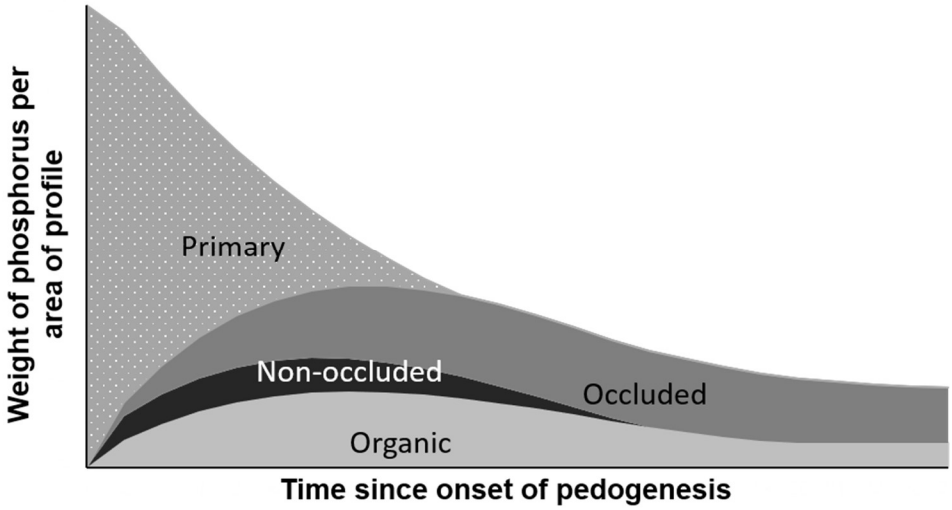

Figure 2-3. Final P transformation model adapted from Walker and Syers (1976). This model differs from the Williams and Walker (1969b) model with an exponential decline of total P rather than a linear decrease. This model also extended the time period on the x-axis,

allowing the model to reach a terminal steady state. The rate of change for each pool of P is dependent on soil forming factors (Jenny, 1941).

Importantly, neither model selected a time period on the X-axis, which indicates that Walker and Syers recognized that different soils would weather at different rates, and one soil will not reach the same point as another soil in the same time period (Fig. 2-3).

Basic chronosequence parameters such as parent material, cause, age, and mean annual precipitation (MAP) for chronosequences spanning a wide range of climates can be found (Table 2-1). The Walker and Syers' (1976) model has been applied to most of these chronosequences successfully and will be discussed in further detail below.

2.4 Ecosystem Retrogression in Response to Pedogenic Processes

2.4.1 Phosphorus Limitation

Prior to the use of the term *retrogression*, knowledge of biomass declines associated with age-related nutrient availability was presented by Chapin et al. (1994) and Vitousek and Farrington (1997). Wardle et al. (2004) initiated the adoption of the term retrogression. Although Vitousek and Farrington (1997) did not use the term retrogression, they applied the Walker and Syers (1976) model of P limitation to the Hawaiian chronosequence and performed a fertilization trial to understand nutrient limitations, using the biomass of trees as a response variable. They found that young soils were N-limited and old soils were limited solely by P. The fertilization experiment also applied different combinations of N, P and other micronutrients to intermediate-aged soils. The application of both N and P caused the greatest increase in tree diameter on intermediate-aged soils, which illustrated the co-limitation of N and P (Vitousek and Farrington, 1997). For information regarding the effects of retrogression on plant communities please see section 2.5 for more details.

Limitation by P can occur on any type of parent material; however, different parent materials may experience different mechanisms of limitation (Vitousek et al., 2010). In the

Hawaiian chronosequence, the soils were formed on volcanic material and were up to 4.1 million years old, representing soils that are P depleted due to age (Vitousek et al., 2010). This is known as "depletion driven" limitation, which is more common in tropical environments over temperate (Sanchez, 1976; Vitousek and Farrington, 1997; Vitousek et al., 2010). Soils with low P parent material (known as "low-P parent material") or barriers to plant roots and water infiltration (known as "soil barriers") may become P limited much faster than other soils (Vitousek et al., 2010).

2.4.2 Phosphorus Changes in Soils – Case Studies

To aid in the evaluation of P limitations during soil development, tables of different chronosequences were developed to explore trends in P fractions with age, P methods, soil sampling depth and soil forming factors (Tables 2-1, A1-1, and A1-2). These chronosequences vary by substrate, age, climate, and biological factors, but they all were heading towards or were displaying a retrogressive state. The main overview paper describing retrogression by Peltzer et al. (2010) identified nine chronosequences in the retrogressive state. At least two additional chronosequences can be included, those of Jurien Bay and Haast (Eger et al., 2011; Laliberté et al., 2012), along with two (Manawatu, Reefton) potentially exhibiting evidence of retrogression, although they have not been fully verified (Walker and Syers, 1976; McDowell et al., 2007).

There are similarities in soil P dynamics for all retrogressive chronosequences limited by P (Peltzer et al., 2010). The most obvious trend is the apparent decline in total P with age in both the surface horizons and with depth (Table A1-1). Total P decline on retrogressive chronosequences can occur linearly (Richardson et al., 2004; Turner et al., 2014), and exponentially (Walker and Syers, 1976). Since Ca-phosphates are generally the most abundant P forms in the parent material, acid-extractable Ca-bound P was the fastest to

decline in all chronosequences because they are more easily solubilized than other P forms (Walker and Syers, 1976). This was a central concept in the P transformational theory of Walker and Syers (1976). Organic P will increase with age to a certain point, followed by a decline (Walker and Syers, 1976; Peltzer et al., 2010). The decline in organic P coincides with shifts in the plant community generally associated with reduced productivity and therefore reduced litter input, or by shifts in vegetation communities towards plants with higher resorption efficiencies, or alternative nutrient acquisition strategies (Richardson et al., 2004; Richardson et al., 2005a; Turner et al., 2007; Peltzer et al., 2010; Hayes et al., 2014). Occluded P and non-occluded P also follow the hump-shaped trend of P, if the chronosequence exhibits enough of an age gradient to capture this trend.

Another common trend in retrogressive chronosequence studies is the increase of the total N: total P ratio (N: P), by concentration, of litter, humus and mineral soil (Tables A1-1 and A1-2). An increase in the N: P ratio in the litter horizons is evident on the Arjeplog, Franz Josef, Glacier Bay, Manawatu, Reefton and Waitutu chronosequences (Table 2-1; Wardle et al., 2004). Cooloola, the Hawaiian substrate gradient and the Reefton chronosequences have slightly increasing N: P ratios in the surface mineral soil (Wardle et al., 2004; McDowell et al., 2007). The implication of increasing P limitation with increasing age is evident in foliage and humus.

Chronosequences followed the Walker and Syers (1976) P transformation model in the surface horizons, such as at the Franz Josef glacier and the San Francisco Volcanic Plateau (Selmants and Hart, 2010; Turner et al., 2012a), and with depth, as on the Central Volcanic Plateau, Manawatu and Reefton, based on analysis using a plethora of methods including the ignition method, modified Hedley extraction and Tiessen and Moir extraction

(Saunders and Williams, 1955; Walker and Adams, 1958; Walker and Syers, 1976; Hedley, 1982; Condron et al., 1990; Tiessen and Moir, 1993; Parfitt et al., 2005; McDowell et al., 2007). Of note, the Hawaiian Substrate Age Gradient followed the Walker and Syers (1976) model, but did not reach terminal steady state due to Asian dust inputs (Chadwick et al., 1999). Phosphorus-NMR data have also been found to follow the Walker and Syers model, with an increase in orthophosphate and orthophosphate monoesters in the surface horizons, followed by a decline (McDowell et al., 2007). Weathering of primary mineral P and increased plant production resulted in the increasing phase, while the decline phase resulted from leaching losses, occlusion of inorganic P, and mineralization of monoesters when P became scarce (McDowell et al., 2007). This trend was also observed on the Franz Josef chronosequence (Turner et al., 2007).

Table 2-1. Long-term chronosequences where Walker and Syers' model has been applied, and soil forming parameters.

Chronosequence	Country	Parent Material	Cause	Climate	MAP (mm)	Initial Age	Oldest Age	Key References
Arjeplog	SWE	Granite boulders, moraine	Secondary Succession	Temp Bor For	750	100	6,000	(Wardle et al., 1997; Wardle et al., 2003; Wardle et al., 2008; Vitousek et al., 2010)
Brooks Peninsula	CAN	Sand grains	Aeolian	Temp Rain For	>3155	<200	>8,000	(Maxwell, 1997)
Central Volcanic Plateau	NZL	Rhyolitic tephra overlying greywacke	Volcanism	Temp Rain For	1600-2400	1,750	14,000	(Parfitt et al., 2005; Richardson et al., 2008)
Cooloola	AUS	Quartz grains	Aeolian	Sub-trop Rain For	1400-1700	10	>600,000	(Thompson, 1981; Walker et al., 2001; Peltzer et al., 2010; Vitousek et al., 2010)
Cox Bay	CAN	Sand grains from greywacke, argillite	Geological uplift	Temp Rain For	3200	127	550	(Singleton and Lavkulich, 1987a, b)
Franz Josef	NZL	Schist, gneiss	Glaciation	Temp Rain For	3800-6000	22	120,000	(Stevens and Walker, 1970; Walker and Syers, 1976; Richardson et al., 2004)
Glacier Bay	USA	Sandstone, limestone with igneous intrusion	Glaciation	Temp Bor For	1400	12	14,000	(Noble et al., 1984; Chapin et al., 1994; Vitousek et al., 2010)
Haast	NZL	Schist, greywacke, argillite	Geological uplift and alluvial processes	Temp Rain For	3455	370	6,500	(Eger et al., 2011; Turner et al., 2012a)
Hawaiian Substrate Age Gradient	USA	Basalt Tephra	Volcanism	Sub-trop Rain For	2500	300	4,100,000	(Crews et al., 1995; Vitousek and Farrington, 1997)
Jurien Bay	AUS	Calcareous to aged quartz sand	Sea level fluctuations	Med Shrub	573	100	>2,000,000	(Laliberté et al., 2012; Turner and Laliberté, 2015)
Manawatu	NZL	Sand from feldspars and quartz	Aeolian	Temp For	850	1	10,000	(Syers and Walker, 1969; Walker and Syers, 1976; McDowell et al., 2007)
Mendocino	USA	Greywacke, sandstone	Geological uplift	Med For	983	100,000	>500,000	(Jenny, 1969; Merritts et al., 1991; Northup et al., 1995)
Mendenhall	USA	Granite	Glaciation	Temp Rain For	>2500	10	>240	(Alexander and Burt, 1996)
Naikoon	CAN	Sand grains from sandstone and shale	Aeolian	Temp Rain For	1242	550	6,500	(Wolfe et al., 2008; Sanborn and Massicotte, 2010)
Reefton	NZL	Granite, greywacke	Alluvium	Temp Rain For	2030	1,000	130,000	(Walker and Syers, 1976; McDowell et al., 2007)
San Francisco Volcanic Field	USA	Volcanic scoria	Volcanism	Semi-arid Desert	336	1,000	3,000,000	(Selmants and Hart, 2008; 2010)
Waitutu	NZL	Mudstone, sandstone	Geological uplift	Temp Rain For	1600-2400	3,000	600,000	(Ward, 1988; Coomes et al., 2005; Parfitt et al., 2005)

Temp = temperate, Sub-trop = sub-tropical, Med = Mediterranean, Rain For = rainforest, Bor For = boreal forest, Shrub = shrub land

2.5 Effects on Ecosystem Composition and Function

2.5.1 Plant Diversity

Not all retrogressive chronosequences respond similarly to retrogression with respect to above-ground plant diversity. On the Franz Josef and Haast chronosequences, plant diversity declined with age, whereas on the Jurien Bay and Hawaiian chronosequences, plant diversity increased with age (Table 2-1; Crews et al., 1995; Richardson et al., 2004; Eger et al., 2011; Laliberté et al., 2012). Researchers have acknowledged that the trends in plant diversity vary on retrogressive chronosequences, and have linked plant diversity to the availability of seeds sources, dispersal, colonization and competition (Walker et al., 2010). Generally, plant species will shift from nutrient-demanding species on younger sites to more stress-tolerant, slow-growing species on older sites, as illustrated for the Waitutu, Mendocino, and Haast chronosequences (Table 2-1; Jenny et al., 1969; Coomes et al., 2005; Eger et al., 2011).

2.5.2 Foliage

Often, foliage N: P ratios are used to examine whether plants are N- or P-limited relative to the Redfield Ratio of 16, developed for plankton using a molar ratio (Redfield, 1958), or the Koerselman and Meuleman (1996) ratio of 14 and 16, developed for plants using concentrations, where a ratio between 14 and 16 suggests a shift in limitation or a stage where co-limitation may occur. For chronosequence studies, the Redfield ratio has been utilized more than the Koerselman and Mueleman ratio (McGroddy et al., 2004). This is an indirect method that has significant drawbacks; however, these ratios can be used to compare sites across a chronosequence or among sites within a fertilization trial. These ratios can be used in humus and foliage; however, foliar ratios correlate better to soil P and show more consistent trends than in humus (Richardson et al., 2008; Wardle et al., 2008). Nutrient ratios

do not provide any indication of the forms and availability of N and P, which limits the interpretation of the data.

Resorption efficiency and proficiency can also be used to understand how plants respond to soil nutrient limitations. Resorption efficiency can be calculated by using the difference in nutrient content in the live and senesced plant foliage divided by the nutrient content of the live foliage (Aerts, 1996; Kobe et al., 2005). The difference between foliage and litter provides an indication of how much of the nutrient is being pulled back into the plant prior to leaf drop (Aerts, 1996; Kobe et al., 2005; Richardson et al., 2005b). Resorption proficiency is the concentration of nutrients in senesced foliage. It shows "the new minimum level to which a plant can reduce an element in senescing leaves" (Killingbeck, 1996).

The use of foliar N: P ratios on chronosequences generally indicates the expected trend of N limitation on young sites, co-limitation of N and P on intermediate aged sites and P limitation on older sites (e.g., Vitousek et al., 1995; Richardson et al., 2004; Parfitt et al., 2005; Izquierdo et al., 2013; Hayes et al., 2014). Foliar P concentrations seem to correlate more strongly to soil P than foliar N to soil N (Izquierdo et al., 2013; Hayes et al., 2014). The trend of foliar N: P ratios may increase to a plateau, like a reverse logistic regression (Richardson et al., 2004; Hayes et al., 2014) or may have a humped-shaped curve that increases to an intermediate age and then declines (Vitousek et al., 1995). This method of looking at plant nutrition and soil nutrient availability is very valuable to explain trends (Koerselman and Meuleman, 1996). Foliar nutrient ratios should be used in conjunction with other methods, and caution should be used when inferring nutrient limitations from foliar nutrient ratios (Koerselman and Meuleman, 1996; Laliberté et al., 2012; Coomes et al., 2013). On the Franz Josef chronosequence, both a young site and old sites had high foliar N:

P ratios (Richardson et al., 2004). This was unexpected as generally foliar N: P is lower on young sites due to N limitation and relatively high P supply (Walker and Syers, 1976; Vitousek et al., 2010). Richardson et al. (2004) could explain this discrepancy because they performed a vegetation survey that detected an N-fixing shrub, which increased N inputs, resulting in P limitation on a young site. Newman and Hart (2015) argue that fertilization trials are required to further evaluate the shift from N to P limitation using foliar nutrient ratios, as there is currently a discrepancy among different chronosequences.

On the Franz Josef chronosequence, resorption proficiency was examined at the community and individual species levels to see if differences between N and P ratios were due to shifting species composition with age or were caused by changing resorption proficiency within species (Richardson et al., 2005b). Foliar and litter N and P concentrations decreased with age, suggesting that resorption became a more important process when soil P became more limiting (Richardson et al., 2005b). On the Jurien Bay chronosequence there was higher N resorption proficiency on young sites and higher P resorption proficiency and efficiency on P limited sites (Hayes et al., 2014). Higher resorption efficiency rates with declining soil fertility have been observed on the Central Volcanic Plateau, Franz Josef and Jurien Bay chronosequences (Richardson et al., 2005b; Richardson et al., 2008; Hayes et al., 2014). The Central Volcanic Plateau, Cooloola, Franz Josef, Glacier Bay, Jurien Bay and Hawaii chronosequences had increasing foliage N: P ratios with age (Wardle et al., 2004; Richardson et al., 2005b; Hayes et al., 2014). There was no increase in N: P ratios in litter with age for the Waitutu chronosequence; however, there was an increasing trend in the live foliage (Wardle et al., 2004). The implication of increasing P limitation with increasing age is

generally increasing N: P ratios in the foliage, and often the humus, and increased efficiency in the use of limiting nutrients.

Some hypothesized that leaf lifespan would increase with declining soil fertility so that plants could conserve nutrients and energy (Aerts and Chapin, 2000; Richardson et al., 2010). On the Franz Josef chronosequence, six indigenous species across the soil fertility gradient were used to examine leaf lifespan (Richardson et al., 2010). Lifespan did not increase with declining soil fertility as predicted. There was no relationship between soil fertility and leaf lifespan for four plant species, and two plant species had declining leaf lifespans with increased P limitation. However, leaf density and thickness increased during retrogression and leaf size decreased (Richardson et al., 2004).

Leaf lifespan may not increase within a species across a fertility gradient, such as on the Franz Josef chronosequence, but plant communities generally shift towards shrubbier, stress-tolerant species with declining soil nutrients (Gaxiola et al., 2010; Peltzer et al., 2010). Dominant plants in the retrogressive phase normally have long-lived leaves and slow tissue turnover compared to the faster growing plants with faster leaf turnover on the younger sites (Wardle et al., 2003; Wardle and Zachrisson, 2005).

2.5.3 Nutrient Acquisition Strategies

Plants can alter the way in which nutrients are accessed by forming symbiotic relationships with mycorrhizae, increasing the number of chemical forms that can be accessed by exuding phosphatase enzymes (Högberg, 1990; Read, 1991; Read and Perez-Moreno, 2003), or altering the supply rates of orthophosphate and absorbing area by increasing root dispersal through the soil (Drew, 1975; Clarkson, 1985; Hodge, 2003; 2004). This can include plants increasing scavenging in soil by rapid root growth, proliferation of roots in nutrient-rich zones, and the growth of root hairs (Francis and Read, 1994; Lambers et

al., 2008; Smith and Read, 1997). The inflow of P can be increased by creating more P-transport proteins, upregulating mRNA that codes for increased P uptake in root hairs and epidermis, or altering the micro-RNA allowing the plant to adapt to nutrient deficiencies (Dong et al., 1999; Huang et al., 2000; Chiou et al., 2006).

Phosphorus forms in soil vary in both accessibility and ease for uptake (Condron et al., 2005; Turner, 2008). Resource partitioning theories of nutrient acquisition are becoming more accepted and can be used to explain the distribution of different plant communities over a nutrient gradient, such as a chronosequence (Lambers et al., 2008; Turner, 2008). On young, undeveloped soils, arbuscular mycorrhizae, ectomycorrhizae, and ericoid mycorrhizae are the dominant mechanisms for nutrient acquisition (Lambers et al., 2008). As soils develop, ectomycorrhizae and ericoid mycorrhizae become more dominant than arbuscular mycorrhizae. Arbuscular mycorrhizae are the most common mycorrhizal association worldwide and can scavenge P in soil, use inorganic P if it is not sorbed, and some arbuscular are thought to be able to use organic P, including inositol orthophosphates, though it has not been definitively proven (Joner et al., 2000; Koide and Kabir, 2000; Lambers et al., 2008; Turner, 2008). Ectomycorrhizae and ericoid mycorrhizae can mine and scavenge for P and release sorbed inorganic P through hydrolysis and mineralize orthophosphate esters (Hill and Richardson, 2007; He et al., 2011).

Once both N and P become limiting in soils, nutrient acquisition strategies shift towards more ancient mechanisms such as mycorrhizae with simple cluster roots that can mine and scavenge P, to non-mycorrhizal plants with simple and compound cluster roots (Shane and Lambers, 2005; Lambers et al., 2006). Cluster roots release carboxylates, which

can acquire P from Al-, Fe- and Ca-P compounds, in addition to releasing phosphatases that can mineralize organic P forms (Shane and Lambers, 2005).

Non-mycorrhizal plants had the lowest foliar N and P contents compared to ecto-, endo- and arbuscular mycorrhizal plants on the Jurien Bay chronosequence (Hayes et al., 2014). Interestingly, the non-mycorrhizal plants had higher levels of foliar Mn which suggests that these plants are increasing the exudation of carboxylate acids which mobilize both P and Mn from minerals (Hayes et al., 2014).

When P fertilizer is applied to plants with nutrient acquisition strategies targeted for nutrient-poor ecosystems they can experience P toxicity due to increased uptake mechanisms (Shane et al., 2004a, b; Shane and Lambers, 2005). This can make fertilizer trials in these environments complicated, because a positive growth effect may not be apparent from P fertilization (Shane et al., 2004a, b; Shane and Lambers, 2005).

2.5.4 Basal Area and Tree Height

The most consistent trend for determining whether a chronosequence is retrogressed is by looking at tree height and/or basal area (BA), which is the cross-sectional area that the tree at 1.3 m off the ground would occupy in a one-hectare area. Tree height and BA both decrease significantly on retrogressed sites (Wardle et al., 2004). When tree BA or height is plotted against age for a retrogressed chronosequence, there is often a severe decline with age after the maximal biomass stage. This is apparent for the six global chronosequences (Arjeplog, Cooloola, Franz Josef, Glacier Bay, Hawaii, and Waitutu) examined by Wardle et al. (2004) and can be inferred for the Haast, Jurien Bay and Mendocino chronosequences (Table 2-1; Jenny et al., 1969; Eger et al., 2011; Laliberté et al., 2012). It has not been verified for the Central Volcanic Plateau, Cox Bay, Manawatu, and Reefton

chronosequences, although significant declines in P have been reported (Walker and Syers, 1976; Singleton and Lavkulich, 1987a, b; McDowell et al., 2007; Richardson et al., 2008).

On the Waitutu chronosequence, BA declined significantly with age, in part due to low P in the soil. However, water table height or waterlogging may also be significant when examining plant height, BA, and diversity, with water table height found to be significantly correlated to declines in BA (Gaxiola et al., 2010; Coomes et al., 2013). The Haast and Jurien Bay chronosequences also have impeded water drainage that potentially influences tree and plant diversity characteristics of these sites (Eger et al., 2011; Turner et al., 2012a; Laliberté et al., 2012).

2.5.5 Bog Formation

Paludification, or bog formation, may be the final process of ecosystem development at some locations (eg., Ugolini and Mann, 1979). The impedance of water flow, often due to cemented horizons, causes bog formation on old sites. During the process of podzolization, for example, a Fe-cemented horizon, known as a placic horizon or Fe pan, develops from the downward movement of organo-mineral complexes that precipitate out at depth (Ugolini and Mann, 1979; Turner et al., 2012a). This in turn prevents the vertical movement of water, promoting the formation of a bog (Ugolini and Mann, 1979; Kitiyama et al., 1997). This process can be a mechanism for retrogression due to soil-barrier limited P, anoxic conditions and resulting shifts in plant communities (Vitousek et al., 2010; Gaxiola et al., 2010; Turner et al., 2012a).

The Haast, Mendocino, and Waitutu chronosequences have formed Fe pans at depth on intermediate-aged to older sites (Jenny, 1969; Turner et al., 2012a; Coomes et al., 2013). Initially, the impeded water flow can increase the amount of available P because the anoxic conditions will reduce ferric oxides and release Fe-bound P (Vitousek et al., 2010; Turner et

al., 2012a). The plant communities will then shift towards more stress-tolerant species that may thrive in waterlogged environments (Grime, 1979; Gaxiola et al., 2010). This phenomenon will not be apparent in all retrogressive chronosequences but is important to include when studying retrogression on soils that have cemented horizons.

3 STUDY AREA

3.1.1 Location

Calvert Island is located on the west coast of British Columbia, roughly 100 km north of Port Hardy on Vancouver Island, and 50 km south of Bella Bella, BC (Fig. 3-1; BC Parks 2015a, b). Calvert Island is separated from the mainland by Fitz Hugh Channel and can only be accessed through boats and float planes. Calvert Island is in the Hakai Lúxvbálís Conservancy area within the Wuikinuxv and Heiltsuk First Nation traditional territory (BC Parks 2015a). The island is roughly 32 km long and ranges in width from 3 to 16 km (Columbia Gazetteer of the World Online, 2016), with the highest point located at the top of Mount Buxton at 1045 m above sea level.

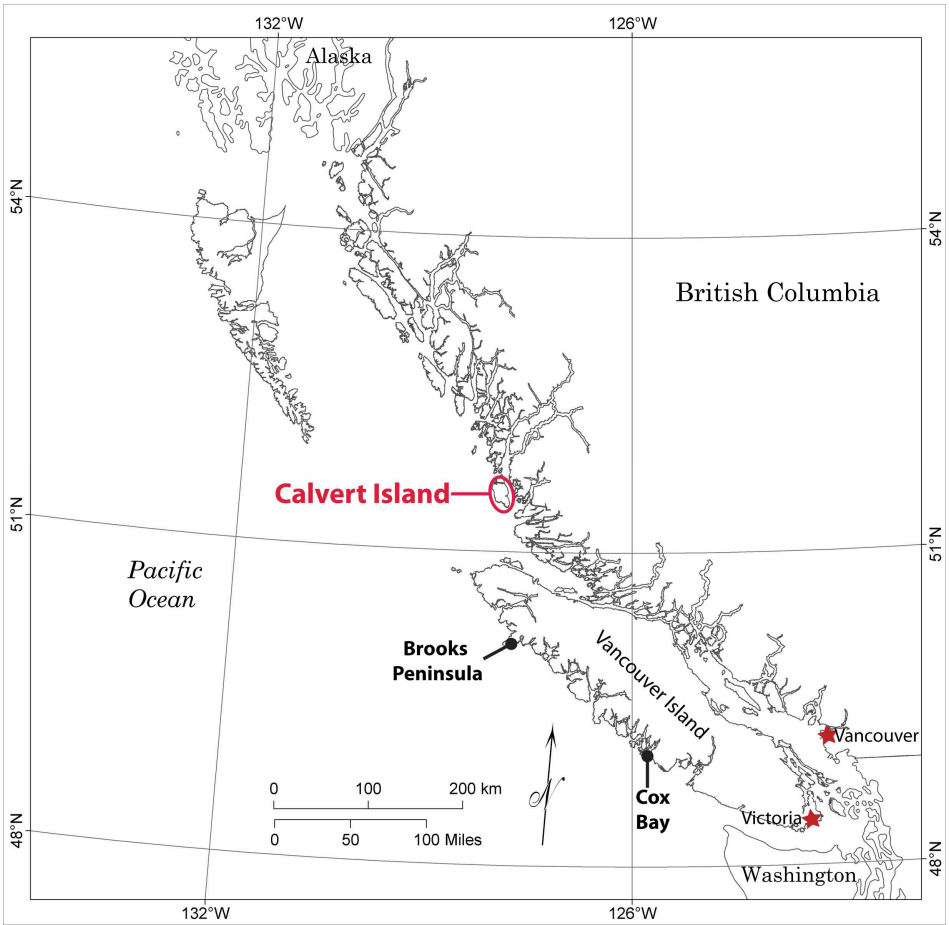

Figure 3-1. Location of Calvert Island (red circle) on the central coast of British Columbia, Canada in relation to the Brooks Peninsula and Cox Bay soil chronosequences.

3.1.2 Chronosequence Ages

Soil ages were determined by Dr. Olav Lian's post-doctoral researcher, Dr. Christina Neudorf, at the University of the Fraser Valley (Neudorf et al., 2015; Fig. 3-2; Table 3-1). Each site was dated by optical stimulated luminescence dating methods that are inherently experimental. The parent material of each site is aeolian dune sand that cannot be dated by radiocarbon methods due to lack of preserved OM. Optical luminescence dating, however, can date mineral grains to the last time they were exposed to light, which is why this technique was used on these sites. A single sample was taken on each site from the C horizon to obtain a minimally altered sample by organic matter, ground water, and eluvial/illuvial processes. Sample ages were determined using the central age model and calibrated for potential errors including anomalous fading and phototransfer effects. The optically derived ages corresponded well to the independently derived radiocarbon ages of adjacent organic samples (Neudorf et al., 2015). Further details on the methods and results can be found in Neudorf et al. (2015).

Figure 3-2. Detailed map of study sites on northwestern Calvert Island, BC, Canada illustrating the locations of the stabilized aeolian dunes and prograding foredune locations that were sampled for this study (adapted from Neudorf et al. 2015). Note: Sample sites are denoted with a red circle.

Table 3-1. The sampling sites used in this study, including chronosequence site name, location, elevation in meters above mean sea level (m amsl) with the standard deviation in brackets, the most accurate age, and the closest landmark (see names in Fig. 3-2), Adapted from Neudorf et al. (2015), with information from Dr. Lian and Derek Heathfield (Lian et al., pers. comm., 2017; Heathfield, pers. comm., 2018)).

Site Name	Location (Lat/Long coordinates)	Elevation (m amsl)	Optically Stimulated Luminescence Age (a BP)	Closest Landmark
CIDS1A	51.6641° -128.1441°	5.52 (0.42)	0	West Beach
CIDS1B	51.6580° -128.1437°	5.83 (0.73)		
CIDS3A	51.6536° -128.1381°	4.73 (0.14)	105 ± 15	West Beach
CIDS3B	51.6535° -128.1379°	4.36 (0.19)		
CIDS4A	51.6564° -128.1386°	8.46 (0.20)	139 ± 17	West Beach
CIDS4B	51.6564° -128.1386°	8.19 (0.15)		
CIDS8A	51.6413° -128.1518°	36.03 (0.38)	3,588 ± 303	Between 4th and 7th Beaches
CIDS8B	51.6414° -128.1518°	34.33 (0.88)		
CIDS9A	51.6600° -128.1457°	9.52 (0.30)	605 ± 50	Between West and North Beaches
CIDS9B	51.6601° -128.1456°	11.22 (0.49)		
CIDS10A	51.6444° -128.1454°	13.51 (0.47)	10,760 ± 864	Dunes behind 3rd Beach
CIDS10B	51.6446° -128.1460°	15.70 (0.33)		
CIDS15A	51.6620° -128.1411°	8.96 (0.22)	4,198 ± 332	Between ponds and North Beach
CIDS15B	51.6622° -128.1411°	10.19 (0.41)		
CIDS16A	51.6661° -128.1178°	6.08 (0.16)	7,236 ± 546	South of Wolf Beach
CIDS16B	51.6661° -128.1180°	6.29 (0.14)		

3.1.3 Vegetation

Calvert Island is situated in the Hectate lowlands ecoregion in the Coastal Western Hemlock zone, Very Wet Hypermaritime subzone, and Central variant (CWHvh2; Banner et al. 2005). Vegetation types include: blanket bogs, bog woodlands, bog forests and zonal forests.

The characteristic tree species within the CWHvh2 variant are western redcedar (*Thuja plicata*), western hemlock (*Tsuga heterophylla*), and yellow cedar (*Chamaecyparis nootkatensis*; Banner et al., 1993). The characteristic shrubs are false azalea (*Menziesia ferruginea*), salal (*Gaultheria shallon*), and Alaskan blueberry (*Vaccinium alaskaense*). The Calvert Island chronosequence has a variety of specific site units within the CWHvh2 classification that also have Sitka spruce (*Picea sitchensis*) and shore pine (*Pinus contorta* var. *contorta*). The younger (105 – 605 a BP) and intermediate-aged sites (3,588 - 4,198 a BP) are productive zonal forests whereas the oldest site (10,760 BP) is a bog woodland with low productivity. The youngest site (~0 a BP) is on a modern foredune with vegetation limited to a sparse grass cover of native dune wildrye (*Elymus mollis)*.

3.1.4 Climate

Calvert Island has a temperate, humid climate that is characterized by heavy precipitation events from October through March (MOE, 2016). The BC Ministry of Forests, Lands and Natural Resource Operations (MOFLNRO) summarized the average climate normals for locations within the CWHvh2 variant from 1961-1990 (Chourmouzis et al., 2009). This long-term data set provides mean temperature and precipitation data that was applicable to the Calvert Island chronosequence (Table 3-2). Climate normal data from Bella Coola were also presented for comparison since this was the closest coastal climate station with long-term climate normals (Environment and Natural Resources, 2018). ClimateBC was

used to estimate climate data on the Northern part of Calvert Island between 1961-1990 and 2001-2010 to examine the decadal averages specific to the site (ClimateBC Map, 2015).

Table 3-2. Climate data for the Coastal Western Hemlock zone, Very Wet Hypermaritime subzone, Central variant (CWHvh2), Bella Coola, and estimated climate data for northern Calvert Island (Chourmouzis et al., 2009; ClimateBC Map, 2015; Environment and Natural Resources, 2018).

Parameter	**Location**			
	CWHvh2	**Bella Coola**	**Calvert Island Field Station (Estimated data)**	
Time Period	1961-1990	1981-2010	1961-1990	2001-2010
Elevation of Reference Station (m)	0-664	18.3	10	10
Mean Annual Precipitation (mm)	3254	1632	2832	2799
Total Mean Annual Snowfall (cm)	N/A	133.8	119	90
Mean Annual Temperature (˚C)	7.7	8.2	8.1	8.7
Mean of Coldest Month (˚C)	2.3	-0.4	3.3	3.3
Mean of Warmest Month (˚C)	14.3	17.0	13.6	14.3

3.1.5 Geology

The geology of Calvert Island is dominated by quartz diorite with secondary lithologies of granodiorite, metasediments, gabbro, and quartz monzonite (Roddick, 1996a). This study, however, will focus only on sandy landforms that range from modern foredunes to recently stabilized or older Holocene, relict sand dunes that are comprised of predominantly quartz sands (Neudorf et al., 2015). The P and Fe concentrations of northern Calvert Island bedrock are significantly lower than farther east in the Coast Mountains (Roddick, 1996a; b).

3.1.6 Geomorphic History

Calvert Island has a unique sea level history whereby the relative sea level (RSL) has remained within 1-2 m of the current sea level for the past 15,000 years, after the retreat of the re-advanced lobe of the Cordilleran Ice Sheet (McLaren et al., 2014; Eamer, 2017; Eamer et al., 2017a). Although unusual, this is possible due to the isostatic rebound of Calvert Island

coinciding with post-glacial eustatic adjustments, creating a sea-level hinge region that may have experienced very little change in relative sea level (McLaren et al., 2014; Shugar et al., 2014; Eamer et al., 2017a). Archaeological records suggest continuous human habitation throughout the Holocene (McLaren et al., 2015). Lagoon cores show consistent diatom presence from 10,700 BP onwards at the current RSL, indicating little to no fluctuation in relative sea level (Andrews and Retherford, 1978; McLaren et al., 2014). The youngest chronosequence sites (~0, 105, 139 a BP) are close to the current shoreline on West Beach; however, the older sites have a more complicated history (Neudorf et al., 2015; Eamer et al., 2017b, c). Some types of coastal sand dunes, such as foredunes, are indicative of past shorelines and are the result of stabilizing vegetation, past climates, and wind patterns (Davidson-Arnott, 2010; Hesp and Walker, 2013). It is unclear how the 4,000+ a BP sites formed because past shorelines are not apparent.

The youngest site in this chronosequence is an established foredune backing West Beach that is vegetated by disturbance-tolerant grasses (predominantly *Elymus mollis*) and other herbaceous plants (Figs. 3-2 and 3-3). This dune provides limiting conditions for plant growth – high disturbance from aeolian sand transport, abrasion, burial, salt spray, highly variable temperatures, and likely moisture deficits (Hesp and Walker, 2013; Eamer et al., 2017c). The next youngest sites (105, 139 BP) are stabilized foredunes backing the modern foredune on West Beach that are colonized by later stage successional tree species including Sitka spruce (*Picea sitchensis*), western hemlock (*Tsuga heterophylla*) and red alder (*Alnus rubra)*. All other chronosequence sites are stabilized dunes formed by aeolian processes (Fig. 3-3; Hesp and Walker, 2013; Eamer, 2017; Eamer et al., 2017c). For detailed plant community information see chapter Six.

Figure 3-3. Representative vegetation across the Calvert Island chronosequence; a) modern, established foredune (0 a BP), b) stabilized, forested dune (605 a BP), c) stabilized, forested dune (3,588 a BP), and a relict, stabilized, forested dune (10,760 a BP).

4 SOIL FORMATION PATHWAYS IN A HYPERMARITIME SAND DUNE CHRONOSEQUENCE, CALVERT ISLAND, BC

4.1 Introduction

Coarse-textured soils in cool or temperate humid environments most often develop into Podzolic soils (McKeague et al., 1983), which are characterized by the accumulation of amorphous organic matter (OM) and/or the enrichment of iron (Fe) and aluminum (Al) in the B horizon (Sanborn et al., 2011). The word Podzol was derived from the Russian words "pod" and "zola" which mean "under ash" and refers to the grey, ashy- looking A horizon (McKeague et al., 1978; Mokma and Buurman, 1982).

Podzolic soils are easily identified in the field by the diagnostic reddish brown to black B horizon (Bh, Bhf, or Bf) and the often associated, bleached A horizons (Ae or Ahe; Sanborn et al., 2011). Podzols mainly develop in climates where precipitation exceeds evapotranspiration (McKeague et al., 1983). Cool, wet climates slow decomposition, promoting the accumulation of OM on the surface (McKeague et al., 1983). Organic matter includes animal and plant matter, ranging from fresh litter inputs to entirely humified material, as well as soil microorganisms that may be living or dead (Schaetzl and Anderson, 2005). Reduced decomposition and greater OM accumulation enhance the production of mobile organic acids that are involved in formation of organic- (Bh or Bhf) or Fe- and/or Al-enriched (Bf) B horizons (Lundström et al., 2000; Sauer et al., 2007). In Canada, Podzols can form in perhumid and humid climates and are not limited by temperature (McKeague et al., 1983). They cover 14.3% of Canada's land mass and are most commonly found under coniferous forests with acidic litter and minimal bioturbation (Schaetzl and Anderson, 2005; Sanborn et al., 2011). Podzolic soils can form in upland and lowland environments; however, their characteristic genetic horizons and their thickness will differ with slope position and soil

moisture regime (McKeague et al., 1978; Sanborn et al., 2011). Soils that are not subject to mass movement and erosion will exhibit more strongly developed Podzolic B horizons (McKeague et al., 1978). Due to their coarse texture and low water-holding capacity, they are important areas of groundwater recharge (Sauer et al., 2007).

There are three proposed mechanisms of podzolization that can act independently, subsequently or in tandem; however, two are more widely discussed (Lundström et al., 2000; Schaetzl and Anderson, 2005; Sauer et al., 2007; Sanborn et al., 2011). The three mechanisms are: i) organo-mineral complexation, ii) proto-imogolite formation, and iii) the metal reduction movement mechanism (Farmer et al., 1980; Anderson et al., 1982; Farmer and Fraser, 1982; Skjemstad et al., 1992; Sanborn et al., 2011).

The first mechanism involves exudates from plant roots, fungi and soil microbes and incomplete litter decomposition, which provide organic acids that can dissolve and chelate Fe and Al from soil minerals (Lundström et al., 2000; Sauer et al., 2007; Sanborn et al., 2011). These organic acids and subsequent organo-metal complexes then move down through the organic horizons and eluvial horizon and are subsequently immobilized in the B horizon. Over 80% of Al found in the eluvial horizon of Podzols has been linked to OM, thus supporting this mechanism (Petersen, 1976; Lundström, 1993).

The second mechanism is the proto-imogolite theory that involves the transport of Al, Fe and Si in inorganic colloids of hydroxy-Fe-Al-orthosilicate that are deposited in the B horizon, where the Al and Si are precipitated as allophanic-type materials (Farmer et al., 1980; Farmer and Fraser, 1982; Farmer and Lumsdon, 2001). This process has been inferred from the presence of allophanic materials in Bf horizons (van Breemen et al., 2000). These short-range-order minerals cannot form in the presence of organic acids, so the two

mechanisms cannot occur simultaneously (van Breemen et al., 2000). The presence of allophane has been documented in many soil types world-wide, including Podzols (Young et al., 1980; Farmer, 1982; Parfitt, 1990; Jansen et al., 2005). Allophane has a positive charge at low pH and can sorb P and OM, which in turn can reduce nutrient cycling and decomposition rates (Parfitt, 1977; Parfitt and Henmi, 1982; Parfitt, 1990). Allophane is not a discretely defined compound; rather, it represents a spectrum of short-range order minerals with an average Al: Si atomic ratio of 2 (Parfitt, 1990). In New Zealand, Parfitt and Kimble (1989) identified allophanic compounds with Al: Si ratios ranging from 0.4-4.0.

The third mechanism relies on the translocation of reduced organically-complexed Fe to the B horizon where it is immobilized by the oxidation of organic acids (Skjemstad et al., 1992; Sauer et al., 2007). This mechanism relies on the interaction of all podzolization mechanisms because the proto-imogolite transported downward from the A horizon to the B horizon absorbs OM within the B horizon and any mobile Fe or Al (Skjemstad et al., 1992). Eventually, enough OM would accumulate in the upper B horizon that a redox gradient would form between the first B horizon and lower horizon, most likely through the development of a cemented horizon and the presence of seepage, promoting the reduction and dissolution of Fe to a greater depth (Skjemstad et al., 1992). This mechanism of podzolization is responsible for the separation of Al- and Fe-enriched horizons, with Fe-enriched horizons at a greater depth due to greater mobility and the movement by reduced Fe (Skjemstad et al., 1992).

Once Al, Fe and Si are transported to the B horizon, formation of a Podzolic B horizon involves their stabilization by one or more of: an increase in pH, change in soil redox status, OM decomposition, decreasing C: metal ratios with depth, or adsorption of OM to soil

surfaces (McKeague et al., 1971; Ugolini and Dahlgren, 1991; Gustafsson et al., 1995; Lundström et al., 2000). For example, soluble organic complexes have a net negative charge and as they move down the soil profile they will bind to cations in the soil to balance the charge (McKeague et al., 1971; Petersen, 1976). Once the saturation point of the organo-metal complex is reached, it will be immobilized at the zero point of charge and subsequently precipitate (McKeague et al., 1971; Petersen, 1976). If microorganisms decompose the organic component of the organo-metal complex, this will release metal cations into solution that can be immobilized by precipitation or sorption (Lundström et al., 1993; Gustafsson et al., 1995). As the organo-metal complex moves down the soil profile, it may encounter an increase in pH, a water table, or a lithological discontinuity that will promote its immobilization and precipitation (Gustafsson et al., 1995; Schaetzl and Anderson, 2005)

Podzolization within the coastal temperate rainforest, extending from northern California to south-east Alaska, is rapid because of the high rainfall, and can result in a variety of genetic soil types, depending on the topography, water table position and parent materials (Banner et al., 2005; D'Amore et al., 2015). Soils with high water retention dominate the landscapes, most often in association with shallow organic soils (Banner et al., 2005). Due to high rainfall and high leaching, nutrient-poor soils are common. In these coastal temperate rainforests, there is a wide range of site productivity, from productive forests to bog forests to blanket bogs, resulting from the varied types of soil development (Banner et al., 2005).

In forested soils of this region, imperfectly drained Podzols and Folisols with thick forest floors (FF) are dominant, but other Organic soils can also form (Banner et al., 2005). Forest floor (FF) refer to all surface organic horizons present on a site (inclusive of L, F, and

H horizons). Elsewhere in the landscapes, Regosols and Brunisols form on floodplains and Gleysols form where saturation occurs during most of the year (Banner et al., 2005). Podzols in this region often develop characteristic Fe-cemented placic horizons and/or humic- and/or Al-cemented ortstein horizons, or duric horizons (Sanborn et al., 2011). Placic horizons are usually thin (< 5 mm), consisting of multiple variegated reddish brown to black layers (Sanborn et al., 2011; D'Amore et al., 2015). Morphologically, placic horizons are generally irregular or involuted in appearance and are most often cemented by Fe and/or manganese (Mn; McKeague et al., 1968; Moore, 1976; Sanborn et al., 2011). The mechanism of placic horizon formation is not fully understood, but may be caused by the precipitation of metals in response to a change in redox, pH, and/or texture or by the precipitation of organo-metal complexes (Lavkulich et al., 1971; McKeague et al., 1983; Lapen and Wang, 1999). Ortstein horizons are thicker, cemented Podzolic B horizons that cover greater than one-third of the exposed pedon face, and are cemented by humic materials, Fe, or Al, depending on which podzolization mechanisms are active. Duric horizons are cemented horizons that appear similar in colour to the parent material, except that they are strongly cemented and do not qualify as Podzolic B horizons (Sanborn et al., 2011).

Rates of Podzol development vary globally with climate, parent material and plant communities (Sauer et al., 2008). Even within Canada, the time required to form Podzols can range from, for example, 371 years at Cox Bay, BC, to an estimated 12,400 years in subarctic Quebec (Singleton and Lavkulich, 1987a; LaFortune et al., 2006). Sauer et al. (2008) completed a comprehensive overview of podzolization rates for over 25 chronosequences around the world. Some Podzols in south east Alaska near the Mendenhall glacier formed in

less than 240 years (Alexander and Burt, 1996), whereas soils in the southern Alps of New Zealand required greater than 8,000 years (Birkeland, 1989).

Podzol formation rates have been documented across Canada in a range of climates, most often in coastal environments (Sanborn et al., 2011; Sanborn, 2016). On the coast of BC, there are three documented soil chronosequences that provide evidence for rates of pedogenesis in the Coastal Western Hemlock (CWH) zone: Cox Bay, Naikoon, and Brooks Peninsula (Singleton and Lavkulich, 1987a, b; Maxwell, 1997; Sanborn and Massicotte, 2010). The Cox Bay chronosequence extended only 550 years (Singleton and Lavkulich, 1987a, b), while the Brooks Peninsula spans 8,000 years but the site ages were poorly constrained (Maxwell, 1997). The Naikoon chronosequence spanned 6,500 years and was well-constrained, with ages determined by optically stimulated luminescence dating (see Wolfe et al., 2008); however, limited research has been performed at this site, particularly related to forest productivity and nutrient availability (Sanborn and Massicotte, 2010). The limited body of existing research on chronosequences in BC suggests the need for more studies examining soil development across the full Holocene time period, with more robust dating methods.

The present study aimed to infer the rates and potential pathways of pedogenesis along a hypermaritime chronosequence on the central coast of BC spanning almost 11,000 years. Sites used in this study were dated by optically stimulated luminescence techniques, which provides good time constraints for the age of each site (Neudorf et al., 2015), unlike previous studies using dendrochronology or inferring soil ages from radiocarbon dates obtained for adjacent peat deposits (Singleton and Lavkulich, 1987a; Maxwell, 1997). The post-glacial relative sea level history and related landscape evolution and geomorphology of

this site is well documented (McLaren et al., 2014; Shugar et al., 2014; Neudorf et al., 2015; Eamer, 2017; Eamer et al., 2017a, b), and provided a unique study area with the opportunity to determine how long important processes take in this hypermaritime environment, such as mature Podzol development, and formation of placic and ortstein horizons.

The objective of this study was to determine if the Calvert Island chronosequence displayed patterns of development over time that have been observed elsewhere in the region, such as the Cox Bay, Naikoon and Brooks Peninsula chronosequences (Singleton and Lavkulich, 1987a, b; Maxwell, 1997; Sanborn and Massicotte, 2010). It was was hypothesized that with increasing soil age, the pH and base cation status of the soil would decline due to the temperate climate, coarse-texture of the soils and the high rainfall (Table 3-2; Singleton and Lavkulich, 1987a, b; Maxwell, 1997; Sanborn and Massicotte., 2010). These chemical changes were hypothesized to be associated with stronger morphological development in the soil profiles with increasing age, resulting in the formation of Podzolic B horizons and mature Podzols (Singleton and Lavkulich, 1987a, b; Maxwell, 1997; Sanborn and Massicotte, 2010).

4.2 Methods

4.2.1 Study Area

This chronosequence was located on Calvert Island on the central coast of BC (Fig. 3-1). The elevation of each site was estimated using aerial Lidar from a 3 m digital elevation model (Fig. 3-2; Table 3-1). All sites were within walking distance from the Calvert Island field station of the Hakai Institute (51° 39’ 16” N, 128° 7’ 51” W).

4.2.2 Site Selection and Description

Research sites were visited in the summer of 2015 to verify that each site met the requirements for a soil chronosequence, including: progressive soil development; minimal disturbance; similar soil parent material, topography, geomorphology, and climate; and similar vegetation cover within the dune (Jenny, 1941; Walker et al., 2010). All sites were sampled in spring 2016.

A total of eight sandy landforms were examined in this study, with ages ranging from a modern beach (~0 years old) to 10,760 years old (Table 3-1). Two sampling locations were examined on each sand dune to capture the variability of soil formation within the dune. Sampling locations were chosen in locations that reflected a stable landscape position. When possible, sampling locations were chosen on stable, upland positions that were flat to gently sloping, with well to moderately well-drained conditions. Any deviations from these criteria were noted and can be found in the results section and Appendix 2.

4.2.3 Soil Sampling

Soil sampling was completed in accordance with the Canadian System of Soil Classification (SCWG, 1998) whereby a soil pit, approximately one m^3 and over 1 m deep, was used to expose the soil genetic horizons. The horizons were classified based on colour, texture, and evidence of pedogenic/soil forming processes, and each were sampled separately. Samples from the lowest horizons were sampled first to minimize cross-contamination from upper horizons.

4.2.4 Sample Preparation

All soil samples were air dried and ground to 2 mm. For cemented horizons, a mortar and pestle were used to disaggregate the sample and a coffee grinder was used for organic samples.

4.2.5 Soil Characterization

Samples were sent to the Analytical Chemistry Laboratory of the BC Ministry of Environment in June 2016 for soil characterization. These samples were analysed for: total C, exchangeable cations, pH, pyrophosphate- and oxalate-extractable Al, Fe, and Si, and total elemental analysis (including Al, Ca, Na, K and P). These properties were utilized to fully classify the pedons per SCWG (1998).

Exchangeable cations were extracted using 0.1 M barium chloride and analysed using ICP-OES (Hendershot et al., 2008). The pH was analysed using an adapted procedure from Kalra and Maynard (1991), with a 1:1 soil to water and 1:2 soil to 0.01 M calcium chloride ($CaCl_2$) ratio for mineral soils. Depending on the viscosity of the organic samples, the soil: water ratios used ranged from 2:3 to 1:9 and between 1:2 and 1:9 for 0.01 M $CaCl_2$. The pH determined using 0.01 M $CaCl_2$ was used for soil classification (Kalra and Maynard, 1991; SCWG, 1998).

Sodium pyrophosphate (0.1 M) and acidified ammonium oxalate (0.2 M) were used to extract Fe, Si, and Al from mineral samples, followed by ICP-OES analysis (McKeague and Day, 1966; Courchesne and Turmel, 2008). Pyrophosphate-extractable Fe (Fe_p) and Al (Al_p) represent organically-complexed Fe and Al, whereas oxalate extractable Fe (Fe_o) and Al (Al_o) represent amorphous and organically complexed Fe and Al. Therefore, the difference between oxalate- and pyrophosphate-extractable Fe and Al provides an indication of how much of these elements occur in non-crystalline forms (Farmer and Fraser, 1982; Gustafsson et al., 1995).

Closed-vessel microwave acid digestion followed by ICP-atomic emission spectrophotometry (AES) was used for total elemental analysis of the organic samples (Kalra and Maynard, 1991), whereas high temperature fusion with lithium metaborate/lithium

bromide using a Claisse M4 Fluxer, followed by ICP-OES was used to analyse total elements on the mineral samples (Claisse, 2003).

4.2.6 Soil Mass

Determination of soil mass was calculated using two different methods dependent on soil type. It is difficult to get an accurate bulk density of the FF because they are very deep and easily compacted. For mineral horizons that were not cemented, a slide hammer soil corer was utilized on a ledge of undisturbed soil (Blake and Hartge, 1986). For mineral soils with cementation, a clod was broken off from the profile, weighed (wet weight), coated in paraffin, and the volume was measured by the displacement method and the weight was converted to dry weight by measuring the moisture content of a subsample of the clod (Blake and Hartge, 1986). Mineral soil bulk density was calculated for each soil horizon when possible; however, some horizons were thin and multiple horizons were captured in one sample.

For the organic horizons, a high-power drill with a steel coring tube was utilized to sample the entire FF to calculate its mass per unit area (Nalder and Wein, 1998). Where the organic horizon thickness exceeded the length of the drill coring tube (>20 cm), the slide hammer was used to obtain bulk density cores from organic horizons exposed on the soil pit walls (Blake and Hartge, 1986).

4.2.7 Chemical Weathering Indexes

The chemical index of alteration (CIA) provides an indication of the amount of weathering within a soil by calculating the molar ratio of a relatively immobile element, Al, to the sum of Al and more mobile elements (Ca, Na, K), expressed in oxide form using concentrations from lithium metaborate fusion (Equation 1; Nesbitt and Young, 1982). To minimize the effects of sampling procedure on the CIA calculations, the sand samples used to

optically date these soils were used as the reference parent material, because sampling to the C horizon in each pedon was not feasible (Appendix 4; Neudorf et al., 2015). Samples from CIDS1, CIDS2, CIDS3 and CIDS4 (~0 to 139 a BP) were used for the average parent material values because it was assumed that they represented the least weathered samples (Neudorf et al., 2015). The CIA was calculated for each horizon in each pedon. Calcium was corrected (CaO*) to represent only Ca occurring in silicate minerals by deducting an estimate of Ca present as apatite equal to the P oxide concentration (P_2O) multiplied by ten and divided by three.

$$CIA = \left(\frac{Al_2O_3}{Al_2O_3 + CaO^* + Na_2O + K_2O}\right) * 100\% \qquad Equation\ 1$$

The eluvial/illuvial coefficient (EIC) was also calculated for each horizon to examine the enrichment or depletion of an element within a soil horizon relative to the concentration of an immobile element within the soil horizon and parent material (Equation 2; Muir and Logan, 1982; Schaetzl and Anderson, 2005). Titanium can be mobile within Podzols because of its solubility in oxalic acid, which is prevalent in organic horizons; thus, Zr was used as the immobile element due to its lower variability and greater immobility within forested dune soils (Dumon and Vigneaux, 1979; Tejan-Kella et al. 1991; Skjemstad et al. 1992). The EIC for all profiles were calculated for Ca, Na, K, P, and Si using concentrations (mg kg^{-1}) determined by lithium metaborate fusion.

$$EIC = \left(\left(\frac{Sh}{Rh}\Big/\frac{Sp}{Rp}\right) - 1\right) * 100 \qquad Equation\ 2$$

The terms Sh and Rh are the concentrations of the element of interest in the sample horizon (Sh) and parent material (or reference horizon, Rh), respectively, divided by the

concentration of the immobile element (Zr) in the sample horizon divided by the concentration of Zr in the parent material.

4.2.8 Data Analysis

Due to the nature of chronosequence studies, replicates on each site were used to look at the variability of soil development and associated chemical parameters within each dune. Only averaged values of the two replicates were used for data analysis to avoid pseudoreplication. The coefficient of variation and standard deviation were calculated from the two replicates to examine variability within a dune. Since each profile had unique genetic horizons and associated thicknesses, a weighted average was calculated for all horizon types (FF, A and B) for all data unless otherwise noted.

Allophane presence was examined using the estimated allophane concentration of each horizon determined by calculating the Al: Si ratio of inorganic, non-crystalline Al and multiplying the oxalate-extractable Si concentration of each horizon by a factor determined by Parfitt (1990). Graphs were created to illustrate trends of CIA, EIC, and pyrophosphate- and oxalate-extractable Al and Fe with depth. Weighted averages for 10 cm increments were calculated for the depth graphs. Podzolic B thickness and FF depth were also explored but no trends were apparent.

4.3 Results

4.3.1 Chemical Properties

The greatest decline in pH measured in water was between 0 and 105 years, corresponding to Ae development and FF accumulation (Fig. 4-1; Appendix 2). The average pH of each horizon fluctuated little after 105 years (Fig. 4-1). The pH within the FF decreased throughout, with the L horizon being the most basic and the H horizon being the most acidic (Appendix 2).

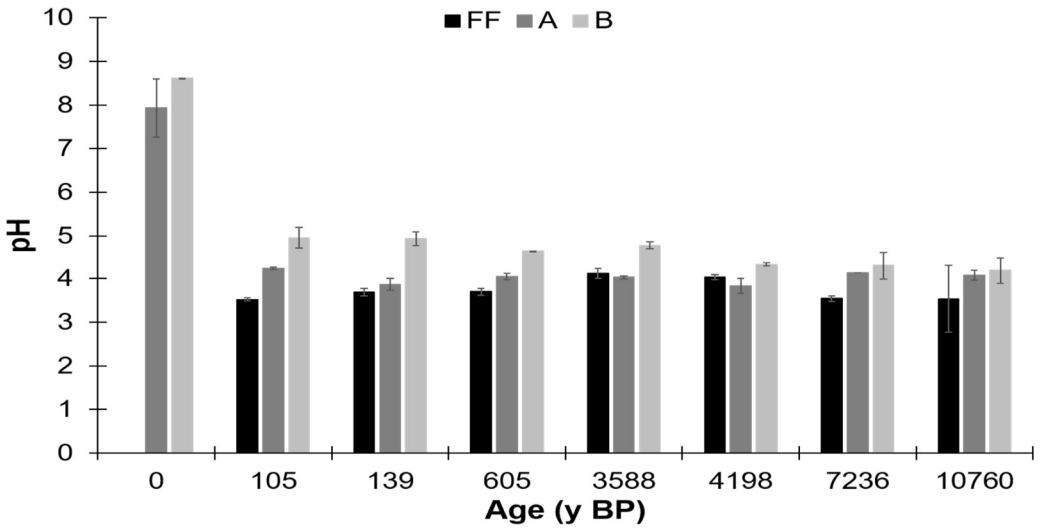

Figure 4-1. Average weighted pH (H_2O) of the forest floor (FF), A and B mineral horizons with one standard deviation indicated by the bars (n=2; Note: the youngest site (0 a BP) did not have a FF or a B horizon, so there are no FF data and the BC horizon was used instead of a B horizon).

The FF maintained appreciable concentrations of exchangeable base cations, extracted with $BaCl_2$, with increasing age, particularly on the 3,588 a BP and 4,198 a BP sites (Fig. 4-2 a). The greatest base cation concentration in the A horizon was found on the youngest site (~0 a BP) and the least was found on the oldest site (10,760 a BP). The concentration of base cations was the least in the B horizon compared to all horizon types (Fig. 4-2a). Overall, Al^{3+} increased in concentration with increasing age (Fig. 4-2b), although there was a large spike of Al^{3+} on the 7,236 a BP site in the FF, and there was a peak of Al^{3+} in the A horizon on the 4,198 a BP site (Fig. 4-2b).

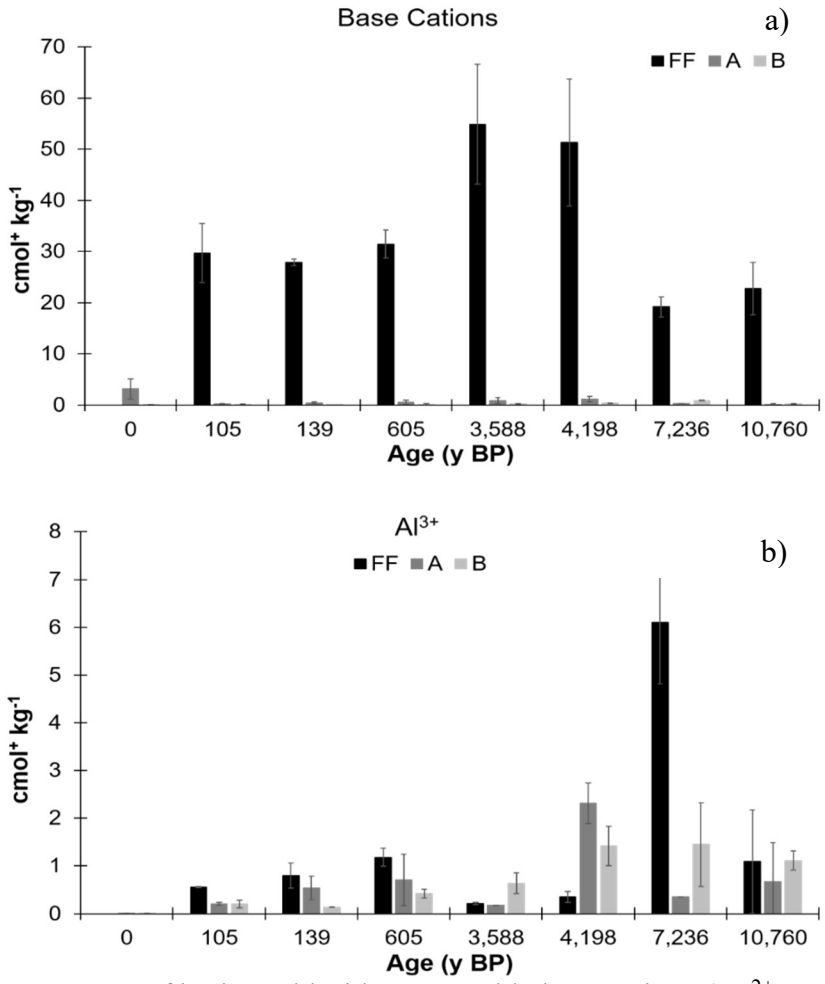

Figure 4-2. Average sum of barium chloride-extractable base cations (Ca^{2+}, Mg^{2+}, Na^{+}, and K^{+}) and aluminum cation (Al^{3+}) of each soil horizon with one standard deviation indicated by the bars; forest floor (FF), A and B mineral horizons (n=2) (Note: the youngest site (0 a BP) did not have a FF or a B horizon, so there are no FF data and the BC horizon was used instead of a B horizon; Hendershot et al., 2008).

The peaks of Fe_p in the depth profile corresponded to the presence of placic horizons, whereas, peaks of Al_p represented either ortstein or placic horizons (Fig. 4-3; Appendix 4). Replicate A on the 3,588 a BP site (CIDS8A) had the greatest concentration of Fe_p followed by the oldest site replicate A (CIDS10A) and then CIDS8B (Fig. 4-3). Site CIDS10A had the greatest Al_p concentration followed by CIDS8B, CIDS8A and CIDS10B for the profiles illustrated.

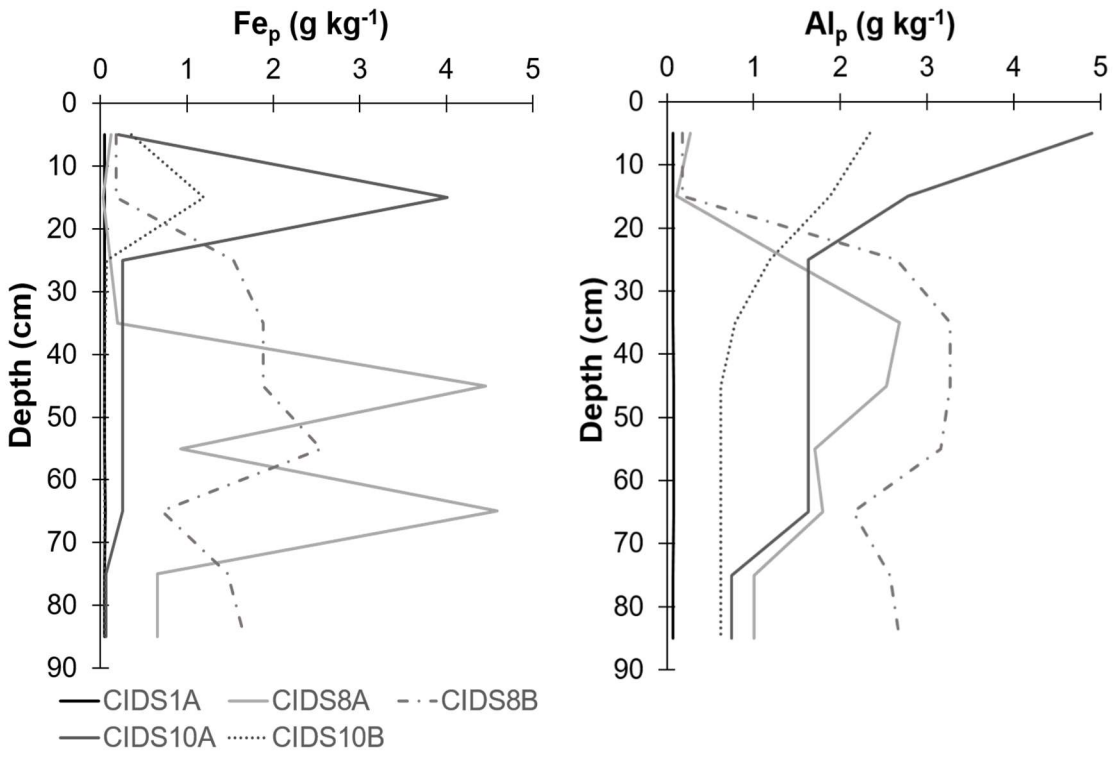

Figure 4-3. Pyrophosphate extractable iron (Fe_p) and aluminum (Al_p) to 90-cm depth for CIDS1A (~0 a BP), CIDS8A and CIDS8B (3,588 a BP) and CIDS10A and CIDS10B (10,760 a BP).

The concentration of non-crystalline Fe (Fe_o -Fe_p) and Al (Al_o-Al_p) increased with increasing age (Fig. 4-4). Peaks in Fe_o -Fe_p did not always correspond to peaks in Fe_p, but often corresponded to the presence of placic horizons (Appendices 2 and 4). For replicate A replicate on the 3,588 a BP site (CIDS8A), the first placic horizon did not have a peak in Fe_o -Fe_p, but the second placic horizon did. Overall, the concentration of Fe_o -Fe_p decreased with increasing depth (Fig. 4-4a). Non-crystalline Al was distributed throughout the profile for both replicates on the 3,588 a BP site compared to the youngest site (~0 a BP; Fig. 4-4b). The total amorphous Al concentration increased with increasing age. Replicate B on the oldest site (10,760 a BP; CIDS10B) had an apparent peak of amorphous Al where the Bfc and Bmcj horizons were present. Site CIDS10A did not have a peak of amorphous inorganic Al like CIDS10B but there were appreciable concentrations of amorphous inorganic Al throughout

the entire Bmcj (Fig. 4-4b). Interestingly, the proportion of total Fe that was oxalate-extractable was much greater than for Al (Appendix 2).

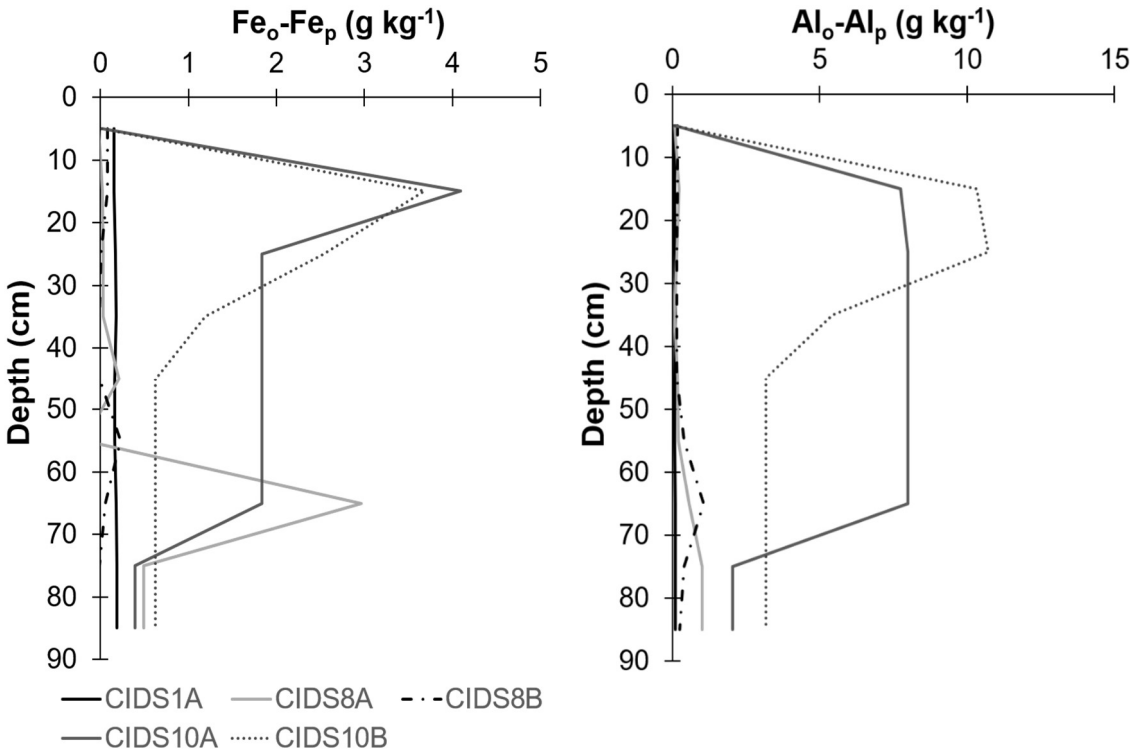

Figure 4-4. Amorphous inorganic Fe (Fe_o -Fe_p) and Al (Al_o-Al_p) to 90-cm depth for CIDS1A (~0 a BP), CIDS8A and CIDS8B (3,588 a BP) and CIDS10A and CIDS10B (10,760 a BP).

Estimated allophanic materials increased in abundance with increasing age (Fig. 4-5). The youngest site, ~0 a BP (CIDS1A), had a consistent, but minimal, concentration of estimated allophane throughout the entire profile. Soil depth profiles indicated increasing concentrations of allophane with increasing age, because small peaks of allophane occurred within the 3,588 a BP sites (CIDS8A and 8B), and an increased concentration of allophane occurred in the oldest sites (10,760 a BP; CIDS10A and 10B; Fig. 4-5). The accumulation of allophane also occurred closer to the surface in the older soils, whereas, it was just below 50 cm depth after 3,500 years (Fig. 4-5) Interestingly, the 4,198 a BP site (CIDS15) had the greatest concentration of allophane compared to all other soil profiles (Appendix 4).

Allophane concentration increased with increasing age and was evident in all soil horizons, particularly Ae, Bhc and Bfc horizons (Appendices 2 and 4).

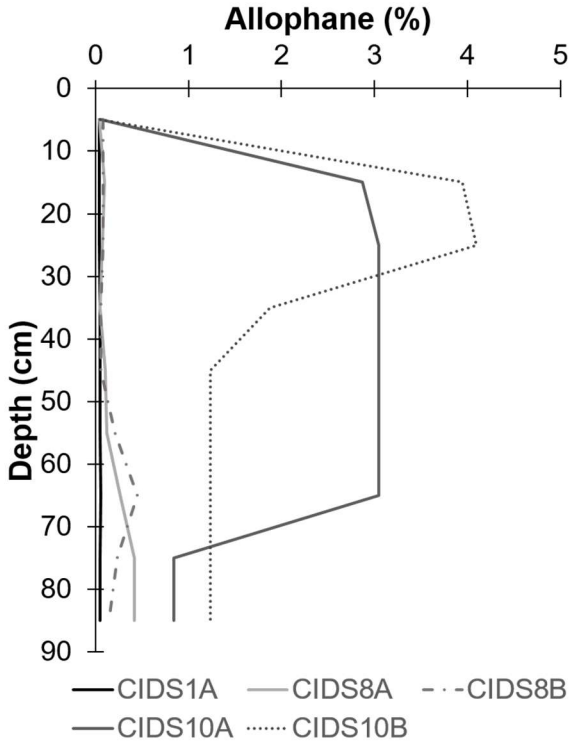

Figure 4-5. Soil depth profile for estimated allophane (%) for CIDS1A (~0 a BP), CIDS8A and CIDS8B (3,588 a BP) and CIDS10A and CIDS10B (10,760 a BP) using methods from Parfitt (1990).

4.3.2 Chemical Weathering Indices

The average CIA for the unweathered parent material calculated from the optical dating samples was 61 ± 1 (n=4). The CIA for the youngest soil at CIDS1A (~0 a BP) was less than unweathered parent material, suggesting that it was enriched rather than depleted of mobile oxides (Fig. 4-6). Replicates CIDS8A and 8B showed similar CIA values with increasing depth. The first 20 cm of mineral soil at CIDS8A and 8B had a comparable CIA to the unweathered parent material, followed by an increased CIA after 20 cm, reaching a plateau around 63. Although the CIA depth profiles for CIDS10A and 10B looked different, they both followed similar trends, with the greatest CIA in the Bfc and Bmcj horizons (Fig.

4-6). For the soil profiles not depicted in Fig. 4-6, the CIA ratio increased with increasing age, indicating greater weathering with increasing time (Appendix 4).

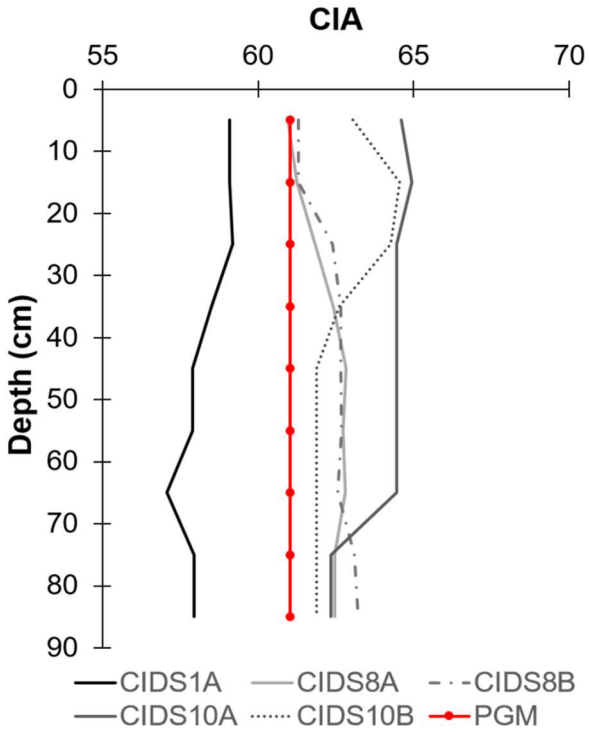

Figure 4-6. Depth profiles of CIA values in the < 2mm fraction for select profiles; CIDS1A (0 a BP), CIDS8A, and B (3,588 a BP), CIDS10A, and B (10,760 a BP), with reference values for the assumed parent geological material used for optical dating (Neudorf et al., 2015).

Total P was enriched on site CIDS1A, with the EIC exceeding 50 in the top 30 cm and the enrichment declined with increasing depth (Fig. 4-7a). Both CIDS8A and 8B (3,588 a BP) illustrated significant depletion of P in the first 20 cm corresponding to the Ae and/or Ahe horizons. CIDS8A maintained P depletion up to 40 cm, which marks the transition area to the placic horizon, whereas P depletion was less pronounced after 20 cm in CIDS8B. Both CIDS10A and 10B (10,760 a BP) showed enrichment of P in the upper Bhc horizon, followed by significant P depletion within 10 cm to 95 cm depth for CIDS10A and, between 10 and 30 cm depth for CIDS10B (Fig. 4-7a; Appendix 4).

The Ca EIC ratios showed similar trends for all sites older than 3,500 years (Fig. 4-7b). The youngest site, CIDS1A had an enrichment of Ca throughout the depth profile. Within 105 years, depletion of Ca within pedons was evident; however, there was a greater depletion of Ca on CIDS3 (105 a BP; Ca EIC = -7 to -57) compared to CIDS4 (139 a BP; Ca EIC = 26 to -25; Appendix 4). All the sites older than 605 years showed depletion of Ca, particularly in Bhc or ortstein horizons (Fig. 4-7b).

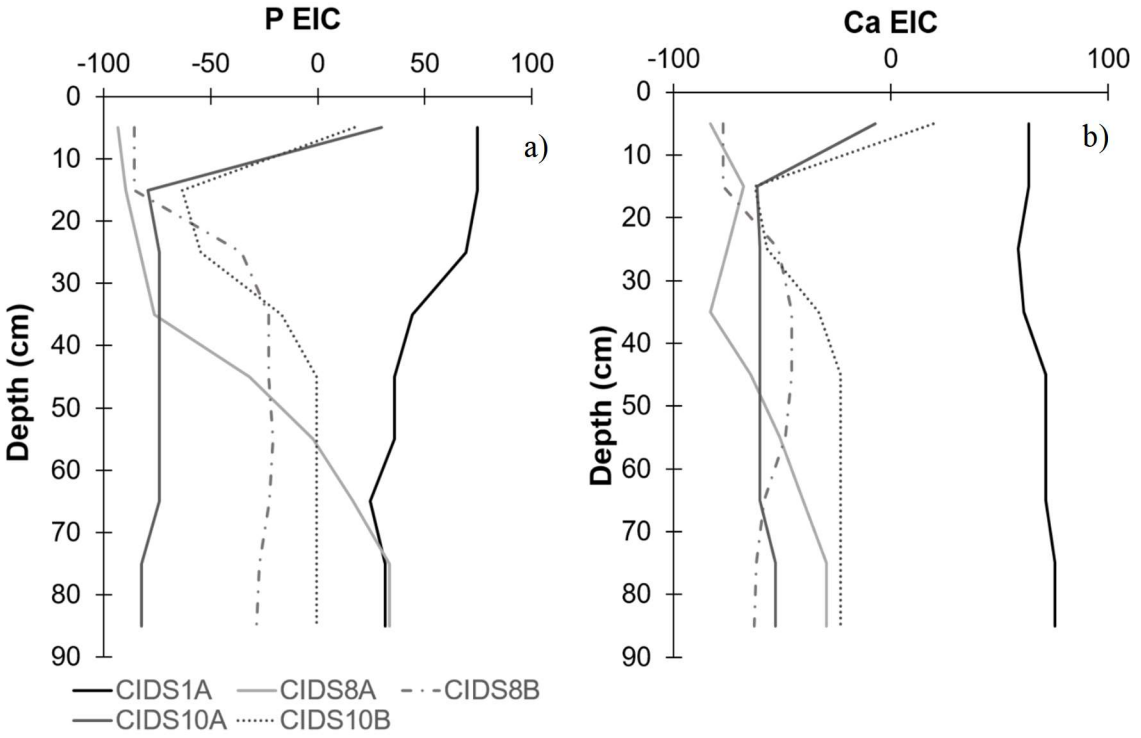

Figure 4-7. Depth profiles of eluvial/illuvial coefficients (EIC) for P (a) and Ca (b) in the < 2mm fraction for select profiles; CIDS1A (0 a BP), CIDS8A, and B (3,588 a BP), CIDS10A, and B (10,760 a BP) using Zr as the resistant reference element.

4.3.3 Soil Morphology

Pedons on the youngest site (~0 a BP), an established foredune, were classified as Cumulic Regosols (CU.R) with evidence for establishment of early successional plants followed by progressive burial (Fig. 4-8; Appendix 2; SCWG, 1998). Within 105 to 139 years, on stabilized, forested foredunes, sites had bleached eluvial horizons and showed

evidence of progressive FF accumulation (Table 4-1; Fig. 4-8; Appendix 2). Pedons on these sites were classified as Eluviated Dystric Brunisols (E.DYB). The FF on the 139 y BP site was considerably thinner than the 105 y BP site (ranges from 9 - 10 cm thick; Tables A2-3 to A2-6) and was most likely caused by landscape position because the 139 y BP site was on the top of an established, forested foredune with rapidly drained soils, whereas the 105 y BP site was in a lower elevation position that may act as a catchment. After 605 years, pedons had developed diagnostic organic-enriched B horizons and ortstein cemented horizons on an established, forested dune with evidence of tree fall. Pedons on the 605 a BP site were classified as E.DYB (Table 4-1).

Within 3,500 years, mature Podzols had formed on an established, forested, dune-capped tombolo (Eamer, 2017), two types of cemented horizons (ortstein, placic) had formed and pedons met the criteria for an Ortstein Humic Podzol (OT.HP; Fig. 4-8; Appendix 2). The pedons on the 4,198 a BP site, on an established, relict, forested foredune, were also classified as OT.HP. The 7,236 a BP site was an established, forested foredune and had the thickest FF of all sites making it a Humic Folisol (H.FO). Replicate B was sampled at the original site where the optical stimulated luminescence dating sample was obtained though it was a wetter replicate due to the site microtopography and the apparent weathering depth was considerably greater than for any other pedon, with the Bh horizon transitioning to a BC at 2.23 m. Had the FF been thinner on the 7,236 a BP site, the pedon at CIDS16A would have been classified as an Orthic Humic Podzol (O.HP) and the pedon at CIDS16B would have been an OT.HP. The two pedons classified on the oldest site, 10,760 a BP (CIDS10; an established, bog forest dune), did not meet the same soil classification great group, although comparable horizonation was apparent. The pedon at CIDS10A was classified as a Placic

Humic Podzol (P.HP; Fig. 4-8), whereas the pedon at CIDS10B was classified as an E.DYB because the Podzolic B horizon at CIDS10B was not thick enough to meet the criteria (10 cm thick; Table 4-1; Appendix 2; SCWG, 1998). This site was interesting because of the presence of a beige organic layer that felt "silty". Generally, humified H horizons are dark brown, so the presence of a light beige humified layer was intriguing.

Most soil horizons remained structureless with increasing age, which means that there was no orderly arrangement of soil particles around the planes of weakness (CANSIS, 1982). A shift in the kind of structureless condition from single-grained to massive occurred with increasing age, where single-grained refers to a loose mass of individual soil particles and massive refers to a coherent mass of soil particles that do not exhibit a distinct arrangement (Table 4-1; CANSIS, 1982). Soil textures other than sand were present in some Ae and Ahe horizons after 3,500 years (Table 4-1). Root restriction and seepage occurred on most sites older than 3,500 years (Appendix 2). Evidence of fire was prevalent on all chronosequence sites after 3,588 years. Charcoal was found in older soils within the organic horizon on sites >3,500 years and more modern fires scars on living trees were apparent on sites >7,000 years. The prevalence of tree scarring on the 7,236 a BP site was less than on the 10,760 a BP site; most trees at on the oldest site (10,760 a BP) with a DBH > 9 cm had fire scars (particularly evident on *Pinus contorta* var. *contorta*; Appendices 2 and 3). The date of the most recent fire on sites older than 3,500 years is unknown (Hoffman et al., 2016a, b).

Table 4-1. Pedon classification, site series and soil morphology including bulk density (Db; Banner et al., 1993; SCWG, 1998).

Pedon Age (BP) Classification	Site Series (BEC): dominant plant species[a]	Horizon (CSSS)	Depth (cm)	Colour (moist)	Structure[b]	Texture[c]	Db (g/cm^3)
CIDS1A	modern established dune: dune grass	C	0-27	5Y 6/2	SG	S	1.36
0		Ahb	27-34	2.5Y 4/2	SG	S	1.28
CU.R		C2	34-62	5Y 6/2	SG	S	1.18
		Ahb2	62-67	2.5Y 5/2	SG	S	1.17
		BC	67-116	5Y 5.5/1	SG	S	1.17
CIDS1B	modern Established dune: dune grass	C	0-13	2.5Y 6/2	SG	S	1.33
0		Ahb	13-18	5Y 3/2	MA, SG	S	1.16
CU.R		BC	18-92	5Y 6/2	SG	S	1.25
		C2	92-111+	5Y 7/1	SG	S	1.25
CIDS3A		organic layer: S/L 28-26 / Fm 26-22 / Hw 22-0					
105 ± 15	15 Ss: Hw/Dr/Ss	Ae	0-3	2.5Y 5/2	SG	S	1.20
E.DYB		Bmj	3-58	10YR 4/3	SG	S	1.25
		BC	58-93+	2.5Y 4/3	SG	S	1.37
CIDS3B		organic layer: S/L 37-35 / Fm 35-33 / Hw 33-0					
105 ± 15	15 Ss: Hw/Dr	Ae	0-3	2.5Y 5/2	SG	S	1.20
E.DYB		Bhj	3-26	10YR 4/4	SG	S	1.22
		Bm	26-55	2.5Y 4/3	SG	S	1.37
		BC	55-120+	2.5Y 5/3	SG	S	1.46
CIDS4A		organic layer: S/L 9-8 / Fa 8-7 / Hh 7-0					
139 ± 17	01 CwHw: Ss/Hw/Cw	Ae	0-3	2.5Y 5/2	SG	S	0.98
E.DYB		Bhj	3-23	10YR 4/3	SG	S	1.25
		Bm	23-73	2.5Y 5/3	SG	S	1.37
		BC	73-111+	2.5Y 6/8	SG	S	1.25
CIDS4B		organic layer: S/L 10-8 / Fm 8-6 / Hh 6-0					
139 ± 17	01 CwHw: Hw/Ss	Ae	0-5	10YR 4/1	SG	S	0.93
E.DYB		Bhj	5-19	10YR 3/4	SG	S	1.20
		Bm	19-64	2.5Y 6/3	SG	S	1.31
		BC	64-103+	2.5Y 6/3	SG	S	1.36
CIDS9A		organic layer: S/L 25-23 / Fm 23-18 / Hh 18-5 / Hw 5-0					
605 ± 50	03a CwYc: Hw/Dr	Ae	0-6	5Y 7/1	SG	S	0.96
E.DYB		Bhj	6-36	10YR 3/2	MA, SG	S	1.26
		Bhc	36-39	7.5YR 2.5/3	MA	S	1.26
		Bmj	39-90	10YR 3/	MA, SG	S	1.35
		BC	90-112+	2.5Y 4/4	MA	S	1.33
CIDS9B		organic layer: L 4-3 / Fm 3-1 / Hi 1-0					
605 ± 50	03a CwYc: Cw/Dr	Ahe	0-13	10YR 4/2	SG	S	0.86
E.DYB		Hwb	13-33	7.5YR 2.5/1	-	-	0.10
		Bm	33-58	2.5Y 5/4	MA	S	1.14
		Bhjcj	58-113	10YR 3/2	MA	S	1.14
CIDS8A		organic layer: L 37-34 / Fm 34-15 / Hw 15-0					
3,588 ± 303	14 Ss: Hw/Cw/Ss	Ahe	0-6	10YR 5/4	MA	LS	1.42
OT.HP		Ae	6-25	2.5Y 6/2	SG	S	1.42
		Bhc	25-43	10YR 2/2	MA	S	1.56
		Bfc1	43-45	2.5YR 2.5/3	MA	S	1.76
		Bm1	45-65	7.5YR 3/2	SG	S	1.42
		Bfc2	65-67	5YR 3/4	MA	S	1.76
		Bm2	67-95	10YR 3/4	MA	S	1.41
		BC	95-163+	2.5YR 5/4	SG	S	1.41

Pedon Age (BP) Classification	Site Series (BEC): dominant plant species[a]	Horizon (CSSS)	Depth (cm)	Colour (moist)	Structure[b]	Texture[c]	Db (g/cm^3)
CIDS8B		organic layer: L 28-27 / Fa 27-10 / Hw 10-0					
3,588 ± 303	14 Ss:	Ae	0-22	2.5Y 6/2	SG	S	0.96
OT.HP	Hw/Ss	Bhc	22-57	5YR 2.5/1	MA	S	1.24
		Bfcj1	57-58	7.5YR 2.5/2	MA	S	1.29
		Bh	58-72	7.5YR 3/2	MA	S	1.29
		Bhcj2	72-106	5YR 2.5/1	MA	S	1.29
CIDS15A		organic layer: S/L 20-18 / Fm 18-14 / Hh 14-0					
4,198 ± 332	01 CwHw:	Ae	0-4	10YR 4/1	MA	SL	0.68
OT.HP	Hw/Ss/Cw	Ahe	4-12	10YR 3/2	MA	SL	0.68
		Bhc	12-21	10YR 2/1	MA	LS	1.29
		Bfcj	21-23	2.5YR 2.5/3	MA	S	1.64
		Bmcj	23-49	10YR 4/6	MA	S	1.66
		BC	49-103+	2.5YR 5/4	SG	S	1.28
CIDS15B		organic layer: S/L 18-16 / Fm 16-13 / Hh 13-0					
4,198 ± 332	01 CwHw:	Ae	0-9	10YR 4/3	SBK	L	0.68
OT.HP	Hw/Cw/Yc	Ahe	9-14	10YR 3/1	MA	LS	0.68
		Bhc	14-28	10YR 2/1	MA	S	1.25
		Bhc2	28-38	10YR 3/6	MA	S	1.24
		Bh	38-43	7.5YR 2.5/2	MA	S	1.24
		Bfc	43-45	2.5YR 2.5/4	MA	S	1.63
		Bm	45-128+	2.5Y 5/4	MA	S	1.32
CIDS16A		organic layer: S/L 0-3 / Fa 3-8 / Hw 8-35 / Oh 35-55					
7,236 ± 546	11 CwYc:	Bhc	55-64	5YR 2.5/2	MA	S	1.18
HU.FO	Cw/Hw/Yc/Pc	Bhcj	64-80	10YR 3/3	MA	S	1.04
		Bfc	82-81	5YR 3/4	MA	S	1.58
		Bm	81-136+	10YR 4/4	MA	S	1.31
CIDS16B		Organic layer: S/L 0-4 / Fm 4-12 / Hw 12-45 / Oh 45-63					
7,236 ± 546	11 CwYc:	Bhc	63-85	7.5YR 2.5/2	MA	S	1.31
HU.FO	Cw/Hw/Hw	Ae	85-86	2.5Y 4/2	SG	S	1.25
	Yc/Pc	Bmcj	86-103	7.5YR 2.5/3	MA	S	1.25
CIDS10A		organic layer: Lv 28-27 / Fm 27-24 / Hh1 24-10 / Hh2 10-0					
10,760 ± 864	11 CwYc:	Bhcj	0-10	10YR 2/1	MA	LS	0.87
P.HP	Cw/Yc/Hw/PC	Ae	10-12	10YR 7/1	SG	-	0.87
		Bfc	12-15	5YR 4/4	MA	S	1.49
		Bmcj1	15-70	2.5Y 7/3	MA	S	1.27
		BCg1	70-138	2.5Y 7/3	MA	S	1.27
CIDS10B		organic layer: S/L 28-25 / Fm 25-20 / Hh1 20-14 / Hh2 14-0					
10,760 ± 864	11 CwYc:	Bhc	0-7	10YR 2/1	MA	LS	0.96
E.DYB	Cw/Hw/Pc	Ae	7-10	2.5Y 5/3	SG	S	0.96
		Bfc	10-13	5YR 4/6	MA	S	1.23
		Bmcj	13-33	10YR 5/8	MA	S	1.23
		BC	33-90+	5Y 6/2	MA	S	1.31

[a] Tree species (Banner et al., 1993): red alder (Dr), western redcedar (Cw), yellow cedar (Yc), western hemlock (Hw), and shore pine (Pc)

[b] Structure (FAO, 2006): single grain (SG), massive (MA) and subangular blocky (SBK)

[c] Texture (SCWG, 1998): sand (S), sandy loam (SL), and loamy sand (LS)).

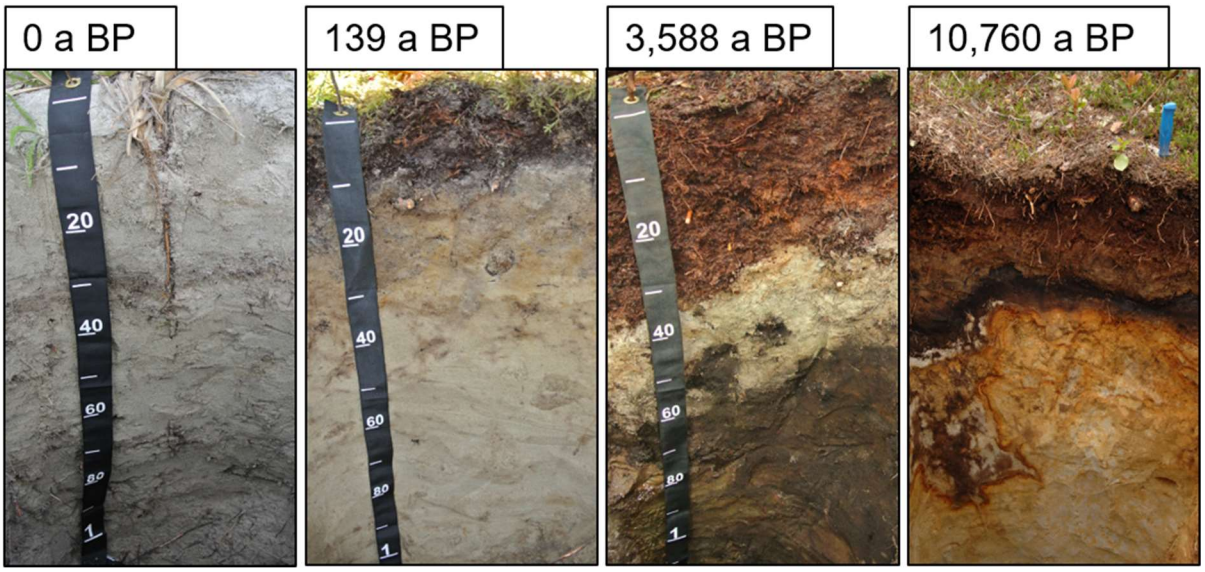

Figure 4-8. Representative soil profiles from the youngest to the oldest sites on the Calvert Island Chronosequence, BC. The youngest site (0 a BP, CIDS1A) is a Cumulic Regosol, the 139 a BP (CIDS4B) is an Eluviated Dystric Brunisol, the 3,588 a BP (CIDS8B) is an Ortstein Humic Podzol, and the 10,760 a BP (CIDS10A; knife handle is 11 cm) sites is a Placic Humic Podzol.

4.4 Discussion

4.4.1 Exploration of Chronosequence Assumptions

Soil chronosequences are invaluable for the study of soil development because the space-for-time substitution allows for the examination of changes occurring on a longer time scale than any human lifespan (Jenny, 1941; Walker et al., 2010). There are limitations to the use of chronosequence studies; however, particularly related to the succession of different plant communities with age (e.g., Johnson and Miyanishi, 2008) but it is possible to use chronosequences in an appropriate context to produce reliable data such as examining soil development between temporally linked sites (Walker et al., 2010). It is important to remember, however, that a chronosequence is subject to variability in all environmental factors that control soil and broader ecosystem development, and that deviations from "ideal" may exist such as differences in landscape position, drainage or specific plant species.

The Calvert Island chronosequence has robust time control from the use of optically stimulated dating techniques that included corrections for errors (Neudorf et al., 2015) as well as detailed interpretation of post-glacial landscape evolution (Eamer, 2017; Eamer et al., 2017a, b). All dunes used in this study were established or stabilized dunes and aeolian in origin (Neudorf et al., 2015; Eamer, 2017; Eamer et al., 2017a, b, c). Drainage appeared to be similar across all sites, aside from sites where cemented horizons impeded water flow, which was expected with age in the CWH zone (Banner et al., 2005). Sites CIDS3 (105 a BP) and CIDS16 (7,236 a BP) were lower elevation sites, which resulted in a wetter microclimate though drainage and degree of soil development were comparable to sites of similar age.

All parent material (C) and/or transition horizons (BC) were comparable and did not provide any indications to suggest that the parent material was not the same (e.g. no differences in carbonate content, texture, colour, etc.). All dunes were confirmed to be aeolian sand dunes (Eamer, 2017; Eamer et al., 2017c). It was assumed that similar environmental conditions were experienced on each dune at the same age; however, confirmation of this assumption is not possible. For example, on CIDS9B, there was evidence of recent treefall, but we could not confirm that treefall also occurred on all older sites when they were ~600 years old. Radiocarbon dating of buried wood horizons could be performed where remnants of fallen trees have not been fully degraded to further investigate the history of treefall.

Over the duration of the Calvert island chronosequence there have been fluctuations in climate such as cooler, drier climate conditions during the retreat of the Cordilleran ice sheet following the last glacial maximum and a warmer, wetter climate during the early Holocene period (Eamer, 2017; Eamer et al., 2017a). All long-term chronosequences will

have experienced fluctuations in climate owing to the millennial time-scale of these studies. Some chronosequences have significant changes in climate, such as the Hawaiian chronosequence, where soil development in the current climate may only take one-third of the time that it would take to form the same soil in previous climates (Hotchkiss et al., 2000). Variations in climate are important to document and include within the analysis of chronosequence studies as it is impossible to have a natural experiment without this variation.

Aeolian activity is controlled by sediment availability, moisture, and wind regime, and aeolian landform records may also be controlled by other environmental mechanisms including changes in relative sea level and climate (Hesp and Walker, 2013; Eamer, 2017; Eamer et al., 2017a). On Calvert island, sediment availability and moisture conditions are well-documented whereas long-term wind conditions are not fully understood (Eamer et al., 2017a; Walker, pers. Comm., 2018). The Calvert island chronosequence was formed on aeolian landforms, which reflect the interplay between these factors. The oldest stabilized, relict dune started to form 14 to 10.5 kya while cold and dry conditions persisted and promoted the development of large dune systems (Eamer, 2017; Eamer et al., 2017a). By 10.5 to 8.5 kya, the oldest dune (10,760 y BP; CIDS10) started to stabilize because of a reduced sediment supply and, potentially, the warmer, wetter climate. Between 8.5 and 5.6 kya, a large foredune formed behind north beach (4,198 y BP; CIDS15) in response to a new supply of subaerial sediment and likely changes in beach width and littoral circulation in the west beach embayment. By 5.6 to 4.2 kya, the tall dune on the tombolo between 4th and 7th beach (3,588 y BP; CIDS8) stabilized and became vegetated during a warm, wet climate. More recently, rapid shoreline progradation rates have occurred on west beach between 1.8

and 0.4 kya (1.2 m a^{-1}) and 0.4 kya to present (0.69 m a^{-1}). Coincidently, dune stabilization rates have also been high during this period, as is found elsewhere on the British Columbia coast (0 y BP (CIDS1); 105 y BP (CIDS3); 139 y BP (CIDS4); Eamer, 2017; Eamer et al., 2017a; Heathfield and Walker 2011).

Though there was significant change in the climate within the past 11,000 years, Eamer (2017) found minor occurrences of coastal strawberry and crowberry 15.1 to 14.7 kya and 840 a BP pollen from Sitka spruce, shore pine, red alder and cedar were found near Hood Lake (found north east of CIDS9). The paleobotanical record shows that early successional plant species were present on Calvert Island when the oldest site, 10,760 a BP, was formed and tree species currently dominant on Calvert Island were also present 840 a BP. This suggests that the biological community was similar across the chronosequence and the expected successional trends of early successional species to high productivity forests to low productivity forests with increasing age were apparent, which was typical in the CWH zone (Banner et al., 2005).

Therefore, the Calvert Island sites collectively met the requirements for a chronosequence study (Jenny, 1941; Walker et al., 2010), albeit with some variation within climate and topography, as they appeared to have experienced a convergent, successional trajectory with low frequency and severity of disturbance (Walker et al., 2010).

4.4.2 Changes in Soil Chemical Properties with Time

4.4.2.1 Exchangeable Cations

The base cation concentration in the FF was significantly higher than in the mineral soil, most likely due to surface enrichment from litter fall and the close proximity to the ocean resulting in sea spray (Figs. 3-1 and 3-2). The peak of base cations within the FF on CIDS8 (3,588 a BP) and CIDS15 (4,198 a BP) may be attributed to the dominant yellow and

redcedar litterfall that is known to have a high Ca content; this would increase the buffering capacity within the FF (Fig. 4-2; Appendices 3 and 4; Radwan and Harrington, 1986). All sites were within approximately 310 m from the shoreline, with CIDS8 (3,588 a BP) and CIDS15 (4,198 a BP) closest to the shoreline (140 m). On the west coast of Vancouver Island, Cordes (1972) documented that annual sea spray deposits 250 g m^{-2} of Na, 22 g m^{-2} of Mg, 8.9 g m^{-2} of K and 7.0 g m^{-2} of Ca on recent dunes (Sondheim et al., 1981). However, the mineral horizons had continual depletion of base cations, and the increased removal of Ca and P with depth indicated by the EIC (Figs. 4-2 and 4-7).

With increased weathering and podzolization it was expected that the base cations would leach out of the mineral soil, reducing the base cation abundance (Tiessen et al., 1984; Sauer et al., 2007). This was apparent after 105 years in the A and B horizons with a drastic decline in base cations (Figs. 4-1 and 4-2). Overall, the EIC for all mineral horizons depicted the expected trends for P and Ca with increasing depletion with increasing age, except for the youngest site (~0 a BP) that had an enrichment of Ca and P (Fig. 4-7). The enrichment of P within the mineral horizons on the youngest site may be due to the input of phosphate ions within sea spray or aeolian deposition of coastal sediment. The BC horizon did not have as great a decline as the A and B horizons because the BC horizon is a transition horizon to the C horizon, which implies less weathering and removal of cations (Fig. 4-2).

Potential inputs from seaspray were originally thought to cause the enrichment of Ca within the mineral soil in the youngest site; however, the actual concentration of Ca within each soil horizon was comparable to the reference parent material and exchangeable Ca within the mineral horizons did not account for a considerable proportion of total Ca (2.0%; Appendix 4). The cause for enrichment of Ca in the youngest site may be attributed to lower

concentrations of reference element Zr, that in turn, increased the EIC; additionally, there was little clay within these soils ($\%_{\text{clay in B horizon}}$ = 2.4%; SD = 1.7) and few mechanisms to retain these cations. (Appendix 4). After 100 years of weathering, Ca became depleted and the depth of depletion increased with increasing age. The Bhc or ortstein horizons were the most Ca-depleted soil horizons, which also corresponded to the higher CIA values, indicating greater weathering in Bhc horizons (Figs. 4-6 and 4-7b).

Granite and granodiorite are the most prevalent bedrock in the surrounding area, and it is possible that the bedrock could have been reworked into the sand that is the parent material of this chronosequence (Roddick, 1996a; Neudorf et al., 2015). Generally, CIA values for granite and granodiorite are between 45 and 55 (Nesbitt and Young, 1982). It was expected that some mobile elements were removed from the original bedrock prior to deposition on these sandy landforms because there are many processes that could weather the original bedrock into sand grains, including glaciation, wind erosion, solution weathering through precipitation, biological weathering and coastal processes. The length of time it took to weather the original rock into these sand grains is currently being researched in partnership with the Hakai Institute.

Using unpublished data from Roddick (1996b), CIA values calculated for the rock samples taken from Calvert and Hectate Island had a mean CIA value of 63 (SD = 1), ranging between 60 and 64. The parent material of this chronosequence had a CIA of 61 (SD = 1) which was within the range of rock samples taken from the geological survey (Fig. 4-6; Appendix 4). The range of CIA values for this soil chronosequence did not vary considerably with age (56-67) compared to the geological survey rock samples and the parent material (Fig. 4-6; Appendix 4).

The relatively insignificant change in CIA on Calvert Island with increasing age was unexpected, considering that these soils were classified as mature Podzols after 3,588 years and exhibit strong morphological characteristics including the reddish-brown placic horizons and dark, organic cemented B horizons (Table 4-1; Appendix 2). The weathering regime on the Calvert Island chronosequence may be severe enough that congruent dissolution of the mineral matrix is occurring and there is limited formation of secondary minerals considering that these soils were extremely acidic, receive large amounts of precipitation and were in a temperate climate (Tables 1-2 and 2-1; McBride, 1994). There was no evidence for the accumulation of secondary mineral weathering products in the portions of these pedons that were examined, so it is possible that if they were formed, they were transported to a depth that was not sampled (Ugolini et al., 1977).

The primary cementing agents in placic horizons were organically-complexed Fe and Al, whereas ortsteins were cemented by organically-complexed Al and organic material (Figs. 4-3 and 4-4; Appendix 2). Some developing ortsteins that were weakly cemented were not enriched in organic material, such as Bmcj horizons, and organically-complexed Al was the likely cementing agent, consistent with findings by McKeague and Wang (1980), Lapen and Wang, (1999) and Sanborn et al. (2011). Estimated allophane concentrations increased with age, and the depth where allophane peaked became closer to the soil surface with increasing age (Fig. 4-5).

Base cation leaching within the mineral horizons was evident from changes in base cation concentrations, and EIC values, and the associated drop in pH with increasing age. These changes were accompanied by increasing concentrations of organically-complexed and inorganic-Fe and -Al, and the accumulation of allophane closer to the surface of the soil with

age. These trends in soil properties illustrate the trajectory of soil development along the Calvert Island chronosequence where podzolization plays a leading role.

4.4.2.2 Comparison of Soil Chemical Properties with Similar Studies

The loss of base cations and decline in pH with progressive soil development on the Calvert Island chronosequence was comparable to the declines along the Naikoon, Cox Bay, Cooloola, Jurien Bay and Haast chronosequences (Table 2-1; Singleton and Lavkulich, 1987a; Sanborn and Massicotte, 2010; Turner et al., 2012a; Chen et al., 2015; Turner and Laliberté, 2015). Both the Naikoon and Cox Bay chronosequences also exhibited a plateau of pH after ~100 and ~371 years respectively, compared to ~105 years for the Calvert Island chronosequence (Singleton and Lavkulich, 1987a; Sanborn and Massicotte, 2010). On the Haast chronosequence, base cation concentration and pH declined in mineral soils with increasing age, comparable to the Calvert Island chronosequence (Turner et al., 2012a). Mass balance calculations were also performed on the Haast chronosequence and illustrated an increased depletion of Ca and P with depth with increasing age comparable to the EIC values from Calvert Island (Eger et al., 2011). On the Cox Bay chronosequence, the FF had a greater concentration of base cations (Ca, Mg and K) than the mineral soils and did not show a trend of declining base cations with increasing age, similar to the FF on the Calvert Island chronosequence (Singleton and Lavkulich, 1987a). The mineral soils on the Cox Bay chronosequence did have declining concentrations of exchangeable Ca and Mg with age, like on Calvert Island.

Compared to soils in other parts of the world such as Guyana or South Africa with CIA values close to 100, the soils on Calvert Island were not severely weathered compared to the parent material (Nesbitt and Young, 1982). For comparison, the CIA values from the

Damma Glacier chronosequence in Switzerland with quartz, biotite and K-feldspar parent material ranged from 55 to 65 within the first 10 cm of the surface (Bernasconi et al., 2011). On Holocene beach and fluvial sands in northwest Mexico, beach sands had CIA values ranging from 58 to 66, like the Calvert Island chronosequence, though the fluvial sands were more weathered than beach sands due to the loss of easily weathered feldspars, with CIA values ranging from 58 to 78 (Carranza-Edwards et al., 1994). On Baffin Island, CIA values were used to understand the variability of glacial erosion with CIA values < 35 on recently exposed surfaces and up to >80 on older upland, exposed surfaces (Refsnider and Miller, 2013). Within the Yukon, the Wounded Moose paleosol pedons had an average CIA of 75 (Daviel et al., 2011) indicating significant weathering, whereas Orthic Dystric Brunisols on the Lewes Plateau had CIA values ranging from ~50 up to ~65 with depth, corresponding to the transition from the weakly weathered surficial veneer of loess to the older, locally-derived colluvial and residual materials (Dampier et al., 2011). The Calvert Island CIA values were most comparable to Holocene beach sands from northwest Mexico (Fig. 4-6; Appendix 4; Carranza-Edwards et al., 1994).

Like the Calvert Island chronosequence Fe-enriched and Fe-enriched cemented horizons, on the Naikoon, Cox Bay and Haast chronosequences had a greater concentration of Al_p and Fe_p than other horizons, which suggests that organically-complexed Al and Fe were responsible for these Fe enriched horizons, rather than amorphous forms of Fe and Al (Figs. 4-3 and 4-4; Singleton and Lavkulich, 1987a; Sanborn and Massicotte, 2010; Eger et al., 2011). The organic-enriched B horizons on the Haast chronosequence had higher concentrations of Al_p than Bfc horizons like the organic-enriched horizons on the Calvert Island chronosequence (Eger et al., 2011).

The presence of allophane has been documented in many soil types world-wide, including Podzols (Young et al., 1980; Farmer, 1982; Parfitt, 1990; Jansen et al., 2005). Mokma et al. (2001) identified allophane in samples from lower mineral horizons ranging from 900 to 10,700 years on a sandy chronosequence with Podzols in Finland but did not estimate the concentration of allophane within these samples. Allophane was also identified in Danish Podzols with unknown ages by Mossin et al. (2002). Along the Cooloola chronosequence, allophane was identified in all profiles with increasing concentrations of allophane associated with increased aged (Skjemstad et al., 1992). The Cooloola chronosequence is much older than the Calvert Island chronosequence (spans from the Holocene to the Pleistocene), so the intermediate- to old-aged sites on the Calvert Island chronosequence are comparable to the younger sites on Cooloola (Tejan-Kella et al., 1990; Skjemstad et al., 1992). Ferro-Humic Podzols on Vancouver Island, which has a comparable climate, also had a substantial concentration of estimated allophane in the Bhf horizons (Sanborn and Lavkulich, 1989).

4.4.3 Soil Development and Proposed Mechanisms of Podzolization Along the Calvert Island Chronosequence

Within the first 100 years of soil development on this hypermaritime chronosequence, the morphological changes suggest that podzolization was the dominant soil forming process (Fig. 4-8). This rapid development can be attributed to the temperate climate and high rainfall (currently 2800 mm y^{-1}; Table 3-2). It took < 105 years of pedogenesis to develop a FF and an eluvial horizon. Between 139 and 605 years, the development of an organic-enriched, weakly cemented horizon had occurred. By ~3,500 years a mature Podzol had formed, with characteristic ortstein and placic horizons (Table 4-1).

The origin of the silty-feeling beige, organic horizon is not understood. Previous records of the beige organic horizon were in Humisols that were deposited when the ecosystem was functioning as a bog (Banner, 1983). It is common in bogs to find this beige organic horizon that is called sedimentary peat and it moves by water transport between bogs. On the Calvert Island chronosequence this beige organic horizon could not have formed in a bog because the oldest site, (10,760 a BP; CIDS10) is in an upland position in a discharge location. It is possible that fine glacial sediment could have been deposited on the oldest dune from the proximal glaciofluvial plain that contained fine sediment after drainage of the glacial meltwater by aeolian processes (Eamer, 2017; Eamer et al., 2017b).

Organic matter-enriched cemented horizons formed prior to the increase in concentration of allophane, so it is expected the organo-metal complexation mechanism occurred prior to the proto-imogolite theory (Figs. 4-3, 4-4 and 4-8; Appendices 2 and 4). Since cemented horizons formed between 139 and 605 a BP of soil development they could act as a barrier and impede the movement of organic or inorganic sols. Therefore, the Al in the allophanic materials may have been derived from organo-metal complexes that were deposited prior to formation of water-restricting features, and could have been enhanced by the upward movement of Al derived from parent material with ground water fluxes (Dahlgren and Ugolini, 1989; Ugolini and Dahlgren, 1991).

Bedrock in the study area was inherently low in Fe compared to values determined along a ~ 200 km transect spanning the Coast Range, extending eastward from Calvert Island (Roddick, 1996a; b). The average total Fe values for the transect were 4.0% (SD=2.0) while the average Fe values for sampling locations on Calvert and Hectate Island were 1.6% (SD=1.7; Roddick, 1996a; b). Local bedrock was ultimately the source of glacial sediment

that had been reworked into the sand forming the dunes of the chronosequence. Low Fe values, particularly below 5%, which were prevalent on this chronosequence, influenced the path of pedogenesis because low Fe promotes podzolization over brunification and the development of Mor and Moder humus forms rather than Mull forms (Douchaufour and Souchier, 1978). The maximum Fe_p concentration for placic horizon on the Calvert Island chronosequence was on the 3,588 a BP site, replicate A, but the concentration was still appreciably low in comparison to other Podzols (Sauer et al., 2007).

Low Fe parent materials are often also low in clay, and are often acidic which causes a lower decomposition rate compared to high Fe and clay parent materials (Douchaufour and Souchier, 1978; Schaetzl and Anderson, 2005). When Fe is release from primary minerals it is subsequently complexed with organic materials because there is little to no clay competing for Fe. These Fe-organic complexes are soluble and can move to depth promoting podzolization, whereas, soils with higher Fe and clay form insoluble Fe-clay-organic complexes (Douchaufour and Souchier, 1978; Schaetzl and Anderson, 2005). Soils that have low Fe parent material also have low ratios of cation: anions, which also promotes the movement of organo-metal complexes (Douchaufour and Souchier, 1978). Since the soils on the Calvert Island chronosequence were dominated by Mor and Moder humus forms, had a maximum Fe concentration of 4% and the dominance of organic-enriched Bh horizons rather than Bhf or Bf horizons, this indicates that the low Fe parent material influenced the path of pedogenesis on the sequence of soils and that the organo-metal complex podzolization mechanism must have occurred prior to the formation of allophane. Also, the movement of reduced organically-complexed Fe must have occurred after the organo-metal complex

mechanism since Fe-cemented horizons occur below organic- and/or Al-cemented horizons similarly to Skjemstad et al. (1992).

4.4.3.1 Comparison of Podzolization Rates with Similar Studies

Mature Podzols formed at Calvert Island between 605 and 3,588 years, which was most comparable to Naikoon (Fig. 4-8; Tables 2-1 and 4-1; Sanborn and Massicotte, 2010). Cox Bay has a slightly wetter and warmer climate, so it makes sense that podzolization would proceed more rapidly than on Calvert Island (Singleton and Lavkulich, 1987a). Soils at Cox Bay lacked placic horizons, presumably due to their youthfulness, or it could be related to the parent material composition. Formation of placic required between 1,200 and 5,000 years on the Brooks Peninsula and between 800 and 3,100 years at Naikoon (Maxwell, 1997; Sanborn and Massicotte, 2010). In the Calvert Island chronosequence, ortstein horizons started forming between 139 and 605 years, while placic horizons appeared between 605 years and 3,588 years (Table 4-1). Similar to the Naikoon chronosequence, placic horizons on Calvert Island were not enriched in Mn like those in Newfoundland (McKeague, 1968; Moore; 1976; Sanborn and Massicotte, 2010).

The rates of podzolization within Canada are highly variable because of the range of climates, parent materials, and length of pedogenesis. For instance, in subarctic Quebec, it was estimated that it will take 12,400 years to meet the requirements for a Podzolic soil assuming a linear increase in Fe_p with increasing age (Lafortune et al., 2006), whereas Podzol formation was identified on the Hudson Bay chronosequence after 2,300 years and after ~1,200 years in southern James Bay (Protz et al., 1984; Protz et al., 1988). Within soils near the St. Lawrence River, Quebec, it took 5,000 to 6,000 years to form a placic horizon (Moore, 1976) compared to the 605 to 3,588 years required on Calvert Island; however, the

mean annual precipitation (MAP) near the St. Lawrence River is roughly one-third the MAP on Calvert Island, so slower pedogenesis was expected. Dubois et al. (1990) documented locations in Quebec where ortstein development occurred in less than 420 years, which was consistent with the Calvert Island chronosequence where ortstein horizons started forming between 139 and 605 years. Similar to Calvert Island, ortsteins on the east coast of Canada are primarily cemented by organic-Al complexes (McKeague and Wang, 1980; Lapen and Wang, 1999).

The North American coastal temperate rainforest biome extends along the coastal margin from California to Alaska and is characterized by MAP > 1400 mm, so comparison with other sites within the coastal temperate rainforest is particularly useful for comparison with the Calvert Island chronosequence (D'Amore et al., 2012). Calvert Island is situated in the perhumid coastal temperate rainforest, as is southeast Alaska (Fig. 3-1). In southeast Alaska, at the Mendenhall glacier chronosequence with > 2500 mm of MAP (Table 2-1), Spodosols can form within 300 years or less, with characteristic Bf and C horizons apparent after 100 years (Alexander and Burt, 1996). Placic horizons can form within 500 years in southeast Alaska (Ugolini and Mann, 1979). Within 6,000 to 8,000 years in Lituya Bay, Alaska, Podzolic soil horizons developed with the rapid formation of placic horizons followed by paludification and the reduction/removal of Fe from the soil profile (Ugolini and Mann, 1979). Podzolization rates in southeast Alaska are comparable to those on Calvert Island.

Sauer et al. (2008) examined Podzol development in southern Norway on sandy beach deposits. Initial signs of podzolization first occurred between 3,800 and 4,300, years with fully mature Podzols by 6,600 years. This rate of Podzolization was slower than on

Calvert Island, most likely due to the lower mean annual temperature (MAT) and significantly lower MAP. Another study in southern Sweden by Mokma et al. (2004) found that it took 1,520 years to form a Podzolic horizon and an estimated 4,780 years to form a fully mature Podzol. It should be noted that Mokma et al. (2004) lacked sites between 1,800 and 8,300 years of age. In Germany near the Mittelburg glacier, podzolization was apparent after 100 years and all sites from 1,500 to 7,000 years were mature Podzols that had comparable Podzolic features suggesting these soils were at steady state after only 1,500 years (Jenny, 1941; Stevens and Walker, 1970). In northern Sweden near Lake Ragunda, podzolization was apparent within 100 years and mature Podzols were formed within 1,000 years (Tamm, 1920).

In the southern hemisphere on the Cooloola chronosequence spanning > 700,000 years in Australia, it took roughly 7,500 years to form a mature Podzol in a humid, subtropical environment (Table 2-1; Thompson, 1981; Chen et al., 2015). Evaporation and transpiration would most likely be greater in Cooloola than Calvert Island resulting in less moisture available for rapid podzolization. Proto-imogolite allophanic materials were found in the Bhs and Bh horizons in Cooloola, suggesting that Podzolic mechanisms present in Cooloola were comparable to Calvert Island, just at different rates (Skjemstad et al., 1992). In a slightly cooler climate than at Cooloola, sand dunes near Woy Woy, Australia, had significant depletion of carbonates within 100 years, and formation of Fe Podzols after 2,000 years and humus Podzols after 3,000 years (Burges and Drover, 1953). The MAP was comparable to Cooloola, but the MAT was lower because it is further from the equator. Cooler environments lead to less evaporation and more moisture that can be used to facilitate faster podzolization due to the formation of organic acids and subsequent leaching.

The Haast chronosequence in New Zealand is an example of rapid Podzol development in a climate both warmer and wetter than the Calvert Island chronosequence (Table 2-1; Eger et al., 2011; Turner et al., 2012a). This series of soils were formed on foredune ridges and has a uniform parent material of quartzo-feldspathic sand (Eger et al., 2011). It was estimated that within the first 100 years there was rapid acidification and leaching of basic cations since a Brunisol was present on the 370-year-old dune (Eger et al., 2011). By 1,000 years, Podzolic horizons had begun to form and progressive thickening of the FF and development of an eluviated A horizon was present on the 2,000-year-old dune (Turner et al., 201a2). Within 3,903 years, the dunes met the criteria for a Spodosol and had developed a placic horizon (Turner et al., 2012a). The Haast chronosequence was the most comparable chronosequence to the Calvert Island chronosequence because the climate is wet and warm causing a rapid weathering rate, the parent materials were similar and the rate of podzolization was comparable. The Calvert Island chronosequence developed characteristic placic humic Podzols between 605 and 3,588 years, compared to Haast that took between 3,384 and 3,903 years. It was valuable to have a comparable chronosequence to Calvert Island that has the development of a placic horizon since not all Podzols will develop these genetic horizons.

Formation of placic horizons is enhanced in environments where the precipitation greatly exceeds evapotranspiration (Turner et al., 2012a). For example, placic horizons were formed in the Cropp River Basin within 1,500 years with > 10,000mm of MAP (Tonkin and Basher, 2001), whereas placic horizons did not form in Cooloola, southern Norway, or southern Sweden (Thompson, 1981; Mokma et al., 2004; Sauer et al., 2008; Turner et al., 2012a). Interestingly, placic horizons are prevalent in northeastern Taiwan, particularly in

finer soils derived from shale and sandstones in areas with > 3200 mm MAP (Wu and Chen, 2005; Jien et al., 2013). Due to the change in texture between the albic and cambic horizon, Wu and Chen (2005) hypothesized that during storms, water would become perched between these horizons and thus the deposition of Fe occurred with the change in redox potential. The formation rates of cemented horizons were comparable throughout Canada, when MAP, MAT and parent material were considered.

4.5 Conclusion

This study provides a thorough exploration of soil development on Calvert Island within the CWH zone on the longest documented soil chronosequence on the coast of BC. Soil development on the Calvert Island chronosequence was rapid due to the hypermaritime environment and relatively coarse-textured parent material. Within 105 years of development, the forest floor established, an eluvial horizon developed and the pedons were classified as E.DYB compared to the CU.R on the youngest site. It took between 605 and 3,500 years to form a fully mature Podzol with characteristic placic (P.HP) and ortstein (OT.HP) horizons; however, weakly-formed cemented horizons were present at the 605-year-old site. This rate of soil development was comparable to the Cox Bay and Naikoon chronosequences in BC and the Haast chronosequence in New Zealand. There was an increase in amorphous Fe and Al with increasing age, with maximum concentrations of organically-complexed Fe and Al occurring in placic and ortstein horizons. The organo-metal complexation mechanism appeared to be the dominant mechanism involved in podzolization during the first few thousand years of chronosequence development, followed by formation of allophanic materials. The movement of reduced organically-complexed metals also occurred because Fe-cemented horizons (placic) occurred below organic- and/or Al-cemented horizons (ortstein). All soils had relatively low CIA values, suggesting minimal

loss of mobile cations relative to Al from primary minerals, even though the soils had strong morphological features and were classified as mature Podzols after 3,588 years. The hypotheses of this chapter were fulfilled on the Calvert Island chronosequence since mature Podzols formed by 3,588 years with characteristic Podzolic B horizons and strong morphological characteristics. It was also evident that prior to podzolization there was a drastic decline in pH and base cations that allowed for podzolization to progress. Future projects on the Calvert Island chronosequence could investigate the origin of the beige organic horizon and the concept of congruent weathering could be examined using soil pore water and leachate collection and analysis, as well as using scanning electron microscopy to look at the surface of mineral grains .

5 PHOSPHORUS DYNAMICS ACROSS A HOLOCENE CHRONOSEQUENCE, CALVERT ISLAND, BC

5.1 Introduction

Phosphorus (P) is one of the most limiting nutrients to plant growth worldwide along with nitrogen (N), and both are integral to the productive functioning of an ecosystem (Walker and Syers, 1976). It has been widely documented that with increasing soil age, total soil P within the mineral soil declines. The Walker and Syers (1976) P transformation model is the most cited paper regarding soil P decline and the behaviour of different operationally-defined soil P pools with increasing soil age (e.g. Crews et al., 1995; Vitousek and Farrington, 1997; Parfitt et al., 2005). Generally, studies examining how P pools change with age only study the surface organic or upper mineral horizons, limiting the understanding of connections and differences among different horizons within a soil profile. Different soil horizons are influenced by different processes that affect the quantity and forms of P. For instance, the litter horizon (L horizon) receives constant inputs from the overstory that are modified and humified biologically to create the fermentation (F) and humified (H) organic horizons, while the mineral horizons are more influenced by geological processes including mineral sorption and illuviation of organo-metal complexes from the organic horizons (Lundström et al., 2000; Sauer et al., 2007; Sanborn et al., 2011).

Declining P with increasing age has been widely documented on soil chronosequences spanning many climates, parent materials, disturbance regimes and age ranges (Peltzer et al., 2010). Depending on the soil forming factors, each chronosequence may become depleted of P by different mechanisms (Vitousek et al., 2010). Sandy chronosequences, such as Cooloola, Cox Bay and Jurien Bay, have inherently low P parent material, which means that there are low concentrations of P within the rocks or parent

material for weathering and plant uptake (Vitousek et al., 2010; Turner et al., 2012a; Chen et al., 2015; Turner and Laliberté, 2015). Since the total amount of P within low-P parent materials is lower than higher-P parent materials, they can become depletion-driven faster than soils with greater initial P concentrations (Vitousek et al., 2010). Depletion-driven refers to the loss of inorganic and dissolved organic P via weathering and subsequent leaching, which generally takes millions of years but can occur faster with low-P parent materials (Vitousek et al., 2010). Other forms of P limitation may be caused by barriers to root exploration, such as placic horizons, or transactional P limitations caused by the slow release of P from minerals compared to other nutrients (Vitousek et al., 2010). The Walker and Syers (1976) model states that Ca-P forms will be the first P forms to be exploited because they are generally the most abundant P forms in the parent material and are more easily solubilized than other P forms; as soil ages and P becomes scarcer, organic and occluded forms of P will dominate. Occluded P is inorganic or organic P that is tied up within mineral matrices (Walker and Syers, 1976; Crews et al., 1995; McDowell et al., 2007).

To understand the cycling of P within a soil it is necessary to characterize and measure the concentrations of organic P, especially within P-limited systems due to the increasing dominance of organic P with age (Walker and Syers, 1976). Currently, P nuclear magnetic resonance spectroscopy (P-NMR) is the only method able to simultaneously characterize all the forms of organic P within a soil sample (Cade-Menun, 2005). Solution P-NMR is the most common method to characterize soil organic P compared to solid state NMR because paramagnetic ions present within intact samples cause line broadening and decrease the signal-to-noise within spectra. The spin-spin relaxation time (T2) between nuclei in solid samples also decreases the length of time that nuclei can remain excited,

increasing line-broadening (Cade-Menun, 2005). The most commonly used extractant for soil organic P analysis by P-NMR is combined sodium hydroxide (NaOH) and ethylenediaminetetraacetic acid (EDTA; Cade-Menun and Liu, 2014).

Although P dynamics have been extensively studied on soil chronosequences, P-NMR has not been widely applied. Most researchers used fractionation methods such as Chang and Jackson's (1957) modified procedure (Tiessen and Moir, 1993) and the modified Hedley (1982) procedure (McDowell and Condron, 2000) to quantify different pools of P along chronosequences (e.g. Walker and Syers, 1976; Izquierdo et al., 2013; Chen et al., 2015). To date, P-NMR analysis has been performed on soil samples from the Haast, Franz Josef, Västerbotten, Manawatu and Reefton chronosequences (Table 2-1; McDowell et al., 2007; Turner et al., 2007; Vincent et al., 2013; Turner et al., 2014). McDowell et al. (2007) proposed that within mineral horizons, pyrophosphates, diesters (including DNA) and the recalcitrant *myo*- and *scyllo*-IHP would increase with soil age in chronosequences, as shown by Manawatu and Reefton because specific organic P forms including DNA, glucose-6-phosphate (G6P) and IHP strongly sorb onto Fe and Al at low pH onto or within soil peds (Parfitt, 1979; Shang et al., 1990; Celi and Barberis, 2007). Mineral soil on the Franz Josef chronosequence was dominated by DNA that was correlated to OM and to *myo*- and *scyllo*-IHP and other monoesters on the oldest site that were sorbed to amorphous metals (Turner et al., 2007). Whereas on the Haast chronosequence, microbial P compounds dominated the organic horizon, illustrating the importance of microbial cycling of P in the FF (Turner et al., 2014). Phosphorus-NMR can also be performed on foliage samples which can be used to link the forms of P found within the L horizon to the surrounding plant species; however, the

origins of many P compounds remain unknown (Makarov et al., 2002; Makarov et al., 2005; Smernik et al., 2015).

Within the coastal western hemlock (CWH) zone in British Columbia, P is often limiting due to low P parent material and rapid weathering within the temperate, hypermaritime climate (Prescott et al., 1993; Kranabetter et al., 2003; Kranabetter et al., 2013). Many soils in the CWH zone have organic-cemented horizons (Bhc) known as ortstein horizons and Fe- enriched cemented horizons (Bfc) known as placic horizons (Banner et al., 1993; Green and Klinka, 1994). These cemented horizons can impede water flow and can initiate paludification (Ugolini and Mann, 1979; Sanborn et al., 2011; Turner et al., 2012a). A short chronosequence in Cox Bay, within the CWH zone, had a sharp decline in Ca-P within 371 years, associated with rapid podzolization (Singleton and Lavkulich, 1987a, b). Other longer chronosequences such as the Naikoon chronosequence on Graham Island and the Brooks Peninsula chronosequence on Vancouver Island also exhibit rapid podzolization and the development of placic horizons, but P forms in these soils have not been studied in detail (Maxwell, 1997; Sanborn and Massicotte, 2010).

This study aimed to examine how the broad pools of P changed with time on a hypermaritime, Holocene chronosequence within the CWH zone, and to specifically examine how soil organic P compounds varied with increasing age in the organic and mineral soil horizons as well as in dominant foliage species. It was hypothesized that with increasing age, organic P would become an increasingly dominant pool of soil P. An increase in the dominance of DNA was expected in the organic horizons and an increase in *myo*- and *scyllo*-IHP was expected in the mineral horizons based on previous studies (Walker and Syers; 1976; McDowell et al., 2007; Turner et al., 2012a; Turner et al., 2014). Organic P forms

within foliage were also expected to coincide with the forms of organic P within the L horizon since foliage provides a consistent influx of nutrients.

5.2 Methods

5.2.1 Study Area and Site Selection

The chronosequence was located on Calvert Island on the west coast of British Columbia (Figs. 1-4 and 1-5), and was dated by optically stimulated luminescence dating techniques (Neudorf et al., 2015; Table 3-1).

Eight sandy landforms were examined in this study, with ages ranging from a modern established foredune (~0 years old (a BP) to a 10,760 a BP stabilized, relict dune (Table 3-1). Two sampling locations were examined on each sand dune to capture the variability of soil formation within the dune and age. Sampling locations were chosen to best reflect a stable landscape position. Any deviations from these criteria were noted and can be found in Appendix 2.

5.2.2 Sample Collection and Preparation

Soil sampling was completed in accordance with the Canadian System of Soil Classification (SCWG, 1998), which was used to classify and sample the soil genetic horizons. Details of the specific methods related to soil classification can be found in Chapter Four. Two soil samples were taken from each genetic horizon; one sample was air-dried and used for basic chemical analysis and one that was immediately dried at 60˚C until constant weight for P-NMR analysis to prevent hydrolysis and degradation of P compounds (Cade-Menun, 2005; McDowell et al., 2007). All dried soil samples were sieved to < 2 mm. For cemented horizons, a mortar and pestle was used to disaggregate the sample and a coffee grinder was used to grind organic samples.

Bulk density or mass per area measurements were taken in each soil horizon when possible and were used to calculate the mass of certain elements per a set depth of soil profile. Bulk density samples were sealed in plastic bags in the field, and then oven-dried in the lab at 105 ˚C to constant weight. Detailed methods determining soil mass can be found in Chapter Four.

To examine P forms in surrounding plants, foliage was collected from the three most dominant tree or shrub species in a 5-m radius plot around each soil pit using an adapted Ballard and Carter (1986) method. Foliage samples were pruned off by hand when possible and intact, green foliage was retrieved off the ground if hand sampling was not feasible. All foliage samples were dried at 60˚C until constant weight. Dried foliage samples were ground using a coffee grinder and were stored individually in Ziploc bags prior to analysis.

Foliage samples were grouped by average total P concentration with group 1 consisting of the 105 and 139 a BP sites (CIDS3 and CIDS4), group 2 consisted of sites spanning 605 to 4,198 a BP (CIDS8, CIDS9 and CIDS15) and group 3 consisted of sites spanning 7,236 to 10,760 a BP (CIDS16 and CIDS10). To examine trends in foliage with increasing age, two tree species that spanned all age classes, except for the recent dune, were analysed in composited samples created with equal weights of each dried sample at the laboratory in the Agriculture & Agri-Food Swift Current Research and Development Centre. Western hemlock (*Tsuga heterophylla*; Hw) was present on 13 of the 16 sites and western redcedar (*Thuja plicata*; Cw) was present on 6 of the 16 sites.

5.2.3 Total, Organic and Mehlich-3 Phosphorus Analysis

Samples for soil characterization were sent to the Analytical Chemistry Laboratory of the BC Ministry of Environment in June 2016. Total organic P was determined using the ignition method with 0.5M sulfuric acid and analysed colorimetrically using a Cary-60

UV/vis spectrophotometer (Saunders and Williams, 1955; Walker and Adams, 1958; O'Halloran and Cade-Menun, 2008). The Mehlich-3 method was used to extract exchangeable nutrients including P, Na, K, Ca, Mg, Cu, Zn, Mn and Fe, and the extracts were analysed on a Teledyne Leeman Labs Prodigy dual-view inductively coupled plasma-optical emission spectrophotometer (ICP-OES) with a sea spray nebulizer (Mehlich, 1984; Kalra and Maynard, 1991). Closed-vessel microwave acid digestion with ICP-atomic emission spectrophotometry (ICP-AES) was used for total P analysis on the organic samples (Kalra and Maynard, 1991); high temperature fusion with lithium metaborate/lithium bromide using a Claisse M4 Fluxer followed by ICP-OES was used to analyse total P on the mineral samples (Claisse, 2003).

Foliage and L horizon samples were analysed at the Swift Current Research and Development Centre in autumn, 2016. Organic P was determined using the ignition method and total P was determined using the Parkinson-Allen digestion method (1975) for both foliage and L horizon samples. All extracts were analysed for molybdate-reactive P (MRP) using the Murphy and Riley (1962) colorimetric method.

5.2.4 Phosphorus NMR

5.2.4.1 Extraction

Previous analysis (Cade-Menun, pers. comm., 2016) indicated that there was very little organic P within non-organic-enriched horizons in samples from these sites, so only a subset of samples were analysed with P-NMR. From each replicate plot, L, H and organic-enriched mineral horizons were analysed, as well as the composited foliage samples. Different masses of each sample type were extracted because of differences in P and organic matter concentrations. For the L horizon and foliage samples, 1 g (dry weight) was used, whereas 3 g was used for H horizons and 10 g was used for mineral samples. Each sample

was placed in a 50-mL sample tube with 30-mL of 0.5 M NaOH + 0.1 M Na_2EDTA and shaken for 4 hours in the dark at ~20C. Next, the samples were centrifuged for 15 minutes at 12,000 x *g*. A 1-mL subsample of the supernant was diluted (1:10) with DI water for total P analysis and was analysed using ICP-OES to determine the concentrations of P, Al, Ca, Fe, Mg, and Mn in extracts. The remaining supernants were filtered through Whatman 42 in a Buchner funnel to remove OM from the sample, washing with DI. The filtrates were placed in clean 50-mL centrifuge tubes, frozen, and then lyophilized until dry (~3 days).

The freeze-dried extracts of the H horizon and mineral soil samples were sent to the Stanford Magnetic Resonance Laboratory (SMRL) at Stanford University in July 2016 for NMR analysis by Dr. Corey Liu. The L horizon and composited foliage samples were analysed in the fall of 2016 at the Saskatchewan Structural Sciences Centre (SSSC) at the University of Saskatoon by Dr. Barbara Cade-Menun from the Agriculture & Agri-Food Swift Current Research and Development Centre.

5.2.4.2 NMR Analysis

At SMRL, the freeze-dried extracts were prepared for P-NMR analysis by adding 0.5 – 1.5 ml of D_2O, 0.5 ml H_2O, 0.5 – 4.0 ml of NaOH-EDTA extracting solution and 0.5 – 1.0 mL of 10 M NaOH to increase the sample pH above 12 (Cade-Menun, 2005; Cade-Menun and Liu, 2014). Samples were centrifuged at 3260 x *g* for 5 minutes. The spectra were obtained on a Varian Inova 600-MHz spectrometer (202.5 MHz for P) with a 10-mm broad band probe. The NMR parameters were: 45˚ (0.22-µs) pulse, 4.5-s pulse delay, 0.5-s acquisition time, 20˚C, and no proton decoupling. Sample LAN30 (7,236 a BP; CIDS16B, Bhc horizon) was very viscous and had a very low paramagnetic ion (Fe, Mn) content so a 9.5 s pulse delay was used on this sample only. To optimize spectral resolution and the

signal-to-noise ratio (S/N), the first few samples were run for longer periods of time in 4-hour blocks to understand the samples and achieve the best S/N with minimal degradation. Total NMR analysis for the H and mineral horizon samples ranged from 8 – 16 h, to achieve an acceptable S/N, which varied with sample factors such as concentrations of P, Fe and Mn, and viscosity from OM.

At the University of Saskatchewan, the freeze-dried supernants of the L horizon and foliage samples were prepared by adding 0.6 ml of D_2O, H_2O and the NaOH-EDTA extracting solution, as well as 0.4 mL of 10 M NaOH to increase the sample pH above 12. Some samples were very viscous so an additional 0.4 mL each of D_2O and NaOH-EDTA extracting solution were added to LN20 (Cw-G1), LN2 (~0 a BP; CIDS1B, thatch), LN5 (139 a BP; CIDS4A, L), LN7 (3,588 a BP; CIDS8A, L), LN9 (605 a BP; CIDS4B, Hh), LN16 (10,760 a BP; CIDS10B, L), LN23 (7,236 a BP; CIDS15A, Hh) and LN24 (7,236 a BP; CIDS15A, Bhc). Sample LN2 formed a precipitate after preparation so the sample was diluted with water to filter the precipitate out. All samples were centrifuged at 3260 x *g* for 5 minutes. Spectra were obtained on a Bruker Avance 500 MHz spectrometer (202.5 MHz for P) with a 10-mm broadband probe. The NMR parameters were: 45˚ (0.13-μs) pulse, 4.5-s pulse delay, 0.5-s acquisition time, 21˚C, and no proton decoupling. Analysis times ranged from 4 – 8 hours. The pulse widths at SMRL and the SSSC were measured and subsequently adjusted for the individual instruments, resulting in small differences; however, the parameters are comparable.

During sample analysis at both SMRL and SSSC, selected samples were spiked with different reference compounds after initial NMR analysis, to confirm peak identifications within the monoester region. The chemical shifts of compounds were slightly different for

each sample type (L vs. H vs. mineral horizons), so a few samples of each sample type were spiked. Spiking compounds included: *myo*-IHP, adenosine monophosphate (AMP), α- and β-glycerophosphate, glucose-1-phosphate, G6P, and phosphocholine, all dissolved in NaOH-EDTA, as described in Cade-Menun (2015). At SMRL, six samples were spiked; eight samples were spiked at the SSSC.

5.2.4.3 Processing and Peak Interpretation

Spectra were processed using NMR Utility Transform Software (NUTS, Acorn NMR, Livermore, CA, 2000 edition). The integral trace of each spectrum was manually manipulated for baseline correction. The orthophosphate peak was easily identified in all spectra for every sample type, so it was used to standardize the spectra by adjusting its chemical shift to 6.000 ppm in all samples.

The entire spectrum for each sample (30 to -30 ppm) was first analysed using 7 Hz line broadening, and areas for the broad groupings of phosphonates (30 to 7 ppm), monoesters plus orthophosphate (7 to 2.5 ppm), diesters (2.5 to -4.4 ppm), and polyphosphates (-4.4 to -30 ppm) were calculated. Each broad grouping was further analysed with 2 Hz line broadening to display the peaks in more detail. There was no indication that there were any P compounds outside the 30 and -30 ppm; thus, the areas of peaks for the P compounds within the spectral window added up to 100% of the extracted P. Concentrations of P compounds were determined by multiplying the percentage of each P compound by the concentration of P extracted by NaOH-EDTA. Peak assignments were determined using spiking and published literature (Doolette et al., 2009; Cade-Menun, 2015). Peaks in the spectra were grouped into inorganic and organic forms. Inorganic P included orthophosphate, pyrophosphate and total polyphosphates; the rest were considered to be organic P.

Some monoesters are the result of alkaline hydrolysis of RNA and phospholipids during NMR analysis (Makarov et al., 2002; Turner et al., 2003b), which can overestimate the concentration of monoesters in the original soil prior to extraction and analysis. Glycerophosphates are degradation products of phospholipids and AMP is a degradation product of RNA (Makarov et al., 2002; Turner et al., 2003b; Doolette et al., 2009; Cade-Menun, 2015). Therefore, monoester and diester concentrations were corrected by adding the concentrations of α- and β-glycerophosphates, and AMP to the total diester concentration, and subtracting them from the total monoester concentration.

5.2.5 Data Analysis

Data were analysed with STATA 14 IC. Linear and non-linear regression analysis was performed on the mass of total P and organic P to a 1 m depth. The following models were used to examine the data: linear, second order polynomial, Michaelis-Menton, logarithmic and exponential models (decay or increase). Akaike's information criteria were used to determine which model fit best (Gotelli and Ellison, 2004). To examine variability within a dune, the standard deviation was used.

Some P compounds (e.g. IHP and DNA) became increasingly dominant with age within the soil samples; thus, parametric pair-wise correlations and non-parametric Spearman correlations were used to test the relationship with other soil parameters. The Shapiro-Wilk normality test and visual examination of box plots using Stata 14 IC, for each horizon type (α=0.05) were also performed. Only parameters known to correlate with the concentration of IHP and DNA were analysed using correlation analysis (Turner et al., 2007; 2014).

5.3 Results

5.3.1 Soil Mass Phosphorus (Total and Organic)

The average mass of total P declined linearly with age, while organic P displayed a hump-shaped curve that peaked around 4,000 years (Fig. 3-1). The variability of total P was greatest on the youngest sites, (~0 y; SD = 39 mg kg^{-1}; 105 y; SD = 32 mg kg^{-1}). The lowest within-dune variabilities for total P were on intermediate-aged sites (3,588 y; SD = 4 mg kg^{-1}; 4,198 y; SD = 7 mg kg^{-1}; Fig. 5-1).

Multiple exponential models and one linear model were applied to the total organic P mass data and the best fitting second-order exponential equation was chosen (Fig. 5-1). The within-dune variability for organic P mass was greatest after 3,588 a BP (SD = 17 mg kg^{-1}) and ~0 a BP (SD = 11 mg kg^{-1}) and lowest after 605 a BP (SD = 1 mg kg^{-1}) and 7,236 a BP (SD = 1 mg kg^{-1}).

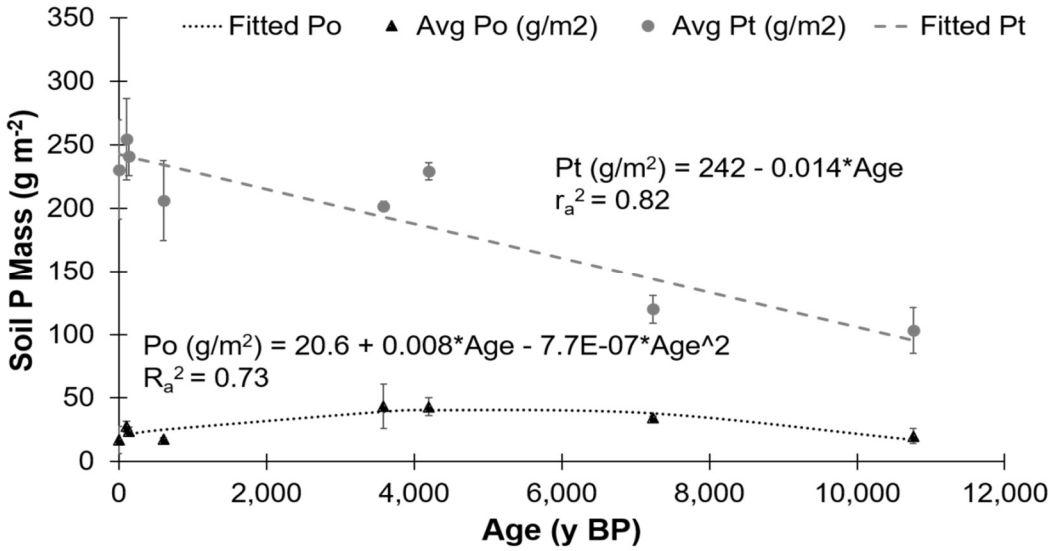

Figure 5-1. Average mass of total and organic phosphorus (P) to a 1 m depth with the associated linear and non-linear regression formula, respectively, and associated r-value (n=8). Total P (Pt) was determined by acid digestion for organic samples and fusion for mineral samples (Kalra and Maynard, 1991; Claisse, 2003). Organic P (Po) was determined by the ignition method (Saunder and Williams, 1955). Note: standard deviation indicated by error bars (n=2).

5.3.2 Mehlich-3 Extractable Elements

The L horizon had the greatest extractable P via the Mehlich-3 method followed by the H horizon with the lowest concentration of extractable P within the mineral horizons (Fig. 5-2; Mehlich, 1984). With increasing age, the Mehlich-extractable P concentration and standard deviation declined in all sample types (Fig. 5-2).

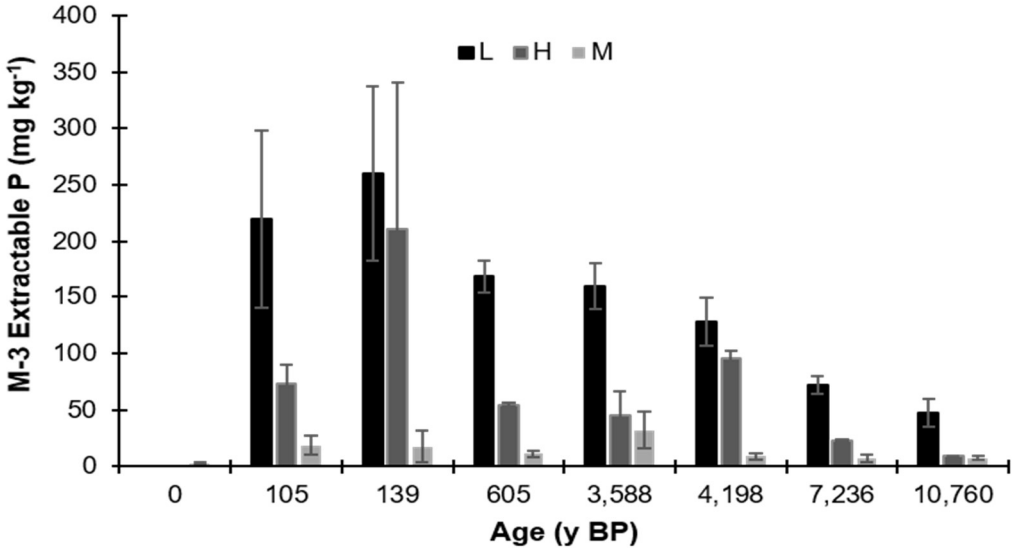

Figure 5-2. Average Mehlich-3 extractable phosphorus (M-3 Extractable P) concentration within the select litter (L), humic-enriched organic (H) and mineral horizon (M) samples used for P-NMR analysis (Mehlich, 1984). Note: standard deviation indicated by error bars (n=2).

The average sum of Ca+Mg extracted by Mehlich-3 within the L horizon remained relatively stable with age, exhibiting only a slight decline in the sum of cations with increasing age (Fig. 5-3a). The H horizon samples maintained a stable concentration of Ca+Mg until ~4,200 years followed by a decline (Fig. 5-3a). There was a drastic decline in Ca+Mg in the mineral horizon samples between 0 and 105 years (Fig. 5-3a). The L horizon had the greatest concentration of Ca+Mg followed by the H horizon and then the mineral horizon (Fig. 5-3a).

Conversely, the mineral horizons had the greatest Fe+Al concentration followed by the H horizon and then the L horizon (Fig. 5-3b). The L and H horizons had a slight increase in Fe+Al with age compared to a much larger increase with age in the mineral horizon (Fig. 5-3b). Within the mineral horizons, Fe+Al concentration peaked around 4,000 years (Fig. 5-3b). The H horizon after 7,236 a BP had an unusually high Fe+Al concentration that was not consistent with other H horizon samples (Fig. 5-3b).

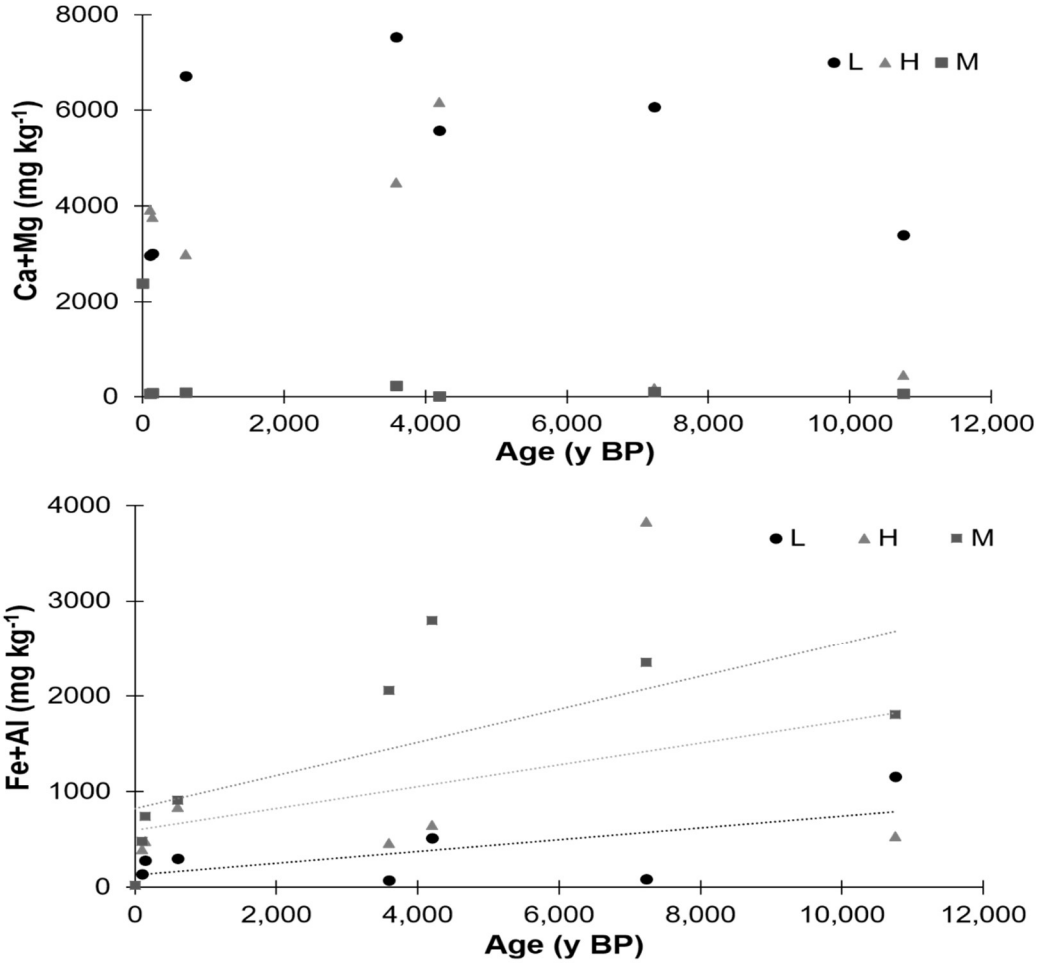

Figure 5-3. Average Mehlich-3 extractable calcium (Ca) + magnesium (Mg) (a) and iron (Fe) + aluminum (Al) (b) concentration within the select litter (L), humic-enriched organic (H) and mineral horizon (M) samples used for P-NMR analysis (n=2) (Mehlich, 1984).

5.3.3 Phosphorus Recovery in NaOH-EDTA Extracts

Foliage samples of Hw and Cw had the highest P recovery rates (> 79%) with NaOH-EDTA while Salal had a slightly lower recovery rate (> 66%; Table 5-1). The L horizon

samples extracted with NaOH-EDTA also had high recovery of total P (> 73%) compared to the H (29 - 66%) and mineral horizons (10- 53%; Table 5-1). The recovery rate for the L horizon remained consistent across all ages (73 - 88%; Table 5-1). The youngest site was not forested, so thatch, a loose organic horizon found in grassy areas, was used instead of an L horizon sample.

The recovery of total P in the H horizon was significantly less than in the L horizon, with the lowest recoveries after 105 a BP (29%) and 3,588 a BP (31%; Table 5-1). All other sites had recovery rates between 42 and 66% for total P within the H horizon (Table 5-1).

Although total P within the mineral horizon declined with increasing age, the recovery of P within NaOH-EDTA extracts increased (Table 5-1). The lowest total P recovery for mineral samples was on the youngest sites, ~0 and 105 a BP with 10 and 12% recoveries, respectively. The highest recovery of total P was on the oldest site, 10,760 a BP, with a 53% recovery (Table 5-1).

Interestingly the recovery of organic P within the NaOH-EDTA extract, determined by adding all organic forms of P identified within the P-NMR spectra together, was greatest in the mineral horizons with recoveries ranging from 39 (105 a BP) to 169% (139 a BP; Table 5-1). The recovery of organic P within the L horizon was greatest after 105 a BP (72%) and lowest after 7,236 a BP (28%) illustrating a decline of organic P recovery with age. The H horizon recovery rates for organic P were between 16 (3,588 a BP) and 47% (7,236 a BP; Table 5-1).

Table 5-1. Average total (Pt) and organic P (Po) concentrations within select soil horizons (litter (L), humic-enriched organic (H) and mineral (M) horizons) and composite foliage samples (western hemlock (Hw), western redcedar (Cw), and Salal), determined by acid digestion (Kalra and Maynard, 1991) or fusion methods (Claisse, 2003) for Pt and the ignition method for Po (Saunders and Williams, 1955), and the recovery rate within the NaOH-EDTA extracts. Total P within the NaOH-EDTA extract was determined by ICP-OES and Po was calculated by summing all organic forms of P identified within the P-NMR spectra together. Note: one standard deviation is within the brackets.

Horizon/ Species	Age (a BP)	Site	Pt (mg kg^{-1})	Po (mg kg^{-1})	P Recovery in NaOH-EDTA (%)	
					Pt	Po
L	0	CIDS1	586 (81)	-	73 (1)	-
L	105	CIDS3	857 (57)	531 (112)	88 (5)	72 (5)
L	139	CIDS4	561 (91)	448 (23)	81 (3)	50 (0)
L	605	CIDS9	836 (163)	548 (29)	83 (2)	60 (20)
L	3,588	CIDS8	481 (18)	432 (65)	75 (7)	37 (7)
L	4,198	CIDS15	449 (30)	388 (52)	78 (2)	46 (6)
L	7,236	CIDS16	252 (21)	426 (45)	76 (8)	28 (2)
L	10,760	CIDS10	179 (43)	229 (34)	76 (3)	33 (6)
H	0	CIDS1	-	-	-	-
H	105	CIDS3	632 (96)	440 (42)	29 (6)	19 (1)
H	139	CIDS4	827 (204)	439 (14)	49 (8)	28 (7)
H	605	CIDS9	359 (237)	272 (161)	66 (37)	42 (23)
H	3,588	CIDS8	263 (19)	188 (8)	31 (11)	16 (4)
H	4,198	CIDS15	777 (56)	522 (33)	42 (0)	19 (3)
H	7,236	CIDS16	331 (126)	281 (95)	48 (29)	47 (29)
H	10,760	CIDS10	187 (83)	135 (54)	42 (1)	35 (11)
M	0	CIDS1	234 (5)	17 (18)	10 (5)	94 (62)
M	105	CIDS3	291 (2)	25 (1)	12 (4)	39 (4)
M	139	CIDS4	148 (8)	14 (12)	26 (3)	169 (123)
M	605	CIDS9	182 (88)	20 (7)	32 (28)	147 (57)
M	3,588	CIDS8	250 (6)	73 (24)	33 (5)	87 (14)
M	4,198	CIDS15	165 (12)	65 (24)	42 (5)	97 (27)
M	7,236	CIDS16	167 (18)	35 (5)	34 (1)	126 (9)
M	10,760	CIDS10	115 (16)	40 (24)	53 (31)	139 (15)
Hw	0-139	G1	1266	-	97	-
Hw	605-4,198	G2	1003	-	104	-
Hw	7,236-10,760	G3	515	-	84	-
Cw	0-139	G1	1406	-	92	-
Cw	605-4,198	G2	916	-	79	-
Cw	7,236-10,760	G3	521	-	86	-

Horizon/ Species	Age (a BP)	Site	Pt (mg kg^{-1})	Po (mg kg^{-1})	P Recovery in NaOH-EDTA (%)	
					Pt	Po
Salal	3,588	CIDS8A	929	-	73	-
Salal	3,588	CIDS8A	977	-	66	-
Salal	4,198	CIDS15B	782	-	68	-

5.3.4 Chemical Shifts

The chemical shifts of peaks within the L horizon and foliage samples, H horizons and mineral horizons varied slightly within the different sample types (Tables 5-2 to 5-4). The chemical shifts of peaks in the L horizon and foliage samples were most comparable to the mineral horizon samples while the chemical shifts of peaks in the H horizon samples, except pyrophosphate, were generally downfield of the other sample types. For the unknown peak at 5 ppm and DNA, the H horizon samples had the most downfield chemical shift followed by the L horizon and foliage samples and lastly, the mineral horizons (Tables 5-2 to 5-4).

For the broader compound classes (i.e. phosphonates and monoester 1), the standard deviation for chemical shifts was greater than for better-defined compounds (i.e. *myo*-IHP and DNA; Tables 5-2 to 5-4). Within the broader compound classes, the mineral horizons had higher standard deviations for an individual peak compared to the L horizon and foliage, and H horizon samples (Tables 5-2 to 5-4).

Table 5-2. Chemical shifts of peaks detected in ^{31}P-NMR spectra for litter horizon and foliage samples, present in thirteen or more of the 25 samples.

Category	P Form or Compound Class	Chemical Shift (ppm)
Inorganic P		
	Orthophosphate	6.00 ± 0.00
	Pyrophosphate	-4.41 ± 0.14
	Polyphosphates	-4.19 ± 0.08, -4.79 ± 0.21, -5.27 ± 0.33, -7.37 ± 0.38, -13.11 ± 0.51, -17.07 ± 0.65, -18.58 ± 0.38, -20.25 ± 0.47, -22.08 ± 0.66, -24.28 ± 0.67, -26.13 ± 0.62, -27.78 ± 0.45
Organic P		
	Phosphonates	28.39 ± 0.41, 27.30 ± 0.46, 26.39 ± 0.57, 24.36 ± 0.70, 20.72 ± 0.68, 18.04 ± 0.56, 16.28 ± 0.77, 14.81 ± 0.81, 8.43 ± 0.33
Orthophosphate Monoesters		
	myo-IHP	5.62 ± 0.07, 4.68 ± 0.07, 4.24 ± 0.09, 4.17 ± 0.09
	scyllo-IHP	3.81 ± 0.10
	neo-IHP	6.49 ± 0.09, 4.35 ± 0.07
	D-*chiro*-IHP 4e/2a	6.67 ± 0.10, 5.41 ± 0.14, 4.07 ± 0.10
	D-*chiro*-IHP 4a/2e	6.30 ± 0.08, 4.85 ± 0.08, 4.41 ± 0.07
	Unknown	5.14 ± 0.06
	Glucose 6-phosphate	5.30 ± 0.06
	α-glycerophosphate	4.97 ± 0.06
	ß-glycerophosphate	4.62 ± 0.07
	Mononucleotides	4.52 ± 0.07, 4.45 ± 0.04, 4.38 ± 0.03, 4.33 ± 0.03
	Choline phosphate	3.93 ± 0.09
	Monoester 1	6.89 ± 0.06, 6.75 ± 0.07, 6.22 ± 0.03, 6.16 ± 0.02
	Monoester 2	5.89 ± 0.02, 5.80 ± 0.03, 5.72 ± 0.03, 5.46 ± 0.06, 5.07 ± 0.05, 4.75 ± 0.03
	Monoester 3	3.65 ± 0.05, 3.44 ± 0.04, 3.29 ± 0.06, 3.14 ± 0.07, 2.95 ± 0.06, 2.80 ± 0.05, 2.59 ± 0.05
Orthophosphate Diesters		
	Other Diester 1	2.47 ± 0.04, 2.30 ± 0.06, 2.03 ± 0.08, 1.61 ± 0.07, 1.45 ± 0.05, 1.02 ± 0.12, 0.60 ± 0.08, 0.41 ± 0.07, 0.07 ± 0.07, -0.17 ± 0.10, -0.34 ± 0.09
	DNA	-0.49 ± 0.11, -0.75 ± 0.11
	Other Diester 2	-0.95 ± 0.09, -1.13 ± 0.09, -1.59 ± 0.07, -1.80 ± 0.05, -2.12 ± 0.13, -3.05 ± 0.09

Table 5-3. Chemical shifts of peaks detected in ^{31}P-NMR spectra for the H horizon samples, present in seven or more of the 14 samples.

Category	P Form or Compound Class	Chemical Shift (ppm)
Inorganic P		
	Orthophosphate	6.00 ± 0.00
	Pyrophosphate	-4.31 ± 0.20
	Polyphosphates	-4.00 ± 0.13, -7.25 ± 0.40, -9.28 ± 0.66, -14.08 ± 0.56, -19.22 ± 0.23, -20.61 ± 0.18, -27.72 ± 0.70
Organic P		
	Phosphonates	31.70 ± 0.58, 28.07 ± 0.71, 20.56 ± 0.52, 19.55 ± 0.38, 18.80 ± 0.28, 12.06 ± 0.34
Orthophosphate Monoesters		
	myo-IHP	5.69 ± 0.08, 4.74 ± 0.09, 4.36 ± 0.09, 4.27 ± 0.08
	scyllo-IHP	3.91 ± 0.07
	neo-IHP	6.58 ± 0.07, 4.45 ± 0.09
	D-*chiro*-IHP 4e/2a	6.76 ± 0.07, 5.51 ± 0.09, 4.16 ± 0.07
	D-*chiro*-IHP 4a/2e	6.38 ± 0.07, 4.93 ± 0.08, 4.52 ± 0.09
	Unknown	5.24 ± 0.08
	Glucose 6-phosphate	5.41 ± 0.10
	α-glycerophosphate	5.06 ± 0.10
	ß-glycerophosphate	4.69 ± 0.08
	Mononucleotides	4.62 ± 0.07, 4.54 ± 0.04, 4.48 ± 0.04, 4.42 ± 0.02
	Choline phosphate	4.05 ± 0.08
	Monoester 1	6.94± 0.05, 6.19 ± 0.04, 6.09 ± 0.02, 6.42 ± 0.06
	Monoester 2	5.89 ± 0.04, 5.72 ± 0.12, 5.16 ± 0.04, 4.77 ± 0.03, 5.31 ± 0.12
	Monoester 3	3.76 ± 0.07, 3.40 ± 0.07, 2.73 ± 0.10, 3.00 ± 0.08
Orthophosphate Diesters		
	Other Diester 1	1.74 ± 0.11, 1.42 ± 0.14, 1.10 ± 0.15, 0.67 ± 0.08, 0.41 ± 0.05, 0.27 ± 0.07
	DNA	-0.39 ± 0.10, -0.69 ± 0.11
	Other Diester 2	-1.07 ± 0.11, -1.40 ± 0.11, -1.66 ± 0.08, -1.97 ± 0.11, -2.24 ± 0.13

Table 5-4. Chemical shifts of peaks detected in ^{31}P-NMR spectra for mineral soil horizons, present in eight or more of the 16 samples.

Category	P Form or Compound Class	Chemical Shift (ppm)
Inorganic P		
	Orthophosphate	6.00 ± 0.00
	Pyrophosphate	-4.10 ± 0.33
	Polyphosphates	-3.86 ± 0.32, -4.22 ± 0.13, -5.46 ± 0.93, -7.41 ± 0.56, -9.45 ± 0.65, -11.06 ± 0.77, -14.09± 0.68, -17.60 ± 0.60, -19.98 ± 0.75, -22.29 ± 0.49, -23.14 ± 0.35, -24.65 ± 0.30, -26.00 ± 0.62, -29.58 ± 0.68, -31.92 ± 0.94
Organic P		
	Phosphonates	33.67 ± 0.70, 32.13 ± 0.88, 28.88 ± 0.70, 26.73 ± 0.58, 24.85 ± 0.80, 21.50 ± 0.58, 20.15 ± 0.51, 19.01 ± 0.29, 12.85 ± 0.59
Orthophosphate Monoesters		
	myo-IHP	5.64 ± 0.16, 4.66 ± 0.17, 4.27 ± 0.19, 4.18 ± 0.18
	scyllo-IHP	3.81 ± 0.18
	neo-IHP	6.53 ± 0.18, 4.39 ± 0.19
	D-*chiro*-IHP 4e/2a	6.67 ± 0.17, 5.42 ± 0.18, 4.09 ± 0.18
	D-*chiro*-IHP 4a/2e	6.32 ± 0.16, 4.84 ± 0.18, 4.44 ± 0.18
	Unknown	5.07 ± 0.13
	Glucose 6-phosphate	5.33 ± 0.17
	α-glycerophosphate	4.96 ± 0.18
	ß-glycerophosphate	4.60 ± 0.18
	Mononucleotides	4.66 ± 0.09, 4.49 ± 0.17, 4.41 ± 0.20, 4.26 ± 0.19
	Choline phosphate	3.95 ± 0.20
	Monoester 1	6.89 ± 0.16, 6.43 ± 0.26, 6.19 ± 0.15
	Monoester 2	5.86 ± 0.04, 5.75 ± 0.11, 5.47 ± 0.17, 5.23 ± 0.12, 5.01 ± 0.17, 4.81 ± 0.14
	Monoester 3	3.72 ± 0.15, 3.58 ± 0.12, 3.35 ± 0.13, 3.15 ± 0.09, 2.93 ± 0.11, 2.65 ± 0.11
Orthophosphate Diesters		
	Other Diester 1	2.33 ± 0.09, 2.04 ± 0.11, 1.66 ± 0.18, 1.31 ± 0.15, 1.03 ± 0.10, 0.65 ± 0.23, 0.42 ± 0.20, 0.13 ± 0.20, -0.33 ± 0.25
	DNA	-0.54 ± 0.27, -0.83 ± 0.22
	Other Diester 2	-1.33 ± 0.19, -1.44 ± 0.20, -1.82 ± 0.26, -2.28 ± 0.24, -2.61 ± 0.12, -3.09± 0.18, -3.55 ± 0.16

5.3.5 Phosphorus-NMR Results in Foliage and Soil Horizons

With increasing age, the proportion of orthophosphate declined in both Hw and Cw species, while corrected diesters, corrected monoesters, total polyphosphates, and phosphonates increased in proportion (Fig. 5-4a). All salal samples were within a single age grouping and were used to determine the forms of P within salal and compare them to those in Hw and Cw. The salal in age group 2 had a moderate proportion of orthophosphate and corrected diesters, followed by corrected monoesters, total polyphosphates and phosphonates (Fig. 5-4a). For both Hw and Cw, the concentration of all forms of P declined with increasing age, with the most significant decline in orthophosphate while corrected diesters and monoesters maintained an appreciable concentration (Fig. 5-4b).

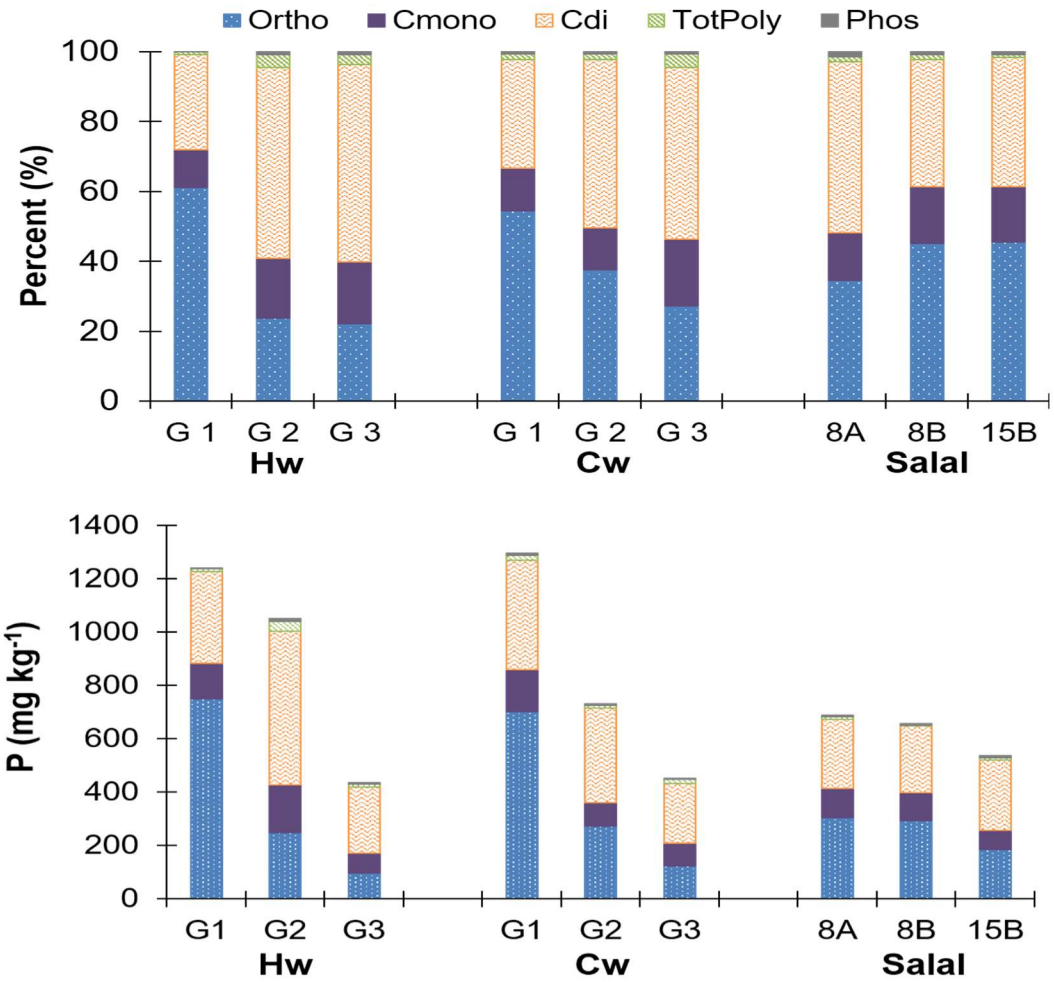

Figure 5-4. Proportion (a) and concentration (b) of total phosphorus (P) of main P compounds within NaOH-EDTA extracts examined using P-NMR of three foliage species western hemlock (Hw), western redcedar (Cw) and salal by age groupings (G1, G2, G3) or by site (CIDS8A (3,588 a BP), 8B (3,588 a BP), 15B (4,198 a BP)). Abbreviations are as follows; orthophosphate (ortho), corrected orthophosphate diesters (Cdi), corrected orthophosphate monoesters (Cmono), total polyphosphates (totPoly) and phosphonates (phos). Age groupings were made based on soil total P concentrations with G1 representing ages 105 – 139 years, G2 representing 605 – 4,198 years and G3 representing 7,236 to 10,760 years.

Proportions and concentrations of broad P compound classes (e.g. phosphonates, polyphosphates) within the L horizon varied less than in the H and mineral horizons (Figs. 5-5 to 5-7). The proportion of total corrected monoesters in the L horizon remained similar throughout the chronosequence, ranging from 15.5% (3,588 a BP) to 18.6% (4,198 a BP) of extracted total P (Fig. 5-5a). The proportion of corrected diesters increased with increasing

age in the L horizon, with 24.7% of extracted P as corrected diesters on the youngest site (~0 a BP) to 37.6% of total P on the oldest site (10,760 a BP; Fig. 5-5a). The proportions of orthophosphate and total polyphosphates were variable with increasing age in the L horizon and slightly declined with age, whereas the proportion of phosphonates was constant with age, ranging from 0.7 to 0.8% of extracted P (Fig. 5-5a).

In the L horizon, the concentration of all P compound classes of extracted P declined with increasing age (Fig. 5-5b). There was an apparent shift in the dominance of different P compounds with age in the L horizon. On the youngest site with thatch rather than L horizon, orthophosphate dominated followed by total polyphosphates > corrected diesters > corrected monoesters > phosphonates (Fig. 5-5). Within the first 100 years, corrected diesters became the most dominant form of P followed by orthophosphate > total polyphosphates > corrected monoesters > phosphonates (Fig. 5-5). By 10,000 years, corrected diesters and orthophosphate still dominated but the proportion of corrected monoesters increased while total polyphosphates declined (Fig. 5-5).

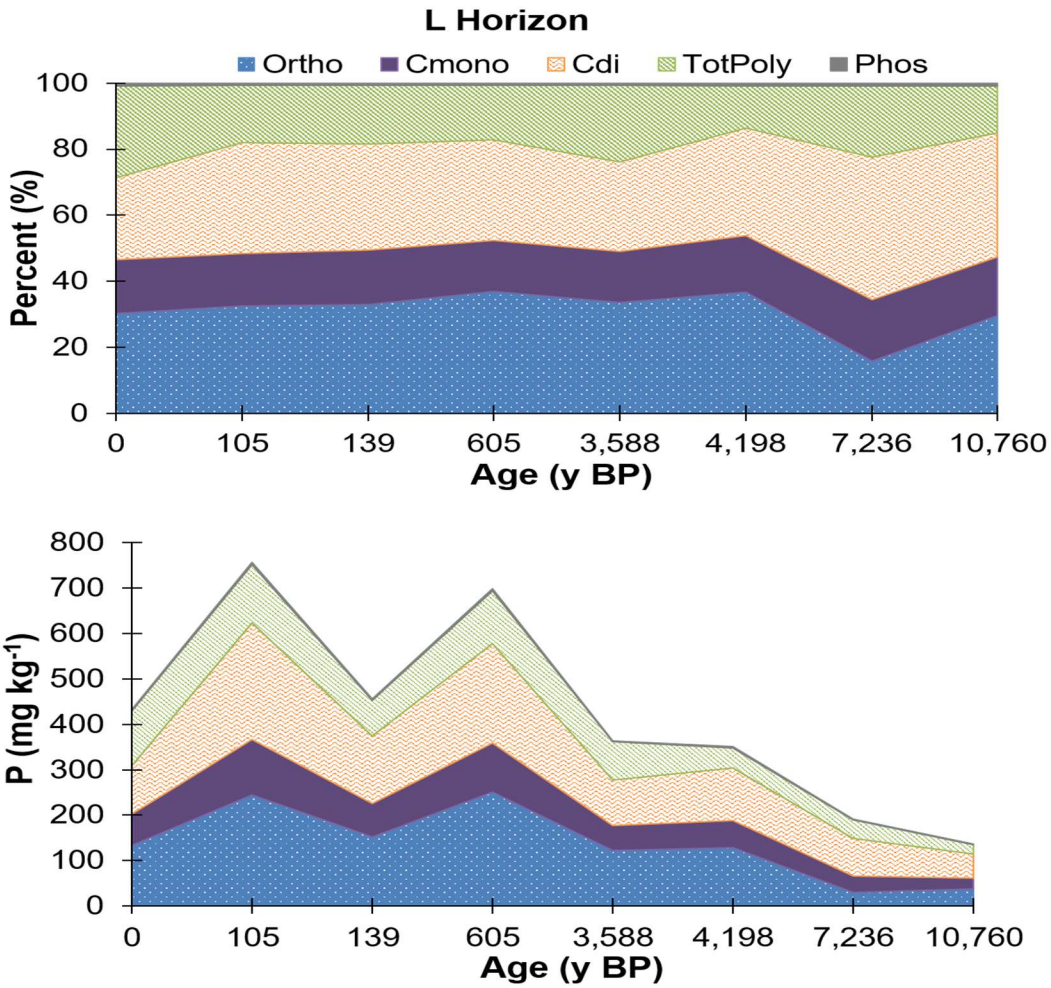

Figure 5-5. Average proportion (a) and concentration (b) of P with NaOH-EDTA extracts examined using P-NMR for the main groupings of P compounds in the litter soil horizon (L): corrected orthophosphate diesters (Cdi), corrected orthophosphate monoesters (Cmono), orthophosphate (ortho), total polyphosphates (totPoly) and phosphonates (phos) (n=2).

Within the H horizons, orthophosphate represented a considerable portion of the extracted P on all sites up until ~7000 years, and then declined (Fig. 5-6). Sites aged 139 a BP and 4,198 a BP had the greatest proportion of orthophosphate (ortho = 61% and 55%, respectively) compared to all other sites (Fig. 5-6a). The lowest proportions of orthophosphate were on sites aged 7,236 a BP and 10,760 a BP (ortho = 9% and 22%, respectively; Fig. 5-6a). The concentration of orthophosphate also declined with increased age (Fig. 5-6b). Corrected monoesters and diesters, in H horizon samples, increased in proportion and concentration with increasing age (Fig. 5-6). Within the H horizon, the

proportion of phosphonates did not vary with increasing age; however, they did not constitute a large portion of the extracted P (2.2 - 4.6%; Fig. 5-6). There was no obvious trend in the proportion of total polyphosphate within the H horizon samples, with the lowest proportion of total polyphosphates after 139 a BP (9%) and 7,236 a BP (6%; Fig. 5-6a). The concentrations of phosphonates and total polyphosphates did decline with increasing age in H horizon samples (Fig. 5-6b).

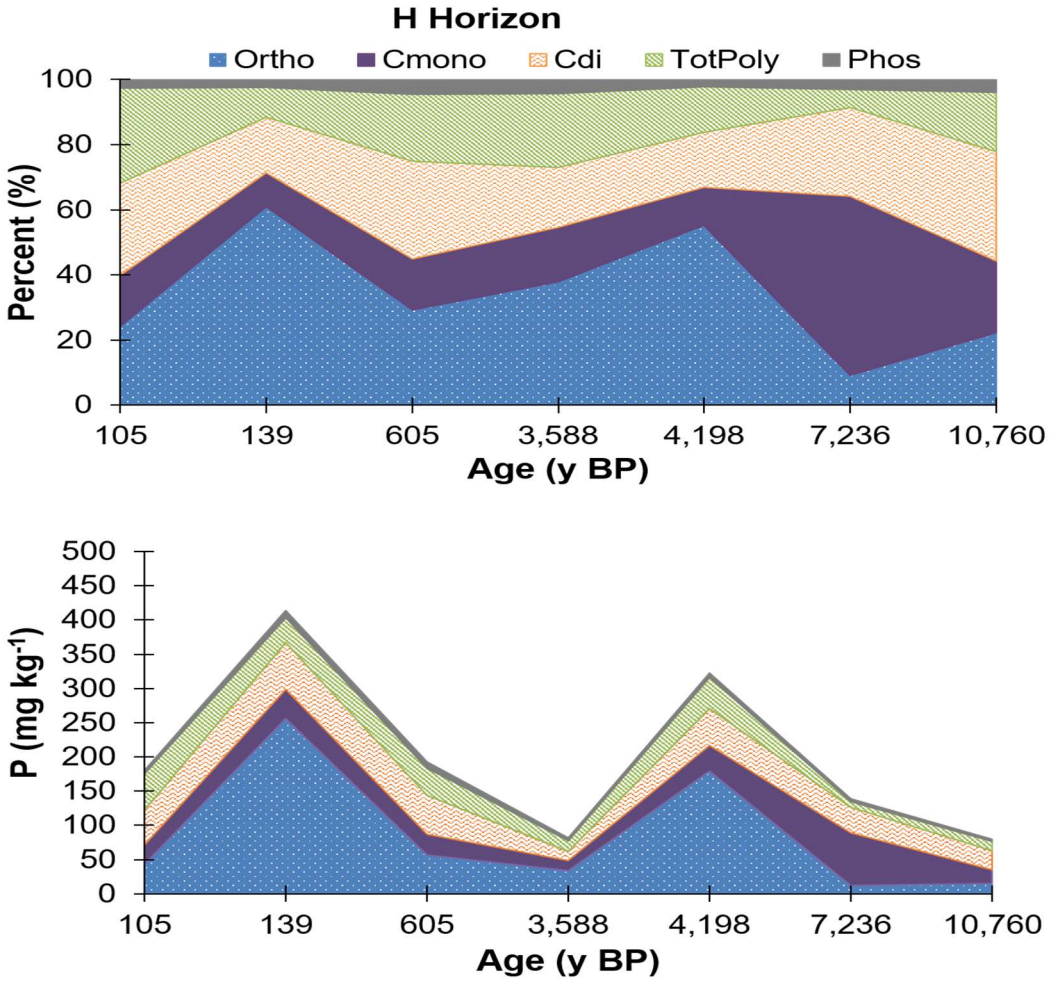

Figure 5-6. Average proportion (a) and concentration (b) of P with NaOH-EDTA extracts examined using P-NMR for the main groupings of P compounds in the humic-enriched organic horizon (H): corrected orthophosphate diesters (Cdi), corrected orthophosphate monoesters (Cmono), orthophosphate (ortho), total polyphosphates (totPoly) and phosphonates (phos) (n=2).

Within the mineral horizons, the proportion and concentration of orthophosphate declined with increasing age and was associated with an apparent increase in the proportions of corrected monoesters and diesters with age (Fig. 5-7). The proportions of total polyphosphates and phosphonates did not fluctuate significantly with age even though the concentration of phosphonates increased minimally with increasing age (Fig. 5-7).

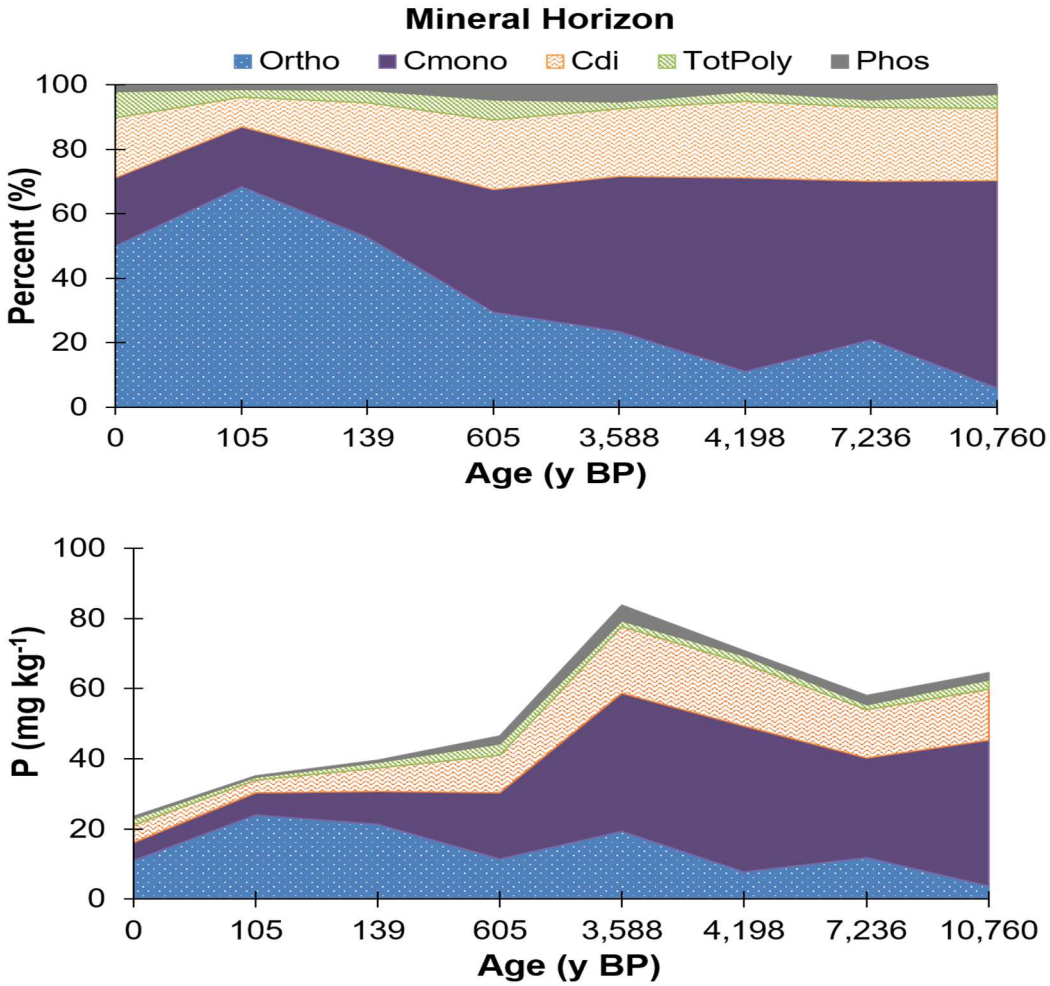

Figure 5-7. Average proportion (a) and concentration (b) of P within NaOH-EDTA extracts examined using P-NMR for the main groupings of P compounds in the mineral horizon: corrected orthophosphate diesters (Cdi), corrected orthophosphate monoesters (Cmono), orthophosphate (ortho), total polyphosphates (totPoly) and phosphonates (phos) (n=2).

5.3.5.1 Detailed Phosphorus-NMR Trends

Select identifiable P compounds and compound classes were examined in more detail to determine the changes in these forms within sample types (Table 5-5). Unidentified

monoester and diester concentrations can be found in Appendix 5. Forest floor and all foliage samples were mostly dominated by monoesters resulting from the degradation of diesters during sample analysis (nucleotides, α- and β-glycerophosphates; Table 5-5). The H horizons were also dominated by DNA, nucleotides and β-glycerophosphates but *myo*- and *chiro*-IHP had higher concentrations than α-glycerophosphate (Table 5-5). Interestingly, the mineral horizons were dominated by *myo*- and *scyllo*-IHP followed by DNA, nucleotides and glycerophosphates. The IHP stereoisomer with the greatest concentration within L horizon and foliage samples was *myo*-IHP followed by *chiro*-, *scyllo*- and *neo*-IHP; however, *neo*-IHP was not measurable within Cw (Table 5-5).

Table 5-5. Concentration of select organic P compounds within NaOH-EDTA extracts of selected soil horizons and composited foliage species (L = litter horizon; H = humic-enriched organic horizon; M = mineral horizon; Hw = western hemlock; Cw = western redcedar), α and β glycerophosphates (glyc), DNA, nucleotides (nucl), *myo*-, *scyllo-, chiro-,* and *neo*-inositol hexakisphosphates (IHP). Note: standard deviation is within brackets; n=2.

Horizon/ Species	Site	α-glyc (mg kg-1)	β-glyc (mg kg-1)	DNA (mg kg-1)	Nucl (mg kg-1)	*myo*-IHP (mg kg-1)	*chiro*-IHP (mg kg-1)	*scyllo*-IHP (mg kg-1)	*neo*-IHP (mg kg-1)
L	CIDS1	18.9 (1.1)	34.8 (5.8)	9.5 (1.7)	28.3 (3.4)	15.9 (8.1)	13.7 (1.6)	3.6 (1.1)	2.6 (0.3)
L	CIDS3	38.8 (0.7)	80.5 (2.6)	35.5 (13.2)	59 (0.5)	15.3 (0.8)	19.4 (0.2)	4.5 (0.5)	4.5 (0.5)
L	CIDS4	23.3 (5)	48.2 (7.3)	14.4 (3.4)	34.5 (7.9)	13.2 (5.2)	13.4 (1.4)	2.7 (0.3)	2.7 (0.3)
L	CIDS9	37.6 (15)	72.9 (32)	35.3 (20.4)	43.4 (6.8)	14.8 (4.4)	22.5 (1.1)	4.2 (0.7)	4.2 (0.7)
L	CIDS8	20.3 (2.2)	39.9 (5.5)	4.3 (2.3)	21 (5.1)	8.2 (0.7)	10 (0.9)	2.2 (0.1)	2.2 (0.1)
L	CIDS15	16.5 (0.8)	32.9 (1.4)	23 (0.7)	25.7 (2.7)	10.3 (2.5)	10.1 (0.5)	2.1 (0.2)	2.1 (0.2)
L	CIDS16	12.6 (0.5)	25.3 (1.1)	16.2 (2.8)	17.7 (0.9)	6.1 (0.2)	6.1 (0.2)	1 (0)	1 (0)
L	CIDS10	10 (5.3)	20 (10.7)	5.7 (0.1)	10.4 (4.8)	5.8 (1.7)	3.2 (0.8)	0.9 (0.1)	0.9 (0.1)
H	CIDS1	-	-	-	-	-	-	-	-
H	CIDS3	2.8 (0.6)	5.5 (1.2)	15.8 (1.1)	12 (2.5)	5.5 (2.2)	2.8 (0.6)	1.4 (0.2)	0.7 (0.2)
H	CIDS4	5.6 (1.1)	11.4 (2.7)	21.2 (6.9)	9.8 (0.4)	4.8 (2.2)	11.5 (7)	4.8 (2.2)	2.3 (1.2)
H	CIDS9	4.7 (2.2)	9.4 (4.4)	19.3 (0.7)	11.3 (1.7)	4.4 (0.3)	4 (0.2)	2.1 (1.5)	1 (0.1)
H	CIDS8	1.1 (0.5)	2.3 (0.9)	2.5 (2)	3 (2.1)	1.5 (1.1)	2.6 (1.6)	0.9 (0.9)	0.5 (0.4)
H	CIDS15	3.6 (0.2)	7.1 (0.9)	13.9 (6.2)	12.1 (1.5)	4.3 (0.8)	8.7 (0.6)	1.6 (0.1)	1.6 (0.1)
H	CIDS16	3.2 (1.3)	5.8 (1.8)	5.5 (1.3)	9.2 (0)	17.1 (4.7)	6.5 (0.4)	13 (7.7)	1.2 (0.3)
H	CIDS10	1.6 (0.5)	3.1 (0.9)	10.7 (7.6)	4.2 (2.7)	3.3 (3.3)	2 (1.1)	2 (2.4)	0.3 (0.1)
M	CIDS1	0.9 (0.7)	1.6 (1.2)	0.4 (0.5)	1.3 (1.3)	0.9 (0.4)	0.9 (0.5)	0.5 (0.2)	0.1 (0.1)
M	CIDS3	0.2 (0)	0.5 (0.1)	0.8 (0.7)	0.7 (0.3)	1.4 (0.4)	1.2 (0.3)	0.8 (0.1)	0.4 (0.2)
M	CIDS4	0.6 (0)	1 (0)	1.8 (1.5)	1.2 (0.3)	2.2 (0.4)	1.6 (0.6)	1.4 (1)	0.3 (0.1)
M	CIDS9	0.8 (0.4)	1.5 (0.8)	4.1 (3.2)	1.4 (0.4)	7.7 (6.5)	1.6 (0.7)	3.2 (2.8)	0.4 (0)
M	CIDS8	1.5 (0.3)	2.6 (0.4)	5 (0.9)	5 (4.4)	12.2 (2.4)	3.1 (0.5)	10.1 (0.5)	0.9 (0.6)
M	CIDS15	1.2 (0.2)	1.8 (0.5)	6.1 (1.1)	3.7 (0.3)	15.5 (3.2)	2.8 (0.2)	9.7 (2.4)	0.9 (0.1)
M	CIDS16	0.7 (0)	1.2 (0.2)	5.3 (1.5)	2.7 (0.3)	9.4 (4.9)	2.1 (0.1)	6.9 (2.3)	0.7 (0)

Horizon/ Species	Site	α-glyc (mg kg-1)	β-glyc (mg kg-1)	DNA (mg kg-1)	Nucl (mg kg-1)	*myo*-IHP (mg kg-1)	*chiro*-IHP (mg kg-1)	*scyllo*-IHP (mg kg-1)	*neo*-IHP (mg kg-1)
M	CIDS10	0.8 (0.5)	1.2 (0.7)	4 (1)	2.6 (2.7)	14 (8.7)	2.4 (1.5)	8.7 (5.8)	1 (1.1)
Hw	G1	57.7	106.8	78.6	24.6	16.0	17.2	8.6	8.6
Hw	G2	63.6	121.0	128.3	97.0	34.4	33.4	6.3	6.3
Hw	G3	24.6	49.6	61.3	34.1	13.4	11.7	2.6	2.6
Cw	G1	52.8	104.3	75.9	78.5	34.8	25.7	0.0	0.0
Cw	G2	58.8	116.8	101.6	29.0	25.4	8.0	0.0	4.4
Cw	G3	34.5	69.5	61.5	26.0	17.5	17.1	0.0	2.7
Salal	CIDS8A	23.7	47.3	20.3	47.3	23.7	23.0	4.1	4.1
Salal	CIDS8B	22.6	45.2	17.4	49.7	22.6	19.4	3.9	3.9
Salal	CIDS15B	30.3	63.9	31.9	53.2	13.3	13.8	3.2	3.2

5.3.6 Monoester: Diester Ratios

Current P-NMR studies correct monoester and diester concentrations for degradation (Makarov et al., 2002; Turner et al., 2003b; Doolette et al., 2009; Cade-Menun, 2015). However, to compare current data with previous studies where correction for degradation was less common, both the original (M:D) and corrected monoester: diester (cM:D) ratios must be reported (Table 5-6).

The foliage species had comparable M:D and cM:D to the L horizon, with the M:D being greater than one and the cM:D being less than one (Table 5-6). Within the L horizon, both original and corrected M:D ratios declined with increasing age (Table 5-6). The M:D ratio remained greater than 1 in the L horizon for the whole chronosequence; however, the cM:D ratio was less than 1 (Table 5-6). The M:D ratio in the H horizons were all greater than 1, whereas the cM:D was less than one at all sites except intermediate-aged sites (3,588 a BP and 7,236 a BP). The mineral horizons exhibited different trends for monoesters and diesters than the L and H horizons because both M:D and cM:D for all samples were greater than 1; however, the M:D was relatively stable with increasing age whereas cM:D increased with age (Table 5-6).

The cM:D of all foliage species ranged from 0.3 to 0.4. The L horizon cM:D ranged from 0.4 (7.236 a BP) to 0.6 (~0 and 3,588 a BP) while the H horizons ranged from 0.5 (105 and 605 a BP) to 1.1 (3,588 a BP) with the exception of the 7,236 a BP site, which had a cM:D of 2.0 (Table 5-6). The mineral horizons cM:D ranged from 1.2 (~0 a BP) to 2.8 (10,760 a BP). The L horizon and foliage samples had the greatest degradation of P compounds (15 – 29%) within the NaOH-EDTA extract when compared with the H (7 – 13%) and mineral horizons (4 – 15%; Table 5-6).

Table 5-6. Uncorrected (M:D) and corrected monoester:diester (cM:D) ratio and percent of degradation within NaOH-EDTA extracts of selected soil horizons and composited foliage species (L = litter horizon; H = humic-enriched organic horizon; M = mineral horizon; Hw = western hemlock; Cw = western redcedar). Note: standard deviation is within brackets.

Horizon/ Species	Age (a BP)	Site	M:D	cM:D	Degradation (%)
L	0	CIDS1	6.6 (0.3)	0.6 (0.1)	19 (3)
L	105	CIDS3	4.1 (0.3)	0.5 (0.1)	24 (3)
L	139	CIDS4	4.7 (0.1)	0.5 (0.1)	24 (4)
L	605	CIDS9	4.5 (1.1)	0.5 (0.2)	22 (4)
L	3,588	CIDS8	8.4 (1.8)	0.6 (0.0)	22 (1)
L	4,198	CIDS15	3.5 (0.6)	0.5 (0.1)	22 (1)
L	7,236	CIDS16	3.4 (0.0)	0.4 (0.0)	29 (1)
L	10,760	CIDS10	5.8 (3.0)	0.5 (0.1)	29 (10)
H	0	CIDS1	-	-	-
H	105	CIDS3	1.6 (0.1)	0.5 (0.1)	11 (2)
H	139	CIDS4	1.7 (0.4)	0.6 (0.2)	7 (2)
H	605	CIDS9	1.7 (0.1)	0.5 (0.1)	13 (4)
H	3,588	CIDS8	6.0 (6.9)	1.2 (0.9)	8 (1)
H	4,198	CIDS15	1.9 (0.0)	0.7 (0.1)	7 (0)
H	7,236	CIDS16	5.0 (1.0)	2.0 (0.1)	13 (1)
H	10,760	CIDS10	1.5 (0.1)	0.6 (0.2)	11 (0)
M	0	CIDS1	15.9 (10.6)	1.2 (0.5)	15 (6)
M	105	CIDS3	4.8 (1.1)	1.8 (0.0)	4 (2)
M	139	CIDS4	4.0 (1.9)	1.4 (0.4)	8 (2)
M	605	CIDS9	3.4 (0.1)	1.7 (0.3)	8 (0)
M	3,588	CIDS8	5.8 (0.7)	2.3 (0.8)	11 (5)
M	4,198	CIDS15	5.1 (0.3)	2.3 (0.4)	10 (1)
M	7,236	CIDS16	3.9 (0.3)	2.0 (0.5)	8 (1)
M	10,760	CIDS10	4.8 (1.8)	2.8 (0.5)	7 (1)
Hw	0-139	G1	2.2	0.4	15
Hw	605-4,198	G2	1.6	0.3	27
Hw	7,236-10,760	G3	1.4	0.3	25
Cw	0-139	G1	2.4	0.4	18
Cw	605-4,198	G2	2.0	0.2	28
Cw	7,236-10,760	G3	2.4	0.4	29
Salal	3,588	CIDS8A	1.8	0.4	17
Salal	3,588	CIDS8B	1.8	0.4	18
Salal	4,198	CIDS15B	2.0	0.3	28

5.3.7 Relationships of Select Organic Phosphorus Compounds with Soil Chemical Parameters

Only soil chemical parameters with statistically significant correlation coefficients ($p < 0.05$) are listed in Table 5-7. Of the parameters analysed with correlation analysis, total C was correlated to IHP in the mineral horizons (Table 5-7). Within the mineral horizons, IHP and DNA concentration were positively correlated to Al_o (amorphous, organically-complexed Al), and Al_o+ Fe_o (Table 5-7).

Table 5-7. Correlation coefficients between inositol hexakisphosphate (IHP) and DNA determined by solution P-NMR and select soil chemical parameters; oxalate (o) extractable Al, oxalate extractable iron (Fe) and Al (Fe_o+Al_o), and total carbon within the mineral horizon samples analysed on the Calvert Island chronosequence.

	Mineral Horizon	
	IHP	**DNA**
Al_o	0.86***	0.79*
Fe_o+Al_o	0.87***	0.81*
Total Carbon	0.91***	-

[1] Significance at the 5, 1, and 0.1% level indicated by *, **, and ***, respectively.

Mehlich 3 extractable P within select samples used for 31P-NMR and orthophosphate concentration determine through 31P-NMR spectral analysis were significantly correlated ($r_s = 0.9413$, $p < 0.0001$; Fig. 5-8).

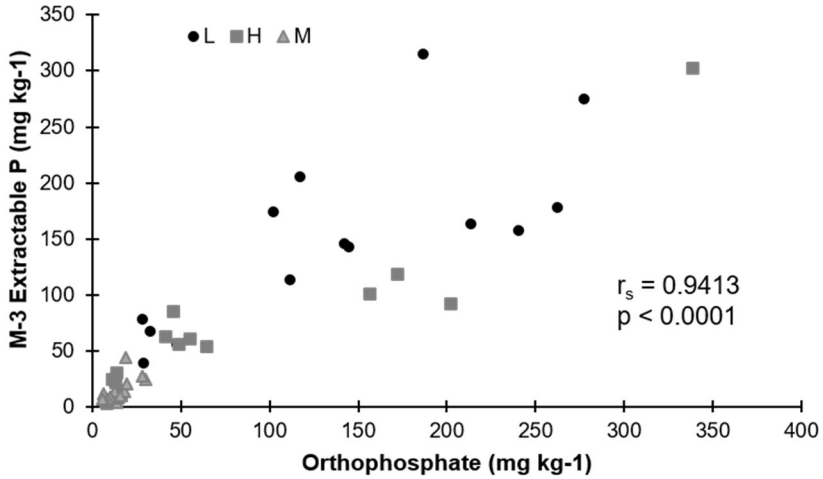

Figure 5-8. Average Mehlich-3 extractable phosphorus (M-3 Extractable P) concentration within the select litter horizon (L), humic-enriched organic horizon (H) and mineral horizon

(M) samples used for P-NMR analysis with associated orthophosphate concentration determined by ^{31}P-NMR spectroscopy and spearman correlation coefficient (n=2) (Mehlich, 1984).

5.4 Discussion

5.4.1 Total Soil Profile Phosphorus Trends

Fractionation analysis was not performed on the Calvert Island chronosequence, so the P fractionations listed in Walker and Syers (1976) cannot be compared to the data here; however, total P, organic P, exchangeable P, and the sum of exchangeable Ca+Mg and Fe+Al, supplemented by P-NMR data, provide an adequate data set to see if the Calvert Island chronosequence follows the general trends of the Walker and Syers model (1976; (Figs. 5-2 to 5-8).

The mass of total P to a 1 m depth followed a linear decline with age, rather than the typical exponential decline suggested by Walker and Syers (1976; Fig. 5-1). Originally, the Williams and Walkers (1969b) model for P transformations hypothesized that total P would decline linearly with increasing time; however, Walker and Syers (1976) adjusted the model by suggesting that total P would decline exponentially. Some of the chronosequence studies used to create the Walker and Syers (1976) model detected linear declines of total P with time, such as Franz Josef (Stevens and Walker, 1970) and Manawatu (Syers and Walker, 1969); however, it is expected with time that total P will plateau, creating an exponential model. Therefore, the Calvert Island chronosequence may currently exhibit a linear decline of total P to 1 m depth with increasing age, but may be on an exponential trajectory in the longer-term (Fig. 5-1).

On Calvert Island, organic P displayed a hump-shaped curve that increased until ~4,000 years, followed by a decline (Fig. 5-1), which is characteristic of organic P in the Walker and Syers (1976) P model and is comparable to long-term chronosequences including

those at Hawaii, Franz Josef, Reefton and Haast (Walker and Syers, 1976; Crews et al., 1995; Eger et al., 2011). Since organic P followed the Walker and Syers (1976) model and total P declined similarly to the initial decline phase of the model, it is hypothesized that primary mineral P rapidly declined within the first 4,000 years and was accompanied by an increase in occluded and non-occluded P forms, which can be seen in the decline of Mehlich-3 extractable P with increasing age in all horizons and the dramatic loss of Mehlich-3 extractable Ca and Mg within 105 years in the mineral horizon and the progressive accumulation of Fe and Al (Figs. 5-2 to 5-3). Exchangeable Ca and Mg declined with increasing age on the Haast, Mendocino and Jurien Bay chronosequences (Northup et al., 1995; Eger et al., 2011; Turner and Laliberté, 2015), similarly to Calvert Island (Figs. 5-2 to 5-3).

5.4.2 Correction for Degradation of Diesters

In solution P-NMR, many monoesters are the result of alkaline hydrolysis of RNA and phospholipids (Makarov et al., 2002; Turner et al., 2003b). Some researchers, such as Schneider et al. (2016), acknowledge this limitation and present data with multiple different correction factors while others like Vincent et al. (2013) choose to define the correction factor and provide original data with degradation rates. In 2011, He et al. used a correction factor, later used by Schneider et al. (2016), that seemed to most accurately reflect enzymatic hydrolysis of diesters (α and β glycerophosphates, and nucleotides), so this correction factor was used in this study. Original data are also included to compare to previous studies not utilizing correction factors.

Extraction of organic P with NaOH-EDTA used with P-NMR is currently the most quantitative method to recover organic P within high organic content samples and mineral samples (Cade-Menun and Preston, 1996; Cade-Menun et al., 2000; Turner et al., 2005). The

recovery of P in NaOH-EDTA extracts from the foliage and L horizon samples was the greatest of all sample types and did not fluctuate significantly with age (Table 5-1). Interestingly, the organic P recovery declined with increasing age in the L horizon samples, with 72% of the organic P recovered on the site aged 105 a BP to 28% recovery after 7,236 a BP (Table 5-1). The reduced recovery of organic P in the L horizon with age may have been caused by differences in humification processes that may have incorporated organic P within organic matter (Celi and Barberis, 2007), reducing the solubility in NaOH-EDTA, or perhaps since the soils were significantly older and more weathered, the ignition method could have overestimated the organic P concentration by converting previously insoluble inorganic P compounds into soluble compounds during ignition (Condron et al., 1990).

In the H horizons, the lowest recoveries of total P were in the wood-enriched H horizons (Hw) compared to humic-enriched organic horizons (Hh), and the recovery of organic P increased with age in all H horizons (Table 5-1; Appendices 2 and 4). The recovery of total P within the mineral horizon was the lowest of all horizon types; however, the recovery of organic P increased with increased age (Table 5-1).

The recovery of total P within this study is comparable to the recovery rates found within Podzols on Vancouver Island, with 71 - 95% recovery within the LF layer, 32-95% recovery in the H horizon and 4-64% recovery within mineral horizons (Cade-Menun et al., 2000). On the Franz Josef chronosequence, Turner et al. (2007) also had lower recovery rates on young soils compared to older mineral soils.

With increasing age, organic forms of P dominate and are more easily extractable with NaOH-EDTA than precipitated P forms (Bowman and Moir, 1993; Turner et al., 2003a; Turner, 2008). The youngest site (~0 a BP) was minimally weathered and received daily

influxes of sea spray rich in basic cations, increasing pH relative to the older samples (~0 a BP: pH = 7.9; 10,760 a BP: pH= 3.7; Appendix 4). Higher-pH samples generally have lower recoveries because P bound by Ca and Mg is harder to extract with NaOH-EDTA than P bound to Fe and Al (Turner et al., 2003a; McDowell et al., 2005; Turner and Blackwell, 2013). With increasing age, both the H and mineral horizons became more enriched in Fe and Al, which corresponds to an increase in the recovery organic P (Fig. 5-3b).

It is important to note that the mechanisms of P recovery with NaOH-EDTA are not fully understood and more studies should be completed comparing the extract and the residual P in the remaining sample after extraction with NaOH+EDTA (e.g. Turner, 2008; Cade-Menun and Liu, 2014).

5.4.3 Chemical Shifts

The chemical shifts for each sample type varied slightly among sample types, with the H horizon samples producing chemical shifts that were downfield of the L horizon, foliage and mineral horizon samples (Tables 5-2 to 5-4). For most mineral horizons, foliage and L horizon, the chemical shifts of identified P compounds and compound classes were comparable with the mineral samples generally being a little upfield from the foliage and L horizon samples (Tables 5-2 and 5-4). The unknown peak around 5.00 ppm also follows these trends because the H horizons were the furthest downfield followed by foliage and L horizon samples, and then mineral horizons. Since the chemical shift of the unknown peak is consistent within sample type, it may be the 4 axial/2 equatorial conformation of *neo*-IHP (Turner et al., 2012b; Cade-Menun, 2015).

Since all samples were analysed at constant temperature at a pH > 12, the difference in chemical shifts among sample types may have been caused by differences in ionic strength, paramagnetic content or the OM content (Gorenstein, 1984; Crouse et al., 2000;

McDowell and Stewart, 2005; Cade-Menun, 2015). The presence of Fe and Al will influence the chemical shift; however, the change between horizons is not fully explained by the paramagnetic content since the H horizon samples were furthest downfield followed by L horizon and foliage samples and then mineral horizons. This suggests that the difference in chemical shift may have been caused by the greater concentration of OM within the different H and mineral horizon samples.

The mineral horizons generally had higher standard deviations for chemical shifts compared to the foliage and L horizon samples and the H horizons (Tables 5-2 to 5-4). The mineral samples had considerably less P than the other samples and generally had noisier spectra that could have resulted in more variation of chemical shifts (Table 5-1; Appendix 5).

5.4.4 Changes in Phosphorus Among Sample Types

Within foliage on chronosequences, total P can decline linearly, exponentially or with a hump shape. On the Cooloola chronosequence, total P declined with increasing age with a greater decline in *Banksia* sp. than *Leptospermun* sp. (Chen et al., 2015). On the Volcanic Plateau and Franz Josef chronosequences, total P within the foliage displayed a hump shape while Waitutu declined consistently (Parfitt et al., 2005). On the Mendocino chronosequence, the series spanned long enough that a plateau in foliar P was achieved after 330,000 years for three tree species (Izquiredo et al., 2013). Lastly, in a comparable environment to Calvert Island, the Glacier Bay chronosequence showed a humped decline in total P within Spruce and a consistent decline within Alder species (Chapin et al., 1994). In the current study, Cw and Hw did not reach a detectable plateau in foliar P on the Calvert Island chronosequence, potentially due to the composite nature of the samples, but total P did consistently decline with age (Table 5-1).

Foliage samples for all species were dominated by corrected diesters and orthophosphate followed by corrected monoesters, total polyphosphates and phosphonates (Fig. 5-4). The L horizon was comparable to the foliage samples, except there was an increase in the proportion of total polyphosphates that was greater or equal to the concentration of corrected monoesters (Figs. 5-4 and 5-5). The H horizon samples had more fluctuation of compound class dominance among sites, but overall orthophosphate, corrected diesters and corrected monoesters dominated. Compared to the foliage and L horizon samples, the H horizon samples had a slight increase in polyphosphates and phosphonates, but had a decline in pyrophosphate (Figs. 5-4 to 5-6). Lastly, the mineral horizons samples did not follow the same trends as the previous sample types; instead, corrected monoesters and orthophosphate dominated the P forms (dependent on the site) followed by corrected diesters, total polyphosphates and phosphonates (Figs. 5-4 to 5-7).

It appears that there was little alteration to the litter inputs in the L horizon compared to the fresh foliage samples, because the proportions of main compound classes were similar even though the total P concentration of the L horizon was less than the foliage samples (Figs. 5-4 and 5-5). When transitioning from the L horizon to the H horizons, the main difference is the increased dominance of polyphosphates instead of pyrophosphates (Figs. 5-5 and 5-6). The H horizons are well-humified humic or wood-enriched horizons with an abundance of mycelia, and within mycelium, P is transported as polyphosphate granules (Makarov et al., 2002; Oberson and Joner, 2005; Bünemann et al., 2008); thus, an increase in polyphosphate can be tied to the increased fungal cycling of nutrients. Pyrophosphates are a shorter form of polyphosphate and may be a storage compound for microbes, explaining the increased proportion within the L horizon compared to the foliage and the decline when

transitioning to the more active H horizon (Condron et al., 1990). They may also originate from degradation of polyphosphates during extraction and NMR analysis (Cade-Menun et al., 2005).

The most interesting shift in the main P compound classes is between the H horizon and the mineral horizons; corrected monoesters and orthophosphate dominated the mineral horizon, rather than orthophosphate and corrected diesters in all other sample types, and the proportion of phosphonates increased (Figs. 5-6 and 5-7). Mineral horizon samples dominated by orthophosphate had a lower concentration of corrected monoesters and the sites dominated by corrected monoesters had lower concentrations of orthophosphate (Fig. 5-7). The increased proportion of corrected monoesters can be attributed to an increase in the dominance of IHP (Fig. 5-7; Table 5-5). The increased proportion of phosphonates may be due to the imperfectly drained nature of the soils older than 600 years caused by the formation of ortstein and placic horizons, because phosphonates appear to accumulate in cool, wet, acidic environments (Appendix 2; Newman and Tate, 1980; Cade-Menun, 2005).

The processes controlling P forms in the foliage are directly related to the specific plant species, the mycorrhizal association and the rhizosphere community, and in turn control the inputs to the L horizon. Forest floors are a dynamic interface between surrounding plant species and the H and mineral horizons, and are influenced by vegetation, temperature, moisture and active microbial biomass (Barnes et al., 1994). The forms of P within the foliage and L horizon will influence the H horizon but the direct effect may be diminished by increased biological alteration within the well-humified H horizon from the abundance of mycelia (Appendix 2). Beneath the H horizon, the organic-enriched mineral horizon is controlled by drastically different processes than the overlying horizons because the chemical

composition of the mineral horizons determines how P compounds are stabilized in the soil, rather than being flushed through the soil during large rain events. The buildup of corrected monoesters suggests that the controlling process in the mineral horizons is sorption, which is corroborated with the increase of amorphous and exchangeable Fe and Al in the mineral horizon compared to the other horizons. In addition, the presence of roots declined with age in the mineral horizons and no identifiable mycelia were found, which would limit the biological aspects of P cycling (Fig. 5-3b; Greaves and Webley, 1969).

Specific forms of organic P forms within the foliage and L horizon were dominated by DNA and by the diester degradation products α- and β- glycerophosphates and nucleotides (Table 5-5). The H horizon also resembled the foliage and L horizon composition except that DNA was dominant, followed by nucleotides and then glycerophosphates (Table 5-5). The L and H horizons have definite links to the P forms found in the foliage; however, the mineral horizons do not follow the same trend. For the mineral horizons *myo*- and *scyllo*-IHP are the most dominant forms of organic P in the selected forms followed by DNA, nucleotides and *chiro*-IHP and minimal concentrations of glycerophosphates (Table 5-5).

The *myo* stereoisomer of IHP is found commonly in seeds, where it is known as phytate. The other stereoisomers of IHP are either microbially produced like *neo*-IHP (Martin et al., 2000) or epimerized from *myo*-IHP (Smith and Clark, 1951; Caldwell and Black, 1958; Cosgrove, 1980; Turner and Richardson, 2004; Giles et al., 2011) because *chiro*-, *scyllo*-, and *neo*-IHP have not been found in appreciable quantities in plant tissue (Turner et al., 2007). This current study shows that all stereoisomers of IHP were found in plant foliage in varying concentrations depending on the plant species (Table 5-5). Redcedar and salal foliage had all four IHP stereoisomers, whereas Hw had all stereoisomers except *scyllo*-IHP. However,

since foliage was not always collected directly from the plants and was not sterilized prior to extraction, microbial alteration and epimerization may have occurred and influenced the IHP forms and concentrations (Table 5-5).

The uncorrected M:D ratio was much more variable than the cM:D within all samples types (Table 5-6). The M:D ratio of all samples was greater than one, suggesting the dominance of monoesters over diesters, whereas the cM:D was less than one in the foliage and L horizon, between 0.5 and 2 in the H horizons and greater than one in the mineral horizons (Table 5-6). This suggests that diesters, including degradation products, dominated the foliage, L horizon and sometimes the H horizon, while monoesters were more dominant in the mineral horizon (Table 5-6). These data are consistent with the above conclusion, suggesting minimal alteration of the foliage within the L horizon, greater biological cycling and alteration in the H horizon and the dominance of chemisorption processes in the mineral horizons.

5.4.5 Changes in Phosphorus with Age

With increasing age, the concentration of total P decreased for all sample types, and organic P increased and then declined for all samples, with the maximum at different ages depending on the sample type (Table 5-1). The concentration of total P within the NaOH-EDTA extracts also declined with increasing age for foliage, L horizon and H samples whereas the concentration increased with age in the mineral samples due to greater recovery and possibly the increased dominance of organic P with age, and different stabilization mechanisms compared to the L and H horizon samples (Figs. 5-3 to 5-6b).

For most samples, with increasing age the proportion of orthophosphate declined while corrected monoesters and diesters increased (Figs. 5-4 to 5-7a). All samples including foliage, and L, H and mineral horizon samples had declining proportions of orthophosphate,

with the L horizon exhibiting the least change (Figs. 5-4 to 5-7a). It is consistent with the literature that orthophosphate will decline with age since it is a more labile form of P released from primary minerals, plant material and microbes and is subsequently immobilized into less labile forms of P, such as IHP, or incorporated into plant tissues (Vitousek and Farrington, 1997; McDowell et al., 2007; Bünemann et al., 2008). Orthophosphate and Mehlich 3 P concentrations were strongly correlated ($p < 0.0001$), so the declining concentration of orthophosphate was correlated with a decline in extractable P illustrating the increased recalcitrance of the newly dominant organic forms of P with increasing age (Figs. 5-2 to 5-8).

Corrected monoester proportions increased with increasing age for foliage, some H horizons and most mineral horizon samples (Figs. 5-4, 5-6, and 5-7a). The L horizon did not show a consistent increase in corrected monoesters (Fig. 5-5a). Foliage samples had an increase in *myo*- and *chiro*-IHP while the select H horizons (3,588 and 7,236 a BP) had an increase in *myo*-, *scyllo*- and *chiro*-IHP and monoester 2 and 3 (Figs. 5-4 and 5-6a). The mineral horizon samples had increased *myo*- and *chiro*-IHP and monoesters 1, 2, and 3 (Fig. 5-7a; Appendix 5). It is consistent with current literature that *myo*- and *scyllo*-IHP increased in proportion with increasing age in the H and mineral horizon samples (McDowell et al., 2007; Turner et al., 2007; Turner et al., 2014) even though the concentration did decline between 7,236 and 10,760 years (Figs. 5-6 and 5-7b).

Corrected monoesters, including IHP, increased with age in the H and mineral horizons because IHP can easily sorb onto humic materials, clays or form insoluble precipitates, making them less likely to be mineralized (Goring and Bartholomew, 1952; Condron et al., 1990; Turner et al., 2002; Giles et al., 2011). With increasing age, Al_o

concentrations increased in the mineral horizons because podzolization moves organically-complexed Al and Fe to depth, where they can precipitate as short-range order allophanic materials or remain bound to OM (Appendix 4; Gustafsson et al., 1995; Lundström et al., 2000). Short-range order allophanic type materials and Fe are known to sorb organic P compounds including IHP, inositol monophosphate, glucose-6-phosphate and DNA (Shang et al., 1990; Celi et al., 1999; Celi and Barberis, 2007; Yan et al., 2014; Jørgensen et al., 2015). Jørgensen et al. (2015) examined IHP stabilization by selective dissolution of minerals in three different soils and found that in the temperate rainforest, on the Haast chronosequence, IHP were completely removed when the mineral grains were digested with hydrofluoric acid. This suggested that all IHP were sorbed on amorphous metals that were extracted by acid-ammonium oxalate. This finding is consistent with the Calvert Island chronosequence where the IHP and Al_o+Fe_o concentrations were strongly correlated ($p < 0.05$; Table 5-5; Fig. 5-9).

The youngest site, ~0 a BP, with a buried Ah horizon had on average 0.01% Al_o and reached a maximum around 7,236 a BP with 0.63% Al_o and declined to 0.40% around 10,760 a BP (Appendix 4). Shang et al. (1996) compared sorption of IHP, G6P and orthophosphate on short range, non-crystalline Al and found that IHP sorbed the strongest and formed multi-ring complexes making IHP more biologically unavailable compared to orthophosphate and G6P. Li et al. (2013) identified the bonding structure of IHP to Al as mostly bidentate binuclear inner sphere surface complexes with minimal monodentate complexes. Inner sphere complexes are tightly held within the soil matrix and are sometimes considered somewhat irreversible due to the nature of the bond (McBride, 1994; Li et al., 2013). Monodentate complexes can desorb more easily than bidentate complexes, but the rate of

desorption may be up to three orders of magnitude longer (McBride, 1994). This explains why IHP builds up in the mineral horizons enriched in oxalate extractable Al.

Corrected diesters increased in proportion in all sample types, with only slight increases within the L and H horizon samples (Figs. 5-4 to 5-7a). The increase in corrected diesters within the foliage and L horizon can be attributed to increases in DNA, RNA, and phospholipids (Figs. 5-4 and 5-5a; Makarov et al., 2002). The H horizons had an increased proportion of DNA, while the mineral horizons had increased DNA, diester 1 and diester 2 (Figs. 5-6 and 5-7a). Diesters including RNA and phospholipids are generally more labile in soils than monoesters because they only have one ionizable proton instead of the two found in monoesters, reducing their adsorption capacity; thus, diesters are more commonly found in solution and are subsequently more easily mineralized (Makarov et al., 2002; Condron et al., 2005; Celi and Barberis, 2007; Vincent et al., 2013). However, DNA can be sorbed onto humic materials and within the interlayers of clays at low pH, explaining the accumulation of DNA in these samples (Greaves and Wilson, 1969; Levy-Booth et al., 2007; Turner et al., 2007).

Within mineral horizons, significant correlations were identified between IHP and DNA with Al_o, and Fe_o+Al_o (Table 5-7). Since the concentrations of IHP and DNA increased with increasing concentration of amorphous organic and inorganic Al, this suggests that Al is most likely the main binding element within the mineral horizon on these sites. Iron and Al correlated to IHP and DNA although Fe was not significantly correlated to IHP and DNA by itself, possible due to the inherently low Fe concentrations in these soils (Roddick, 1996a; b; Sauer et al., 2007). Total C was positively correlated to IHP within the mineral horizon samples, which may be caused by the chemical composition of IHP which inherently has C

within it, but doesn't eliminate the potential for IHP to be sorbed on humic materials. In previous studies DNA was found to sorb on humic materials (Greaves and Wilson, 1969; Levy-Booth et al., 2007; Turner et al., 2007), so a positive correlation between total C (surrogate for organic C since no carbonates are present) and DNA was expected; however, no significant correlation was found in any horizon type. Either DNA was not one of the compounds contributing to total C or DNA was not stabilized by C within these soils. It would be interesting to further examine the mechanisms and kinetics for IHP and DNA sorption within these soils.

The proportion of total polyphosphates increased within foliage samples and declined in L horizon samples (Figs. 5-4 and 5-5a). Phosphonates increased in the L and mineral horizons, with a slight increase in the H horizons (Figs. 5-5 to 5-7 a). The increase in phosphonates may be attributed to the increasingly wetter conditions with age since placic and ortstein horizons formed between 600 and 3,500 years and can impede water flow, making conditions wetter, cooler and more acidic. This is ideal for the formation and accumulation of phosphonates, because these conditions limit bacterial activity and subsequently phosphonatase enzyme production (Appendix 2; Tate and Newman, 1982; Hawkes et al., 1984; Condron et al., 2005).

With increasing age, there were no apparent trends for the M:D and cM:D ratios within the foliage, L and H horizons, though sites aged 3,588 and 7,236 a BP had higher cM:D within the H horizons due to the increased dominance of IHP and monoesters 2 and 3 (Table 5-6). With increasing age, the cM:D ratio increased in the mineral horizon samples due to the accumulation and sorption of IHP compounds (Table 5-6).

5.4.6 Comparison with Similar Studies

Cade-Menun (1995) performed solution (NaOH-EDTA) P-NMR on soils from the CWH zone within Cw dominated forests. Unlike the Calvert Island soils, the L and H horizon were dominated by uncorrected monoesters and diesters followed by orthophosphate with the monoesters and diesters being almost double the orthophosphate, whereas orthophosphate was the most dominant P form within the extracts on Calvert Island in the L and H horizons followed by uncorrected monoesters and diesters (Appendix 5). The mineral horizons from Cw sites presented in Cade-Menun (1995) were dominated by orthophosphate and monoesters which is similar to Calvert Island. Further identification of specific organic P forms was not performed for the Cade-Menun (1995) study but it would be interesting to see if the uncorrected monoesters dominating the LFH layers contained a larger proportion of diester degradation products and if the monoesters in the mineral horizons were mainly IHP like the soils found on Calvert Island.

The effects of fire were also investigated within Cw-Hw forests by Cade-Menun et al. (2000). Post-fire LF and H horizons displayed an increase in inorganic P following fire since fire mineralizes organic P forms to orthophosphate (Macadam, 1987; DeBano and Klopatek, 1988; Tomkins et al., 1991). After 10 years the effects of fire were diminished, and inorganic P concentrations were comparable to old growth forests. On sites aged 7,236 and 10,760 a BP on the Calvert Island chronosequence had evidence of a fire history because shore pine (*Pinus contorta* var. *contorta*), also known as lodgepole pine, had visible fire scars and charcoal fragments were found in soils greater than 3,500 years (Appendices 2 and 3). Hoffman et al. (2016a, b) documented fire chronology on northern Calvert Island and Hectate Island spanning 13,000 years and found that there was a fire-free period between roughly 7,500 and 5,500 years BP, with most fires occurring within the last 1,000 years. This

suggests that all charcoal found on this chronosequence may be assumed to be less than 5,500 years BP. The L and H horizons on Calvert Island do not have an apparent increase in orthophosphate on sites aged 7,236 and 10,760 a BP, so the fires that did occur may not have been severe or were long enough ago that the effects of fire have diminished.

Preston and Trofymow (2000) also performed solution P-NMR (NaOH+Chelex) within the CWH zone, comparing the west and east side of Vancouver Island. The east side was in the very dry variant while the west side was in the very wet variant with mean temperature and precipitation that are comparable to the Calvert Island chronosequence. The young mineral soils on Calvert Island (0-139 y) are comparable to the mineral soils on the west coast of Vancouver Island, with orthophosphate dominating followed by uncorrected monoesters, and diesters (Appendix 5). The west coast soils used in Preston and Trofymow (2000) were characteristic of forests with nutrient restrictions and cool, wet conditions within the CWH zone that are also characteristic of the Calvert Island chronosequence.

Since the Walker and Syers (1976) publication, over 15 chronosequences have been studied that meet the requirements for their P transformational model. Most studies have examined how total P and organic P change with age in the mineral horizons and some that look at the organic horizons. Fewer studies examine how the P within foliage changes and none have examined how P in the L horizon changed unless they were studying microbial biomass in the other organic horizons.

Within the H horizons, total P declined consistently at the Volcanic Plateau, Franz Josef and Waitutu sites at rates less than in the mineral horizons (Parfitt et al., 2005), which is comparable to the Calvert Island chronosequence with the exception of the 4,198 a BP site (Table 5-1). Unlike Calvert Island, total P declined exponentially on the Haast

chronosequence, reaching a stable concentration after only 1,000 years coinciding to the development of a mature Podzol (Turner et al., 2012a).

The concentration of total P within mineral horizons declined with age on chronosequences across the world, with significant declines at the Cooloola, Jurien Bay, Franz Josef, Reefton, Manawatu, Waitutu and Mendocino sites (Syers and Walker, 1969; Walker and Syers, 1976; Parfitt et al., 2005; Izquiredo et al., 2013; Chen et al., 2015; Turner and Laliberté, 2015). The Haast chronosequence and the Hawaiian Substrate Age Gradient both had rejuvenating dust inputs that buffered the total P concentration within the soil, but a significant decline with age was still apparent (Eger et al., 2013). Haast also had an increase in total P following the formation of placic horizons, most likely due to the reduction and subsequent mobilization of Fe, but this was not seen on Calvert Island (Crews et al., 1995; Kurtz et al., 2001; Eger et al., 2011; Turner et al., 2012a). The Cox Bay chronosequence has a very similar climate to Calvert Island and though total P data were not reported, a linear decline of Ca-P was apparent in the first 550 years to 1 m depth and an exponential decline of Ca-P occurred in the first 10 cm of mineral soil (Singleton and Lavkulich, 1987b). The Calvert Island chronosequence does not have Ca-P data, but a significant decline of extractable Ca and Mg occurred within 7,000 years in the H horizon and 105 years in the mineral horizon (Fig. 5-3a). Total Ca declined consistently within the mineral horizon with age, whereas total Ca exhibited a hump-shaped curve with age and total Mg declined consistently within the H and mineral horizons (Appendix 4).

Organic P is more likely to have a hump-shaped decline, which is characteristic of the Walker and Syers (1976) model; as orthophosphate becomes scarcer with increasing age, soil microorganisms are forced to mineralize less-labile forms of P including organic P forms,

which are subsequently immobilized and transformed within the microorganisms (Quiquampoix and Mousain, 2007). Within organic horizons, the Volcanic plateau, Franz Josef, and Waitutu chronosequences exhibited a humped decline of organic P with increasing age (Parfitt et al., 2005). The same hump-shaped curve was seen in the mineral horizons on the Reefton, Manawatu, Hawaiian Islands, Jurien Bay, Franz Josef, Cooloola and Mendocino chronosequences (Walker and Syers, 1976; Crews et al., 1995; Richardson et al., 2004; Parfitt et al., 2005; Eger et al., 2011; Izquiredo et al., 2013; Chen et al., 2015; Turner and Laliberté, 2015). The concentration of total organic P to 1 m depth, including the FF, on the Calvert Island chronosequence was also hump-shaped when plotted against age (Fig. 5-1).

Studies that have used P-NMR on chronosequences have used uncorrected data with the exception of Vincent et al. (2013) on the Väserbotten chronosequence, though the other studies note that due to the degradation of diesters, total diesters are underestimated (McDowell et al., 2007; Turner et al., 2007; Turner et al., 2014). The Väserbotten chronosequence did not have a significant decline in total P with age so it isn't directly comparable to the Calvert Island chronosequence, but it is interesting to note that Vincent et al. (2013) found that ~40% of non-IHP monoesters were degradation products of RNA. This illustrates the need to correct for degradation of organic P compounds within NaOH-EDTA extracts.

On the Franz Josef, Haast, Manawatu and Reefton chronosequences the proportions of DNA, pyrophosphates, *myo*- and *scyllo*-IHP increased with increasing age in the mineral horizon (McDowell et al., 2007; Turner et al., 2007; Turner et al., 2014). Similar increases in DNA, *myo*- and *scyllo*-IHP were observed in the mineral horizons on Calvert Island; however, an increase in pyrophosphates was not apparent. Interestingly, the potential

sorption mechanisms for DNA on the Franz Josef and Calvert Island chronosequences differ, with humic material stabilizing DNA on Franz Josef (Turner et al., 2007), and non-crystalline amorphous and organic Al on Calvert Island (Table 5-7). The organic horizon was analysed with P-NMR on the Haast chronosequence and had an increase in phospholipids (0.5-2.0 ppm), DNA and total polyphosphates (Turner et al., 2014). On Calvert Island, the H horizon had an increase in corrected monoesters and diesters with age that can be attributed to an increase in DNA, phospholipids, RNA, *myo*- and *scyllo*-IHP and the monoester 2 category. Total polyphosphates were variable with age on Calvert Island, so a clear trend was not apparent. Interestingly, phosphonates were not detected in the organic horizon on Haast (Turner et al., 2014), whereas phosphonates were detectable on all sites on Calvert Island and slightly increased in proportion with age. This suggests that wetter, more acidic soil conditions on Calvert Island compared to Haast caused a reduction in bacterial activity (Tate and Newman, 1982; Hawkes et al., 1984; Condron et al., 2005). Further studies of this site are warranted to confirm.

Turner et al. (2014) presented a figure of the total IHP concentration and amorphous Al+Fe with increasing age on Franz Josef, and the IHP concentration mirrored the amorphous Al+Fe concentration. The total IHP concentration exhibited a hump shape with the decline coinciding with the decline in amorphous Fe+Al. The decline in IHP may have been due to biological utilization of these compounds or due to a decline in the stabilization sites for IHP (Turner et al., 2014). In the Calvert Island chronosequence, IHP was also correlated to available and amorphous Al, and Al_o+ Fe_o although Fe alone was not correlated with IHP (Table 5-7). When Al_o+ Fe_o and total IHP concentration were graphed with age for the Calvert Island chronosequence, the IHP and Al_o+ Fe_o concentration curves were similar,

but the concentration of IHP increases or declines before Al_o+ Fe_o which is not like the Turner et al. (2014) data (Fig. 5-9; Table 5-5; Appendix 4). Turner et al. (2014) concluded that the changes in IHP concentration with age were most likely related to changes in P availability and organic P utilization rather than a change in P sorption sites. This is also supported by the Calvert Island data, where IHP concentration changed prior to Al_o+ Fe_o concentration that ended up mirroring the IHP concentration change.

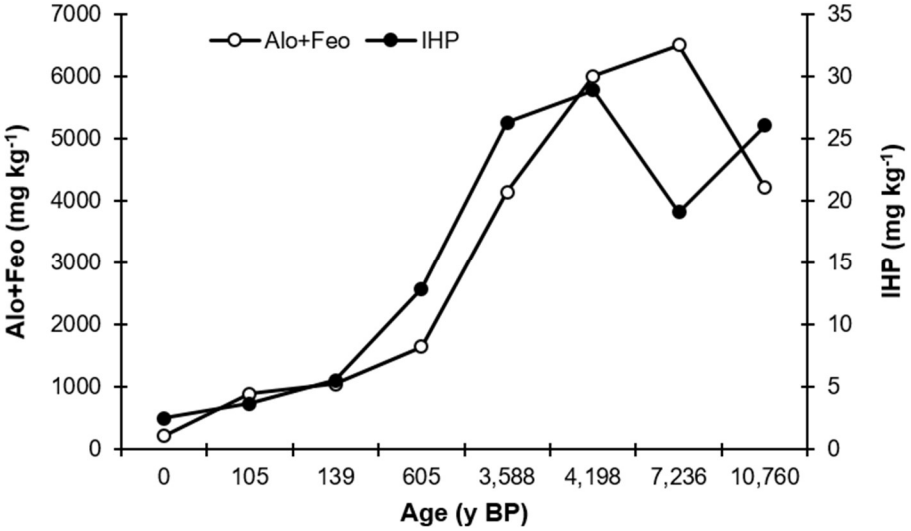

Figure 5-9. A comparison of inositol hexakisphosphate (IHP) including the *myo*-, *scyllo*-, D-*chiro*- and *neo*-IHP stereoisomers and amorphous aluminum (Al_o) and iron (Fe_o) extracted in acid-ammonium oxalate for the Calvert Island chronosequence.

The M:D ratio within mineral soil on the Manawatu and Reefton chronosequence declined with increasing age similarly to Calvert Island (McDowell et al., 2007). However, once the correction for monoesters and diesters was applied, the cM:D actually increased with age on Calvert Island. Due to the increased dominance of IHP with age on Manawatu and Reefton, the cM:D might also be comparable to Calvert Island, reflecting an increased dominance of corrected monoesters with age (McDowell et al., 2007).

5.5 Conclusion

Different processes controlled the amount and forms of P within different sample types. The L horizon had lower concentrations of total P than the foliage samples, but the forms of organic P within the L horizon were directly comparable to the foliage samples. The H horizons had similar forms of P as the L horizon, but there was a larger proportion of DNA and nucleotides than the L horizon and an increase in *myo*- and *scyllo*-IHP. The proportion of phosphonates increased within H horizons, most likely due to differences in the soil microclimate including wetter condition, different microbial communities due to a lower pH or different nutrient concentrations than the exposed L horizon. The main differences in P forms between the L and H horizon can be explained by microbial degradation and scavenging, because the OM within the H horizon was fully humified and the buildup of biological by-products was apparent. The mineral horizons were considerably different from the organic horizons, with a much lower total P concentration and an increased proportion and concentration of IHP and DNA with increasing age that was correlated to the increased concentration of available and amorphous Al forms.

With age, total P to a 1 m depth declined linearly while organic P displayed a hump-shaped curve, both of which are comparable to the Walker and Syers P model for ageing soils. As hypothesized, organic P became a more dominant pool of soil P with increasing age. In all sample types, orthophosphate declined with increasing age while the proportion of corrected diesters increased with age. A slight increase in the proportion of corrected diesters was seen in the foliage, and L and H horizon samples and a large increase in corrected monoesters within the mineral horizon was observed. The increase of corrected diesters in the L and H horizons were not due to an increased proportion of DNA with age as expected,

but rather because of the increased proportion of α- and β-glycerophosphates. The increase in corrected monoesters in the mineral horizon was due to the increased concentration of IHP and DNA; confirming the hypothesis that *myo*- and *scyllo*-IHP would increase with age. The increased concentration of IHP and DNA within the mineral horizon were correlated to total C and the increased concentration of organic and inorganically-bound amorphous Al. Also, the decline in exchangeable Ca+Mg coincided with an increase in exchangeable Al+Fe.

Overall the Calvert Island chronosequence was comparable to other chronosequences where the Walker and Syers P model has been successfully applied. The P results from the surrounding CWH zone were also comparable to the soils found on Calvert Island. This is the first time that the foliage, L, H and mineral horizons were examined in depth with P-NMR. In Hw and salal, *scyllo*-IHP was identified though it has previously not been found in plant matter, but foliage samples were not always taken directly from the trees due to sampling limitations and samples were not sterilized prior to analysis. Future research should examine sterilized Hw and salal samples to determine if *scyllo*-IHP is found in plant matter, or if it is a product of microbial degradation.

6 EVIDENCE OF ECOSYSTEM RETROGRESSION ON CALVERT ISLAND, BC

6.1 Introduction

Soil development occurring in stable landscape positions in the absence of catastrophic disturbance provides a unique situation for studying ecosystem succession (Wardle et al., 2004). In the past, studies focussed on the establishment and upbuilding seral stages, with most of the focus on the maximal biomass stage (Vitousek and Farrington, 1997; Wardle et al., 2004; Peltzer et al., 2010). Without a catastrophic disturbance, that maximal biomass phase in late primary or secondary succession cannot continue indefinitely; rather, primary productivity undergoes a decline phase following the maximal biomass stage (Wardle et al., 2004). This decline phase is known as ecosystem retrogression, which is the pronounced decline in primary productivity in aboveground biomass accompanying ageing soils in diverse environments (Wardle et al., 2004). Retrogression has been documented on 11 chronosequences worldwide ranging from xeric grasslands to humid subtropical forests, and exhibits characteristic changes in ecological functioning (Table 2-1; Wardle et al., 2004; Peltzer et al., 2010; Eger et al., 2011; Laliberté et al., 2012).

A simple metric used to determine if retrogression has occurred is tree basal area (BA), which is defined as the cross-sectional area of trees using the diameter at breast height (DBH) per hectare (Westman and Whitaker, 1975; Wardle et al., 2004; Peltzer et al., 2010). Most commonly the progressive buildup and maximal biomass phase are followed by a decline phase, creating a hump-shaped trend in BA over time (Wardle et al., 2004). In chronosequences exhibiting retrogression, plant diversity can either decline with increasing age (e.g. Franz Josef, Haast) or increase (e.g. Jurien Bay, Hawaii; Crews et al., 1995; Richardson et al., 2004; Walker et al., 2010; Eger et al., 2011; Laliberté et al., 2012). There is a marked shift in plant communities with age, regardless of plant diversity, with more

nutrient-demanding species on younger sites and more stress-tolerant, slow-growing species on older sites, as illustrated by the Waitutu, Mendocino, and Haast chronosequences (Jenny et al., 1969; Coomes et al., 2005; Eger et al., 2011). Soil microorganism communities also shift with age on retrogressive chronosequences, from bacterial-dominated systems on younger sites to fungal-dominated systems on older sites with greater nutrient limitations (Wardle et al., 2004; Williamson et al., 2005).

Variations in nitrogen (N) to phosphorus (P) ratios (N: P) of foliage and soil horizons have been used to identify possible limiting nutrients (van den Driessche, 1974; Ballard and Carter, 1986; Koerselman and Meuleman, 1996; Wardle et al., 2004). Across a range of chronosequences worldwide, these ratios generally indicate a shift from N limitation on young sites, to co-limitation by N and P on intermediate-aged sites and P limitation on older sites (Vitousek et al., 1995; Richardson et al., 2004; Parfitt et al., 2005; Izquierdo et al., 2013; Hayes et al., 2014). Over time, foliar and organic soil horizon N: P ratios may increase to a plateau, like a reverse logistic regression (Richardson et al., 2004; Hayes et al., 2014) or be hump-shaped (Vitousek et al., 1995; Wardle et al., 2004).

Nutrient ratios can only indicate potential nutrient limitations; a fertilization trial is the only true way to determine if a growth limitation exists, as indicated by an increase in plant growth directly associated with the nutrient addition (Koerselman and Meuleman, 1996; Laliberté et al., 2012). Nitrogen to P (N: P) ratios are frequently used in foliar and soil analysis but the method stemmed from ocean research where Redfield (1958) determined the ideal N: P ratio for ocean plankton, otherwise a limitation may exist. Koerselman and Meuleman (1996) further refined this ratio by examining 40 different studies using biomass N: P ratios within different ecosystems and determined that a N: P ratio < 14 indicated N

limitation whereas an N: P ratio > 16 indicated P limitation. In 2004, Güsewell suggested that within plant biomass an N: P ratio < 10 was N-limited and > 20 was P-limited. The ratio of N: organic P (N: Po) is a good indicator of N limitation within mineral soils because N mineralization has been found to be negatively related to N: Po and 90% of the variation of N mineralization rates was explained by N: Po ratios and total N concentration (Carlyle and Nambiar, 2001). With age, the N: Po ratio is expected to increase with increasing age and a C:Po ratio greater than 200 was associated with P-deficient soils (McGill and Cole, 1981).

Ecosystem retrogression can be caused by nutrient limitations, most commonly from N or P, or changes in soil that make them unfavourable for plant growth such as formation of a physical barrier (Vitousek et al., 2010). Retrogression can occur on all types of parent materials, though the mechanisms causing limitations to primary productivity may be different (Vitousek et al., 2010). For instance, some soils may have had adequate supplies of P in the past, but as the soils age significantly the reserve of P within the parent material became depleted, such as on the Hawaiian chronosequence (Vitousek and Farrington, 1997; Vitousek et al., 2010); other soils may have been inherently low in P from low-P parent materials, causing plant growth limitations faster with age than in soils developed on higher-P parent materials, such as the Cooloola chronosequence (Walker et al., 1983; Wardle et al., 2004; Vitousek et al., 2010). Physical barriers to plant growth such as cementation and waterlogging also can limit plant productivity due to impedance of roots and the mobilization of P under reducing conditions, as has occurred at Glacier Bay, Alaska (Noble et al., 1984; Chapin et al., 1994; Vitousek et al., 2010).

In the coastal temperate rainforest zone of British Columbia, there are extensive low-productivity forests dominated by western redcedar (*Thuja plicata;* Cw*)* and western

hemlock (*Tsuga heterophylla*; Hw; Banner et al., 2005; D'Amore et al., 2012) and shore pine (*Pinus contorta var. contorta*). Within the North Coast Timber Supply Area in British Columbia, within the Coastal Western Hemlock (CWH) zone very wet, hypermaritime variant (CWHvh2; Fig. 3-1), these low-productivity forests account for 12% of the supply area or 235,000 ha (Banner et al., 2005). Due to the increasing value of Cw and yellow cedar (*Chamaecyparis nootkatensis*; Yc), these lower-productivity areas became of interest economically for timber and fibre production, so a greater ecological understanding was needed and the factors affecting productivity were assessed (Banner et al., 2005). Banner et al. (2005) identified three factors that affected the productivity of these cedar-hemlock forests in the CWHvh2 variant: bedrock geology, soil drainage, and disturbance history. For example, a soil formed on metamorphic rocks with good drainage and frequent disturbance supported more productive forests than soils formed on igneous rock with poor drainage and limited disturbance (Banner et al., 2005).

Though there has been extensive forestry research within the North Coast Timber Supply Area, there is little knowledge about pedogenesis, including the time required to develop low-productivity forests and nutrient-limited soils (Banner et al., 1993; Banner et al., 2005). On the coast of British Columbia, there have been three documented soil chronosequences that have examined rates of pedogenesis in the CWH zone: Cox Bay, Naikoon, and Brooks Peninsula (Singleton and Lavkulich, 1987a, b; Maxwell, 1997; Sanborn and Massicotte, 2010). The Cox Bay chronosequence extended only 550 years (Singleton and Lavkulich, 1987a, b), while the Brooks Peninsula spanned 8,000 years, but the site ages were poorly constrained (Maxwell, 1997). The Naikoon chronosequence was well constrained, with ages determined by optically stimulated luminescence dating; however, limited research

has been performed, particularly related to forest productivity and nutrient availability (Sanborn and Massicotte, 2010). This limited body of existing research suggests the need for more study of the links between pedogenesis and forest productivity within the CWH biogeoclimatic zone.

This study aimed to examine soil development, P dynamics and forest productivity along a ~11,000-year chronosequence on Calvert Island within the CWHvh2 biogeoclimatic variant (Neudorf et al., 2015). On the coast of British Columbia, soils can be low in P and develop root restrictions with age caused by high water tables, high acidity and the development of cemented soil horizons (Banner et al., 1993; Banner et al., 2005; Kranabetter et al., 2005; Sanborn et al., 2011). The Calvert Island chronosequence provides a unique area where the parent material is coastal and aeolian sands so the main factors influencing above-ground productivity would be soil drainage and disturbance history, which influence nutrient availability (Banner et al., 2005).

The purpose of this chapter was to determine if ecosystem retrogression was evident on the older sites within the Calvert Island Chronosequence since changes in soil morphology and declines in total P were apparent. The first research hypothesis is that forest productivity would reach a maximum on the intermediate-aged sites followed by a decline (Wardle et al., 2004; Peltzer et al., 2010; Izquierdo et al., 2013) that would be caused by restrictions caused by soil development and P availability (Walker and Syers, 1976; Wardle et al., 2004; Banner et al., 2005; Sanborn et al., 2011). The second research hypothesis is that total carbon (C), N and P would follow the expected trends of the Walker and Syers (1976) P model. The third research hypothesis was that with increasing age, there would be a shift towards plant species adapted to nutrient-poor conditions (Jenny et al., 1969; Coomes et al., 2005; Eger et al.,

2011). The fourth and final hypothesis is that the N: P ratios would increase in foliage and humus with increasing age, similar to those illustrated in Wardle et al. (2004).

6.2 Methods

6.2.1 Study Area

This chronosequence was located on Calvert Island on the west coast of British Columbia (Figs. 1-4 and 1-5), and was dated by optically stimulated luminescence dating techniques (Table 3-1; Neudorf et al., 2015). Eight sandy landforms including beaches and coastal dunes were examined in this study, with ages ranging from that of a modern, established foredune (~0 a BP) to 10,760 a BP on a stabilized, relict coastal dune (Table 3-1).

6.2.2 Sample Collection and Analysis

Two pedons were sampled at each site and samples were taken from all genetic horizons. All soil samples were air dried and ground to 2 mm. For cemented horizons, a mortar and pestle were used to disaggregate the sample and a coffee grinder was used for organic samples. Soil was also sampled for bulk density and is explained in Chapter Four.

Total C analyses were completed to classify the soil samples as mineral (< 17 % organic C (OC)) or organic (> 17% OC; SCWG, 1998). In this study, total C was assumed to be OC as there were no carbonates in these soils. Total C, N and S were analysed by the Dumas ignition method, using a ThermoFischer Scientific Flash 2000 CHNS analyser (McGill and Figueiredo, 1993; Horneck and Miller, 1998). Details on the other methods and analyses of the soil samples can be found in chapters Four and Five, and appendices Two, Four and Five.

Foliage was collected from the three most dominant tree or shrub species in a 5-m radius plot around each pedon using an adapted Ballard and Carter (1986) method. Foliage samples were pruned by hand when possible and intact, green foliage was retrieved from the

ground if hand sampling was not feasible. Sampling was not limited to current year foliage because it was not possible to separate current and past year foliage on the older sites since there was clustered leaf growth and slow growth rates. All foliage samples were dried at 60˚C until repeated measures of weight were constant with time. Dried foliage samples were ground using a coffee grinder and were stored individually at room temperature in sealed Ziploc bags prior to analysis.

Individual foliage samples were analysed for total C and N using the same method for the soil samples (McGill and Figueiredo, 1993; Horneck and Miller, 1998). Total P was analysed at the Agri-Food and Agriculture Canada Swift Current Research and Development Center using Parkinson-Allen (1975) acid digestion and the Murphy and Riley (1962) colorimetric method. Western hemlock was one of the dominant tree species on 13 of the 16 sites, while Cw was dominant on 6 of the 16 sites but spanned all age classes.

6.2.3 Basal Area

Basal area is a surrogate method used to assess above-ground tree biomass and is the most common method used on chronosequences to determine whether ecosystem retrogression is occurring (Wardle et al., 2008; Gaxiola et al., 2010). The National Forest Inventory protocols were adapted for calculation of BA in this study (NFI, 2008). A fixed-radius plot of 3.99 m was used. The first BA plots were completed on a narrow dune and only 3.99-m radius plots could fit along the dune. All trees over 9 cm at DBH were measured to one mm, whereas trees less than 9 cm DBH were tallied according to size class (0-2.9, 3.0-5.9, and 6.0-8.9 cm DBH). Basal area was replicated three times per site. On foredunes, plots ran lengthwise along the dune.

6.2.4 Data Analysis

All data were analysed with STATA 14 IC data and statistical analysis software. Linear and non-linear regression analyses were performed on the mass of total C, N and P mass to a one m depth. For each element, the following models were used to examine the data; linear, second order polynomial, Michaelis-Menton, logarithmic and exponential models (decay or increase). Akaike's information criteria was used to determine which model fitted best (Gotelli and Ellison, 2004) and only models that realistically represented pedogenic processes were used (Schaetzl et al., 1994). For example, total C may exhibit an exponential increase at the beginning stages of succession; however, that trend cannot be maintained throughout all successional states because studies have shown that it will plateau or accumulate at decreasing rates with time (Schaetzl et al., 1994; Wardle et al., 2004). Therefore, it was best to choose a model that illustrated long-term trends more accurately, such as a Michaelis-Menton or a second-order polynomial model.

Correlation analysis was performed on the mass of C, N, and P (total and organic) within a 1-m control section of the soil profile, including the forest floor (FF), where the FF includes all surface organic horizons (eg., L, F and H horizons), and the C, N, and P (total and organic) mass to a 30-cm depth of mineral soil and N and P concentrations within Hw. The presence of cementation, seepage and FF thickness were also noted. The Shapiro-Wilk normality test and visual examination of box plots using Stata 14 IC for each parameter (α=0.05) were performed. Only organic P to a 30-cm depth of mineral soil was not normally distributed so non-parametric correlation (Spearman) was used. The presence of cementation was a categorical variable so non-parametric correlation was also used on these data. Parametric pair-wise correlations (pwcorr) were used to test all other soil parameters. The Bonferroni multiple comparison correction factor was utilized in all correlation analysis.

6.2.5 Site Series and Ground Cover Estimation

A small Daubenmire frame (0.1 m^2) was used to determine the percent cover by category, including moss, rock, wood, bare mineral soils, and plant litter (ABMI, 2014). Ground cover determination was replicated three times surrounding each pedon, so a total of six Daubenmire plots were completed per site. The frame was randomly thrown onto the ground to capture representative locations.

Using the BC Ministry of Forests Land Management Handbook No. 25 for describing terrestrial ecosystems in the field, the most appropriate site series within the CWHvh2 variant was identified for each replicate (MOFLR, 2010). Dominant plant species were also noted by Lee-Ann Nelson and Lori Johnson for each replicate including trees, shrubs and all ground cover species.

6.3 Results

6.3.1 Ecosystem Succession and Soil Development

The youngest site was the only site with bare ground and a dominant cover of grass, forbs and herbaceous plants with a significant proportion of litter (thatch on the youngest dune) cover (Fig. 6-1). With increasing age, the proportion of litter cover declined while shrubs (< 0.5 m), forbs and herbaceous plants increased in abundance. The proportion of forbs and herbaceous plants were inversely related to shrub cover (0.5 m). Lichen and trees (< 0.5 m) were only dominant on the oldest site, 10,760 a BP. Wood cover was present on most sites, but represented a greater proportion of cover after 105 and 3,588 a BP. The proportion of moss was greatest after 139 and 7,236 a BP (Fig. 6-1).

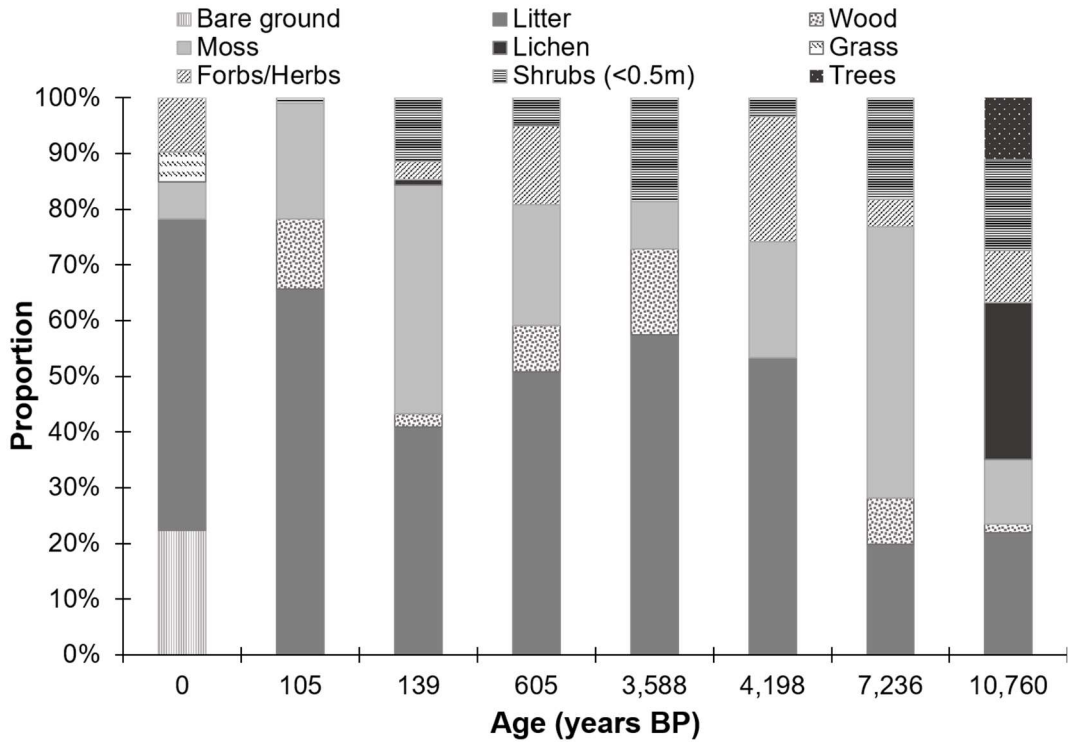

Figure 6-1. Percent cover of dominant cover classes found on each site (n=6).

Basal area was variable along the chronosequence, indicated by the error bars and variation in average values (Fig. 6-2). The youngest site did not have any trees over 1.3 m height (Appendix 3). With increasing landform age, the average BA increased up until ~3,588 years (stage 5) followed by a decline, with the exception of the site aged 605 a BP (CIDS9; stage 4; Fig. 6-2). Within the 605 a BP site, there was not a consistent successional stage due to the prevalence of tree fall and young Cw trees (Appendices 2 and 3).

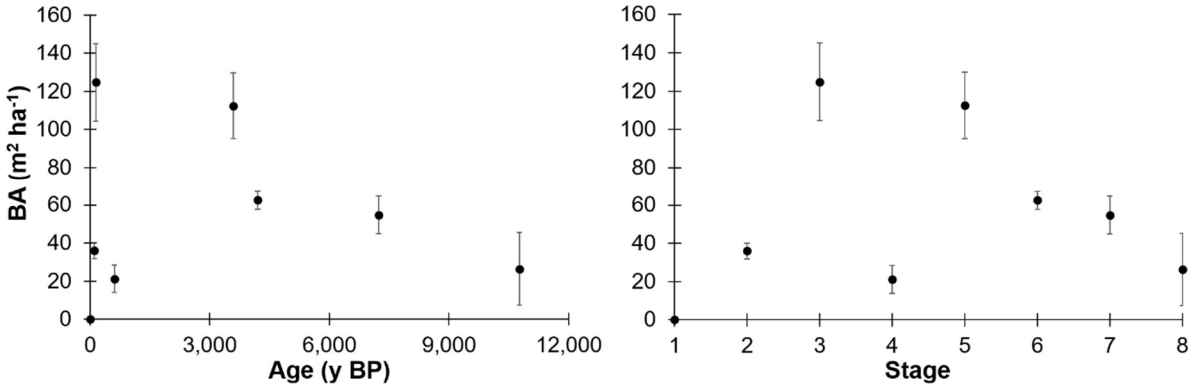

Figure 6-2. Tree basal area (BA) on each site by age (a) and chronosequence stage (b) with stage one equivalent to 0 a BP and stage eight represents 10,760 a BP (n=3). Standard deviation is indicated by error bars.

Representative photographs of the youngest site, ~0 a BP, an intermediate site, 3,588 a BP, and the oldest site, 10,760 a BP, display the build-up phase, maximal biomass phase and decline phase, respectively, illustrating the decline in aboveground biomass with increasing age (Fig. 6-3).

With increasing age, the forest floor (FF; inclusive of the L, F and H horizons) thickness did not continually increase; rather, the depth fluctuated depending on the site conditions (Fig. 6-4). By 605 years a organic-enriched cemented ortstein had started to form and by 3,588 years strongly developed ortstein and placic horizons had formed (Fig. 6-4). These cemented horizons prevailed on all sites older than 605 years. Basal area was greatest on the 139 and 3,588 a BP site, followed by a decline and an associated shift towards trees species that are known to grow in more nutrient-poor conditions, shore pine (*Pinus contorta* var. *contorta*; Pc) and Yc (Figs. 6-2 and 6-4, Appendix 3; Banner et al., 2005).

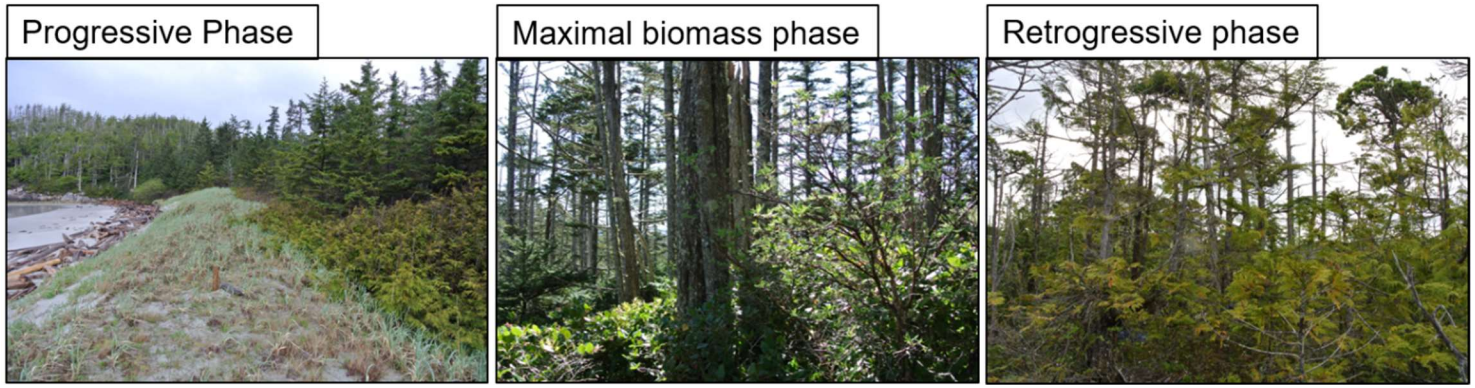

Figure 6-3. Characteristic photographs of the three successional stages present on the Calvert Island chronosequence; the progressive (build-up) phase (~0 a BP; CIDS1), maximal biomass phase (3,588 a BP; CIDS8) and the retrogressive (decline) phase (10,760 a BP; CIDS10).

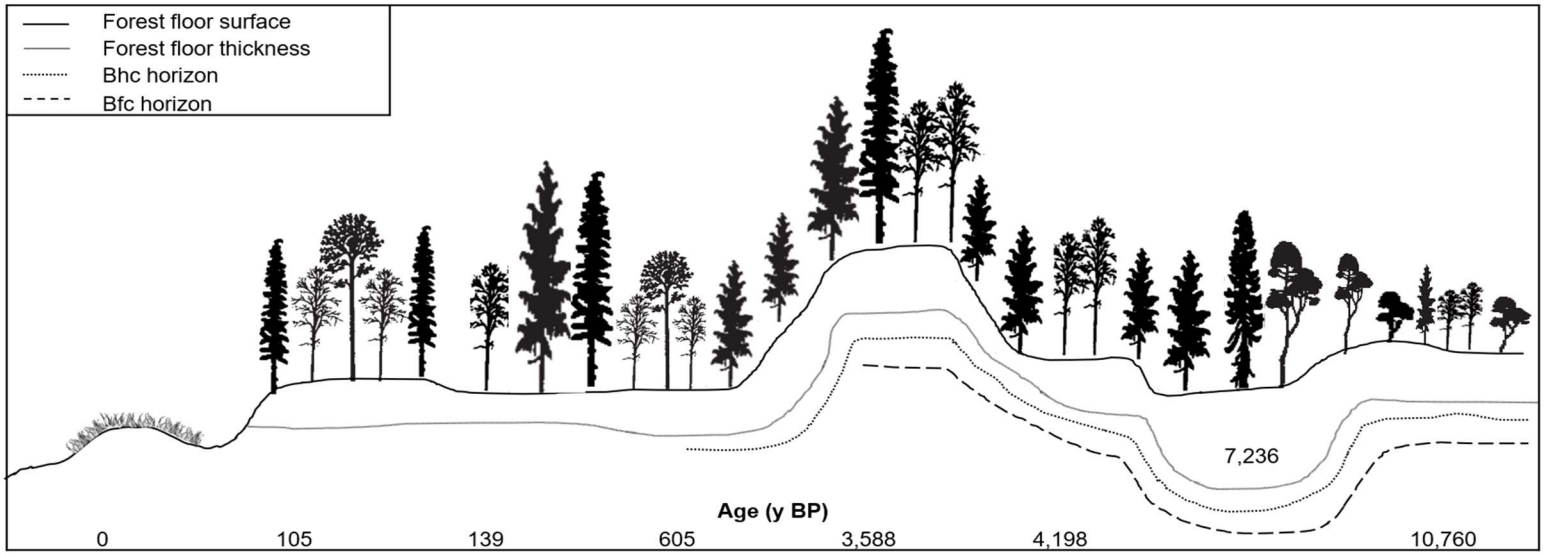

Figure 6-4. Visual depiction of soil and forest development with increasing age along the Calvert Island chronosequence including the development of cemented ortstein (Bhc) and placic (Bfc) horizons with age and the dominance of stunted tree growth on the oldest sites. Note that diagram is not to scale. Tree icons adapted from Banner et al. (1993).

Plant communities on the Calvert Island chronosequence shifted from early successional plant communities on the youngest site (~0 a BP) to climax plant communities on intermediated-aged site (3,588 and 4,198 a BP), followed by a less-productive plant community that were adapted to poorer soil conditions by 10,760 years (Table 6-1). The youngest site had an early seral stage plant community consisting mostly of grasses (dune wildrye (*Elymus mollis*) and red fescue (*Festuca rubra*)) with other species that grow easily on recently disturbed landscapes including yarrow (*Achillea millifolium)*, Indian paintbrush (*Castilleja miniata*), strawberry (*Fragaria chilonensis*) and peavine (*Lathyrus japonicus;* Table 6-1). Red alder (*Alnus* rubra; Dr) was only present on sites aged 105 and 605 a BP. Sitka spruce (*Picea sitchensis*; Ss) was present on most intermediated-aged sites from 105 years to 4,198 years (Table 6-1). After 7,236 years, Yc, mountain hemlock (*Tsuga mertensiana*) and shore pine (*Pinus contorta* var. *contorta*; Pc) became more dominant tree species and were associated with an increase in the presence of sphagnum moss and Labrador tea (*Ledum groendlandicum*; Table 6-1).

Table 6-1. Biogeoclimatic (BEC) site series classification for each site and presence and absence data from plant surveys (n=2) using Latin and common plant names (X indicates presence) (Green and Klinka, 1994).

Latin Name	Common Name	Site Age (a BP) and BEC Site Series Classification							
		~0	**105**	**139**	**605**	**3,588**	**4,198**	**7,236**	**10,760**
		N/A	15 - Ss	01 - CwHw	03a - CwYc	14 - Ss	01 - CwHw	11 - CwYc	11 - CwYc
Achillea millifolium	Yarrow	X							
Alnus rubra	Red alder		X		X				
Arctostaphylos uva-ursi	Kinniknick							X	
Blechnum spicant	Deer fern		X	X	X		X	X	
Castilleja miniata	Indian paintbrush	X							
Chamaecyparis nootkatensis	Yellow cedar							X	X
Cladina portentosa	Coastal reindeer lichen								X
Coptis asplenifolia	Goldthread							X	X
Cornus canadensis	Bunchberry				X		X	X	X
Elymus mollis	Dune wildrye	X							
Empetrum nigrum	Crowberry								X
Festuca rubra	Red fescue	X							
Fragaria chilonensis	Coastal strawberry	X							
Gaultheria shallon	Salal		X	X	X	X	X	X	X
Hylocomium splendens	Step moss				X		X		
Lathyrus japonicus	Purple peavine	X							
Ledum groendlandicum	Labrador tea							X	X
Lonicera involucrata	Black Honeysuckle				X				
Menziesia ferruginea	False azalea				X	X	X	X	X
Mianthemum dilatatum	False lily of the valley		X		X		X	X	X
Picea sichensis	Sitka spruce		X	X		X	X		
Pinus contorta	Shore pine							X	X
Polystichum munitum	Sword fern		X						
Pterdium aquilinum	Bracken fern		X		X				
Rhytidiadelphus loreus	Lanky moss				X		X		
Rubus spectabilis	Salmonberry		X		X	X			
Smilacina racemosa	False Solomon's seal				X				
Sphagnum sp.	Sphagnum							X	X
Thuja plicata	Redcedar			X	X	X	X	X	X
Tsuga heterophylla	Western hemlock		X	X	X	X	X	X	X
Tsuga mertensiana	Mountain hemlock							X	
Vaccinium parvifolium	Red Huckleberry			X					
-	Upland moss		X	X		X	X	X	X
Vaccinium sp.	-		X		X		X	X	

6.3.2 Carbon, Nitrogen and Phosphorus

The mass of C to one m depth, including the FF, increased with age up to 7,200 years BP and then plateaued, and was fit with a Michaelis-Menton non-linear model (Fig. 6-5). The highest C mass was present on the 7,236 a BP site (47261 g m^{-2}, CV=20%) and the lowest was on the youngest site (~0 a BP; 6262 g m^{-2}, CV=11%). The 105 a BP site had more C to 1 m depth compared to the 139 a BP site (15129 g m^{-2}, CV_{105}=4% vs. 8126 g m^{-2}, CV_{139}=39%). Total C on the oldest site (10,760 a BP; 23897 g m^{-2}, CV=27%) was less than on the 7,236 a BP site.

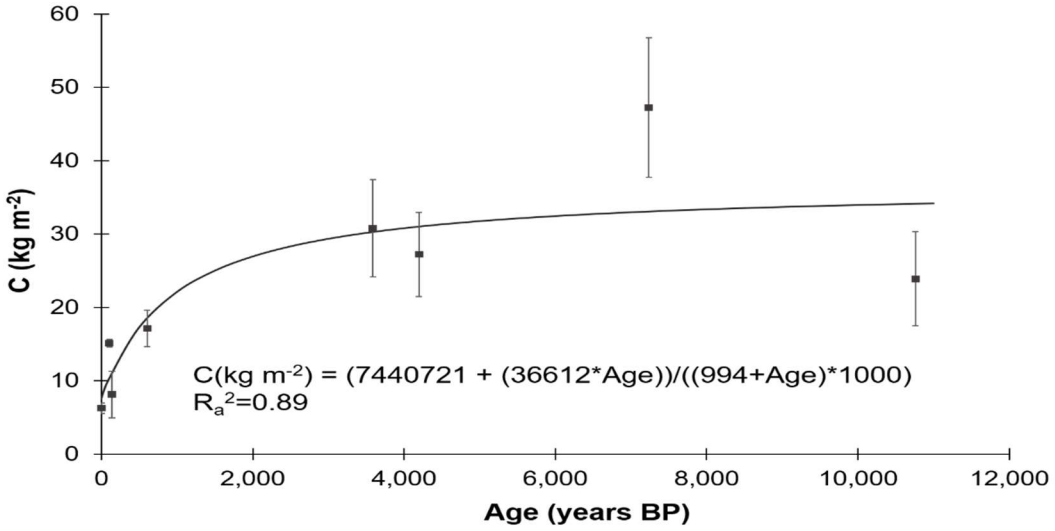

Figure 6-5. Average mass of carbon (C) to 1 m depth for each site including the forest floor with one standard deviation (n=2).

The mass of total P was greatest on the youngest sites followed by a decline, whereas N mass was least on the youngest sites, increased to a maximum around 7,200 years BP and then declined (Fig. 6-6). Total P exhibited a linear decline with age. The 105 a BP site had the greatest total P mass (254 g m^{-2}, CV=13%) compared to the oldest site (10,760 a BP), which had the least (103.3 g m^{-2}, CV=18%). A second-order polynomial model fitted the total N data best. Total N mass was least on the youngest site (~0 a BP; 68 g m^{-2}, CV=15%)

and greatest on the 7,236 a BP site (871 g m^{-2}, CV=17%). Interestingly the 105 a BP site had higher total N mass (361 g m^{-2}, CV=8%) than the 139 a BP site (172 g m^{-2}, CV=29%).

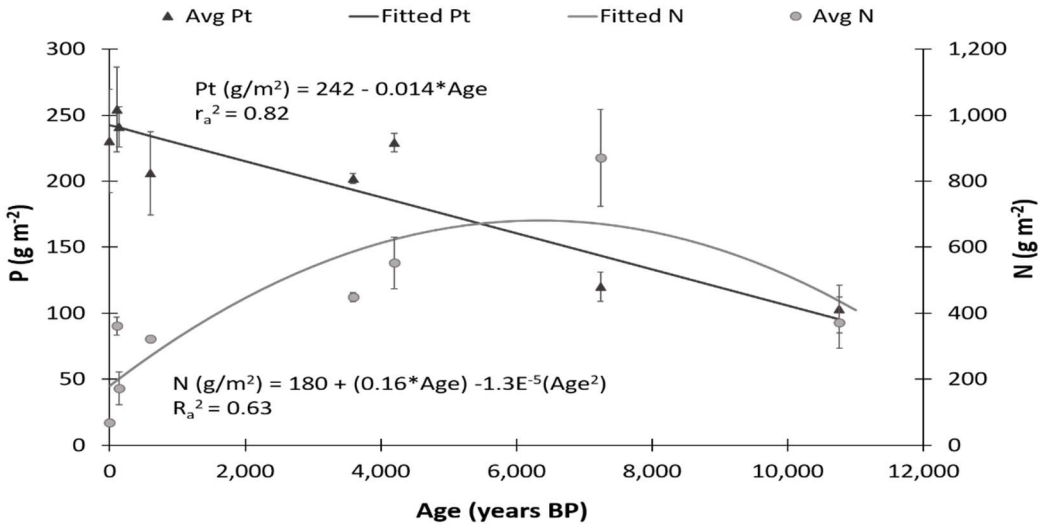

Figure 6-6. Average mass of total phosphorus (Pt) and nitrogen (N) to 1 m depth for each site including the forest floor with one standard deviation (n=2; note: two axis).

6.3.3 Nutrient Ratios

Within the foliage samples of Cw and Hw, there was a slight increase in the N: P ratio with increasing age ranging from 6.9 (139 a BP) to 10.1 (10,760 a BP) for Cw and 3.8 (605 a BP) to 10.9 (7,236 a BP; Fig. 6-5a). The N: P of litter also increased slightly with age ranging from 8.4 (139 a BP) to 14.8 (10,760 a BP Fig. 6-5a). The C: P increased considerably with increasing age in both foliage species (Cw; 366 (139 a BP) to 1108 (10,760 a BP): Hw; 271 (605 a BP) to 979 (10,760 a BP)) and the litter (492 (139 a BP) to 1259 (10,760 a BP)); Fig. 6-5b). The N to organic P ratio was consistent in the litter with age (14.5 (3,588 a BP) to 21.5 (105 a BP); Fig. 6-5c) whereas the C to organic P ratio increased considerably (936 (139 a BP) to 1668 (10,760 a BP); Fig. 6-5d).

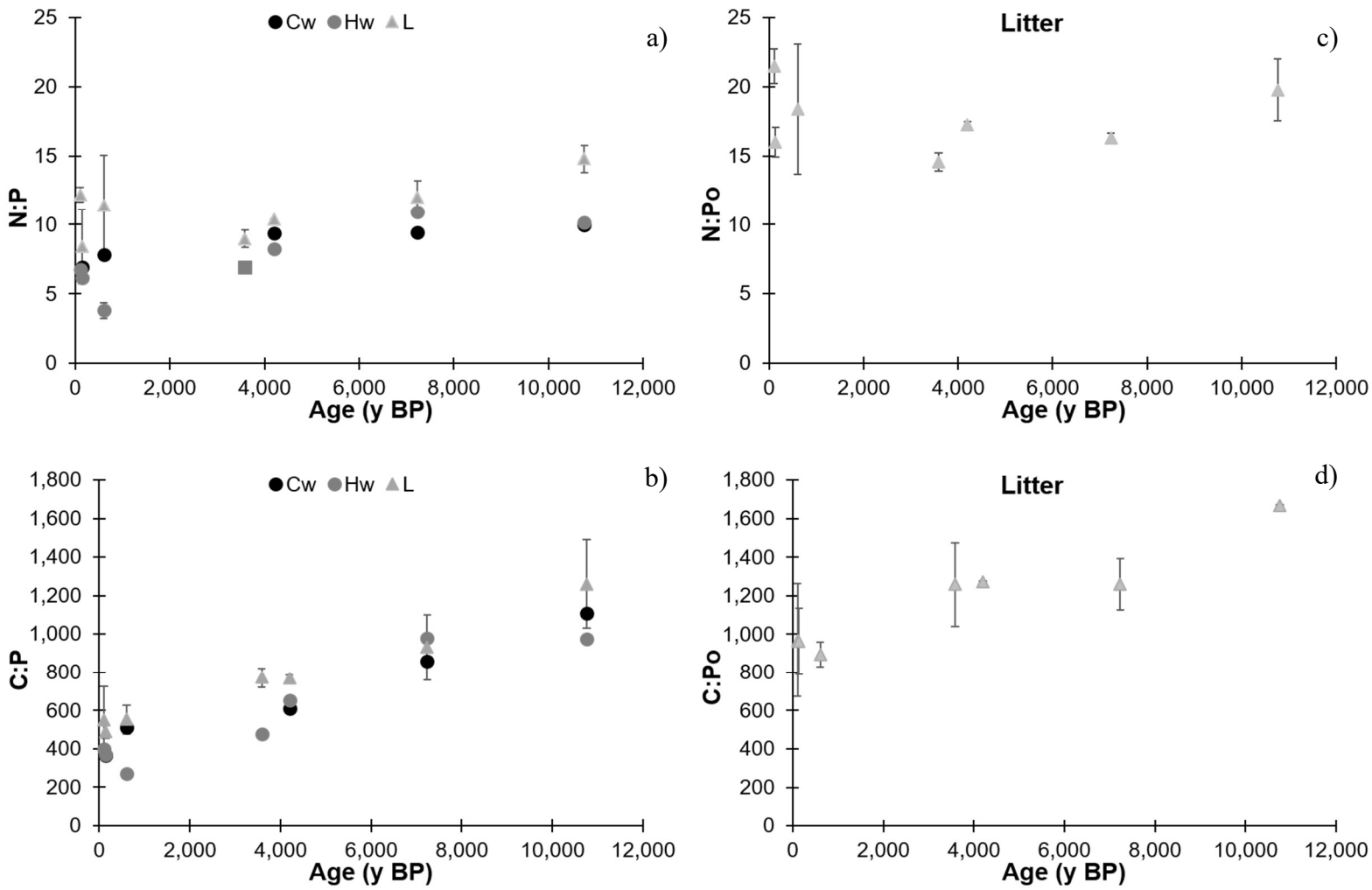

Figure 6-7. Nitrogen to phosphorus ratios (N: P) (a) and carbon to phosphorus (C: P) ratios (b) within foliage samples of western redcedar (Cw) and western Hemlock (Hw), and litter samples along the Calvert Island chronosequence and nitrogen to organic phosphorus (N: Po) ratios (c) and C: Po ratios (d) for litter (n=2 except for select foliage samples without duplicates).

Up until 7,000 years the C: P and C: Po ratios within the FH horizon remained relatively consistent (with the exception of a peak on the 3,588 a BP site) and then increased with age (Table 6-2). The N: P ratios within the FH horizon were consistent along the chronosequence, whereas the N: Po ratios were variable but overall unchanged with age (Table 6-2). Peaks in all nutrient ratios within the mineral horizons were observed on CIDS9 (Table 6-2). The C: P and C: Po ratios within the mineral horizon increased with age, with the largest increase between 139 and 3,588 a BP (with exception of the 605 a BP site; Table 6-2). The N: P ratio within the mineral horizon was less than one for the first 105 years, followed by an increase to four (10,760 a BP) with exception of the 605 a BP site. The N: Po ratio ranged from five (~0 a BP) to 22 (10,760 a BP), illustrating an increase with increasing age (Table 6-2).

Table 6-2. Nutrient ratios for the fermentation and humic organic horizons (FH) and the upper 30 cm of mineral soil (M) including carbon (C) to phosphorus (P), C to organic P (Po) and nitrogen (N) to P and Po. The standard deviation is noted in the brackets (n=2).

Type	**Age**	**Site**	**C: P**	**C: Po**	**N: P**	**N: Po**
FH	105	CIDS3	804 (108)	1170 (101)	2 (0)	27 (1)
	139	CIDS4	556 (70)	1085 (67)	1 (0)	19 (0)
	605	CIDS9	764 (96)	1087 (166)	2 (0)	23 (2)
	3588	CIDS8	1332 (68)	1906 (73)	2 (0)	23 (0)
	4198	CIDS15	678 (37)	1025 (60)	2 (0)	23 (3)
	7236	CIDS16	1343 (124)	1710 (108)	2 (0)	30 (2)
	10760	CIDS10	1667 (196)	2178 (326)	2 (0)	26 (0)
M	0	CIDS1	23 (7)	338 (140)	0 (0)	5 (5)
	105	CIDS3	9 (3)	187 (119)	0 (0)	5 (3)
	139	CIDS4	24 (6)	299 (122)	1 (0)	9 (2)
	605	CIDS9	818 (1120)	1717 (1767)	8 (11)	20 (12)
	3588	CIDS8	205 (133)	1095 (738)	2 (1)	12 (5)
	4198	CIDS15	383 (66)	1127 (263)	6 (0)	17 (1)
	7236	CIDS16	135 (26)	789 (181)	3 (0)	17 (3)
	10760	CIDS10	233 (181)	1101 (165)	4 (3)	22 (2)

6.3.3.1 Foliar Nitrogen and Phosphorus

Nitrogen declined from 9.7 g kg^{-1} after 139 a BP to 4.5 g kg^{-1} after (10,760 a BP within Cw, and between 8.0 g kg^{-1} after 105 a BP to 5.1 g kg^{-1} after 10,760 a BP within Hw (Table 6-3). Within Cw, P declined from 1.4 g kg^{-1} after 139 a BP to 0.4 g kg^{-1} after 10,760 a BP (Table 6-3). The concentration of P within Hw declined from 1.2 g kg^{-1} after 105 a BP to 0.5 g kg^{-1} after 10,760 a BP with a peak in foliar P concentration on the 605 a BP site with 1.8 g kg^{-1} (Table 6-3).

Table 6-3. Foliar nutrient concentrations for western redcedar (Cw) and western hemlock (Hw) for nitrogen (N) and phosphorus (P) along the Calvert Island Chronosequence.

Species	Age	N (g kg^{-1})	P (g kg^{-1})
Cw	139	9.7	1.4
Cw	605	7.5	1.0
Cw	4,198	7.6	0.8
Cw	7,236	5.5	0.6
Cw	10,760	4.5	0.4
Hw	105	8.0	1.2
Hw	139	8.0	1.3
Hw	605	6.7	1.8
Hw	3,588	7.3	1.1
Hw	4,198	6.2	0.8
Hw	7,236	5.5	0.5
Hw	10,760	5.1	0.5

6.4 Discussion

6.4.1 Ecosystem Succession

The youngest site in the Calvert Island chronosequence (~0 a BP), which was a modern established coastal foredune, had a distinct plant community because of the disturbance regime created by proximity to the ocean and the constant erosional and depositional processes of aeolian and littoral processes occurring near or on this dune. Bare ground and thatch made up most of the ground cover on the youngest site, with smaller proportions of grass, forbs and herbaceous species (Fig. 6-1). With increasing age, there was

a shift towards less litter cover on all sites with an associated increase in forbs, herbaceous plants and shrubs < 0.5 m tall. The proportion of forbs and herbaceous plants was inversely related to shrub cover. The younger (stabilized, forested foredunes) to intermediate (relict dunes) sites on this chronosequence had the greater above ground biomass, measured by BA (Fig. 6-2). With a more developed overstory, less light reaches the FF, preventing the establishment of a large population of understorey plants; instead, the soil surface is litter dominated. On the oldest relict dune, there was declining tree BA and, most likely an associated increase in the amount of sunlight able to penetrate, which promoted the growth of understorey plants and decreased the proportion of litter cover (Fig. 6-2).

Interestingly, the oldest relict dune (10,760 a BP) was the only site with a considerable proportion of lichen, and trees < 0.5 m tall. Generally, lichen cover is associated with drier sites and a reduced cover of moss (Banner et al., 1993; Green and Klinka, 1994), though on the oldest site (10,760 a BP) there was more lichen cover than moss, even though there was sphagnum moss, indicating wetter conditions. On the west coast of British Columbia, it is common to find reindeer lichen (*Cladonia* spp.) growing within and around fens and bogs as well as forming blankets on top of moss in areas less well-drained than the oldest site on the Calvert Island chronosequence (Munger, 2008). The BA on the oldest relict dune (10,760 a BP) was much less than the intermediate-aged sites and the health of the trees was diminished, as indicated by the krummholz phenotypes and fire scars (Fig. 6-2; Appendix 2). The reduced BA and stunted growth of trees may have provided a good location for the establishment of small trees because of the decrease in canopy cover.

Banner et al. (2005) found that an increase of moss cover was associated with lower productivity sites and the decline in soil drainage, so moss cover was expected to be greatest

on the wettest sites; however, that was not the case. Sites ages 139 and 7,236 a BP had the greatest proportion of moss cover, but the 139 a BP site was a well-drained site with less understorey cover than other sites, such as those aged 105 and 605 a BP, so litter and moss dominated the ground cover, with moss commonly living on decomposing logs and detritus. The 7,236 a BP site was a wetter microsite, so a large proportion of moss cover was expected. To fully understand how vegetation cover correlates with age and site drainage on this chronosequence, future studies should examine percent cover by stratum rather than grouping all types of cover under 0.5 m into the same visual area. Woody debris cover was greatest on the 105 a BP site, where there were many fallen and dead trees, and on the 3,588 a BP site, where debris from salal was dominant.

Basal area along the Calvert Island chronosequence had a hump-shaped curve as expected for a retrogressed chronosequence. Unfortunately, the successional stage throughout the 605 a BP site was not consistent because there was a large portion that had experienced significant tree fall. One of the BA measurement plots had to be in a relatively open shrub area, and one was in a recent tree fall area with many young redcedars. Only one of the three BA plots were in a mature forest so there was high variability within the 605 a BP site BA data (Appendix 3). Tree fall is an important aspect of the natural disturbance regime in a mature forest, but it is difficult to discern whether tree fall occurred on each site of the chronosequence around the same time (~ 600 a BP) or not. Tree fall occurs frequently on Calvert Island, mainly during winter storms, because the trees are shallow rooted; trees rarely live longer than 300 years (Walker, pers. comm., 2018). If the 605 a BP site was not disturbed, it would be expected that the period of maximal biomass would be between 139 to 3,588 years.

The younger- to intermediate-aged sites (105 – 4,198 y) are the only sites on the chronosequence with Ss and Dr, which are species commonly found on higher-productivity forest sites on the coast of British Columbia. The older sites (7,236 – 10,760 y) became increasingly dominated by Yc, Pc, and mountain hemlock that are indicative of poorer site conditions and low productivity (Banner et al., 2005; Kranabetter et al., 2005). The older sites also had Labrador tea and sphagnum moss, commonly found on wetter, poorly drained sites (Banner et al., 2005). The younger and intermediate-aged sites had more productive forest types CWHvh2 – 01 CwHw Salal and 15-Ss Kindbergia whereas the older sites were 11-CwYc goldthread, which are classified as low-productivity forests (Kranabetter et al., 2005).

With increasing age, it is apparent that there was a change in soil morphology along the Calvert Island chronosequence that affected soil drainage and may be related to the shift towards species adapted to nutrient-poor conditions and those adapted to poorly drained soils including Labrador tea and Crowberry (*Empetrum nigrum*; Banner et al., 2005). The BA also followed the characteristic hump-shaped curve (Wardle et al., 2004), so it can be assumed that the Calvert Island chronosequence was experiencing ecosystem retrogression on the latter stages of the chronosequence. Retrogression may be caused by changes in soil morphology or nutrient limitations, most often of which are N or P (Wardle et al., 2004; Turner et al., 2012a; Coomes et al., 2013).

6.4.2 Changes in Nutrients with Age

6.4.2.1 Total Carbon, Nitrogen and Phosphorus Within Soil

On Calvert Island, total C followed the expected trend of increasing to a maximum and plateauing with increasing age (Fig. 6-5; Wardle et al., 2004; Wardle et al., 2008; Peltzer et al., 2010; Rossi and Rabenhorst, 2016). Total P declined linearly with age, which is

characteristic of the initial stage of the Walker and Syers (1976) model (Figs. 1-3 and 4-6). Total P content is expected to plateau eventually, exhibiting a trend that would more closely resemble an exponential trajectory (Syers et al., 1969; Stevens and Walker, 1970; Walker and Syers, 1976). The humped-shaped curve of N mass on the Calvert Island chronosequence is expected on long-term chronosequences (Fig. 6-6); N is not inherited from the parent material and must be fixed biologically, which takes time and energy (Selmants and Hart, 2008; Laliberté et al., 2012; Turner et al., 2012a; Chen et al., 2015).

The variation in the mass of C and N on site CIDS4 can be accounted for by the slightly thicker L and F horizons, which had higher C and N contents, on CIDS4B and a more nutrient enriched Bhj horizon (Appendix 4). Site CIDS10 also had high variability for C and N (CV=27, 21%, respectively) that can be attributed to the lower C content and thinner ortstein horizon at CIDS10B.

6.4.2.2 Potential for Nutrient Limitations

The N: P ratio within Cw and Hw foliage samples did slightly increase with age, though the largest N: P was less than the Redfield and Koerselman and Meulman ratio and suggests no limitation of P to plant growth unlike on the Jurien Bay, Haast, Franz Josef and Mendocino chronosequences (Fig. 6-7a; Richardson et al., 2004; Turner et al., 2012a; Izquieredo et al., 2013; Hayes et al., 2014). Total N and P concentrations in Cw and Hw declined consistently along the Calvert Island chronosequence (Table 6-3). Since foliage sampled was not limited to current year foliage, caution must be used when interpreting the foliar nutrient status (Ballard and Carter, 1986).

The N: P ratios within the litter samples also slightly increased with increasing age just above the Redfield (1958) ratio and within the co-limitation region for Koerselman and

Meuleman (1996) and Güsewell (2004; Fig. 6-7a). Results from a meta-analysis confirmed a global trend where the N: P ratios of litter were greater than in live foliage in all forest types like on the Calvert Island chronosequence (Fig. 6-7a; McGroddy et al., 2004). The mineral soils on Calvert Island had much lower N: P ratios compared to other chronosequences spanning similar ages such as the Haast, Jurien Bay and Cooloola chronosequences (Turner et al., 2012a; Hayes et al., 2014; Chen et al., 2015).

Within the litter the N: Po ratios varied little with increasing age (Fig. 6-7c). Kranabetter et al. (2005) compared N: Po ratios within the FF and mineral soils among forest productivity types within the CWH zone, and also noted little variation. The N: Po ratios within mineral soils on Calvert Island were comparable to the N: Po of the A horizon on the Mendocino chronosequence (Izquierdo et al., 2013).

There was a considerable increase in C: P ratios within Cw, Hw and litter samples and in increase in the C:Po of the FH horizon along the Calvert Island chronosequence similarly to the Haast chronosequence that had a C:P of 1008 after 3903 years (Figs. 6-7b and 6-7d; Turner et al., 2012a). The C:Po of the FH horizons on Calvert Island were ~1,100 after 100 years on Calvert Island and reached a maximum C: Po of 2178 after 10,760 years indicating likely P limitation (Table 6-2). Kranabetter et al. (2005) compared the C: Po ratios within FF among forests of different productivity and found that lower-productivity forest had higher C: Po ratios, like the Calvert Island chronosequence (Fig. 6-7d). Parfitt et al. (2005) evaluated C: Po ratios on the Volcanic Substrate age gradient, and Franz Josef and Waitutu chronosequences within the FH horizon and the first 10 cm of mineral soil. The maximum C: Po ratio within mineral soils was ~1200 after ~100,000 years on the Waitutu

chronosequence, which is comparable to the C: Po on Calvert Island of 1101 after 10,760 years (Table 6-2; Parfitt et al., 2005).

The mass of C, N and P within the soil exhibit similar trends to the nutrient ratios since C increased to a plateau in the soil and P declined with age, the C:P in the soil increased with age, which is also observed in the foliage, litter and organic soils (Figs. 6-5 to 6-7; Tables 6-2 and 6-3). The rate of P loss is greater than the loss of N (after the maximum was reached) in the soil causing an increasing N: P, which is also observed in the foliage, litter and organic soils (Figs. 6-5 to 6-7; Tables 6-2 and 6-3). This suggests that the change in nutrient ratios with age is directly related to the changes in soil nutrient stocks with increasing age.

6.4.3 Soil Development

Until the meta-analysis of Vitousek et al. (2010), retrogression was more frequently associated with a depletion-driven system where P within the soil has been utilized and lost with increasing age, causing a reduction in primary productivity (Walker and Syers, 1976; Wardle et al., 2004). In Vitousek et al. (2010), other causes of retrogression were highlighted such as soil barriers, low P parent material, transactional limitations when releasing P from parent material is difficult, and anthropogenic causes. Two retrogressive chronosequences in Wardle et al. (2004), Waitutu and Glacier Bay, had severe alterations to soil drainage associated with ecosystem succession as well as P limitations. Mendocino is another well-known case study where iron pans formed on older sites, and may be part of the cause for ecosystem retrogression (Table 2-1; Jenny et al., 1969). The Haast chronosequence had placic horizon formation in < 4,000 years and is suspected to have ecological significance in the progression of retrogression (Turner et al., 2012a).

The Calvert Island chronosequence showed evidence for the formation of cemented horizons by 605 years and characteristic placic and ortstein cemented horizons by 3,588 years (Fig. 4-8). After 3,500 years, seepage was identified on all sites except for on the oldest site (10,760 a BP). By 7,236 years, crowberry (*Empetrum nigrum*), Labrador tea (*Ledum groenlandicum*), and sphagnum moss (*Sphagnum* sp.) were present as well as Yc, mountain hemlock and Pc, which are indicators of low-nutrient sites, generally with impeded water drainage (Green and Klinka, 1994; Banner et al., 2005). The same plant species were also identified on the oldest sites on the Glacier Bay chronosequence after 11,000 years (Wardle et al., 2004). Noble et al. (1984) concluded that Podzolization caused the rising of water tables in Glacier Bay, which was further accelerated by the presence of sphagnum moss. Sphagnum moss is a wetland indicator species that can accelerate paludification by further raising the water table, and increasing waterlogging because of the large water holding capacity; this can cause reduced primary productivity, lower evapotranspiration and slower decomposition (Harrington et al., 2001). The Glacier Bay chronosequence is very similar to the Calvert Island chronosequence because they are both within the coastal temperate rainforest and both exhibit retrogression after ~11,000 years (Wardle et al., 2004).

On the Waitutu chronosequence, N and P increased plant growth in a fertilizer trial, suggesting that the oldest sites (> 291,000 years) were N- and P-limited, but there are also strong relationships among drainage conditions and BA, light transmission, litter decomposition and plant communities (Coomes et al., 2013). A deeper water table correlated with greater BA and total P, whereas, shallower water tables were associated with greater light transmission (Coomes et al., 2013). Though P depletion was thought to be the main cause of retrogression (Wardle et al., 2004), the deterioration of soil structure and drainage

may also elicit the same effects via a different pathway such as on the Haast, Glacier Bay, Mendocino and Waitutu chronosequences (Jenny, 1969; Vitousek et al., 2010; Turner et al., 2012a; Coomes et al., 2013; Izquierdo et al., 2013). It is uncertain whether a P limitation directly impeded primary productivity on Waitutu, and in turn reduced evapotranspiration, increasing saturation and creating an environment favouring wetland plants causing paludification, or if P limitation and deterioration of soil drainage acted independently (Coomes et al., 2013).

The Calvert Island chronosequence exhibits retrogression and has declining total P concentrations with increasing age, but it also had changes in soil morphology leading to impeded water drainage and shallow rooting zones (Fig. 6-6; Table 4-1). It is impossible to determine if the cause of retrogression on Calvert Island is from P depletion, soil barriers or both to some extent or other external factors such as climatic change or shifts in the fire regime. Further exploration of water table depth, detailed plant surveys, canopy cover analysis and fertilization trials could provide the necessary information to deduce what the main influential factors are and the contribution of P limitation versus changes in soil drainage caused by Podzolization. Basal area was not significantly correlated with any soil or foliage parameters.

6.5 Conclusion

Ecosystem retrogression is apparent on the latter stages of the Calvert Island chronosequence and is the first chronosequence in BC exhibiting retrogression. With time a hump-shaped curve in BA and a shift towards tree species more tolerant of the declining soil fertility, was apparent, and was associated with low-productivity forests including Pc, Yc, and mountain hemlock as hypothesized. The understory shifted towards shrubbier plants with increasing age and young trees less than 0.5 m tall. Total C, N and P followed expected

trends for ageing chronosequences, with total C increasing to a plateau with increasing age while total N had a hump-shaped trajectory and total P had a linear decline. Total P was characteristic of the Walker and Syers P model. With increasing age, the N: P, N: Po, C: P and C: Po ratios increased with increasing age in the foliage, FF and mineral horizons, indicating the potential for increased P limitation with age, although the N: P ratios rarely exceeded the levels indicative of P limitation. By 3,588 years, placic and ortstein cemented horizons had formed in all soils, causing limitations to root growth and impedance to water infiltration. The Calvert Island chronosequence is comparable to the Haast, Glacier Bay, Mendocino and Waitutu retrogressive chronosequences that had declining P with age and the development of cemented soil horizons. It is evident that the Calvert Island chronosequence is experiencing retrogression though it is not clear whether retrogression was caused by P-limitation or the formation of soil barriers. Most likely P limitation and soil barriers both contributed to retrogression on Calvert Island after ~7,000 years, though future experiments, such as a fertilization trial, could further the understanding of this retrogressive chronosequence. The examination of retrogression on the Calvert Island chronosequence proved our hypotheses to be correct since understory and overstory plant species shifted towards species adapted to poorer nutrient conditions and BA had a humped-shaped curve with increasing age, illustrating retrogression. As expected the N: P ratios in foliage and humus increased with age, but the ratios did not exceed limits indicative of P-limitation.

7 SYNTHESIS

7.1 Summary

The Calvert Island chronosequence spans the longest time interval of any documented soil chronosequence on the coast of British Columbia and is the first in this province where ecosystem retrogression has been explicitly identified. This study is also the first in western Canada to examine organic phosphorus (P) forms in a soil chronosequence using solution P-nuclear magnetic resonance spectroscopy (P-NMR). This chapter summarizes research pertaining to soil development, P dynamics and ecosystem succession, and relates these findings to those of allied research conducted elsewhere on Calvert and Hecate Islands. It was hypothesized that with increasing age, progressive soil development would occur, eventually leading to mature Podzolic soils. An increase in the dominance of organic P was also expected with increasing age, associated with an increase of DNA in organic horizons and *myo*- and *scyllo*-inositol hexakisphosphate (IHP) in the mineral horizons. Lastly, retrogression was expected to be occurring on the oldest sites, illustrated by declining tree basal area and a shift towards plant species adapted to nutrient-poor conditions as well as a shift in nutrient concentrations comparable to the Walker and Syers (1976) model for P transformation. Recommendations for further research on the Calvert Island chronosequence are also presented.

7.1.1 Soil Genesis

The temperate, perhumid climate of the Calvert Island chronosequence provided ideal conditions for rapid pedogenesis. After a mere 100 years, an appreciable forest floor developed, accompanied by formation of B horizons (Bm) and a rapid decline of base cations and pH as expected (Fig. 4-8). Within 600 years, some soil horizons met the requirements for

a Podzolic B horizon and by ~3,500 years, mature Podzols had formed with organic matter-cemented (ortstein) and iron (Fe)-cemented (placic) horizons (Fig. 4-8). With increasing age, the concentrations of amorphous Fe and Al increased, and high concentrations of organically-complexed Al and Fe occurred in the cemented horizons. Two mechanisms of Podzol formation appeared to be involved, with the organo-metallic complex mechanism suggested by initial increases in concentrations of organically-complexed Al and Fe and the development of appreciable forest floors. Subsequently, it was hypothesized that the allophane-imogolite mechanism became active, as indicated by increasing concentrations of allophanic-type materials after ~4,000 years of pedogenesis. Soil development on the Calvert Island chronosequence was comparable to the Cox Bay and Naikoon chronosequences in BC and the Haast chronosequence in New Zealand.

7.1.2 Phosphorus Dynamics

With age, total P to a 1 m depth declined linearly while organic P displayed a hump-shaped curve, both of which are comparable to the Walker and Syers (1976) P model for ageing soils. Phosphorus speciation was analysed using solution P-NMR in all samples in conjunction with other chemical analyses. Different processes controlled P cycling within different sample types, including foliage, organic horizons (L and H horizons) and organic-enriched mineral horizons. As hypothesized, foliage, and L horizons had similar assemblages of P forms as determined by P-NMR, suggesting minimal alteration to the forest floor litter after leaf drop. The H horizons had a similar P composition to the foliage and L horizons, but with an increase in the proportions of DNA, nucleotides, and *myo*- and *scyllo*-inositol hexakisphosphate (IHP) as expected, representing increased microbial activity and the build-up of microbial by-products. The P composition of the organic-enriched mineral

horizons was controlled by geological P cycling rather than biological P cycling, in contrast to the foliage, L and H horizons. The mineral horizon samples had considerably lower total P concentrations and increased proportions and concentrations of IHP and DNA with increasing age, which were correlated to the increased concentrations of exchangeable and amorphous Al forms. Similarly to the hypothesis, IHP increased in dominance with increasing age. However, DNA also increased with increasing age, which was contrary to the original hypothesis.

With increasing age, the proportion of orthophosphate declined in all horizons, corresponding to an increased proportion of monoesters and diesters. The increase of corrected diesters in the L and H horizons were not due to an increased proportion of DNA with age as expected, but rather because of the increased proportion of α- and β-glycerophosphates, which illustrates the significance of biological P cycling. Within the H horizons and mineral horizons, the proportion and concentration of monoesters increases with increasing age because of the sorption of IHP on amorphous, short-range ordered allophanic materials and via humic-metal bonding; confirming the hypothesis that *myo*- and *scyllo*-IHP would increase with age. The increased concentration of IHP and DNA within the mineral horizon were correlated to total C and the increased concentration of organic and inorganically-bound amorphous Al. Overall the Calvert Island chronosequence was comparable to other chronosequences where the Walker and Syers P model has been successfully applied and to the P results from the surrounding CWH zone.

7.1.3 Ecosystem Retrogression

Ecosystem retrogression was apparent in the latter stages of the Calvert Island chronosequence, as indicated by a hump-shaped basal area curve and a shift towards tree

species more tolerant of declining soil fertility in low productivity forests: shore pine, yellow cedar, and mountain hemlock. With increasing age, the understory shifted towards shrubbier plants and trees less than 0.5 m tall. The mass of total carbon (C), P and nitrogen (N) followed expected trends for ageing chronosequences, with C increasing to a plateau around ~3,500, while total P declined linearly, and total N increased to a maximum between ~4,200 and ~7,200 years, followed by a decline. The decline of total P with increasing age is comparable to the initial phase of the Walker and Syers (1976) P model. With increasing age, the N: P, N: Po, C: P and C: Po ratios increased in the foliage, forest floor, and mineral horizons, indicating the potential for increased P-limitation with age. However, the N: P ratios rarely exceeded the levels indicative of P limitation. It was evident that the Calvert Island chronosequence displayed symptoms of retrogression after ~7,000 years, though it was not clear whether this was caused by P limitation or the formation of soil barriers (e.g. placic and ortstein horizons). Most likely declining P reserves and the formation of soil barriers both contributed to retrogression on Calvert Island after ~7,000 years. In accordance with the hypotheses for chapter Six, retrogression has occurred on the Calvert Island chronosequence and was associated with a shift towards shrubbier plant species adapted to lower nutrient concentrations. The N: P ratios in foliage, forest floor and mineral horizons did increase with age as expected but did not exceed levels indicative of P-limitation.

7.2 Comparison and Application

7.2.1 Landscape Evolution on Calvert and Hectate Island

Calvert Island has a unique landscape history because in the last 10,000 years it has had repeated long-term human occupation on multiple sites, along with relatively stable sea levels suggesting that it was a sea level hinge at the last glacial maximum (Shugar et al.

2014; McLaren et al., 2014; 2015; Neudorf et al., 2015). In a small area, Calvert Island contains a multitude of different surficial deposits and landforms that record the complex landscape evolution process on this island, including relict beaches, moraines, glacial and lacustrine sediments, and intertidal mud (Neudorf et al., 2015; Eamer, 2017). The ages of these geological features have been determined with radiocarbon and optically stimulated luminescence dating, with maximum ages exceeding 15,000 years (Neudorf et al., 2015; Eamer, 2017). The geochronology, archeological data and oral histories of the Calvert Island area support the stability of this landscape during the last 10,000 years (McLaren et al., 2014; 2015; Neudorf et al., 2015).

The Calvert Island chronosequence exists because of the unique geomorphic and landscape history in this region (Neudorf et al., 2015; Eamer, 2017; Eamer et al., 2017a, b). On Calvert Island there is evidence of the readvancement of the Cordilleran ice sheet between 14.2 and 13.8 kya (Eamer, 2017; Eamer et al., 2017a). It is rare to find records of glacial readvancement after the last glacial maximum (Eamer, 2017; Eamer et al., 2017a). This readvancement provided a cool, dry climate and large sandy sediment load, likely from Foggy Cove on Calvert Island, that promoted the formation of dune systems on Calvert Island (Eamer, 2017; Eamer et al., 2017a, b). Between 14 and 8.5 kya the relative sea level was a few meters lower than today also promoting the formation of dune systems (McLaren et al., 2014). By the early Holocene (11.7 to 8.3 kya), there was erosion of glacial sediments and a warmer, wetter climate that provided a good environment for the stabilization of the oldest dune (10,760 ya; CIDS10; Eamer, 2017; Eamer et al., 2017b). The relative sea level rose a few meters above the current mean annual sea level between 8.5 and 5.6 kya causing erosion on the coast and the redistribution of these sediments at higher locations, creating

new beaches (eg., CIDS8 and CIDS15; McLaren et al., 2014; Eamer, 2017; Eamer et al., 2017b). By 5.6 to 4.2 kya, the dune complex between 4th and 7th beach (3,588 a BP; CIDS8; Fig. 3-2) and the beach formed behind North Beach (4,198 ya; CIDS15) stabilized because of the warm, wet climate (Eamer, 2017; Eamer et al., 2017b). Between 1.8 and 0.4 kya progradation rates were high on West Beach followed by a little ice age (~0.6-0.4 kya). In the last 400 years, progradation rates have slowed and the climate warmed promoting the stabilization of foredunes behind West Beach (CIDS3 and CIDS4; Eamer, 2017; Eamer et al., 2017b). Eamer (2017) noted that dune activity corresponded to fire activity since fires combusted vegetation and leave the area susceptible to erosion.

7.2.2 Soil Development on Calvert Island and Hectate Island

In 2017, Oliver et al. found that catchments on Calvert and Hecate Islands draining into Kwakshua Channel have some of the highest dissolved organic C (DOC) yields on the Pacific coastal margin. Most of the DOC entering these catchments was of terrestrial origin, most likely derived from the organic matter-rich soils occupying the catchments (Oliver et al., 2017). The examined soils typically had ~35—39 cm of forest floor and ~29—36 cm of mineral soils beneath (Oliver et al., 2017). The soils in the Calvert Island chronosequence were atypical of the surrounding area because much of Calvert Island has thin colluvium (< 1 m; Sanborn, pers. comm., 2018), whereas the chronosequence had thick sand deposits (> 1 m) depth. The forest floor on the chronosequence averaged 28 cm across all sites, which was less than the average thickness of soils examined within the catchments (Oliver et al., 2017). Due to the thick mineral soils found on the chronosequence, commonly containing ortstein and placic horizons, and the accumulation of an appreciable forest floor, it is possible that the Podzols found on the Calvert Island chronosequence may contribute a significant amount of DOC into surface waters and/or the ocean, especially considering the coarse textures and low

water-holding capacities of these sandy Podzols. The soils examined within the Kwakshua catchments rarely had cemented horizons because only well-sorted parent materials (e.g. dune sands, glaciofluvial deposits) tend to develop ortstein and placic horizons (Sanborn, pers. comm., 2018).

On average, the total and organic P concentrations of soils characterized as part of digital soil mapping of the Kwakshua catchments for the Hakai Institute were comparable to those of soils in the Calvert Island chronosequence (Sanborn, pers. comm., 2018). The range of P concentrations from both projects overlapped for most soil horizons including the L, F, H, O, A, B and BC soil horizons. Overall, the organic P concentrations found in the chronosequence were at the lower end of the range from the digital soil mapping project for all horizons, though the chronosequence did include some old soils (> 3,500 years) that have endured significant weathering since formation. The total P concentrations for the chronosequence soils were comparable to those of the digital soil mapping project and had higher, lower or comparable concentrations depending on the horizon and site age (Sanborn, pers. comm., 2017).

Calvert Island has abundant evidence of human occupation for over 13,000 years (McLaren et al., 2014; 2015). Trant et al. (2016) found that the presence of an archeological midden enhanced the growth of trees compared to control areas outside the area of influence of the midden. Soil samples from the control sites outside the midden were taken 30 cm below the litter layer and the average total P concentration was ~0.05% (Trant et al., 2016). The control samples were not classified as organic or mineral soil samples, so the average total P concentrations in the control were compared to the H horizon and the first 30 cm of

the mineral soil on the chronosequence. The H horizon samples had comparable concentrations of total P to the control samples whereas all mineral soils on the chronosequence had less than one half of the concentration of total P (Trant et al., 2016).

7.2.3 Fire Histories and Plant Communities on Calvert and Hectate Island

After ~3,500 years, there was evidence of fire on all Calvert Island chronosequence sites, as indicated by the presence of charcoal in the soils and after 7,236 years of soil development, the presence of fire scars on trees. During the investigation of fire histories on Calvert Island, Hoffman et al. (2016a) found no evidence of fires between 5,500 and 7,500 years and concluded that most fires happened in the last 1,000 years. The temperate rainforest region is resilient to fire because even though it may have ample biomass for fuel, the climate is very wet (~2.8 m precipitation $year^{-1}$) and the environment rarely dries enough to allow for ignition, except in summer droughts (Hoffman et al., 2016a, b; 2017). Hoffman et al. (2017) investigated low- and mixed-severity fires on 15 islands in the coastal temperate rainforest and concluded that lightning and accidental ignition could not account for the type, size and severity of fire observed. Rather, the majority of fires were most likely intentional burnings linked to indigenous habitation. Intentional burning was used as a method to influence plant communities and successional stage, which often coincided with an increase in the number of edible plants (Turner, 1999; 2014; Hoffman et al., 2017).

Further research on the Calvert Island chronosequence, could provide insight into the severity of fire and the time since fire. Chronosequence studies assume that high-severity disturbances are absent and any disturbance that has occurred is minimal, so the investigation of fire histories could be used to confirm the assumption that only low-severity fires may have affected the chronosequence sites (Walker et al., 2010). To understand the timing and

severity of fire on this chronosequence, radiocarbon dating of the charcoal fragments (Gavin et al., 2003; Hoffman et al., 2016a, b), and black C analysis could be utilized, respectively (Wolf et al., 2014).

Certain plant species have been linked to anthropogenic burning, including many *Vaccinium* and *Rubus* species (Turner, 1999; 2014). Plant species along the Calvert Island chronosequence were compared to those linked to anthropogenic burning and there was no evidence of a greater presence of plants linked to anthropogenic burning on the sites that had fire evidence versus those without. The only plant species that had increased presence on sites with fire scars was Labrador tea (*Rhododendron groenlandicum*) but due to the presence of seepage in these cemented soils, the presence of Labrador tea most likely reflects the change in soil moisture (Banner et al., 2005).

7.2.4 Forestry Within the Hypermaritime Coastal Western Hemlock Zone

Retrogression was evident on the latter stages of the Calvert Island chronosequence. The decline in above-ground biomass may have been caused by the formation of cemented soil horizons that impeded root exploration, and/or declining reserves of P with increasing age. The proportion of organic P increased with increasing age and was associated with the dominance of more recalcitrant organic P forms including inositol hexakisphosphates. Soils of western redcedar (Cw) and western hemlock (Hw) dominated forestry sites are generally low in total P, and nutrient limitations may occur in regenerating stands in the Coastal Western Hemlock (CWH) biogeoclimatic zone (Prescott et al., 1993; Kranabetter et al., 2003).

Kranabetter et al. (2005) performed an incubation experiment with low- (Cw-Hw-Salal), medium- (Hw-Sitka spruce (SS)) and high- (Cw-Ss) productivity forest soils to

examine the effect of P fertilization on N cycling. When P was added to the low-productivity soils, extractable inorganic N increased; the same effect was not significant on the medium- and high-productivity soils (Kranabetter et al., 2005). These results suggested that P limitation had occurred on these sites and N may be enhanced with P additions (Kranabetter et al., 2005). This theory was further explored using a ten-year P fertilizer trial in the CWH very wet hypermaritime (CWHvh2) subzone comparing different site preparation methods on low (01-Cw-Hw) productivity sites. No increases in tree growth, foliar N and P, or exchangeable soil P were apparent after ten years, suggesting that the growth of these low-productivity forests was not inhibited by P reserves and could be comparable to those of higher productivity sites if longer rotations or mechanical site preparation were employed (Kranabetter et al., 2013). The low-productivity sites used in these forestry experiments were in the site series 01-Cw-Hw-Salal which is representative of sites aged 139 and 4,198 a BP in the Calvert Island chronosequence. On the chronosequence, site series 01-Cw-Hw-Salal had a lower productivity than site series 14 or 15 with Ss, but had higher productivity compared to site series 11-Cw-yellow cedar (Yc) that was found on the retrogressive sites spanning 7,236 to 10,760 a BP. Thus, the incubation and fertilization trials conducted by Kranabetter et al. (2005; 2013) do not represent the same site series as the retrogressed sites. This does not rule out the potential for P limitation on sites > 7,000 years on the Calvert Island chronosequence. To verify whether P is a limiting factor on the older sites, a fertilizer trial would need to be performed (Koerselman and Meuleman, 1996; Laliberté et al., 2012; Coomes et al., 2013).

7.3 Future Research

This study concluded that retrogression was occurring on the older sites (> 7,000 years) on the Calvert Island chronosequence and was most likely caused by the formation of cemented horizons and declining reserves of P. These findings further the current understanding of soil formation rates in the CWH zone, as well as our knowledge of retrogression globally. Future analyses of changes in the microbial community with increasing soil age may detect successional patterns, such as replacement of bacteria-dominated communities in younger soils by fungal-dominated communities on older, more nutrient poor sites (Wardle et al., 2004; Williamson et al., 2005). Lastly, the origins of many organic P forms are not fully understood and *scyllo*-IHP has never been found in plant matter (Makarov et al., 2002; Makarov et al., 2005; Turner et al., 2007). On the Calvert Island chronosequence, *scyllo*-IHP was identified in western hemlock and salal but to fully determine if *scyllo*-IHP was present in plant matter, sterilized plant samples taken directly from the corresponding species need to be analyzed with solution P-NMR to rule out the possibility that these P forms are microbial by-products within the current samples.

It was expected that with increasing age of soil along the chronosequence, the chemical index of alteration (CIA) value would increase to indicate a greater degree of weathering accompanying the strong morphological changes in the soil; however, the CIA values remained relatively unchanged with increasing age. There was no apparent build-up of secondary weathering products with increasing age, and few soils had textures other than sand, so the soils may be experiencing a weathering and leaching environment severe enough for congruent dissolution to be occurring, with little net change in the composition of the residual mineral solids. To further explore this concept, soil pore water and leachate

collection and analysis could be performed to relate the soluble constituents to the mineral grain chemistry, as well as using methods such as scanning electron microscopy to look at the surface of mineral grains. In conjunction with current watershed monitoring programs through the Hakai Institute, water samples could be collected for analysis of dissolved silica and major cations to estimate rates of chemical denudation, which could be compared to different climatic regimes and rock types globally. This would complement both soil genesis research in the Kwakshua catchments and efforts to understand basin-scale erosion rates by cosmogenic isotope methods (B. Menounos, pers. comm., 2018).

Another project that could be integrated with the Calvert Island chronosequence is to use the recently validated methods employing LiDAR and RapidEye Imagery to examine forest productivity on all chronosequence sites, with a smaller pixel size, to corroborate the current method of measuring basal area manually on each site (Thompson et al., 2016).

8 REFERENCES

Aerts, R. 1996. Nutrient resorption from senescing leaves of perennials: are there general patterns? J. Ecol. **84:** 597—608.

Aerts, R., and Chapin F. S. 2000. The mineral nutrition of wild plants revisited. Adv. Ecol. Res. **30:** 1—67.

Alberta Biodiversity Monitoring Institute (ABMI). 2014. Ecological Recovery Monitoring of Certified Reclaimed Wellsites in Alberta - Field Data Collection Protocols for Forested Lands, Version 2014-05-26. Alberta Biodiversity Monitoring Institute, Edmonton, AB. 96 pp.

Alexander, E.B., and Burt, R. 1996. Soil development on moraines of Mendenhall Glacier, southeast Alaska. I. The moraines and soil morphology. Geoderma **72**: 1—17.

Anderson, H.A., Berrow, M.L., Farmer, V.C., Hepburn, A., Russell, J.D., and Walker, A.D. 1982. A reassessment of Podzol formation processes. J. Soil Sci. **33**: 125—136.

Andrews, J.T. and Retherford, R.M. 1978**.** A reconnaissance survey of late Quaternary sea levels, Bella Bella/Bella Coola region, central British Columbia coast. Can. J. Earth Sci. **15:** 341—350.

Apel, J.R., Pilson, M.E.Q., Reid, J.L., and Osborn, T. 2014. Seawater. [online] http://www.accessscience.com/content/seawater/611350#611350s013 [18 Oct. 2017].

Ballard, T.M. and Carter, R.E. 1986. Evaluating forest stand nutrient status (LMH No. 20). Information Services Branch Ministry of Forests, Victoria, BC. 70 pp.

Banner, A. 1983. Classification and successional relationships of some bog and forest ecosystems near Prince Rupert, British Columbia. MSc, University of British Columbia, Vancouver, BC. 300 pp.

Banner, A., LePage, P., Moran, J., and de Groot, A. 2005. The HyP3 Project: pattern, process, and productivity in hypermaritime forests of coastal British Columbia - a synthesis of 7-year results (Spec. Rep. 10). British Columbia Ministry of Forest, Research Branch, Victoria, BC. 161 pp.

Banner, A., Mackenzie, W., Haeussler, S., Thomson, S., Pojar, J. and Trowbridge, R. 1993. A field guide to site identification and interpretation for the Prince Rupert forest region (LMH No. 26). Information Services Branch Ministry of Forests, Victoria, BC. 281 pp.

Barnes, B.V., Zak, D.R., Denton, S.R. and Spurr, S.H. 1994. Forest Ecology. 4th ed. John Wiley and Sons, Inc., Toronto, ON. 774 pp.

Barrow, N.J. 1978. The description of phosphate adsorption curves. J. Soil Sci. **29**: 447—

462.

Barrow, N.J. 1983. A mechanistic model for describing the sorption and desorption of phosphate by soil. J. Soil Sci. **34**: 733—750.

Barrow, N., and Shaw, T. 1977. Factors affecting the amount of phosphate extracted from soil by anion exchange resin. Geoderma **18:** 309—323.

Barrow, N.J., Bowden, J.W., Posner, A.M., and Quirk, J.P. 1980. Describing the effects of electrolyte on adsorption of phosphate by a variable-charge surface. Aust. J. Soil Res. **18**: 395—404.

BC Parks. 2015a**.** Calvert Island Conservancy. [Online] Available: http://www.env.gov.bc.ca/bcparks/explore/cnsrvncy/calvert_is/ [2016 Jan. 20].

BC Parks. 2015b. Hakai Lúxvbálís Conservancy. [Online] Available: http://www.env.gov.bc.ca/bcparks/explore/cnsrvncy/hakai_luxvbalis/ [2016 Jan. 20].

Beegle, D. 2005. Assessing Soil Phosphorus for Crop Production by Soil Testing. Pahes 123—143 in J. T. Sims, and A. N. Sharpley, eds. Phosphorus: Agriculture and the Environment, Agron. Monogr. 46. ASA, CSSA, and SSSA, Madison, WI.

Bernasconi, S. M., Bauder, A., Bourdon, B., Brunner, I., Bünemann, E., Chris, I., Derungs, N., Edwards, P., Farinotti, D., Frey, B., Frossard, E., Furrer, G., Gierga, M., Göransson, H., Gülland, K., Hagedorn, F., Hajdas, I., Hindshaw, R., Ivy-Ochs, S., Jansa, J., Jonas, T., Kiczka, M., Kretzschmar, R., Lemarchand, E., Luster, J., Magnusson,J., Mitchell, E. A.D., Venterink, H. O., Plötze, M., Reynolds, B., Smittenberg, R. H., Stähli, M., Tamburini, F., Tipper, E. T., Wacker, L., Welc, M., Wiederhold, J. G., Zeyer, J., Zimmermann, S., and Zumsteg, A. 2011. Chemical and biological gradients along the Damma glacier soil chronosequence, Switzerland. Vadose Zone J. **10**: 867—883.

Birkeland, P. W., Burke, R. M., and Benedict, J. B. 1989. Pedogenic gradients for iron and aluminum accumulation and phosphorus depletion in arctic and alpine soils as a function of time and climate. Quatern. Res. **32**: 193-204.

Blake, H.R., and Hartge, K.H. 1986. Bulk density. Pages 363—375 in A. Klute, ed. Methods of Soil Analysis Part 1. Agron. Am. Soc. Agron., Madison, WI.

Blakemore, L.C., Searle, P.L., and Daly, B.K. 1987. Methods for chemical analysis of soils. NZ Soil Bureau Scientific Report 80. Lower Hutt, Department of Scientific and Industrial Research. 103 pp.

Bowman, R.A. 1988. A rapid method to determine total phosphorus in soils. Soil Sci. Soc. Am. J. **52**: 1301—1304.

Bowman, R., and Moir, J. 1993. Basic EDTA as an extractant for soil organic phosphorus.

Soil Sci. Soc. Am. J. **57:** 1516—1518.

Bray, R.H., and Kurtz, L. 1945. Determination of total, organic, and available forms of phosphorus in soils. Soil Sci. **59**: 39—46.

Bünemann, E., Smernik, R., Marschner, P., and McNeill, A. 2008. Microbial synthesis of organic and condensed forms of phosphorus in acid and calcareous soils. Soil Biol. Biochem. **40**: 932—946.

Burges, A., and Drover, D. 1953. The rate of Podzol development in sands of the Woy Woy District, NSW. Aus. J. Bot. **1**: 83—94.

Cade-Menun, B.J. 1995. Phosphorus forms of podzolic soils of northern Vancouver Island and their use by western redcedar. PhD Thesis, University of British Columbia, Vancouver, BC. 227 pp.

Cade-Menun, B.J. 2005. Characterizing phosphorus in environmental and agricultural samples by ^{31}P nuclear magnetic resonance spectroscopy. Talanta **66**: 359—371.

Cade-Menun, B.J. 2015. Improved peak identification in ^{31}P-NMR spectra of environmental samples with a standardized method and peak library. Geoderma **257—258**: 102—114.

Cade-Menun, B.J., and Lavkulich, L.M. 1997. A comparison of methods to determine total, organic, and available phosphorus in forest soils. Commun. Soil Sci. Plant Anal. **28**: 651—663.

Cade-Menun, B.J., and Liu, C.W. 2014. Solution phosphorus-31 nuclear magnetic resonance spectroscopy of soils from 2005 to 2013: A review of sample preparation and experimental parameters. Soil Sci. Soc. Am. J. **78**: 19—37.

Cade-Menun, B.J., and Preston, C. 1996. A comparison of soil extraction procedures for ^{31}P NMR spectroscopy. Soil Sci. **161**: 770—785.

Cade-Menun, B.J., Berch, S.M., Preston, C.M., and Lavkulich, L.M. 2000. Phosphorus forms and related soil chemistry of Podzolic soils on northern Vancouver Island. II. The effects of clear-cutting and burning. Can. J. For. Res. **30**: 1726—1741.

Caldwell, A. G., and Black, C. A. 1958. Inositol hexaphosphate. II. Synthesis by soil microorganisms. Soil Sci. Soc. Am. J. **22**: 293—296.

Callesen, I., Harrison, R., Stupak, I., Hatten, J., Raulund-Rasmussen, K., Boyle, J., Clarke, N., and Zabowski, D. 2016. Carbon storage and nutrient mobilization from soil minerals by deep roots and rhizospheres. For. Ecol. Man. **359**: 322—331.

Carlyle, J.C., and Nambiar, E.K.S. 2001. Relationships between net nitrogen mineralization, properties of the forest floor and mineral soil, and wood production in *Pinus radiata* plantations. Can. J. For. Res. **31**: 889—898.

Carranza-Edwards, A., Rosales-Hoz, L., and Santiago-Pérez, S. 1994. Provenance memories and maturity of Holocene sands in northwest Mexico. Can. J. Earth. Sci. **31**: 1550—1556.

Celi, L., and Barberis, E. 2007. Abiotic stabilization of organic phosphorus in the environment. Pages 113—132 in B.L. Turner, B.L., R. Frossard, and D.S. Baldwin, eds. Organic Phosphorus in the Environment. CABI Publishing, Cambridge, MA.

Celi, L., Lamacchia, S., Ajmone Marsan, F., and Barberis, E. 1999. Interaction of inositol hexaphosphate on clays: Adsorption and charging phenomena. Soil Sci. **164:** 574—585.

Celi, L., Presta, M., Ajmore-Marsan, F., and Barberis, E. 2001. Effects of pH and electrolytes on inositol hexaphosphate interaction with goethite. Soil Sci. Soc. Am. J. **65**: 753—760.

Chadwick, O.A., Derry, L., Vitousek, P.M., Huebert, B J., and Hedin, L.O. 1999. Changing sources of nutrients during four million years of ecosystem development. Nature **397:** 491—497.

Chang, S.C., and Jackson, M.L. 1957. Fractionation of soil phosphorus. Soil Sci. **84**: 133—144.

Chang, S.C., and Juo, S.R., 1963. Available phosphorus in relation to forms of phosphates in soils. Soil Sci. **95**: 91—96.

Chapin, F.S., Walker, L.R., Fastie, C.L., and Sharman, L.C. 1994. Mechanisms of primary succession following deglaciation at Glacier Bay, Alaska. Ecol. Monogr. **64**: 149—175.

Chen, C.R., Hou, E.Q., Condron, L.M., Bacon, G., Esfandbod, M., Olley, J., and Turner, B.L. 2015. Soil phosphorus fractionation and nutrient dynamics along the Cooloola coastal dune chronosequence, southern Queensland, Australia. Geoderma **257-258**: 4—13.

Chien, S.H., Savant, N.K., and Mokwunye, U. 1982. Effect of temperature on phosphate sorption and sorption in two acid soils. Soil Sci. **133**: 160—166.

Chiou, T.J., Aung, K., Lin, S.I., Wu, C.C., Chiang, S.F., and Su, C.L. 2006. Regulation of phosphate homeostasis by microRNA in *Arabidopsis*. Plant Cell **18**: 412—421.

Chourmouzis, C., Yanchuk, A.D., Hamann, A., Smets, P., and Aitken, S.M. 2009. Forest tree genetic conservation status report 1: In situ conservation status of all indigenous British

Columbia species (Tech. Rep. 053). Centre for Forest Conservation Genetics, Forest Genetics Council of B.C., and B.C. Min. For. Range, For. Sci. Prog. Victoria, B.C.

Claisse Inc. 2003. Glass Disks and Solutions by Fusion for Claisse Fluxer Users Manual. 67 pp.

Clarkson, D.T. 1985. Factors affecting mineral nutrient acquisition by plants. Annu. Rev. Plant Physiol. **36**: 77—115.

ClimateBC Map. 2015. Faculty of Forestry, University of British Columbia, Vancouver, BC. [Online] Available: http://climatewna.com/climatena_map/ClimateBC_Map.aspx [2016 Feb. 05].

Columbia Gazetteer of the World Online, 2016. Calvert Island. [Online] Available: http://www.columbiagazetteer.org.login.ezproxy.library.ualberta.ca/main/ViewPlace/22503 [2016 Feb. 05].

Condron, L.M., and Tiessen, H. 2005. Interactions of organic phosphorus in terrestrial ecosystems. Pages 295—308 in B.L. Turner, E. Frossard, and D.S. Baldwin, eds. Organic Phosphorus in the Environment. CABI Publ., Cambridge, MA.

Condron, L.M., Moir, J., Tiessen, H., and Stewart, J. 1990. Critical evaluation of methods for determining total organic phosphorus in tropical soils. Soil Sci. Soc. Am. J. **54**: 1261—1266.

Condron, L.M., Turner, B.L., and Cade-Menun, B.J. 2005. Chemistry and dynamics of soil organic phosphorus. Pages 87—121 in J.T. Sims, and A.N. Sharpley, eds. Phosphorus: Agriculture and the environment. Agron. Monogr. 46. ASA, CSSA, and SSSA, Madison, WI.

Coomes, D.A., Allen, R.B., Bentley, W.A., Burrows, L.E., Canham, C.D., Fagan, L., Forsyth, D.M., Gaxiola, A., Parfitt, R.L., and Ruscoe, W.A. 2005. The hare, the tortoise and the crocodile: the ecology of angiosperm dominance, conifer persistence and fern filtering. J. Ecol. **93:** 918—935.

Coomes, D. A., Bentley, W. A., Tanentzap, A. J., and Burrows, L. E. 2013. Soil drainage and phosphorus depletion contribute to retrogressive succession along a New Zealand chronosequence. Plant Soil **367:** 77—91.

Cordes, L.D. 1972. An ecological study of the Sitka spruce forest on the west coast of Vancouver Island. PhD thesis, The University of British Columbia, Vancouver, BC. 467 pp.

Cosgrove, D.J. 1980. Inositol phosphates: Their chemistry, biochemistry and physiology. Elsevier, Amsterdam, NLD. 191 pp.

Courchesne, F., and Turmel, M.-C. 2008. Extractable Al, Fe, Mn, and Si. Pages 307-312 in M.R. Carter and E.G. Gregorich, eds. Soil sampling and methods of analysis. Taylor & Francis Group, Boca Raton, FL.

Crews, T.E., Kitayama, K., Fownes, J.H., Riley, R.H., Herbert, D.A., Mueller-Dombois, D., and Vitousek, P.M. 1995. Changes in soil phosphorus fractions and ecosystem dynamics across a long chronosequence in Hawaii. Ecology **76**: 1407—1424.

Crouse, D., Sierzputowska-Gracz, H., and Mikkelsen, R. 2000. Optimization of sample pH and temperature for phosphorus-31 nuclear magnetic resonance spectroscopy of poultry manure extracts. Commun. Soil Sci. Plant Anal. **31**: 229—240.

Curran, M.P. 1984. Soil testing for phosphorus availability to some conifers in British Columbia. Msc. Thesis, University of British Columbia, Vancouver, BC. 139 pp.

D'Amore, D.V., Fellman, J.B., Edwards, R.T., Hood, E., and Ping, C.L. 2012. Hydropedology of the North American coastal temperate rainforest. Pages 351-380 in H. Lin, ed. Hydropedology: synergistic integration of hydrology and pedology. Academic Press, Waltham, MA.

Dahlgren, R.A., and F.C. Ugolini. 1989. Formation and stability of imogolite in a tephritic Spodosol, Cascade Range, Washington, USA. Geochim. Cosmochim. Acta **53**:1897–1904.

Dampier, L., Sanborn, P., Smith, C.A.S., Bond, J., and Clague, J.J. 2011. Genesis of upland soils, Lewes Plateau, central Yukon. Part 2: soils formed in weathered granitic bedrock. Can. J. Soil Sci. **91**: 579—594.

Davidson-Arnott, R. 2010. Coastal sand dunes. Pages 228-279 in Introduction to coastal processes and geomorphology. Cambridge University Press, Cambridge, UK.

Daviel, E., Sanborn, P., Tarnocai, C., and Smith, C.A.S. 2011. Clay mineralogy and chemical properties of argillic horizons in central Yukon paleosols. Can. J. Soil Sci. **91**: 83—93.

DeBano, L.F., and Klopatek, J.M. 1988. Phosphorus dynamics of pinyon-juniper soils following simulated burning. Soil Sci. Soc. Am. J. **52**: 271—277.

Dick, W.A., and Tabatabai, M.A. 1977. An alkaline oxidation method for determination of total phosphorus in soils. Soil Sci. Soc. Am. J. **41**: 511—514.

Dong, B., Ryan, P.R., Rengel, Z., and Delhaize, E. 1999. Phosphate uptake in *Arabidopsis thaliana*: dependence of uptake on the expression of transporter genes and internal phosphate concentrations. Plant Cell Environ. **22**: 1455—1461.

Doolette, A., Smernik, R., and Dougherty, W. 2009. Spiking improved solution phosphorus-31 nuclear magnetic resonance identification of soil phosphorus compounds. Soil Sci.

Soc. Am. J. **73**: 919—927.

Drew, M.C. 1975. Comparison of the effects of a localized supply of phosphate, nitrate, ammonium and potassium on the growth of the seminal root system, and the shoot, in barley. New Phytol. **75**: 479—490.

Dubois, J.-M., Martel, Y.A., and Nadeau, L. 1990. Les ortsteins du Québec: répartition geographique, relations géomorphologiques et essai de datation. Can. Geogr. **34**: 303—317.

Duchaufour, P., and Souchier, B. 1978. Roles of iron and clay in genesis of acid soils under a humid, temperate climate. Geoderma **20**: 15—26.

Duff, S.M.G., Sarath, G., and Plaxton, W.C. 1994. The role of acid phosphatases in plant phosphorus metabolism. Physiol. Plant. **90**: 791—800.

Dumon, J.C., and Vigneaux, M. 1979. Mise en evidence d'une certaine mobilité du titane dans les podzols ainsi qu'au laboratoire sous l'influence d'agents organiques. Phys. Chem. Earth **11**: 331—337.

Eamer, J.B.R. 2017. Reconstruction of the late Pleistocene and Holocene geomorphology of northwest Calvert Island, British Columbia. PhD Thesis, University of Victoria, Victoria, BC. 133 pp.

Eamer, J.B.R., Shugar, D.H., Walker, I.J., Lian, O.B., and Neudorf, C.M. 2017c. Distinguishing depositional setting for sandy deposits in coastal landscapes using grain shape. J. Sed. Res. **87**: 1—11.

Eamer, J.B.R., Shugar, D.H., Walker, I.J., Lian, O.B., Neudorf, C.M., and Telka, A.M. 2017a. A glacial readvance during retreat of the Cordilleran Ice Sheet, British Columbia central coast. Quat. Res. **87**: 468—481.

Eamer, J.B.R., Shugar, D.H., Walker, I.J., Neudorf, C.M., Lian, O.B., Eamer, J.L., Bryce, J., and Biln, L. 2017b. Late quaternary landscape evolution in a region of stable postglacial relative sea levels, British Columbia central coast, Canada. Boreas https://doi.org/10.1111/bor.12297.

Eger, A., Almond, P.C., and Condron, L.M. 2011. Pedogenesis, soil mass balance, phosphorus dynamics and vegetation communities across a holocene soil chronosequence in a super-humid climate, south Westland, New Zealand. Geoderma **163**: 185—196.

Eger, A., Almond, P.C., Wells, A., and Condron, L.M. 2013. Quantifying ecosystem rejuvenation: foliar nutrient concentrations and vegetation communities across a dust gradient and a chronosequence. Plant Soil **367**: 93—109.

Environment and Natural Resources. 2018. Canadian climate normal 1981-2010 station data. Bella Coola. Government of Canada, Vancouver, BC. [Online] Available: http://climate.weather.gc.ca/climate_normals/index_e.html [2018 Feb. 07].

Farmer, V. 1982. Significance of the presence of allophane and imogolite in Podzol Bs horizons for podzolization mechanisms: A review. Soil Sci. Plant Nutr. **28**: 571—578.

Farmer, V., and Fraser, A.R. 1982. Chemical and colloidal stability of sols in the Al_2O_3-Fe_2O_3-SiO_2-H_2O system: their role in podzolization. J. Soil. Sci. **33**: 737—742.

Farmer, V., and Lumsdon, D. 2001. Interactions of fulvic acid with aluminium and a proto-imogolite sol: the contribution of e-horizon eluates to podzolization. Eur. J. Soil Sci. **52**: 177—188.

Farmer, V., Russell, J., and Berrow, M. 1980. Imogolite and proto-imogolite allophane in Spodic horizons: evidence for a mobile aluminium silicate complex in Podzol formation. Eur. J. Soil Sci. **31** :673—684.

Food and Agriculture Organization of the United Nations (FAO), 2006. Guidelines for Soil Description. FAO, Rome, ITA. 109 pp.

Francis, R., and Read, D. 1994. The contributions of mycorrhizal fungi to the determination of plant community structure. Plant Soil **159**: 11—25.

Gavin, D.G., Brubaker, L.B., Lertzman, K.P., 2003. Holocene fire history of a coastal temperate rain forest based on soil charcoal radiocarbon dates. Ecology 84, 186–201.

Gaxiola, A., McNeill, S. M., and Coomes, D. 2010. What drives retrogressive succession? Plant strategies to tolerate infertile and poorly drained soils. Funct. Ecol. **24:** 714—722.

Giesler, R., Andersson, T., Lövgren, L., and Persson, P. 2005. Phosphate sorption in aluminum- and iron-rich humus soils. Soil. Sci. Soc. Am. J. **69**: 77—86.

Giesler, R., Petersson, T., and Högberg, P. 2002. Phosphorus limitation in boreal forest: effects of aluminum and iron accumulation in the humus layer. Ecosystems **5**: 300—314.

Giesler, R., Ilvesniemi, H., Nyberg, L., van Hees, P., Starr, M., Bishop, K., Kareinen, T., and Lundström, U.S. 2000. Distribution and mobilization of Al, Fe and SI in three podzolic soil profiles in relation to the humus layer. Geoderma **94**: 249—263.

Giles, C., and Cade-Menun, B.J. 2014. Phytate in animal manure and soils: abundance, cycling and bioavailability. Pages 163—190 in Z. He, and H. Zhang, eds. Applied manure and nutrient chemistry for sustainable agriculture and environment. Springer Science Business Media, Dordrecht, NLD.

Giles, C., Cade-Menun, B.J., and Hill, J. 2011. The inositol phosphates in soils and manures:

abundance, cycling, and measurement. Can. J. Soil Sci. **91**: 397—416.

Gorenstein, D. 1984. Phosphorus-31 NMR: principles and applications. Academic Press, London, UK. 605 pp.

Goring, C., and Bartholomew, W. 1952. Adsorption of mononucleotides, nucleic acids, and nucleoproteins by clays. Soil Sci. **74**: 149—164.

Gotelli, N.J., and Ellison, A.M. 2004. A Primer of Ecological Statistics. Sinauer Associates, Inc., Sunderland, MA. 510 pp.

Greaves, M.P., and Webley, D. 1969. The hydrolysis of *myo*-inositol hexaphosphate by soil microorganisms. Soil Biol. Biochem. **1**: 37—43.

Greaves, M., and Wilson, M. 1969. The adsorption of nucleic acids by montmorillonite. Soil Biol. Biochem. **1**: 317—323.

Green, R.N., and Klinka, K. 1994. A field guide for site identification and interpretation for the Vancouver forest region (LMH No. 28). Research Branch, British Columbia Ministry of Forests, Victoria, BC. 293 pp.

Grime, J. 1979. Primary strategies in the established phase. Plant Strategies and Vegetation Processes. John Wiley and Sons, Chichester, UK, 222 pp.

Gustafsson, J.P., Bhattacharya, P., Bain, D.C., Fraser, A.R., and McHardy, W.J. 1995. Podzolisation mechanisms and the synthesis of imogolite in northern Scandinavia. Geoderma **66**: 167—184.

Güsewell, S. 2004. N: P ratios in terrestrial plants: variation and functional significance. New Phytol **164**: 243—266.

Harrap, F.E.G. 1963. Use of sodium EDTA in the determination of soil organic phosphorus. J. Soil Sci. **4**: 82—87.

Harrington, R. A., Fownes, J.H., and Vitousek, P.M. 2001. Production and resource-use efficiencies in N- and P-limited tropical forests: a comparison of responses to long-term fertilization. Ecosystems **4**: 646—657.

Hawkes, G.E., Powlson, D.S., Randall, E.W., and Tate, K.R. 1984. A ^{31}P nuclear magnetic resonance study of the phosphorus species in alkali extracts of soils from long-term field experiments. Eur. J. Soil Sci. **35**: 35—45.

Hayes, J., Richardson, A., and Simpson, R. 2000. Components of organic phosphorus in soil extracts that are hydrolysed by phytase and acid phosphatase. Biol. Fert. Soils **32**: 279—286.

Hayes, P., Turner, B.L., Lambers, H., and Laliberté, E. 2014. Foliar nutrient concentrations

and resorption efficiency in plants of contrasting nutrient-acquisition strategies along a 2-million-year dune chronosequence. J. Ecol. **102**: 396—410.

He, Z., Olk, D.C., and Cade-Menun, B.J. 2011. Forms and lability of phosphorus in humic acid fractions of Hord silt loam soil. Soil Sci. Soc. Am. J. **75**: 1712—1722.

Heathfield, D.K., and Walker, I.J. 2011. Analysis of coastal dune dynamics, shoreline position, and large woody debris at Wickaninnish Bay, Pacific Rim National Park, British Columbia. Can. J. Earth Sci. **48**: 1185—1198.

Hedley, M.J., Stewart, J.W.B., and Chauhan, B.S. 1982. Changes in inorganic and organic soil phosphorus fractions induced by cultivation practices and by laboratory incubations. Soil Sci. Soc. Am. J. **46**: 970—976.

Hendershot, W.H., Lalande, H., and Duquette, M. 2008. Ion exchange and exchangeable cations. Pages 198-208 in M.R. Carter and E. Gregorich, eds. Soil sampling and methods of Analysis. Taylor & Francis Group, Boca Raton, FL.

Hesp P.A., and Walker I.J. 2013. Coastal Dunes. Pages 328-355 in J.F. Shroder, ed. Treatise on Geomorphology, Volume 11. Academic Press, San Diego, CA.

Hill, J.E., and Richardson, A.E. 2007. Isolation and assessment of microorganisms that utilize phytate. Pages 61—77 in B.L. Turner, A.E. Richardson, and E.J. Mullaney, eds. Inositol Phosphates: Linking Agriculture and the environment. CAB International, Wallingford, UK.

Hodge, A. 2003. Plant nitrogen capture from organic matter as affected by spatial dispersion, interspecific competition and mycorrhizal colonization. New Phytol. **157**: 303—314.

Hodge, A. 2004. The plastic plant: root response to heterogeneous supplies of nutrients. New Phytol. **162**: 9—24.

Hoffman, K., Gavin, D., and Starzomski, B. 2016a. Seven hundred years of human-driven and climate-influenced fire activity in a British Columbia coastal temperate rainforest. R Soc. Open Sci. **3**: 1—14.

Hoffman, K., Gavin, D., Lertzman, K., Smith, D., and Starzomski, B. 2016b. 13,000 years of fire history derived from soil charcoal in a British Columbia coastal temperate rain forest. Ecosphere **7**: 1—13.

Hoffman, K.A., Lertzman, K.P., and Starzomski, B.M. 2017. Ecological legacies of anthropogenic burning in a British Columbia temperate rain forest. J. Biogeogr. [In Press].

Högberg, P. 1990. 15N natural abundance as a possible marker of the ectomycorrhizal habit of trees in mixed African woodlands. New Phytol. **115**: 483—486.

Horneck, D.A. and Miller, R.O. 1998. Determination of total nitrogen in plant tissue. Pages 75-83 in Y.P. Kalra, ed. Handbook of reference methods for plant analysis. CRC Press, Boca Raton, FL.

Hossner, L.R. 1996. Dissolution for total elemental analysis. Pages 49—64 in D.L. Sparks, A.L. Page, P.A. Helmke, R.H. Loeppert, eds. Methods of Soil Analysis Part 3—Chemical Methods. Soil Science Society of America, American Society of Agronomy, Madison, WI.

Hotchkiss, S., Vitousek, P.M., Chadwick, O.A., and Price, J. 2000. Climate cycles, geomorphological change, and the interpretation of soil and ecosystem development. Ecosystems **3**: 522—533.

Huang, C., Barker, S. J., Langridge, P., Smith, F.W., and Graham, R. D. 2000. Zinc deficiency up-regulates expression of high-affinity phosphate transporter genes in both phosphate-sufficient and-deficient barley roots. Plant Physiol. **124**: 415—422.

Izquierdo, J.E., Houlton, B.Z., and van Huysen, T.L. 2013. Evidence for progressive phosphorus limitation over long-term ecosystem development: Examination of a biogeochemical paradigm. Plant Soil **367**: 135—147.

Jansen, B., Nierop, K.G.J., and Verstraten, J.M. 2005. Mechanisms controlling the mobility of dissolved organic matter, aluminium and iron in Podzol B horizons. Eur. J. Soil Sci. **56**: 537—550.

Jenny, H. 1941. Factors of soil formation: a system of quantitative pedology. McGraw-Hill, New York, NY, USA. 281 pp.

Jenny, H., Arkley, R.J., and Schultz, A. 1969**.** The pygmy forest-Podsol ecosystem and its dune associates of the Mendocino coast. Madroño **20:** 60—74.

Jien, S.H., Pai, C.W., Iizuka, Y., and Chiu, C.Y. 2013. Pedogenic processes of placic and spodic horizons in subtropical subalpine forest soils with contrasting textures. Eur. J. Soil Sci. **64**: 423—434.

Johnson, E.A., and Miyanishi, K. 2008. Testing the assumption of chronosequences in succession. Ecol. Lett. **11**: 419—431.

Joner, E.J., Ravnskov, S., and Jakobsen, I. 2000. Arbuscular mycorrhizal phosphate transport under monoxenic conditions using radio-labelled inorganic and organic phosphate. Biotechnol. Lett. **22:** 1705—1708.

Jørgensen, C., Turner, B.L., and Reitzel, K. 2015. Identification of inositol hexakisphosphate binding sites in soils by selective extraction and solution ^{31}P NMR spectroscopy. Geoderma **257-258**: 22-28.

Kalra, Y.P., and Maynard, D.G. 1991. Methods manual for forest soil and plant analysis. For. Can., Northwest Reg., Northern Forestry Center, Edmonton, AB. 125 pp.

Killingbeck, K.T. 1996**.** Nutrients in senesced leaves: keys to the search for potential resorption and resorption proficiency. J. Ecol. **77:** 1716—1727.

Kitayama, K., Schuur, E.A., Drake, D.R., and Mueller-Dombois, D. 1997. Fate of a wet montane forest during soil ageing in Hawaii. J. Ecol. **85:** 669—679.

Kobe, R.K., Lepczyk, C.A., and Iyer, M. 2005. Resorption efficiency decreases with increasing green leaf nutrients in a global data set. J. Ecol. **86:** 2780—2792.

Koide, R., and Kabir, Z. 2000. Extraradical hyphae of the mycorrhizal fungus *Glomus intraradices* can hydrolyse organic phosphate. New Phytol. **148:** 511—517.

Koerselman, W., and Meuleman, A.F. 1996. The vegetation N: P ratio: a new tool to detect the nature of nutrient limitation. J. Appl. Ecol. **33:** 1441—1450.

Kranabetter, J. M., Banner, A., and de Groot, A. 2005. An assessment of phosphorus limitations to soil nitrogen availability across forest ecosystems of north coastal British Columbia. Can. J. For. Res. **35**: 530—540.

Kranabetter, J.M., Banner, A., and Shaw, J. 2003. Growth and nutrition of three conifer species across site gradients of north coastal British Columbia. Can. J. For. Res. **33**: 313—324.

Kranabetter, J.M., LePage, P., and Banner, A. 2013. Management and productivity of cedar-hemlock-salal scrub forests on the north coast of British Columbia. For. Ecol. Manage. **308**: 161—168.

Kruse, J., Abraham, M., Amelung, W., Baum, C., Bol, R., Kühn, O., Lewandowski, H., Niederberger, J., Oelmann, Y., Rüger, C., and Santner, J. 2015. Innovative methods in soil phosphorus research: a review. J. Plant Nut. Soil Sci. **178**: 43—88.

Kuo, S. 1996. Phosphorus analysis. Pages 869–919 in J. M. Bigham ed. Methods of soil analysis. Part 3. chemical methods – SSSA. American Society of Agronomy, Inc., Madison, WI.

Kurtz, A.C., Derry, L.A., and Chadwick, O.A. 2001. Accretion of asian dust to hawaiian soils: isotopic, elemental, and mineral mass balances. Geochim. Cosmochim. Acta **65**: 1971—1983.

Lafortune, V., Filion, L., and Hétu, B. 2006. Émersion des terres et développement des sols bien drainés au Lac Guillaume-Delisle, Québec subarctique. Géogr. Phys. Quat. **60**: 165—181.

Lajtha, K., and Schlesinger, W. H. 1988. The biogeochemistry of phosphorus cycling and

phosphorus availability along a desert soil chronosequence. Ecology **69:** 24—39.

Laliberté, E., Turner, B. L., Costes, T., Pearse, S. J., Wyrwoll, K. H., Zemunik, G., and Lambers, H. 2012. Experimental assessment of nutrient limitation along a 2-million-year dune chronosequence in the south-western Australia biodiversity hotspot. J. Ecol. **100:** 631—642.

Laliberté, E., Turner, B.L., Zemunik, G., Wyrwoll, K.H., Pearse, S.J., and Lambers, H. 2013. Nutrient limitation along the Jurien Bay dune chronosequence: response to Uren & Parsons. J. Ecol. **101:** 1088—1092.

Lambers, H., Raven, J.A., Shaver, G.R., and Smith, S. E. 2008. Plant nutrient-acquisition strategies change with soil age. Trends Ecol. Evol. **23**: 95—103.

Lambers, H., Shane, M.W., Cramer, M.D., Pearse, S.J., and Veneklaas, E.J. 2006. Root structure and functioning for efficient acquisition of phosphorus: matching morphological and physiological traits. Ann. Bot. **98**: 693—713.

Lanoue, A.V.L. 2003. Phosphorus content and accumulation of carbon and nitrogen in boreal forest soils. MSc. Thesis. University of Alberta, Edmonton, AB. 175 pp.

Lapen, D.R., and Wang, C. 1999. Placic and ortstein horizon genesis and peatland development, Southeastern Newfoundland. Soil Sci. Soc. Am. J. **63**: 1472—1482.

Lavkulich, L.M., Bhoojedhur, S., and Rowles, C.A. 1971. Soils with placic horizons on the west coast of Vancouver Island, British Columbia. Can. J. Soil Sci. **51**: 439—448.

Levy-Booth, D.J., Campbell, R.G., Gulden, R.H., Hart, M.M., Powell, J.R., Klironomos, J.N., Pauls, K.P., Swanton, C.J., Trevors, J.T., and Dunfield, K.E. 2007. Cycling of extracellular DNA in the soil environment. Soil Biol. Biochem. **39**: 2977—2991.

Leyton, L. 1948. Mineral nutrient relationships of forest trees. Forestry Abstr. **9**: 399—408.

Li, W., Feng, X., Yan, Y., Sparks, D.L., and Phillips, B.L. 2013. Solid-State NMR spectroscopic study of phosphate sorption mechanisms on aluminum (hydr)oxides. Environ. Sci. Technol. **47**: 8308—8315.

Lindsay, W.L. 1979. Chemical equilibria in soils. John Wiley and Sons, New York, NY.

Lundström, U. 1993. The role of organic acids in the soil solution chemistry of a podzolized soil. J. Soil Sci. **44**: 121—133.

Lundström, U.S., van Breemen, N., and Bain, D. 2000. The podzolization process. A review. Geoderma **94**: 91—107.

Macadam, A.M. 1987. Effects of broadcast slash burning on fuels and soil chemical

properties in the sub-boreal spruce zone of central British Columbia. Can. J. For. Res. **17**: 1577–1584.

Magid, J., Tiessen, H., and Condon, L.M. 1996. Dynamics of organic phosphorus in soils under natural and agricultural systems. Pages 429—466 in Piccolo, A. ed. Humic substances in terrestrial systems. Elsevier, Amsterdam, NLD.

Makarov, M., Haumaier, L., and Zech, W. 2002. Nature of soil organic phosphorus: An assessment of peak assignments in the diester region of ^{31}P NMR spectra. Soil Biol. Biochem. **34**: 1467—1477.

Makarov, M., Haumaier, L., Zech, W., Marfenina, O., and Lysak, L. 2005. Can ^{31}P NMR spectroscopy be used to indicate the origins of soil organic phosphates? Soil Biol. Biochem. **37**: 15—25.

Martin, J. B., Laussmann, T., Bakker-Grunwald, T., Vogel, G., and Klein, G. 2000. Neo-inositol polyphosphates in the amoeba *Entamoeba histolytica*. J. Biol. Chem. **275**: 10134—10140.

Maxwell, R.E. 1997. Soils of Brooks Peninsula. Pages 4.1—4.49 in R.J. Hedba, and J.C. Haggarty, eds. Brooks Peninsula: an ice age refugium on Vancouver Island (Occasional Paper No. 5.). B.C. Min. Environ., Lands and Parks, Victoria, B.C.

McBride, M.B. 1994. Chemisorption and precipitation of inorganic ions. Pages 121—168 in Environmental chemistry of soil. Oxford University Press, New York, NY.

McDowell, R., and Stewart, I. 2005. Peak assignments for phosphorus-31 nuclear magnetic resonance spectroscopy in pH range 5–13 and their application in environmental samples. Chem. Ecol. **21**: 211—226.

McDowell, R.W., Cade-Menun, B.J., and Stewart, I. 2007. Organic phosphorus speciation and pedogenesis: Analysis by solution ^{31}P nuclear magnetic resonance spectroscopy. Eur. J. Soil Sci. **58**: 1348—1357.

McGill, W., and Cole, C. 1981**.** Comparative aspects of cycling of organic C, N, S and P through soil organic matter. Geoderma **26:** 267—286.

McGill, W.B., and Figueiredo, C.T. 1993. Total nitrogen. Pages 201-203 in M.R. Carter, ed. Soil Sampling and Methods of Analysis. Taylor & Francis Group, Boca Raton, FL.

McGroddy, M. E., Daufresne, T., and Hedin, L. O. 2004. Scaling of C: N: P stoichiometry in forests worldwide: implications of terrestrial Redfield-type ratios. Ecology **85**: 2390—2401.

McKeague, J., and Day, J. 1966. Dithionite-and oxalate-extractable Fe and Al as aids in differentiating various classes of soils. Can. J. Soil Sci. **46**: 13—22.

McKeague, J., and Wang, C. 1980. Micromorphology and energy dispersive analysis of ortstein horizons of Podzolic soils from New Brunswick and Nova Scotia, Canada. Can. J. Soil Sci. **60**: 9—21.

McKeague, J., Brydon, J. E., and Miles, N. M. 1971. Differentiation of forms of extractable iron and aluminium in soils. Soil Sci. Soc. Am. Proc. **35:** 33—38.

McKeague, J., Damman, A., and Heringa, P. 1968. Iron-manganese and other pans in some soils of Newfoundland. Can. J. Soil Sci. **48**: 243—253.

McKeague, J., DeConinck, F., and Franzmeier, D. 1983. Spodosols. Dev. Soil Sci. **11**: 217—252.

McKeague, J., Ross, G., Gamble, D., and Mahaney, W. 1978. Properties, criteria of classification and genesis of Podzolic soils in Canada. Pages 27—60 in W. C. Mahaney, ed. Quaternary Soils. Geo Abstracts, Norwich, UK.

McLaren D., Rahemtulla, F., Gitla (White, E.) and Fedje, D. 2015. Prerogatives, sea level, and the strength of persistent places: Archaeological evidence for long-term occupation of the Central Coast of British Columbia. BC Studies **187:** 155—191.

McLaren, D., Fedje, D., Hay, M.B., Mackie, Q., Walker, I.J., Shugar, D.H., Eamer, J.B.R., Lian, O.B. and Neudorf, C. 2014. Post-glacial sea level hinge on the central Pacific coast of Canada. Quat. Sci. Rev. **97:** 148—169.

Mehlich, A. 1984. Mehlich 3 soil test extractant: a modification of Mehlich 2 extractant. Commun. Soil Sci. Plant Anal. **15**: 1409—1416.

Mehta, N.C., Legg, J.O., Goring, C.A.I., and Black, C.A. 1954. Determination of organic phosphorus in soils. 1. Extraction method. Soil Sci. Soc. Am. Proc. **18**: 443—449.

Merritts, D.J., Chadwick, O.A., and Hendricks, D.M. 1991. Rates and processes of soil evolution on uplifted marine terraces, northern California. Geoderma **51**: 241—275.

Ministry of Environment (MOE). 2016. Ecology: Ecoregion Unit Descriptions. [Online] Available: http://www.env.gov.bc.ca/ecology/ecoregions/humidtemp.html#coast [2016 Feb. 05].

Ministry of Forest Lands and Range (MOFLR). 2010. Field manual for describing terrestrial ecosystems, 2nd edition (LMH No. 25). B.C. Ministry of Forest Lands and Range and B.C. Ministry of Environment, Victoria, BC. 266 pp.

Mokma, D., and Buurman, P. 1982. Podzols and podzolization in temperate Regions. Int. Soil Mus. Monogr. **1**: 1—137.

Mokma, D.L., Yli-Halla, M., and Lindqvist, K. 2004. Podzol formation in sandy soils of

Finland. Geoderma **120**: 259—272.

Moore, T. 1976. Sesquioxide-cemented soil horizons in northern Quebec: their distribution, properties and genesis. Can. J. Soil Sci. **56**: 333—344.

Mossin, L., Mortensen, M.,and Nørnberg, P. 2002. Imogolite related to podzolization processes in Danish Podzols. Geoderma **109**: 103—116.

Motomizu, S., Wakimoto, T., and Toei, K. 1983. Spectrophotometric determination of phosphate in river waters with molybdate and malachite green. Analyst **108**: 361—367.

Muir, J., and Logan, J. 1982. Eluvial/illuvial coefficients of major elements and the corresponding losses and gains in three soil profiles. Eur. J. Soil Sci. **33**: 295—308.

Munger, Gregory T. 2008. *Cladonia* spp. In: Fire Effects Information System, U.S. Department of Agriculture, Forest Service, Rocky Mountain Research Station, Fire Sciences Laboratory. [Online]. Available: http://www.fs.fed.us/database/feis//lichens/claspp/all.html [2017 Sep. 21].

Murphy, J., and Riley, J.P. 1962. A modified single solution method for the determination of phosphate in natural waters. Anal. Chim. Acta **27**: 31—36.

Nalder, I.A., and Wein, R.W. 1998. A new forest floor corer for rapid sampling, minimal disturbance and adequate precision. Silva Fenn. **32**: 373—382.

National Forest Inventory (NFI). 2008. Canada's national forest inventory ground sampling guidelines, V. 5. Canadian Forest Service, Victoria, BC. 271 pp.

Negrave, R.W., Prescott, C.E., and Barker, J.E. 2007. Growth and foliar nutrition of juvenile western hemlock and western redcedar plantations on low- and medium-productivity sites on northern Vancouver Island: response to fertilization and planting density. Can. J. For. Res. **37**: 2587—2599.

Neudorf, C.M., Lian, O.B., Walker, I.J., Shugar, D.H., Eamer, J.B.R., and Griffin, L.C.M. 2015. Toward a luminescence chronology for coastal dune and beach deposits on Calvert Island, British Columbia central coast, Canada. Quat. Geochronol. **30**: 275—281.

Nesbitt, H., and Young, G. 1982. Early proterozoic climates and plate motions inferred from major element chemistry of lutites. Nature **299**: 715—717.

Newman, G.S., and Hart, S.C. 2015. Shifting soil resource limitations and ecosystem retrogression across a three million year semi-arid substrate age gradient. Biogeochemistry **124:** 177—186.

Newman, R.H., and Tate, K.R. 1980. Soil phosphorus characterisation by ^{31}P nuclear

magnetic resonance. Commun. Soil Sci. Plant Anal. **11**: 835—842.

Noble, M. G., Lawrence, D. B., and Streveler, G. P. 1984. Sphagnum invasion beneath an evergreen forest canopy in southeastern Alaska. Bryologist **87:** 119—127.

Northup, R.R., Dahlgren, R.A., and McColl, J.G. 1998. Polyphenols as regulators of plant-litter-soil interactions in northern California's pygmy forest: a positive feedback? J. Biogeochem. **42**: 189—220.

O'Halloran, I.P., and Cade-Menun, B. 2008. Chapter 24. Total and organic phosphorus. Pages 265—291 in M.R. Carter, and E.G. Gregorich, eds. Soil sampling and methods of analysis, 2nd ed. Canadian Society of Soil Science and CRC Press, Boca Raton, FL.

Oberson, A., and Joner, E.J. 2005. Microbial turnover of phosphorus in soil. Pages 133—164 in B.L. Turner, E. Frossard, and D.S. Baldwin, eds. Organic Phosphorus in the Environment. CABI Publishing, Cambridge, MA.

Ohno, R., and L.M. Zibilske. 1991. Determinations of low concentrations of phosphorus in soil extracts using malachite green. Soil Sci. Soc. Am. J. **55**: 892—895.

Oliver, A.A., Tank, S.E., Giesbrecht, I., Korver, M.C., Floyd, W.C., Sanborn, P., Bulmer, C., and Lertzman, K.P. 2017. A global hotspot for dissolved organic carbon in hypermaritime watersheds of coastal British Columbia. Biogeosciences **14**: 3743—3762.

Olsen, S.R., Cole, C.V., Watanabe, F.S., and Dean, L.A. 1954. Estimation of available phosphorus in soils by extraction with sodium bicarbonate. U.S.D.A. Circ. 939, U.S. Government Printing Office, Washington, DC. 19 pp. [online] https://archive.org/details/estimationofavai939olse [17 Oct. 2017].

Olsen, S.R., and Sommers, L.E. 1982. Phosphorus. Pages 403—430 in A. L. Page, R. H. Miller, and D. R. Keeney, eds. Methods of soil analysis, part 2. Chemical and biological properties, 2nd ed. American Society of Agronomy, Inc. & Soil Science Society of America, Inc. Madison, WI, USA.

Parfitt, R. 1977. Phosphate adsorption on an Oxisol. Soil Sci. Soc. Am. J. **41**: 1064—1067.

Parfitt, R. 1979. The availability of P from phosphate-goethite bridging complexes. Desorption and uptake by ryegrass. Plant Soil **53**: 55–65.

Parfitt, R. 1989. Phosphate reactions with natural allophane, ferrihydrite and goethite. J. Soil Sci. **40**: 259—369.

Parfitt, R. 1990. Allophane in New Zealand - a review. Soil Res. **28**: 343—360.

Parfitt, R.L., and Henmi, T. 1982. Comparison of an oxalate-extraction method and an

infrared spectroscopic method for determining allophane in soil clays. Soil Sci. Plant. Nutr. **28**:183—190.

Parfitt, R.L., and Kimble, J.M. 1989. Conditions for formation of allophane in soils. Soil Sci. Soc. Am. J. **53**: 971—977.

Parfitt, R.L., Ross, D.J., Coomes, D.A., Richardson, S.J., Smale, M.C., and Dahlgren, R.A. 2005. N and P in New Zealand soil chronosequences and relationships with foliar N and P. Biogeochemistry **75**: 305—328.

Parkinson, J., and Allen, S. 1975. A wet oxidation procedure suitable for the determination of nitrogen and mineral nutrients in biological material. Commun. Soil Sci. Plant Anal. **6**: 1—11.

Peltzer, D.A., Wardle, D.A., Allison, V.J., Baisden, W.T., Bardgett, R.D., Chadwick, O.A., Condron, L.M., Parfitt, R.L., Porder, S., and Richardson, S.J. 2010. Understanding ecosystem retrogression. Ecol. Monogr. **80**: 509—529.

Petersen, L. 1976. Podzols and Podzolization. DSR Forlag, Copenhagen, NLD. 293 pp.

Porder, S. and Ramachandran, S. 2013. The phosphorus concentration of common rocks—a potential driver of ecosystem P status. Plant soil **367:** 41—55.

Prescott, C.E., McDonald, M.A., and Weetman, G.F. 1993. Availability of N and P in the forest floors of adjacent stands of western redcedar – western hemlock and western hemlock – amabilis fir on northern Vancouver Island. Can. J. For. Res. **23**: 605—610.

Preston, C.M., and Trofymow, J.A. 2000. Characterization of soil P in coastal forest chronosequences of southern Vancouver Island: Effects of climate and harvesting disturbance. Can. J. Soil Sci. **80**: 633—647.

Protz, R., Martini, I., Ross, G., and Terasmae, J. 1984. Rate of podzolic soil formation near Hudson Bay, Ontario. Can. J. Soil Sci. **64**: 31—49.

Protz, R., Shipitalo, M., Ross, G., and Terasmae, J. 1988. Podzolic soil development in the southern James Bay Lowlands, Ontario. Can. J. Soil Sci. **68**: 287—305.

Qian, P., Schoneau, J.J., and Karamanos, R.E. 1994. Simultaneous extraction of available phosphorus and potassium with a new soil test: a modification of Kelowna extraction. Commun. Soil Sci. Plant Anal. **25**: 627—635.

Quiquampoix, H., and Mousain, D. 2007. Enzymatic hydrolysis of organic phosphorus. Pages 89—112 in Turner, B.L., Frossard, R., and D.S. Baldwin, eds. Organic Phosphorus in the Environment. CABI Publishing, Cambridge, MA.

Radwan, M., and Harrington, C.A. 1986. Foliar chemical concentrations, growth, and site

productivity relations in western redcedar. Can. J. For. Res. **16**: 1069—1075.

Read, D.J. 1991. Mycorrhizas in ecosystems. Experientia **47**: 376–-391.

Read, D.J., and Perez-Moreno, J. 2003. Mycorrhizas and nutrient cycling in ecosystems – a journey towards relevance? New Phytol. **157**: 475—492.

Redfield, A. C. 1958. The biological control of chemical factors in the environment. Am. Sci. **46:** 205—221.

Refsnider, K.A., and Miller, G.H. 2013. Ice-sheet erosion and the stripping of tertiary regolith from Baffin Island, eastern Canadian arctic. Quat. Sci. Rev. **67**: 176—189.

Richardson, S.J., Allen, R.B., and Doherty, J.E. 2008. Shifts in leaf N: P ratio during resorption reflect soil P in temperate rainforest. Func. Ecol. **22**: 738—745.

Richardson, A.E., George, T.S., Hens, M., and Simpson, R.J. 2005a. Utilization of soil organic phosphorus by higher plants. Pages 165—184 in B.L. Turner, E. Frossard and D.S. Baldwin, eds. Organic Phosphorus in the Environment, CAB International, Wallingford, UK.

Richardson, S.J., Peltzer, D.A., Allen, R.B., and McGlone, M. S. 2005b. Resorption proficiency along a chronosequence: responses among communities and within species. Ecology **86:** 20—25.

Richardson, A.E., and Simpson, R.J. 2011. Soil microorganisms mediating phosphorus availability update on microbial phosphorus. Plant Physiol. **156**: 989—996.

Richardson, A.E., Barea, J.-M., McNeill, A.M., and Prigent-Combaret, C. 2009. Acquisition of phosphorus and nitrogen in the rhizosphere and plant growth promotion by microorganisms. Plant Soil **321**: 305—339.

Richardson, S.J., Peltzer, D.A., Allen, R.B., and McGlone, M. S. 2010. Declining soil fertility does not increase leaf lifespan within species: evidence from the Franz Josef chronosequence, New Zealand. NZ J. Ecol. **34:** 306—310.

Richardson, S.J., Peltzer, D.A., Allen, R.B., McGlone, M.S., and Parfitt, R.L. 2004. Rapid development of phosphorus limitation in temperate rainforest along the Franz Josef soil chronosequence. Oecologia **139**: 267—276.

Roddick, J.A. 1996a. Geology, Rivers Inlet (92M) - Queens Sound Map Areas, British Columbia. Open File 3278. Geological Survey of Canada, Victoria, BC. 102 pp.

Roddick, J.A. 1996b. Rivers Inlet (92 M) bedrock geochemistry. Unpublished raw data. Geological Survey of Canada, Victoria, BC.

Rossi, A.M., and Rabenhorst, M.C. 2016. Pedogenesis and landscape relationships of a Holocene age barrier island. Geoderma **262**: 71—84.

Ryan, P., Delhaize, E., and Jones, D. 2001. Function and mechanism of organic anion exudation from plant roots. Annu. Rev. Plant Physiol. Plant Biol. **52**: 527—560.

Sanborn, P. 2016. The imprint of time on Canadian soil landscapes. Quat. Int. **418**: 165—179.

Sanborn, P., and Lavkulich, L.M. 1989. Ferro-Humic Podzols of coastal British Columbia: I Morphology, selected properties, and classification. Soil Sci. Soc. Am. J. **53**: 511—517.

Sanborn, P., and Massicotte, H. 2010. A holocene coastal soil chronosequence: Naikoon Provincial Park, Graham Island, Haida Gwaii: Progress report. University of Northern British Columbia, Prince George, BC. 53 pp.

Sanborn, P., Lamontagne, L., and Hendershot, W. 2011. Podzolic soils of Canada: Genesis, distribution, and classification. Can. J. Soil Sci. **91**: 843—880.

Sanchez, P.A. 1976. Properties and management of soils in the tropics. John Wiley and Sons, New York, New York, USA. 618 pp.

Sanchez, P.A., and Uehara, G. 1980. Management considerations for acid soils with high phosphorus fixation capacity. Pages 471—514 in Khasawneh F.E., Sample E.C. and E.J. Kamprath, eds. The Role of Phosphorus in Agriculture. American Society of Agronomy, Madison, WI.

Sauer, D., Schülli-Maurer, I., Sperstad, R., Sørensen, R., and Stahr, K. 2008. Podzol development with time in sandy beach deposits in southern Norway. J. Plant Nutr. Soil Sci. **171**: 483—497.

Sauer, D., Sponagel, H., Sommer, M., Giani, L., Jahn, R., and Stahr, K. 2007. Podzol: soil of the year 2007. A review on its genesis, occurrence, and functions. J. Plant Nutr. Soil Sci. **170**: 581—597.

Saunders, W., and Williams, E. 1955. Observations on the determination of total organic phosphorus in soils. Eur. J. Soil Sci. **6**: 254—267.

Schachtman, D.P., Reid, R.J., and Ayling, S.M. 1998. Phosphorus uptake by plants: from soil to cell. Plant Physiol. **116**: 447—453.

Schaetzl, R., and Anderson, S. 2005. Soil genesis and morphology. Cambridge University Press, New York, NY. 817 pp.

Schaetzl, R., Barrett, L., and Winkler, J. 1994. Choosing models for soil chronofunctions and fitting them to data. Eur. J. Soil Sci. **45**: 219—232.

Schneider, K.D., Cade-Menun, B.J., Lynch, D.H., and Voroney, R.P. 2016. Soil phosphorus forms from organic and conventional forage fields. Soil Sci. Soc. Am. J. **80**: 328—340.

Seeling, B., and Zasoski, R.J. 1993. Microbial effects in maintaining organic and inorganic solution phosphorus concentrations in a grassland topsoil. Plant Soil **148**: 277—284.

Selmants, P.C., and Hart, S.C. 2008. Substrate age and tree islands influence carbon and nitrogen dynamics across a retrogressive semiarid chronosequence. Global Biogeochem. Cycles **22**: 1—13.

Selmants, P.C., and Hart, S.C. 2010. Phosphorus and soil development: does the Walker and Syers model apply to semiarid ecosystems? J. Ecol. **91**: 474—484.

Shang, C., Huang, P., and Stewart, J. 1990. Kinetics of adsorption of organic and inorganic phosphates by short-range ordered precipitate of aluminum. Can. J. Soil Sci. **70**: 461—470.

Shang, C., Caldwell, D.E., Stewart, J.W.B., Tiessen, H., and Huang, P.M. 1996. Bioavailability of organic and inorganic phosphates adsorbed on short-range ordered aluminum precipitate. Microb. Ecol. **31**: 29—39.

Shane, M., and Lambers, H. 2005. Cluster roots: a curiosity in context. Plant Soil 274: 101—125.

Shane, M.W., McCully, M.E., and Lambers, H. 2004a. Tissue and cellular phosphorus storage during development of phosphorus toxicity in *Hakea prostrata* (Proteaceae). J. Exp. Bot. **55**: 1033–1044.

Shane, M.W., Szota, C., and Lambers, H. 2004b. A root trait accounting for the extreme phosphorus sensitivity of *Hakea prostrata* (Proteaceae). Plant Cell Environ. **27**: 991–1004.

Shugar, D.H.,Walker, I.J., Lian, O.B., Eamer, J.B.R., Neudorf, C., McLaren, D., and Fedje, D. 2014. Post-glacial sea-level change along the Pacific coast of North America. Quat. Sci. Rev. **97:** 170—192.

Singleton, G.A., and Lavkulich, L.M. 1987a. A soil chronosequence on beach sands, Vancouver Island, British Columbia. Can. J. Soil Sci. **67**: 795—810.

Singleton, G.A., and Lavkulich, L.M. 1987b. Phosphorus transformations in a soil chronosequence, Vancouver Island, British Columbia. Can. J. Soil Sci. **67**: 787—793.

Skjemstad, J., Waters, A.G., Hanna, J.V., and Oades, J.M. 1992. Genesis of Podzols on coastal dunes in Southern Queensland. IV. Nature of the organic fraction as seen by ^{13}C nuclear magnetic resonance spectroscopy. Soil Res. **30**: 667—681.

Smernik, R.J., Doolette, A.L., and Noack, S.R. 2015. Identification of RNA hydrolysis products in NaOH-EDTA extracts using ^{31}P NMR spectroscopy. Commun. Soil Sci. Plant Anal. **46**: 2746—2756.

Smith, D. H., and Clark, F. E. 1951. Anion-exchange chromatography of inositol phosphates from soil. Soil Sci. **72**: 353—360.

Smith, D.H., and Read, D.J. 1997. Mycorrhizal symbiosis. 2nd ed. Academic Press, San Diego, CA. 605 pp.

Smith, F.W., Ellis, B.G., and Grava, J. 1957. Use of acid fluoride solutions for the extraction of available phosphorus in calcareous soils and in soils to which rock phosphate has been added. Soil Sci. Soc. Am. Proc. **21**: 400—404.

Soil Classification Working Group (SCWG). 1998. The Canadian system of soil classification. 3rd ed. Agriculture and Agri-Food Canada, Ottawa, ON. 202 pp.

Sondheim, M., Singleton, G., and Lavkulich, L. 1981. Numerical analysis of a chronosequence, including the development of a chronofunction. Soil Sci. Soc. Am. J. **45**: 558—563.

Stevens, P.R., and Walker, T.W. 1970. The chronosequence concept and soil formation. Q. Rev. Biol. **45**: 333—350.

Stevenson, F.J., and Cole, M.A. 1999. Phosphorus. Pages 279—329 in F.J. Stevenson, and M.A. Cole, eds. Cycles of soil: Carbon, nitrogen, phosphorus, sulfur and micronutrients. Wiley and Sons, Inc., New York, NY.

Syers, J.K., and Walker, T.W. 1969. Phosphorus transformations in a chronosequence of soils developed on wind-blown sand in New Zealand. Eur. J. Soil Sci. **20**: 57—64.

Syers, J. K., Williams, J., Campbell, A. and Walker, T. 1967. The significance of apatite inclusions in soil phosphorus studies. Soil Sci. Soc. Am. J. **31:** 752—756.

Tamm, O. 1920. Markstudier i det Nordsvenska barrskogsområdet. Medd. Statens Skogsförsöksanstalt **17**: 49—300.

Tate, K., and Newman, R. 1982. Phosphorus fractions of a climosequence of soils in New Zealand tussock grassland. Soil Biol. Biochem. **14**: 191—196.

Tejan-Kella, M.S., Chittleborough, D.J., and Fitzpatrick, R.W. 1991. Weathering assessment of heavy minerals in age sequences of Australian sandy soils. Soil Sci. Soc. Am. J. **55**: 427—438.

Thompson, C.H. 1981. Podzol chronosequences on coastal dunes of eastern Australia. Nature **91**: 59—61.

Thompson, C. 1992. Genesis of Podzols on coastal dunes in southern Queensland. I. Field relationships and profile morphology. Soil Res. **30**: 593—613.

Thompson, S.D., Nelson, T.A., Giesbrecht, I., Frazer, G., and Saunders, S. 2016. Data-driven regionalization of forested and non-forested ecosystems in coastal British Columbia with LiDAR and RapidEye imagery. App. Geogr. **69**: 35—50.

Tiessen, H. 2005. Phosphorus dynamics in tropical soils. Pages 253–262 in J. T. Sims and A.N.Sharpley, eds. Phosphorus, agriculture and the environment. ASA-CSSA- SSSA, Madison, Wisconsin, Il.

Tiessen, H., and Moir, J. 1993. Characterization of available P by sequential extraction. Pages 75—86 in M.R. Carter, Ed. Soil sampling and methods of analysis. Lewis Publishers, Boca Raton, Florida, USA.

Tiessen, H., Stewart, J.W.B., and Cole, C.V. 1984. Pathways of phosphorus transformations in soils of differing pedogenesis. Soil Sci. Am. J. **48**: 853—858.

Tomkins, I.B., Kellas, J.D., Tolhurst, K.G., and Oswin, D.A. 1991. Effects of fire intensity on soil chemistry in a eucalypt forest. Aust. J. Soil Res. **29**: 25—47.

Tonkin, P., and Basher, L. 2001. Soil chronosequences in subalpine Superhumid Cropp Basin, western southern alps, New Zealand. New Zeal. J. Geol. Geop. **44**: 37—45.

Tran, T.S., Giroux, M., Guilbeault, J., and Audesse, P. 1990. Evaluation of Mehlich-III extractant to estimate the available P in Quebec soils. Commun. Soil Sci. Plant. Anal. **21**: 1—28.

Trant, A.J., Niljand, W., Hoffman, K.A., Mathews, D.L., McLaren, D., Nelson, T.A., and Starzomski, B.M. 2016. Intertidal resource use over millennia enhances forest productivity. Nat. Commun. **7**: 12491.

Turner, B.L. 2008. Soil organic phosphorus in tropical forests: an assessment of the NaOH-EDTA extraction procedure for quantitative analysis by solution ^{31}P NMR spectroscopy. Eur. J. Soil Sci. **59**: 453—466.

Turner, B.L., and Blackwell, M.S.A. 2013. Isolating the influence of pH on the amounts and forms of soil organic phosphorus. Eur. J. Soil Sci. **64**: 249—259.

Turner, B. L., and Condron, L. M. 2013. Pedogenesis, nutrient dynamics, and ecosystem development: the legacy of TW Walker and JK Syers. Plant Soil **367:** 1—10.

Turner, B.L., and Laliberté, E. 2015. Soil development and nutrient availability along a 2 million-year coastal dune chronosequence under species-rich Mediterranean shrubland in southwestern Australia. Ecosystems **18**: 287—309.

Turner, B.L., and Richardson, A.E. 2004. Identification of *scyllo*-inositol phosphates in soil

by solution phosphorus-31 nuclear magnetic resonance spectroscopy. Soil Sci. Soc. Am. J. **68**: 802—808.

Turner, B.L., Cade-Menun, B.J., Condron, L.M., and Newman, S. 2005. Extraction of soil organic phosphorus. Talanta **66**: 294—306.

Turner, B.L., Cheesman, A.W., and Godage, H.Y.,Riley, A.M. and Potter, B.V.L. 2012b. Determination of *neo*- and D-*chiro*-inositol hexakisphosphate in soils by solution ^{31}P NMR spectroscopy. Environ. Sci. Technol. **46**: 4994—5002.

Turner, B.L., Condron, L.M., Richardson, S.J., Peltzer, D.A., and Allison, V.J. 2007. Soil organic phosphorus transformations during pedogenesis. Ecosystems **10**: 1166—1181.

Turner, B.L., Condron, L.M., Wells, A., and Andersen, K.M. 2012a. Soil nutrient dynamics during Podzol development under lowland temperate rain forest in New Zealand. Catena **97**: 50—62.

Turner, B.L., Cade-Menun, B.J., and Westermann, D.T. 2003a. Organic phosphorus composition and potential bioavailability in semi-arid arable soils of the Western United States. Soil Sci. Soc. Am. J. **67**: 1168—1179.

Turner, B.L., Mahieu, N., and Condron, L.M. 2003b. Phosphorus-31 nuclear magnetic resonance spectral assignments of phosphorus compounds in soil NaOH–EDTA extracts. Soil Sci. Soc. Am. J. **67**: 497—510.

Turner, B.L., Papházy, M.J., Haygarth, P.M., and McKelvie, I.D. 2002. Inositol phosphates in the environment. Biol. Sci. **357**: 449—469.

Turner, B.L., Wells, A., and Condron, L.M. 2014. Soil organic phosphorus transformations along a coastal dune chronosequence under New Zealand temperate rain forest. Biogeochemistry **121**: 595—611.

Turner, N.J. 1999. "Time to burn:" traditional use of fire to enhance resource production by Aboriginal Peoples in British Columbia. Pages 185—218 in R. Boyd, ed. Indians, fire and the land in the Pacific Northwest. Oregon State University Press, Corvallis, OR.

Turner, N.J. 2014. Ancient pathways, ancestral knowledge: ethnobotany and ecological wisdom of indigenous peoples of northwestern North America. McGill-Queen's Press, Montreal, Qu. 1056 pp.

Ugolini, F., and Dahlgren, R. 1991. Weathering environments and occurrence of imogolite/allophane in selected andisols and spodosols. Soil Sci. Soc. Am. J. **55**: 1166—1171.

Ugolini, F.C., and Mann, D.H. 1979. Biopedological origin of peatlands in south east Alaska. Nature **281**: 366—368.

Ugolini, F.C., Dawson, H., and Zachara, J. 1977. Direct evidence of particle migration in the soil solution of a Podzol. Science **198**: 603—605.

United States Department of Agriculture (USDA). 1999. Soil Taxonomy: A Basic System of Soil Classification for Making and Interpreting Soil Surveys. United States Department of Agriculture, Washington, DC.

Uren, N.C., and Parsons, R.F. 2013. Nutritional characteristics of soils on an inferred chronosequence. A comment on Laliberté et al. (2012). J. Ecol. **101:** 1085—1087.

van Breemen, N., Lundström, U.S., and Jongmans, A.G. 2000. Do plants drive podzolization via rock-eating mycorrhizal fungi? Geoderma **94**: 163—171.

Van den Driessche, R. 1974. Prediction of mineral nutrient status of trees by foliar analysis. Bot. Rev. **40:** 347—394.

Vincent, A.G., Turner, B.L., and Tanner, E.V.J. 2010. Soil organic phosphorus dynamics following perturbation of litter cycling in a tropical moist forest. Eur. J. Soil Sci. **61**: 48—57.

Vincent, A.G., Schleucher, J., Gröbner, G., Vestergren, J., Persson, P., Jansson, M., and Giesler, R. 2012. Changes in organic phosphorus composition in boreal forest humus soils: the role of iron and aluminum. Biogeochem. **108**: 485—499.

Vincent, A.G., Vestergren, J., Gröbner, G., Persson, P., Schleucher, J., and Giesler, R. 2013. Soil organic phosphorus transformations in a boreal forest chronosequence. Plant Soil **367**: 149—162.

Vitousek, P.M., and Farrington, H. 1997. Nutrient limitation and soil development: Experimental test of a biogeochemical theory. Biogeochemistry **37**: 63—75.

Vitousek, P.M., Porder, S., Houlton, B.Z., and Chadwick, O.A. 2010. Terrestrial phosphorus limitation: mechanisms, implications, and nitrogen–phosphorus interactions. Ecol. Appl. **20**: 5—15.

Vitousek, P. M., Turner, D. R. and Kitayama, K. 1995. Foliar nutrients during long-term soil development in Hawaiian montane rain forest. J. Ecol. **76:** 712—720.

Walker, J., Thompson, C.H., and Jehne, W. 1983. Soil weathering stage, vegetation succession, and canopy dieback. Pac. Sci. **37**: 471—481.

Walker, L.R., Wardle, D.A., Bardgett, R.D., and Clarkson, B.D. 2010. The use of chronosequences in studies of ecological succession and soil development. J. Ecol. **98**: 725—736.

Walker, P. 1962. Terrace chronology and soil formation on the south coast of NSW. J. Soil

Sci. 13: 178—186.

Walker, T. 1965. The significance of phosphorus in pedogenesis. Pages 295—315 in E.G. Hallsworth and D.V. Crawford (Eds), Experimental Pedology. Lincoln College, Canterbury, NZ.

Walker, T., and Adams, A.F.R. 1958. Studies on soil organic matter: I. Influence of phosphorus content of parent materials on accumulations of carbon, nitrogen, sulfur, and organic phosphorus in grassland soils. Soil Sci. **85**: 307—318.

Walker, T., and Syers, J.K. 1976. The fate of phosphorus during pedogenesis. Geoderma **15**: 1—19.

Wang, C., and Ross, G.J. 1990. Spodosols of Canada. Pages 395—410 in J.M. Kimble and R. Yeck, eds. Proc Fifth Int Soil Corr Meeting (ISCOM V): Characterization, Classification and Utilization of Spodosols. USDA, Washington, DC.

Wang, M., Moore, T.R., Talbot, J., and Richard, P.J. 2014. The cascade of C: N: P stoichiometry in an ombrotrophic peatland: from plants to peat. Env. Res. Lett. **9**: 024003.

Wang, C., Stea, R.R., Ross, G.J., and Holmstrom, D. 1986. Age estimation of the Shulie Lake and Eatonville Tills in Nova Scotia by pedogenic development. Can. J. Earth Sci. **23**: 115—119.

Wardle, D.A., Bardgett, R.D., Walker, L.R., Peltzer, D.A., and Lagerström, A. 2008. The response of plant diversity to ecosystem retrogression: evidence from contrasting long-term chronosequences. Oikos **117**: 93—103.

Wardle, D.A., Hörnberg, G., Zackrisson, O., Kalela-Brundin, M., and Coomes, D.A., 2003. Long-term effects of wildfire on ecosystem properties across an island area gradient. Science **300**: 972—975.

Wardle, D. A., Jonsson, M., Mayor, J. R., and Metcalfe, D. B. 2016. Above-ground and below-ground responses to long-term nutrient addition across a retrogressive chronosequence. J. Ecol. **104**: 545—560.

Wardle, D.A., Walker, L.R., and Bardgett, R.D. 2004. Ecosystem properties and forest decline in contrasting long-term chronosequences. Science **305**: 509—513.

Wardle, D. A., and Zackrisson, O. 2005. Effects of species and functional group loss on island ecosystem properties. Nature **435:** 806—810.

Wardle, D. A., Zackrisson, O., Hörnberg, G., and Gallet, C. 1997. The influence of island area on ecosystem properties. Science **277**: 1296—1299.

Westman, W.E., and Whittaker, R.H. 1975. The pygmy forest region of northern California:

Studies on biomass and primary productivity. J Ecol **63**: 493—520.

Whitton, B.A., Al-Shehri, A.M., Ellwood, N.T.W., and Turner, B.L. 2005. Ecological aspects of phosphatase activity in cyanobacteria, eukaryotic algae and bryophytes. Pages 205—241 in B.L. Turner, E. Frossard and D.S. Baldwin, eds. Organic Phosphorus in the Environment. CAB International, Wallingford, UK.

Williams, J., Syers, J.K., and Walker, T. 1967. Fractionation of soil inorganic phosphate by a modification of Chang and Jackson's procedure. Soil Sci. Soc. Am. J. **31:** 736—739.

Williams, J., and Walker, T. 1969a. Fractionation of phosphate in a maturity sequence of New Zealand basaltic soil profiles: I. Soil Sci. **107**: 22—30.

Williams, J., and Walker, T. 1969b. Fractionation of phosphate in a maturity sequence of New Zealand basaltic soil profiles: 2. Soil Sci. **107**: 213—219.

Williams, J., J.K. Syers, T. Walker, and R. Rex. 1970. A comparison of methods for the determination of soil organic phosphorus. Soil Sci. **110**: 13—18.

Williamson, W.M., Wardle, D.A., and Yeates, G.W., 2005. Changes in soil microbial and nematode communities during ecosystem decline across a long-term chronosequence. Soil Biol. Biochem. **37**: 1289—1301.

Wolf, M., Lehndorff, E., Mrowald, M., Eckmeier, E., Kehl, M., Frechen, M., Pätzold, S. and Amelung, W. 2014. Black carbon: fire fingerprints in Pleistocene loess-palaeosol archives in Germany. Org. Geochem. **70**: 44—52.

Wolfe, S.A., Walker, I.J., and Huntley, D.J. 2008. Holocene coastal reconstruction, Naikoon peninsula, Queen Charlotte Islands, British Columbia (no. 2008-12, 2008). Geological Survey of Canada, Vancouver, BC. 18 pp.

Wood, T.E., Bormann, F.H., and Voigt, G.K. 1984. Phosphorus cycling in a northern hardwood forest: biological and chemical control. Sci. **223**: 341—393.

Wu, S.-P., and Chen, Z.-S. 2005. Characteristics and genesis of inceptisols with placic horizons in the subalpine forest soils of Taiwan. Geoderma **125**: 331—341.

Yan, Y., Li, W., Yang, J., Zheng, A., Liu, F., Feng, X., and Sparks, D.L. 2014. Mechanism of *myo*-inositol hexakisphosphate sorption on amorphous aluminum hydroxide: spectroscopic evidence for rapid surface precipitation. Environ. Sci. Technol. **48**: 6735—6742.

Yang, X., Post, W. M., Thornton, P. E., Jain, A., and Ridge, O. 2013. The distribution of soil phosphorus for global biogeochemical modeling. Biogeosciences **10**: 2525—2537.

Young, A.W., Campbell, A.S., and Walker, T.W. 1980. Allophane isolated from a Podsol

developed on a non-vitric parent material. Nature **284**: 46—48.

Ziadi, N., and Tran, T.S. 2006. Mehlich 3-extractable elements. Pages 81—88 in M.R. Carter and E. Gregorich, eds. Soil sampling and methods of analysis Lewis, 2nd ed. CRC Press, Boca Raton, FL.

APPENDIX 1: LITERATURE SUMMARY TABLES

Table A1- 1. Chronosequences exhibiting phosphorus (P) decline with age and the mechanism of P limitation, status of retrogression and details of what soil horizons, and trends were identified in the following references.

Chronosequences	Mechanism of P Limitation	Retrogressed	Soil Horizon	Soil Trends		References
				Surface Horizons	All Horizons	
Arjeplog	Sink -driven	Yes	Humus (All)	N: P increased	N/A	(Wardle et al., 1997; Wardle et al., 2004; Vitousek et al., 2010)
Central Volcanic Plateau	Not verified	Not verified	Humus (All) Mineral (10cm)	Total P decreased	•Follows Walker and Syers' •Total P is humped with declining trend	(Parfitt et al., 2005; Richardson et al., 2008)
Cooloola	Low P PGM depletion driven	Yes	Mineral (to B horizon)	Slight increase in N: P in sand	Total P declines	(Thompson, 1981; Wardle et al., 2004; Vitousek et al., 2010)
Cox Bay	Not verified	Not verified	Mineral (to 90 cm)	Primary P declined exponentially	Primary P declined linearly	(Singleton and Lavkulicha, 1987a, b)
Franz Josef	Depletion driven	Yes	Humus (All, if present) Mineral (10 cm)	•Follows Walker and Syers' •Total P declined •N: P increased	N/A	(Stevens and Walker, 1970; Parfitt et al., 2005; Richardson et al., 2004; Wardle et al., 2004; Turner et al., 2012a)
Glacier Bay	Soil barrier	Yes	Humus (all) Mineral (10 cm)	N: P increased	Total P declined	(Noble et al., 1984; Chapin et al., 1994; Wardle et al., 2004; Vitousek et al., 2010)
Haast	Low P PGM depletion driven	Yes	Humus (All) Mineral (20 cm)	Total P declined	•Total P declined overall •Iron pan developed after 3,900 years •P mobilized by iron pan	(Eger et al., 2011; Turner et al., 2012a)
Hawaiian Substrate Age Gradient	Depletion driven	Yes	Humus (all) Mineral (all classified)	Minimal increase N: P	•Follows Walker and Syers' •SS not reached due to dust inputs	(Vitousek and Farrington, 1997; Crews et al., 1995; Wardle et al., 2004)
Jurien Bay	Low P PGM Depletion driven	Yes	Humus (all) Mineral (all classified)	Total P decreased in humped pattern	•Total P consistently decreased •Calcrete in stage 4 & 5	(Laliberté et al., 2012; Laliberté et al., 2013; Turner and Laliberté, 2015)
Manawatu	Not verified	Not verified	Humus (all) Mineral (100 cm)	•N: P increased •Mono:diester ratio declined	•Follows Walker and Syers' •Total P declined	(Syers and Walker, 1969; Walker and Syers, 1976; McDowell et al., 2007)
Mendocino	Depletion driven low P PGM	Yes	Litter Mineral (to hardpan)	Available P declined	•Available P declined •Hardpans developed on T3	(Jenny, 1969; Merritts et al., 1991; Northup et al., 1995)
Reefton	Not verified	Not verified	Humus (all) Mineral (64 cm)	•N: P increased •Mono:diester ratio declined	•Follows Walker and Syers' •Total P declined	(Walker and Syers, 1976; McDowell et al., 2007)

Chronosequences	Mechanism of P Limitation	Retrogressed	Soil Horizon	Soil Trends		References
				Surface Horizons	All Horizons	
San Francisco Volcanic Field	Depletion driven sink driven	Yes	Mineral (15 cm)	•Follows Walker and Syers' •Total P declined •Pca still dominates	N/A	(Selmants and Hart, 2008; Selmants and Hart, 2010)
Waitutu	Depletion driven and soil barrier	Yes	Humus (All) Mineral (10 cm)	•N: P increased •Total P declined (mineral) •Slight decline in total P (humus)	N/A	(Ward, 1988; Parfitt et al., 1995; Coomes et al., 2013; Wardle et al., 2004)

Table A1- 2. Vegetation characteristics for retrogressed chronosequences including vegetation diversity, litter and basal area factor (BA). (Note: Baffin Island, Cox Bay, Manawatu and Reefton are not present due to lack of vegetation data).

Chronosequences	Vegetation			References
	Diversity	Litter	BA/Tree Height	
Arjeplog	N/A	No N: P relationship	Decline in BA	(Wardle et al., 1997; Wardle et al., 2004)
Central Volcanic Plateau	N/A	•Resorption proficiency increase •N: P increased	N/A	(Richardson et al., 2008)
Cooloola	N/A	N: P increased	Decline in BA	(Wardle et al., 2004)
Franz Josef	N/A	N: P increased	Decline in BA	(Wardle et al., 2004)
Glacier Bay	N/A	N: P increased	Decline in BA Decline in tree height	(Wardle et al., 2004)
Haast	•Decreased •Shift towards stress tolerant species	N/A	N/A	(Eger et al., 2011; Turner et al., 2012a)
Hawaiian Substrate Age Gradient	N/A	N: P increased (when anomaly was removed)	Decline in BA	(Vitousek et al., 1995; Wardle et al., 2004)
Jurien Bay	Increased	Higher resorption proficiency and efficiency	N/A	(Laliberté et al., 2012, Hayes et al., 2014)
Mendocino	Shift towards stress tolerant species	N/A	N/A	(Jenny, 1969; Izquierdo et al., 2013)
San Francisco Volcanic Field	Vegetation limited by P	N/A	N/A	(Selmants and Hart, 2008; Selmants and Hart, 2010)
Waitutu	Decreased	No N: P relationship	Decline in BA, partially due to water table	(Coomes et al., 2005; Parfitt et al., 2005 ; Wardle et al., 2004)

APPENDIX 2: SITE AND PEDON DESCRIPTIONS

***Site No*:** CIDS1A
Soil Classification: CU.R.

Site Description
Latitude: 51˚39.484’ N
Longitude: 128˚08.643’ W
Elevation: 3 m
Slope Position: Crest
Parent Material: Sandy eolian ridge
Site Series: N/A

Humus Form: N/A
Rooting Depth (cm): 34
Root Restriction Depth (cm): N/A
Seepage Depth (cm): N/A

Comments: Augered from BC to C horizon.

Table A2- 1. Pedon description of CIDS1A.

Horizon Sample #	**Depth (cm)**	**Description**
C CIDS1A-01	0-27	Light olive gray (5Y 6/2 m); sand; single grain; loose; common, very fine roots; gradual, irregular boundary; 23-32 cm thick; moderately alkaline.
Ahb CIDS1A-02	27-34	Dark grayish brown (2.5Y 4/2 m); sand; single grain; very friable; common very fine and few fine roots; clear, broken boundary; 0-9 cm thick; moderately alkaline.
C2 CIDS1A-03	34-62	Light olive gray (5Y 6/2 m); sand; single grain; loose; few fine roots; gradual, smooth boundary; 23-29 cm thick; strongly alkaline.
Ahb2 CIDS1A-04	62-67	Grayish brown (2.5Y 5/2 m); sand; single grain; loose; few fine roots; gradual, wavy boundary; 4-14 cm thick; strongly alkaline.
BC CIDS1A-05	67-116	Gray (5Y 5.5/1 m); sand; single grain; loose; few fine roots; diffuse boundary; strongly alkaline.
C3	116-122+	N/A

*acidity determined by pH in water (CANSIS, 1982)

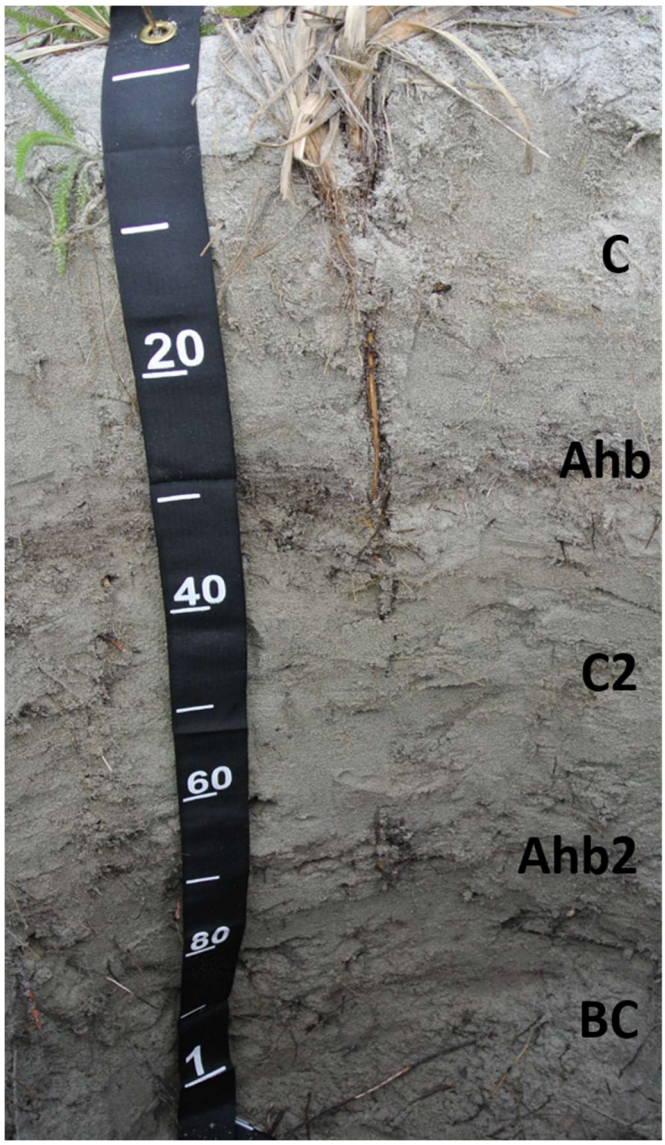

Figure A2- 1. Pedon CIDS1A with horizon designations. Depth is in cm.

***Site No*:** CIDS1B
Soil Classification: CU.R.

Site Description
Latitude: 51˚39.479’ N
Longitude: 128˚08.622’ W
Elevation: 4 m
Slope Position: Crest
Parent Material: Sandy eolian ridge
Site Series: N/A

Humus Form: N/A
Rooting Depth (cm): 92
Root Restriction Depth (cm): N/A
Seepage Depth (cm): N/A

Comments: Higher elevation than CIDS1A. Closer location may have greater erosion due to slope.

Table A2- 2. Pedon description of CIDS1B.

Horizon Sample #	**Depth (cm)**	**Description**
C CIDS1B-01	0-13	Light brownish gray (2.5Y 6/2 m); sand; single grain; loose; few, very fine and fine roots; clear, smooth boundary; 8-17 cm thick; moderately alkaline.
Ahb CIDS1B-02	13-18	Dark olive gray (5Y 3/2 m); sand; friable; massive, single grain; common, very fine and few fine roots; clear, smooth boundary; 4-6 cm thick; mildly alkaline.
BC CIDS1B-03	18-92	Light olive gray (5Y 6/2 m); sand; single grain; loose; common, very fine and fine roots; diffuse, smooth boundary; 73-76 cm thick; strongly alkaline.
C2 CIDS1B-04	92-114+	Light gray (5Y 7/1 d); sand; single grain; loose; few, very fine and fine roots; strongly alkaline.

*acidity determined by pH in water (CANSIS, 1982)

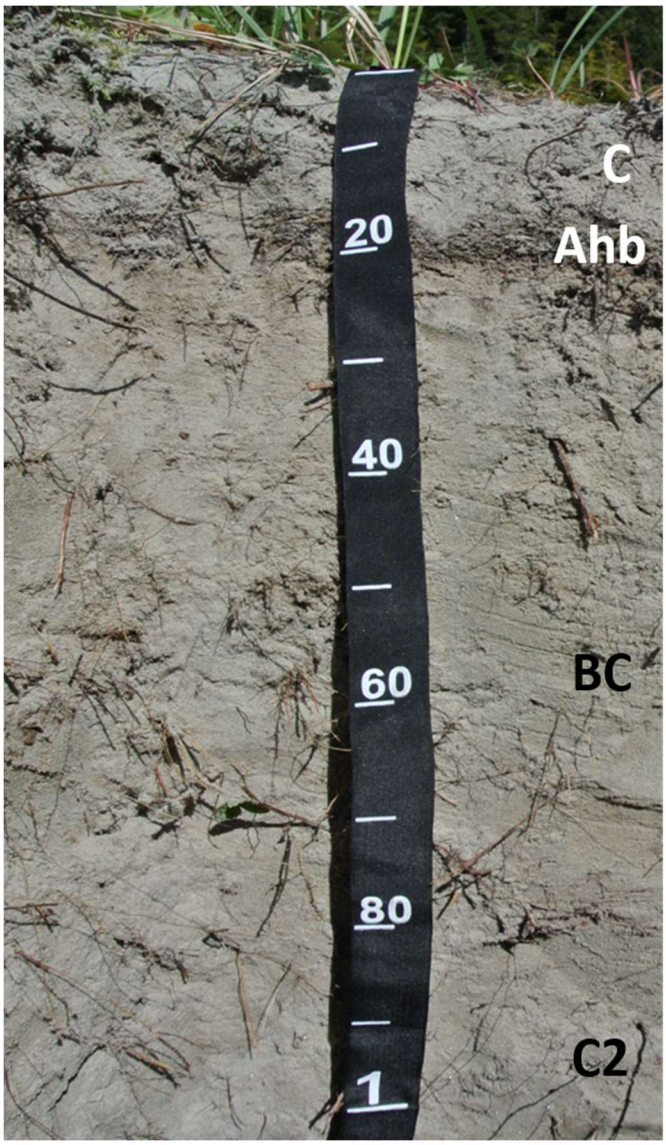

Figure A2- 2. Pedon CIDS1B with horizon designations. Depth is in cm.

***Site No*:** CIDS3A
Soil Classification: E.DYB

Site Description
Latitude: 51˚39.218’ N *Longitude*: 128˚08.285’ W
Elevation: 15 m *Slope Position*: Nearly level
Parent Material: Mesic organic veneer over a sandy eolian ridge
Site Series: 15 Ss

Humus Form: Lignomor *Rooting Depth (cm)*: 50

Root Restriction Depth (cm): N/A *Seepage Depth (cm)*: N/A

Comments: Noted darker banding in BC horizon, colour is noted below.

Table A2- 3. Pedon description of CIDS3A.

Horizon Sample #	**Depth (cm)**	**Description**
S/L CIDS3A-01	28-26	Organic; dark reddish brown (5YR 3/2 m); 1-3 cm thick; extremely acid.
Fm CIDS3A-02	26-22	Organic; very dark brown (7.5YR 2.5/2 m); strong, non-compact matted; common mycelia; abundant, very fine to medium roots; clear, wavy boundary; 2-5 cm thick; extremely acid.
Hw CIDS3A-03	22-0	Organic; very dark brown (10YR 2/2 m); strong, recumbent; abundant, very fine to medium and few coarse roots; abrupt, wavy boundary; 18-27 cm thick; extremely acid.
Ae CIDS3A-04	0-3	Grayish brown (2.5Y 5/2 m); sand; single grain; loose; fine, few roots; gradual, broken boundary; 0-5 cm thick; extremely acid.
Bmj CIDS3A-05	3-58	Brown (10YR 4/3 m); sand; single grain; loose; few, very fine to coarse roots; diffuse, smooth boundary; 52-56 cm thick; strongly acid.
BC CIDS3A-06	58-93+	Olive brown (2.5Y 4/3 m), dark yellowish brown (10YR 4/4 m); sand; single grain; loose; very strongly acid.

*acidity determined by pH in water (CANSIS, 1982)

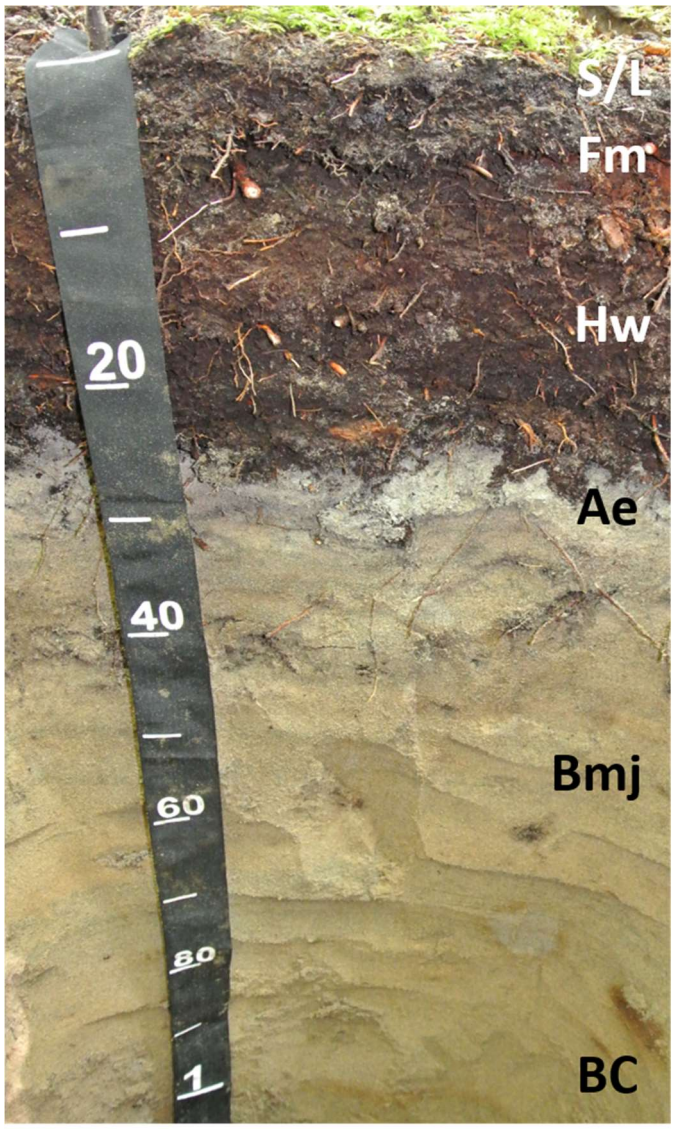

Figure A2- 3. Pedon CIDS3A with horizon designations. Depth is in cm.

***Site No*:** CIDS3B
Soil Classification: E.DYB

Site Description
Latitude: 51˚39.207' N *Longitude*: 128˚08.273' W
Elevation: 14 m *Slope Position*: Nearly level
Parent Material: Mesic organic veneer over a sandy eolian ridge
Site Series: 15 Ss

Humus Form: Lignomor *Rooting Depth (cm)*: 63

Root Restriction Depth (cm): N/A *Seepage Depth (cm)*: N/A

Comments: This site is close to CIDS3A because we wanted to stay on the visible dune and not sample in an ephemeral drainage. Sitka spruce not the dominant tree type on this site because it looks like it has been cut down preferentially.

Table A2- 4. Pedon description of CIDS3B.

Horizon Sample #	**Depth (cm)**	**Description**
S/L CIDS3B-01	37-35	Organic; dark reddish brown (5YR 3/2 m); 1-4 cm thick; extremely acid.
Fm CIDS3B-02	35-33	Organic; very dark brown (7.5YR 2.5/2 m); weak, non-compact matted; common mycelia; abundant, very fine to fine roots; clear, wavy boundary; 1-3 cm thick; extremely acid.
Hw CIDS3B-03	33-0	Organic; black (7.5YR 2.5/1 m); moderate granular; few mycelia; abundant, very fine to fine and few, medium roots; abrupt, wavy boundary; 28-37 cm thick; extremely acid.
Ae CIDS3B-04	0-3	Grayish brown (2.5Y 5/2 m); sand; single grain; loose; few, very fine to fine roots; gradual, broken boundary; 0-10 cm thick; extremely acid.
Bhj CIDS3B-05	3-26	Dark yellowish brown (10YR 4/4 m); sand; single grain; loose; common, very fine to medium roots; gradual, wavy boundary; 7-31 cm thick; very strongly acid.
Bm CIDS3B-06	26-55	Olive brown (2.5Y 4/3 m); sand; single grain; loose; few, very fine to medium roots; diffuse, smooth boundary; 22-45cm thick; very strongly acid.
BC CIDS3B-07	55-120+	Light olive brown (2.5Y 5/3 m); sand; single grain; loose; very strongly acid.

*acidity determined by pH in water (CANSIS, 1982)

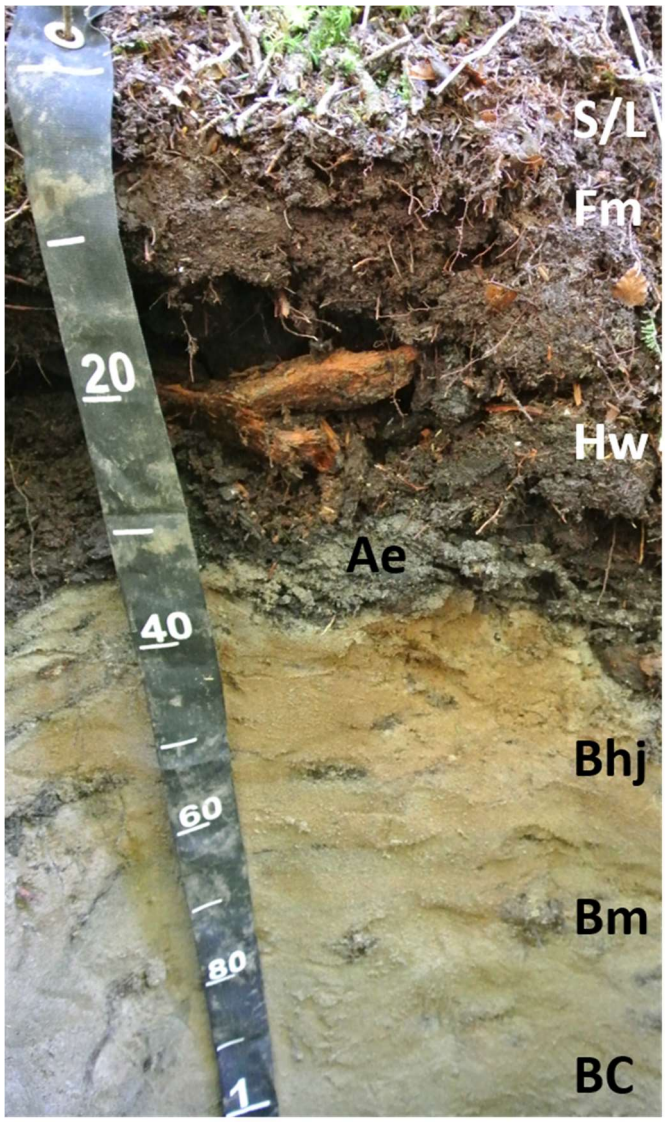

Figure A2- 4. Pedon CIDS3B with horizon designations. Depth is in cm.

***Site No*:** CIDS4A
Soil Classification: E.DYB

Site Description

Latitude: 51˚39.381' N *Longitude*: 128˚08.316' W
Elevation: 14 m *Slope Position*: Crest
Parent Material: Sandy eolian ridge
Site Series: 01 CwHw

Humus Form: Mormoder *Rooting Depth (cm)*: 9
Root Restriction Depth (cm): N/A *Seepage Depth (cm)*: N/A

Table A2- 5. Pedon description of CIDS4A.

Horizon Sample #	**Depth (cm)**	**Description**
S/L CIDS4A-01	9-8	Organic; very dark brown (7.5YR 2.5/2 m); 0-1 cm thick; extremely acid.
Fa CIDS4A-01	8-7	Organic; very dark brown (7.5YR 2.5/2 m); weak, non-compact matted; common mycelia; common, very fine to medium and few, coarse roots; clear, smooth boundary; 0-2 cm thick; extremely acid.
Hh CIDS4A-02	7-0	Organic; very dark brown (7.5YR 2.5/2 m); massive; few mycelia; common, very fine to medium and few coarse roots; abrupt, irregular boundary; 6-9 cm thick; extremely acid.
Ae CIDS4A-03	0-3	Grayish brown (2.5Y 5/2 m); loamy sand; single grain; loose; few, fine and medium roots; gradual, broken boundary; 0-3 cm thick; extremely acid.
Bhj CIDS4A-04	3-23	Brown (10YR 4/3 m); sand; single grain; loose; few, very fine and fine roots; diffuse, wavy boundary; 3-24 cm thick; very strongly acid.
Bm CIDS4A-05	23-73	Light olive brown (2.5Y 5/3 m); sand; single grain; loose; few, fine and medium roots; diffuse, smooth boundary; 45-62 cm thick; strongly acid.
BC CIDS4A-06	73-111+	Olive yellow (2.5Y 6/8 m); sand; single grain; loose; few, medium roots; strongly acid.

*acidity determined by pH in water (CANSIS, 1982)

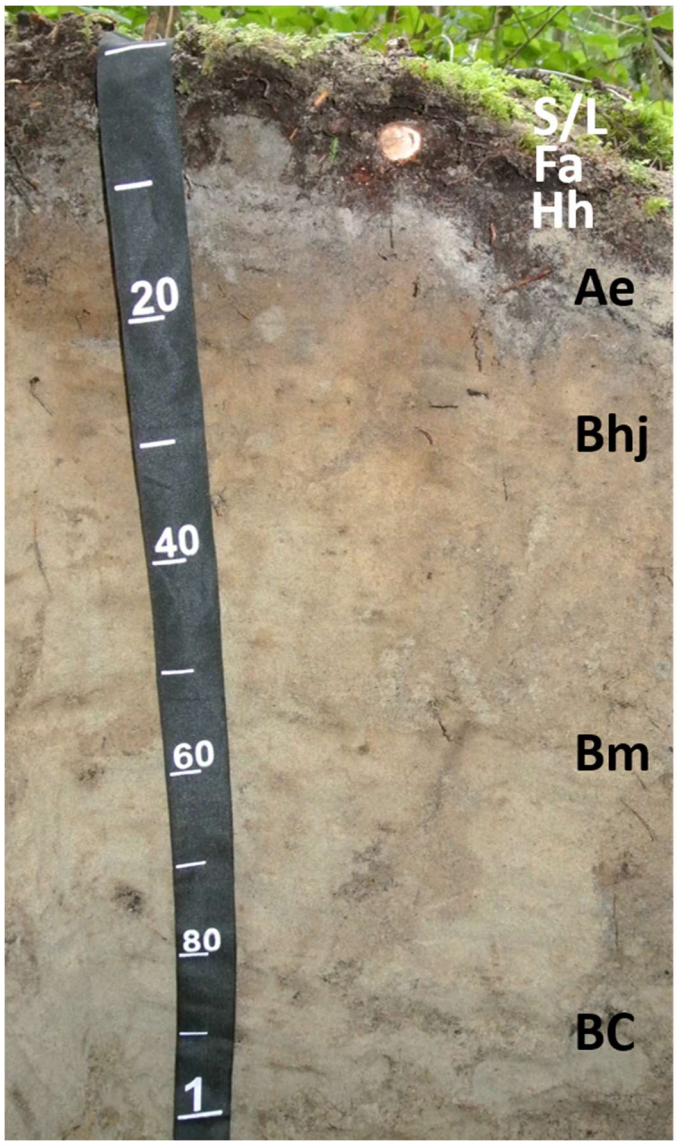

Figure A2- 5. Pedon CIDS4A with horizon designations. Depth is in cm.

***Site No*:** CIDS4B
Soil Classification: E.DYB

Site Description
Latitude: 51˚39.383' N *Longitude*: 128˚08.315' W
Elevation: 13 m *Slope Position*: Middle slope
Parent Material: Mesic organic veneer over a sandy eolian ridge
Site Series: 01 CwHw

Humus Form: Humimor *Rooting Depth (cm)*: 15

Root Restriction Depth (cm): N/A *Seepage Depth (cm)*: N/A

Table A2- 6. Pedon description of CIDS4B.

Horizon Sample #	**Depth (cm)**	**Description**
S/L CIDS4B-01	10-8	Organic; dark brown (7.5YR 3/4 m); 1-3 cm thick; extremely acid.
Fm CIDS4B-02	8-6	Organic; very dusky red (2.5YR 2.5/2 m); weak, non-compact matted; abundant mycelia; abundant, very fine and fine roots; clear, smooth boundary; 1-4 cm thick; extremely acid.
Hh CIDS4B-03	6-0	Organic; black (7.5YR 2.5/1 m); massive; few mycelia; abundant, very fine and medium and few, fine roots; clear, smooth boundary; 6-7 cm; extremely acid.
Ae CIDS4B-04	0-5	Dark gray (10YR 4/1 m); sand; single grain; loose; common, fine and medium, and few, coarse roots; gradual, irregular boundary; 2-17 cm; extremely acid.
Bhj CIDS4B-05	5-19	Dark yellowish brown (10YR 3/4 m); sand; single grain; loose; few very fine and fine roots; gradual, wavy boundary; 6-16 cm thick; extremely acid.
Bm CIDS4B-06	19-64	Light yellowish brown (2.5Y 6/3 m); sand; many, medium to coarse, distinct dark yellowish brown (10YR 3/4 m) mottles; single grain; loose; few, very fine to fine roots; diffuse, smooth boundary; 31-53 cm thick; very strongly acid.
BC CIDS4B-07	64-103+	Light yellowish brown (2.5Y 6/3 m); sand; common, medium to coarse, distinct dark yellowish brown (10YR 3/4 m) mottles; single grain; loose; few, fine roots; very strongly acid.

*acidity determined by pH in water (CANSIS, 1982)

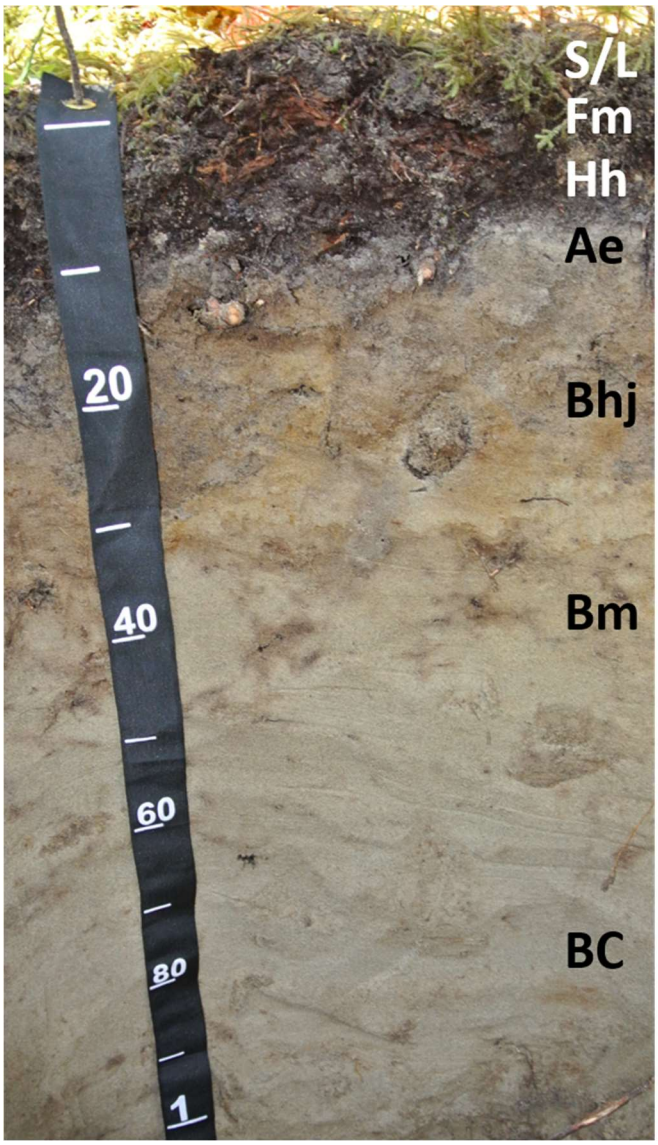

Figure A2- 6. Pedon CIDS4B with horizon designations. Depth is in cm.

***Site No*:** CIDS8A
Soil Classification: OT.HP

Site Description
Latitude: 51˚38.480' N *Longitude*: 128˚09.109' W
Elevation: 27 m *Slope Position*: Upper slope
Parent Material: Mesic organic veneer over a sandy eolian ridge
Site Series: 14 Ss

Humus Form: Lignomor *Rooting Depth (cm)*: 37

Root Restriction Depth (cm): 62 *Seepage Depth (cm)*: 90

Table A2- 7. Pedon description of CIDS8A.

Horizon Sample #	**Depth (cm)**	**Description**
L CIDS8A-01	37-34	Organic; very dark brown (7.5YR 2.5/3 m); medium acid.
Fm CIDS8A-02	34-15	Organic; very dark brown (10YR 2/2 m); weak, non-compact matted; abundant mycelia; abundant, very fine to coarse roots; clear, wavy boundary; 13-27 cm thick; extremely acid.
Hw CIDS8A-04	15-0	Organic; black (7.5YR 2.5/1 m); charcoal in wood; moderate recumbent; few mycelia; common, very fine to coarse roots; clear, irregular boundary; 0-26 thick; extremely acid.
Ahe CIDS8A-05	0-6	Yellowish brown (10YR 5/4 m); loamy sand; massive; friable; few, very fine and fine roots; clear, broken boundary; 3-10 cm thick; extremely acid.
Ae CIDS8A-06	6-25	Light brownish gray (2.5Y 6/2 m); sand; single grain; loose; gradual, wavy boundary; 3-27 cm thick; extremely acid.
Bhc CIDS8A-07	25-43	Very dark brown (10YR 2/2 m); sand; massive; very firm; gradual, wavy boundary; 4-19 cm thick; very strongly acid.
Bfc1 CIDS8A-08	43-45	Dark reddish brown (2.5YR 2.5/3 m), black (7.5YR 2.5/1 m); sand; massive; firm; clear, wavy boundary; 1-4 cm thick; very strongly acid.
Bm1 CIDS8A-09	45-65	Dark brown (7.5YR 3/2 m); sand; single grain; friable; clear, smooth boundary; 3-24 cm thick; very strongly acid.
Bfc2 CIDS8A-10	65-67	Dark reddish brown (5YR 3/4 m); sand; massive; very firm; clear, broken boundary; 1-4 cm thick; very strongly acid.
Bm2 CIDS8A-11	67-95	Dark yellowish brown (10YR 3/4 m); sand; massive; friable; gradual, smooth boundary; 17-19 cm thick; very strongly acid.
BC CIDS8A-12	95-163+	Light olive brown (2.5Y 5/4 m); sand; single grain; loose; strongly acid.

*acidity determined by pH in water (CANSIS, 1982)

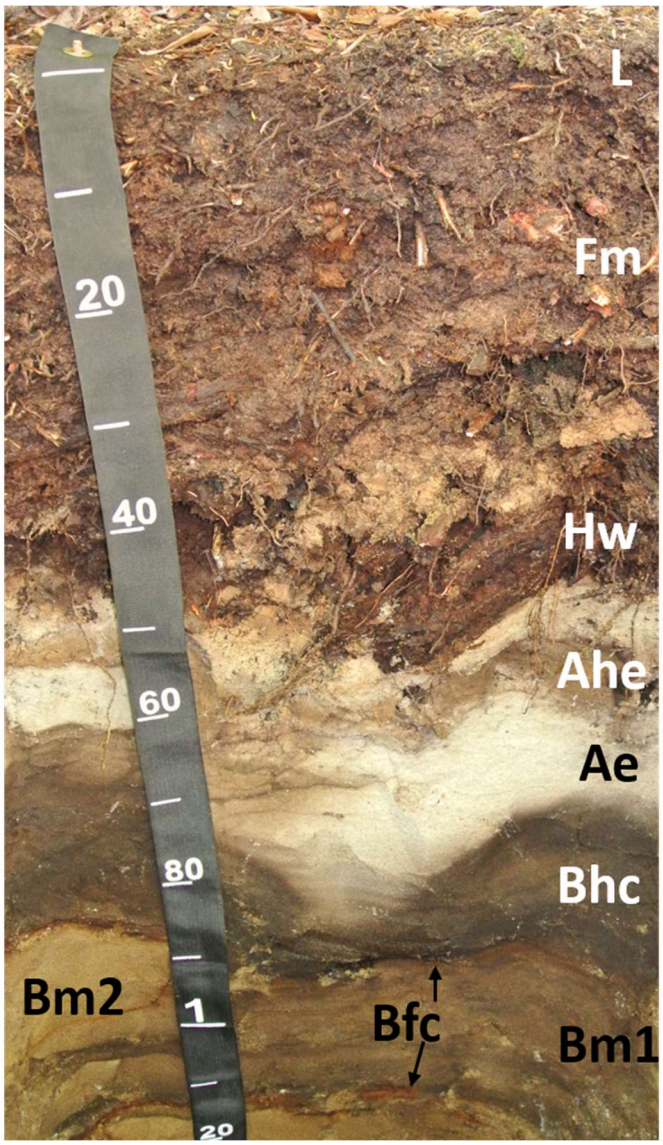

Figure A2- 7. Pedon CIDS8A with horizon designations. Depth is in cm.

***Site No*:** CIDS8B
Soil Classification: OT.HP

Site Description
Latitude: 51˚38.484' N *Longitude*: 128˚09.106' W
Elevation: 28 m *Slope Position*: Crest
Parent Material: Mesic organic veneer over a sandy eolian ridge
Site Series: 14 Ss

Humus Form: Lignomoder *Rooting Depth (cm)*: 50
Root Restriction Depth (cm): 50 *Seepage Depth (cm)*: 80

Comments: Re-dug hole used for optical dating. Well decomposed tree had fallen across one side of pit. 2m below ridge crest.

Table A2- 8. Pedon description of CIDS8B.

Horizon Sample #	**Depth (cm)**	**Description**
L CIDS8B-01	28-27	Organic; dark reddish brown (5YR 3/2 m); 1-3 cm thick; strongly acid.
Fa CIDS8B-02	27-10	Organic; very dark brown (7.5YR 2.5/2 m); weak, granular; abundant mycelia; common, very fine to coarse roots; clear, smooth boundary; 8-24 cm thick; extremely acid.
Hw CIDS8B-03	10-0	Organic; dark reddish brown (5YR 2.5/2 m); strong, recumbent; few mycelia; abundant, very fine and common, fine and medium roots; abrupt, wavy boundary; 0-21 cm thick; extremely acid.
Ae CIDS8B-04	0-22	Light brownish gray (2.5Y 6/2 m); sand; single grain loose; common, very fine and fine roots; gradual, irregular boundary; 9-28 cm thick; extremely acid.
Bhc CIDS8B-05	22-57	Black (5YR 2.5/1 m); sand; massive; firm; gradual, wavy boundary; 8-45 cm thick; very strongly acid.
Bfcj CIDS8B-06	57-58	Very dark brown (7.5YR 2.5/2 m); sand; massive; friable; gradual, broken boundary; 0-1 cm thick; strongly acid.
Bh CIDS8B-07	58-72	Dark brown (7.5YR 3/2 m); sand; massive; friable; gradual, irregular boundary; 5-30 cm thick; very strongly acid.
Bhcj CIDS8B-08	72-106	Black (5YR 2.5/1); sand; massive; firm; very strongly acid.
Bfc CIDS8B-09	106-108	Dark reddish brown (5YR 3/3 m); sand; massive; very firm.
Bm CIDS8B-10	108-119+	Dark brown (10YR 3/3 m); sand; single grain; loose.

*acidity determined by pH in water (CANSIS, 1982)

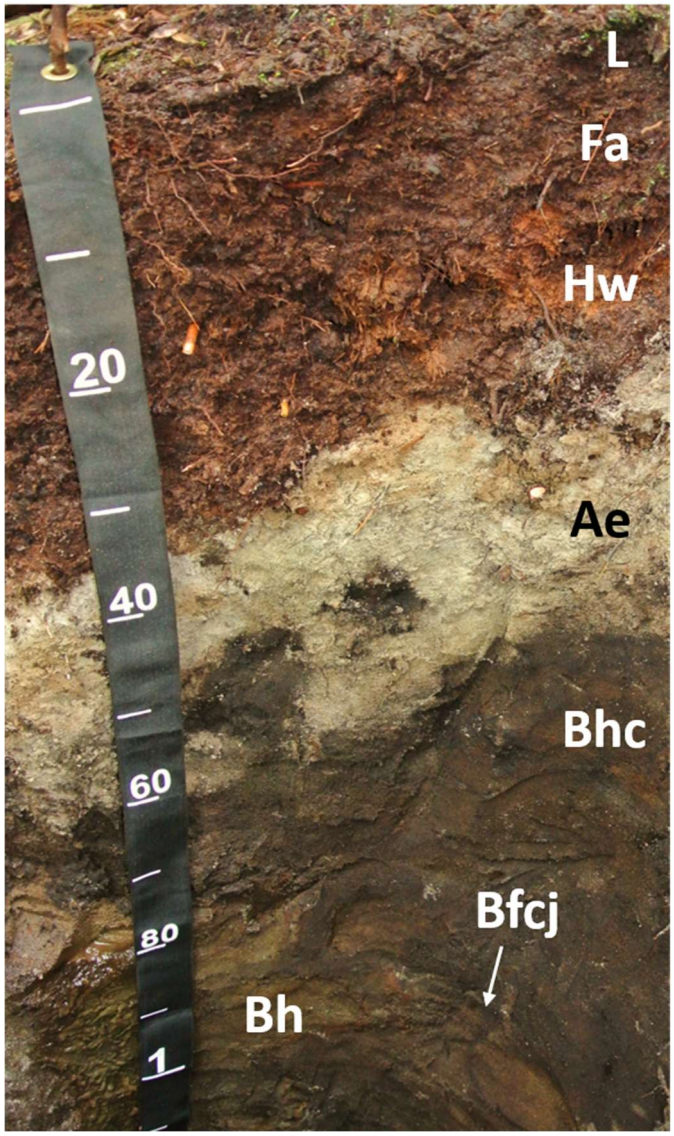

Figure A2- 8. Pedon CIDS8B with horizon designations. Depth is in cm.

***Site No*:** CIDS9A
Soil Classification: E.DYB

Site Description
Latitude: 51˚39.599' N *Longitude*: 128˚08.743' W
Elevation: 14 m *Slope Position*: Crest
Parent Material: Mesic organic veneer over a sandy eolian ridge
Site Series: 03a CwYc

Humus Form: Humimor *Rooting Depth (cm)*: 25

Root Restriction Depth (cm): N/A *Seepage Depth (cm)*: N/A

Comments: Mature forest.

Table A2- 9. Pedon description of CIDS9A.

Horizon Sample #	**Depth (cm)**	**Description**
S/L CIDS9A-01	25-23	Organic; dark reddish brown (5YR 3/2 m); 1-4 cm thick; very strongly acid.
Fm CIDS9A-02	23-18	Organic; dark reddish brown (5YR 2.5/2 m); moderate, non-compact matted; abundant mycelia; abundant, very fine to medium and common, coarse roots; clear, wavy boundary; 3-5 cm thick; extremely acid.
Hh CIDS9A-03	18-5	Organic; black (10YR 2/1 m); weak, granular; abundant mycelia; abundant, very fine to fine and common, medium to coarse roots; clear, irregular boundary; 9-19 cm thick; extremely acid.
Hw CIDS9A-04	5-0	Organic; black (7.5YR 2.5/1 m); moderate, recumbent; common mycelia; abundant, very fine to coarse roots; abrupt, smooth boundary; 0-15 cm; extremely acid.
Ae CIDS9A-05	0-6	Light gray (5Y 7/1 m); sand; single grain; loose; few, very fine to very coarse roots; clear, irregular boundary; 2-8 cm thick; extremely acid.
Bhj CIDS9A-06	6-36	Brown (10YR 3/2 m); sand; massive; friable; few, very fine to medium roots; gradual, irregular boundary; 13-63 cm thick; very strongly acid.
Bhc CIDS9A-07	36-39	Very dark brown (7.5YR 2.5/3 m); sand; massive; firm; clear, broken boundary; 0-7 cm thick; extremely acid.
Bmj CIDS9A-08	39-90	Dark yellowish brown (10YR 3/4 m); sand; massive; very friable; few, fine and medium roots; gradual, smooth boundary; 7-63 cm thick; very strongly acid.
BC CIDS9A-09	90-112+	Olive brown (2.5Y 4/4 m), dark brown (7.5YR 3/3 m); sand; massive; friable; very strongly acid.

*acidity determined by pH in water (CANSIS, 1982)

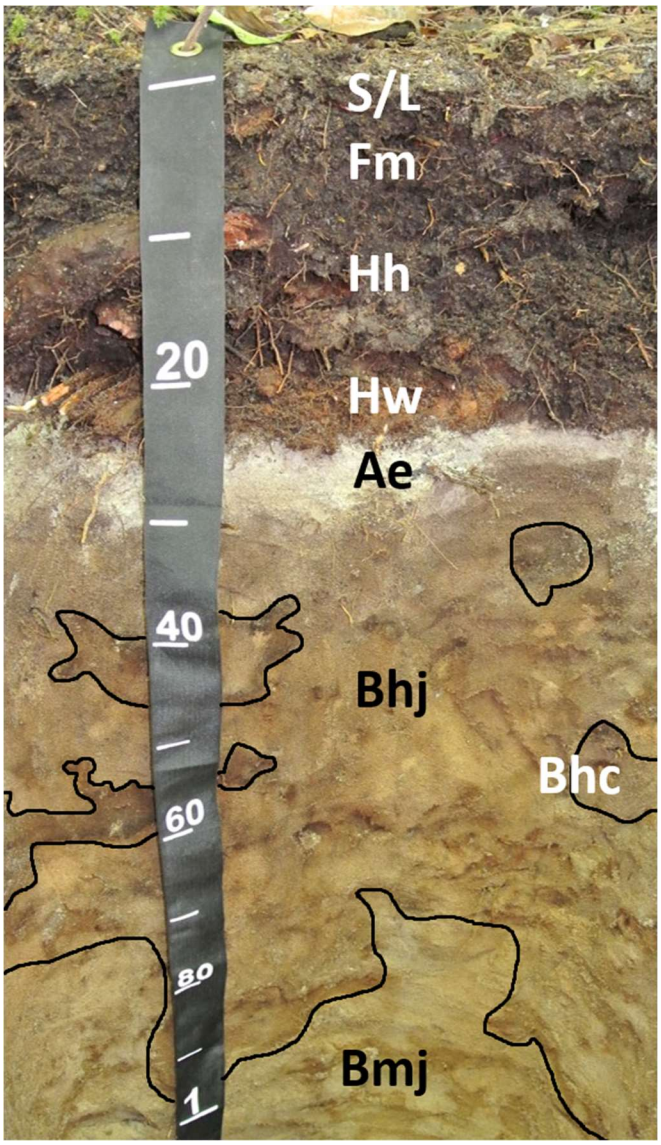

Figure A2- 9. Pedon CIDS9A with horizon designations. Depth is in cm.

***Site No*:** CIDS9B
Soil Classification: E.DYB

Site Description
Latitude: 51˚39.605' N *Longitude*: 128˚08.736' W
Elevation: 12 m *Slope Position*: Upper slope
Parent Material: Mesic organic veneer over a sandy eolian ridge
Site Series: 03a CwYc

Humus Form: Hemimor *Rooting Depth (cm)*: 37

Root Restriction Depth (cm): N/A *Seepage Depth (cm)*: N/A

Comments: Successional stage is not consistent within this dune. This area is in a tree-blow down area that has regenerated with small cedars.

Table A2- 10. Pedon description of CIDS9B.

Horizon Sample #	**Depth (cm)**	**Description**
L CIDS9-01	4-3	Organic; dark brown (7.5YR 3/3 m); 0.5-1 cm thick; very strongly acid.
Fm CIDS9-02	3-1	Organic; very dark brown (10YR 2/2 m); moderate, non-compact matted; common mycelia; abundant, very fine to very coarse roots; gradual, wavy boundary; 1-2 cm thick; extremely acid.
Hi CIDS9-03	1-0	Organic; very dark brown (10YR 2/2 m); moderate, massive; few mycelia; abundant, very fine to very coarse roots; clear, wavy boundary; 0.5-1.5 cm thick; extremely acid.
Ahe CIDS9-04	0-13	Dark grayish brown (10YR 4/2 m); sand; single grain; loose; abundant, very fine to very coarse roots; abrupt, irregular boundary; 3-20 cm thick; extremely acid.
Hwb CIDS9-05	13-33	Organic; black (7.5YR 2.5/1 m); strong, recumbent; common mycelia; abundant, very fine to medium roots; abrupt, irregular boundary; 8-33 cm thick; extremely acid.
Bm CIDS9-06	33-58	Light olive brown (2.5Y 5/4 m); sand; massive; loose; few, very fine to medium roots; gradual, irregular boundary; 5-55 cm thick; extremely acid.
Bhjcj CIDS9-07	58-113	Brown (10YR 3/2 m); sand; massive; friable; few, very fine to coarse roots; gradual, wavy boundary; 33-65 cm thick; very strongly acid.
BC CIDS9-08	113-137+	Light olive brown (2.5Y 5/3 m); sand; common, coarse distinct dark yellowish brown (10YR 3/4 m) mottles; single grain; loose; few, fine roots.

*acidity determined by pH in water (CANSIS, 1982)

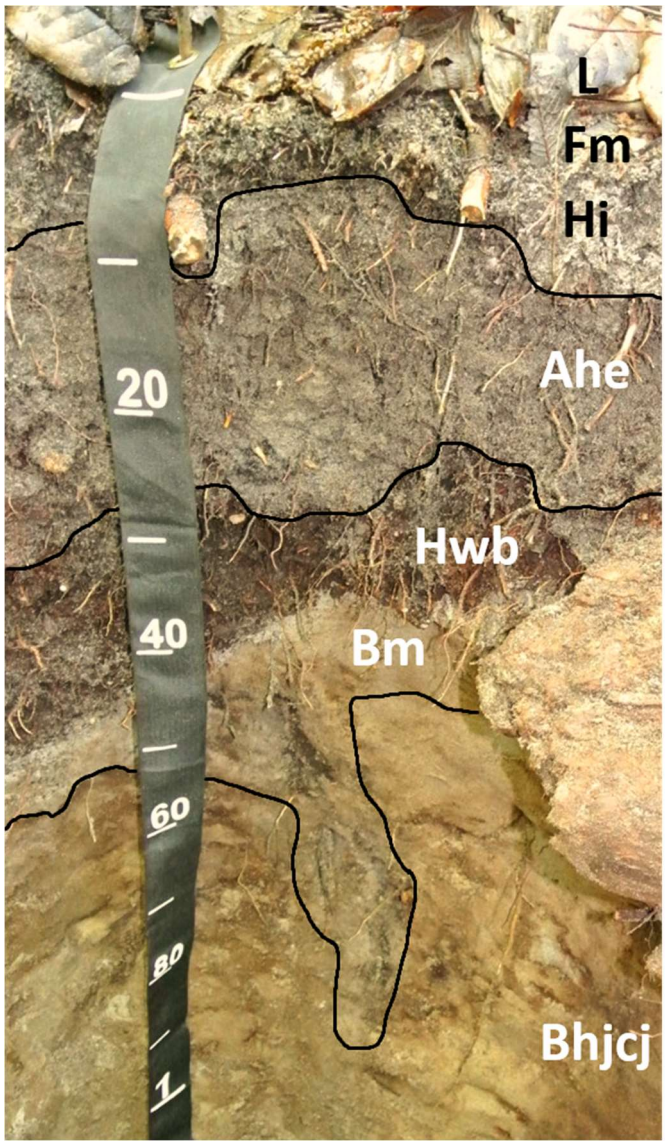

Figure A2- 10. Pedon CIDS9B with horizon designations. Depth is in cm.

***Site No*:** CIDS10A
Soil Classification: P.HP

Site Description
Latitude: 51˚38.663' N *Longitude*: 128˚08.723' W
Elevation: 18 m *Slope Position*: Middle slope
Parent Material: Mesic organic veneer over a sandy eolian ridge
Site Series: 11 CwYc

Humus Form: Humimor *Rooting Depth (cm)*: 28

Root Restriction Depth (cm): 40 *Seepage Depth (cm)*: N/A

Table A2- 11. Pedon description of CIDS10A.

Horizon Sample #	Depth (cm)	Description
Lv CIDS10A-01	28-27	Organic; dark brown (7.5YR 3/2 m); strong, single particle; loose; 1-1 cm thick; extremely acid.
Fm CIDS10A-02	27-24	Organic; very dark brown (7.5YR 2.5/2 m); moderate, granular; friable; abundant mycelia; abundant, very fine to coarse roots; clear, wavy boundary; 3-5 cm thick; extremely acid.
Hh1 CIDS10A-03	24-10	Organic; very dark brown (7.5YR 2.5/3 m); moderate, granular; friable; abundant mycelia; abundant, very fine to medium roots; clear, wavy boundary; 12-16 cm thick; extremely acid.
Hh2 CIDS10A-04	10-0	Organic; yellowish brown (10YR 5/4 m); charcoal bands; weak, fine, subangular blocky; friable; common, very fine to medium roots; abrupt, wavy boundary; 8-12 cm thick; extremely acid.
Bhcj CIDS10A-05	0-10	Black (10YR 2/1 m); loamy sand; massive; firm; few, fine roots; abrupt, irregular and broken boundary; 6-12 cm thick; extremely acid.
Ae CIDS10A-06	10-12	Light gray (10YR 7/1 m); loamy sand; single grain; friable; few, fine roots; abrupt, broken boundary; 0-3 cm thick; extremely acid.
Bfc CIDS10A-07	12-15	Reddish brown (5YR 4/4 m); massive; very firm; few, fine roots; abrupt, irregular boundary; 1-4 cm thick; extremely acid.
Bmcj1 CIDS10A-08	15-70	Pale yellow (2.5Y 7/3 m); sand; massive; firm; gradual, wavy boundary; 10-60 cm thick; extremely acid.
BCg1 CIDS10A-09	70-138	Pale yellow (2.5Y 7/3 m); sand; common, coarse yellowish brown (10YR 5/6 m) mottles; single grain; friable; 60-80 cm thick; extremely acid.
Bmcj2 CIDS10A-10	138-140	Brown (7.5YR 4/3 m); sand; massive; firm; abrupt, smooth boundary; 1-5 cm thick; extremely acid.

Horizon Sample #	Depth (cm)	Description
BCg2 CIDS10A-11	140-165+	Pale yellow (2.5Y 7/3 m); sand; common, coarse light yellowish brown (10YR 6/4 m) mottles; single grain; loose; extremely acid.

*acidity determined by pH in water (CANSIS, 1982)

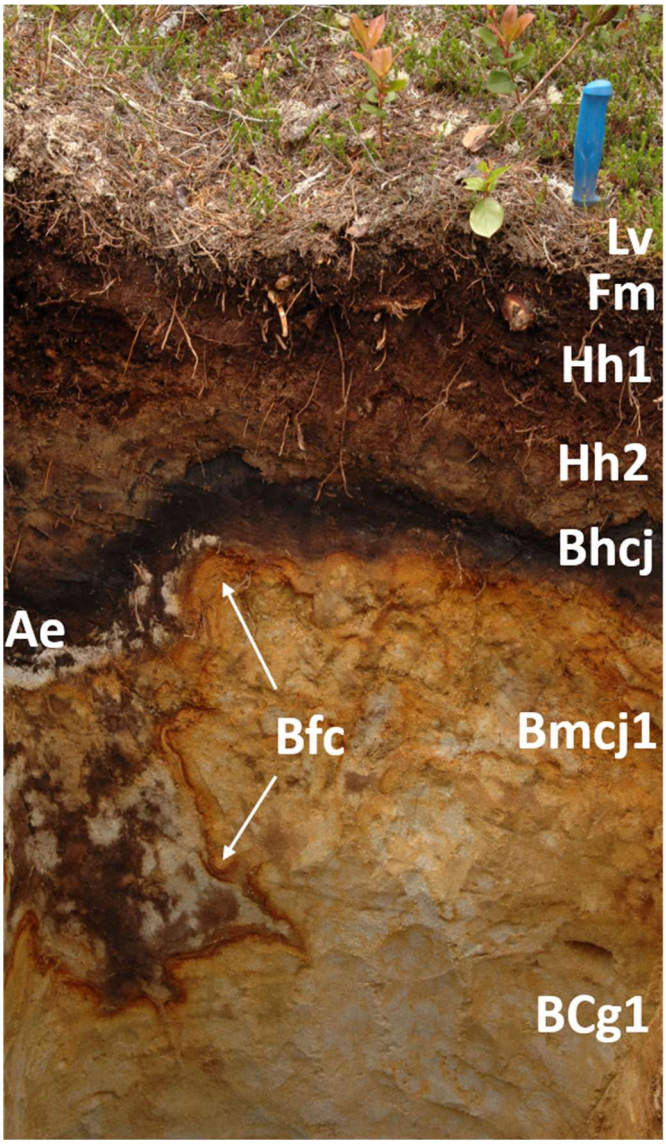

Figure A2- 11. Pedon CIDS10A with horizon designations. Depth is in cm.

***Site No*:** CIDS10B
Soil Classification: E.DYB

Site Description
Latitude: 51˚38.678' N *Longitude*: 128˚08.759' W
Elevation: 20 m *Slope Position*: Upper slope
Parent Material: Mesic organic veneer over a sandy eolian ridge
Site Series: 11 CwYc

Humus Form: Humimor *Rooting Depth (cm)*: 28

Root Restriction Depth (cm): 38 *Seepage Depth (cm)*: N/A

Table A2- 12. Pedon description of CIDS10B.

Horizon Sample #	**Depth (cm)**	**Description**
S/L CIDS10B-01	28-25	Organic; dark brown (7.5 YR 3/2 m); 2-4 cm thick; very strongly acid.
Fm CIDS10B-02	25-20	Organic; very dark brown (7.5YR 2.5/2 m); weak, non-compact matted; common mycelia; abundant, very fine to medium roots; clear, wavy boundary; 2-4 cm thick; extremely acid.
Hh1 CIDS10B-03	20-14	Organic; very dark brown (7.5YR 2.5/2 m); weak, granular; common mycelia; abundant, very fine to fine and few, medium roots; clear, wavy boundary; 3-8 cm thick; extremely acid.
Hh2 CIDS10B-04	14-0	Organic; light yellowish brown (10YR 6/4 m); charcoal bands; medium, blocky; few mycelia; common, very fine to medium roots; clear, irregular boundary; 10-16 cm thick; extremely acid.
Bhc CIDS10B-05	0-7	Black (10YR 2/1 m); sand; massive; firm; few, very fine and fine roots; clear, broken boundary; 3-9 cm thick; extremely acid.
Ae CIDS10B-06	7-10	Light olive brown (2.5Y 5/3 m); sand; single grain; loose; few, very fine to medium roots; gradual, broken boundary; 0-5 cm thick; extremely acid.
Bfc CIDS10B-07	10-13	Yellowish red (5YR 4/6 m); sand; massive; firm; clear, wavy boundary; 1-5 cm thick; extremely acid.
Bmcj CIDS10B-08	13-33	Yellowish brown (10YR 5/8 m); sand; massive; firm; gradual, wavy boundary; 17-26 cm thick; extremely acid.
BC CIDS10B-09	33-204+	Light olive gray (5Y 6/2 m), yellow (2.5Y 7/6 m); sand; massive; friable; extremely acid.

*acidity determined by pH in water (CANSIS, 1982)

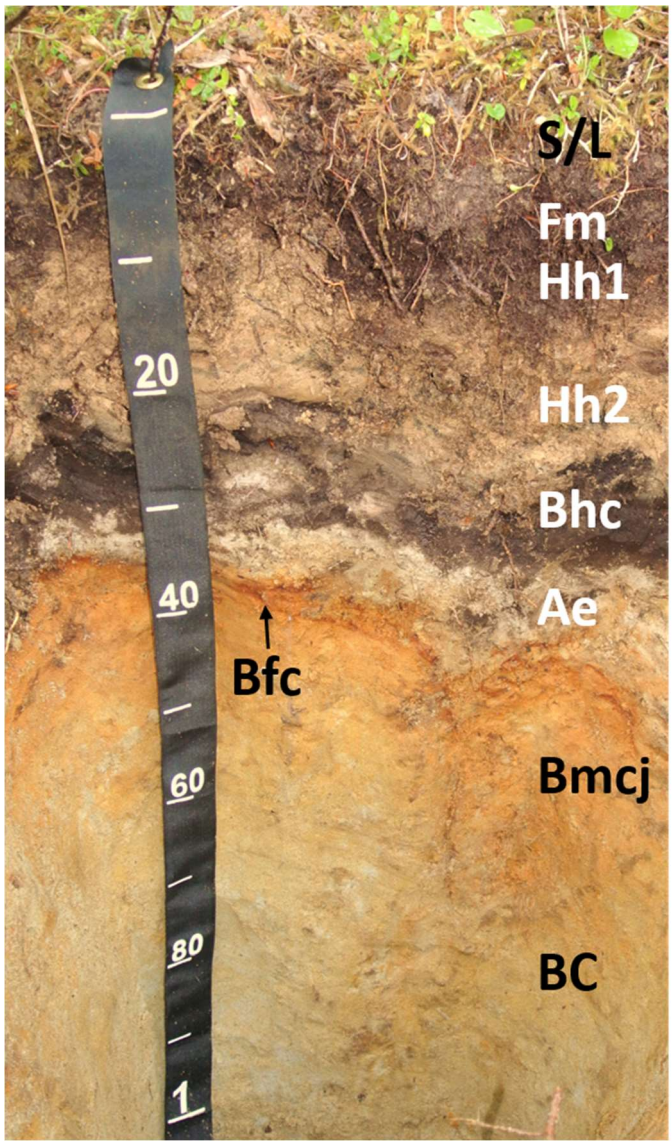

Figure A2- 12. Pedon CIDS10B with horizon designations. Depth is in cm.

***Site No*:** CIDS15A
Soil Classification: OT.HP

Site Description
Latitude: 51˚39.721' N *Longitude*: 128˚08.466' W
Elevation: 19 m *Slope Position*: Nearly level
Parent Material: Mesic organic blanket over a sandy eolian ridge
Site Series: 01 CwHw

Humus Form: Humimor *Rooting Depth (cm)*: 32

Root Restriction Depth (cm): 36 *Seepage Depth (cm)*: 36

Comments: There is no obvious ridge. There is no wetland moss.

Table A2- 13. Pedon description of CIDS15A.

Horizon Sample #	**Depth (cm)**	**Description**
S/L CIDS15A-01	20-18	Organic; dark reddish brown (5YR 3/2 m); 1-2 cm thick; very strongly acid.
Fm CIDS15A-02	18-14	Organic; very dusky red (2.5YR 2.5/2 m); weak, non-compact matted; few mycelia; abundant, very fine to medium roots; clear, wavy boundary; 3-5 cm thick; extremely acid.
Hh CIDS15A-03	14-0	Organic; very dark brown (10YR 2/2 m); moderate, granular; few mycelia; abundant, very fine to very coarse roots; abrupt, wavy boundary; 10-19 cm thick; extremely acid.
Ae CIDS15A-04	0-4	Dark gray (10YR 4/1 m); loamy sand; massive; friable; common, fine and few, medium roots; gradual, broken boundary; 0-9 cm thick; extremely acid.
Ahe CIDS15A-05	4-12	Brown (10YR 3/2 m); sandy loam; massive; friable; abundant, very fine and fine roots; clear, wavy boundary; 5-15 cm; extremely acid.
Bhc CIDS15A-06	12-21	Black (10YR 2/1 m); sand; massive; firm; few, very fine roots; clear, wavy boundary; 6-10 cm thick; extremely acid.
Bfcj CIDS15A-07	21-23	Dark reddish brown (2.5YR 2.5/3 m); sand; massive; very firm; clear, wavy boundary; 1-3 cm thick; extremely acid.
Bmcj CIDS15A-08	23-49	Dark yellowish brown (10YR 4/6 m), dark brown (7.5YR 3/3 m); sand; massive; firm; gradual, smooth boundary; 22-29 cm thick; extremely acid.
BC CIDS15A-09	49-103+	Light olive brown (2.5Y 5/4 m); sand; single grain; loose; very strongly acid.

*acidity determined by pH in water (CANSIS, 1982)

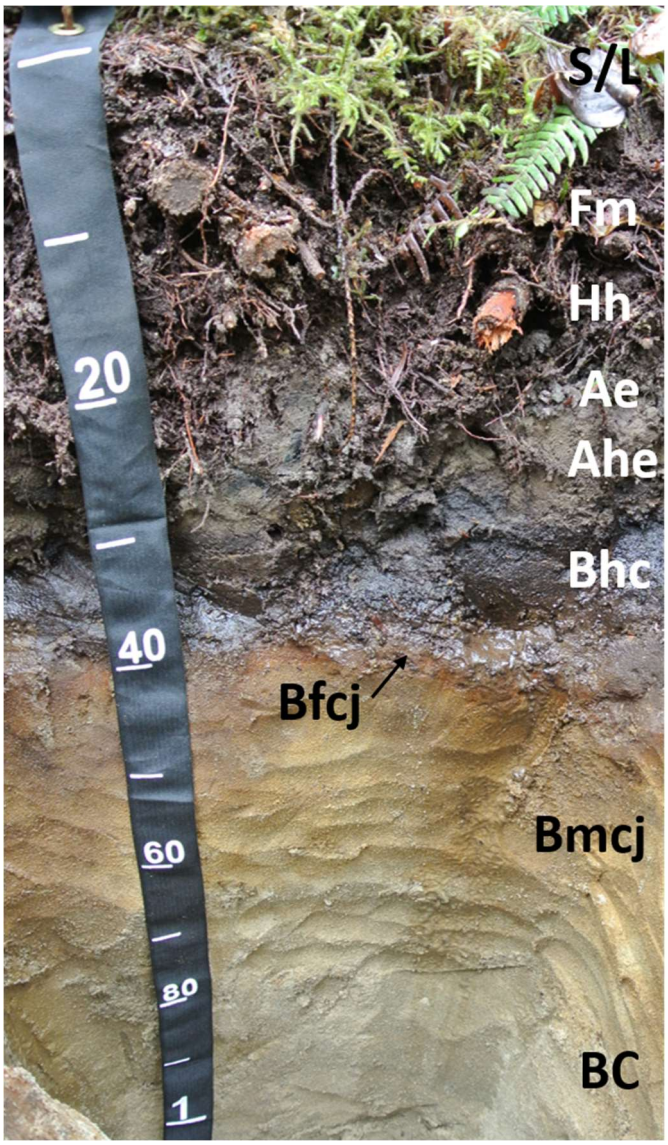

Figure A2- 13. Pedon CIDS15A with horizon designations. Depth is in cm.

***Site No*:** CIDS15B
Soil Classification: OT.HP

Site Description
Latitude: 51˚39.731' N *Longitude*: 128˚08.465' W
Elevation: 16 m *Slope Position*: Nearly level
Parent Material: Mesic organic blanket over a sandy eolian ridge
Site Series: 01 CwHw

Humus Form: Humimor *Rooting Depth (cm)*: 18

Root Restriction Depth (cm): 32 *Seepage Depth (cm)*: 32

Comments: There is no obvious ridge. There is no wetland moss.

Table A2- 14. Pedon description of CIDS15B.

Horizon Sample #	**Depth (cm)**	**Description**
S/L CIDS15B-01	18-16	Organic; dark reddish brown (5YR 3/2 m); 2-3 cm thick; very strongly acid.
Fm CIDS15B-02	16-13	Organic; dark reddish brown (5YR 3/2 m); moderate, non-compact matted; few mycelia; abundant, very fine to coarse roots; clear, smooth boundary; 2-4 cm thick; very strongly acid.
Hh CIDS15B-03	13-0	Organic; very dark brown (7.5YR2.5/2 m); weak, granular few mycelia; abundant, very fine to very coarse roots; abrupt, wavy boundary; 10-13 cm thick; extremely acid.
Ae CIDS15B-04	0-9	Brown (10YR 4/3 m); silt; charcoal bands; subangular blocky; friable; few, very fine roots; gradual, wavy boundary; 3-13 cm thick; extremely acid.
Ahe CIDS15B-05	9-14	Very dark gray (10YR 3-1 m); loamy sand; massive; friable; few, very fine roots; clear, wavy boundary; 3-16 cm thick; extremely acid.
Bhc CIDS15B-06	14-28	Black (10YR 2/1 m), very dark brown (10YR 2/2 m); sand; massive; very firm; clear, wavy boundary; 2-19 cm thick; extremely acid.
Bhc2 CIDS15B-07	28-38	Dark yellowish brown (10YR 3/6 m), black (10YR 2/1 m); sand; massive; firm; few, very fine roots; clear, broken boundary; 3-11 cm thick; extremely acid.
Bh CIDS15B-08	38-43	Very dark brown (7.5YR 2.5/2 m), black (7.5YR 2.5/1 m); sand; massive; friable; few, very fine roots; clear, broken boundary; 1-31 cm thick; extremely acid.
Bfc CIDS15B-09	43-45	Dark reddish brown (2.5YR 2.5/4 m); sand; massive; very firm; abrupt, broken boundary; 1-3 cm thick; very strongly acid.
Bm CIDS15B-10	45-128+	Light olive brown (2.5Y 5/4 m), dark yellowish brown (10YR 3/6 m); sand; massive; firm; extremely acid.

*acidity determined by pH in water (CANSIS, 1982)

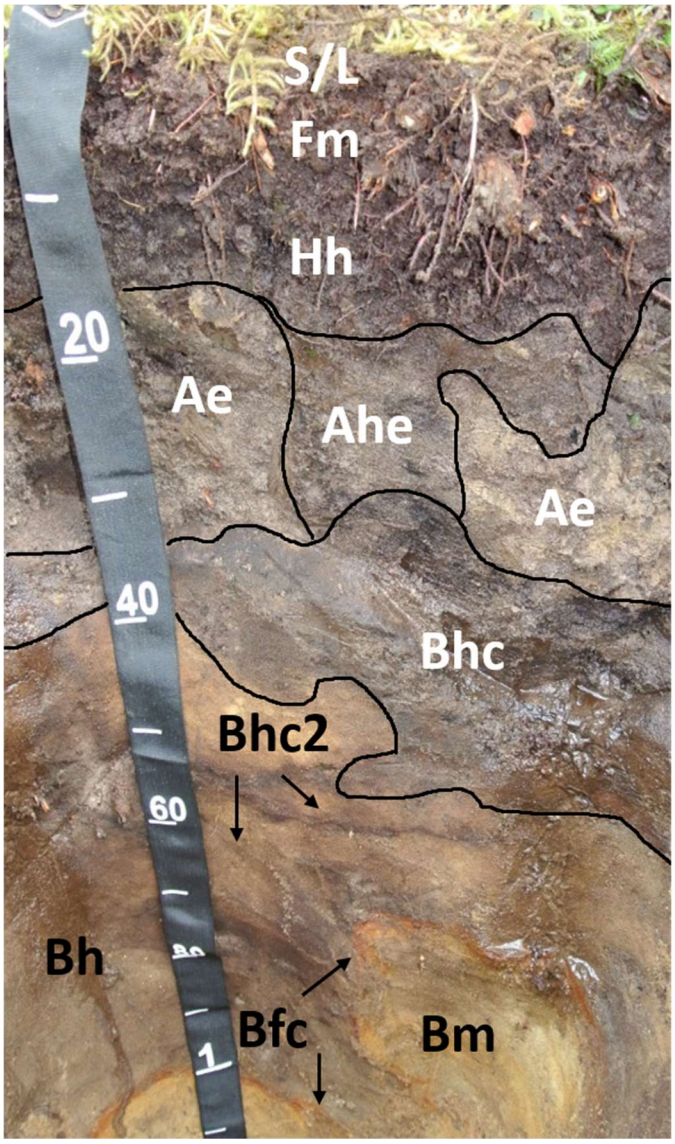

Figure A2- 14. Pedon CIDS15B with horizon designations. Depth is in cm.

***Site No*:** CIDS16A
Soil Classification: HU.FO

Site Description
Latitude: 51˚39.967' N *Longitude*: 128˚07.067' W
Elevation: 14 m *Slope Position*: Nearly Level
Parent Material: Mesic organic blanket over a sandy eolian ridge
Site Series: 11 CwYc

Humus Form: Lignomoder *Rooting Depth (cm)*: 55
Root Restriction Depth (cm): 55 *Seepage Depth (cm)*: 41

Comments: Oh was very hard, seepage occurs in Oh. Site within 15 m of CIDS16B but coordinates of optically dated hole match this location.

Table A2- 15. Pedon description of CIDS16A.

Horizon Sample #	**Depth (cm)**	**Description**
S/L CIDS16A-01	0-3	Organic; dark reddish brown (5YR 3/2 m); 2-4 cm thick; very strongly acid.
Fa CIDS16A-02	3-8	Organic; dark reddish brown (5YR 3/3 m); weak, non-compact matted; common mycelia; abundant, very fine to medium roots; clear, smooth boundary; 3-6 cm thick; extremely acid.
Hw CIDS16A-03	8-35	Organic; black (5YR 2.5/1 m); strong, recumbent; common mycelia; common, very fine and fine roots; abrupt, smooth boundary; 3-29 cm thick; extremely acid.
Oh CIDS16A-04	35-55	Organic; black (10YR 2/1 m); strong, subangular block, recumbent; few mycelia; few, very fine and fine roots; clear, broken boundary; 8-24 cm thick; extremely acid.
Bhc CIDS16A-05	55-64	Dark reddish brown (5Y 2.5/2 m); sandy loam; massive; firm; gradual, broken boundary; 0-17 cm thick; extremely acid.
Bhcj CIDS16A-06	64-80	Dark brown (10YR 3/3 m); sandy loam; charcoal; massive; firm, friable; clear, wavy boundary; 12-22 cm thick; extremely acid.
Bfc CIDS16A-07	80-81	Dark reddish brown (5YR 3/4 m); loamy sand; massive; firm, very firm; gradual, wavy boundary; 0.5-1 cm thick; very strongly acid.
Bm CIDS16A-08	81-136+	Dark yellowish brown (10YR 4/4 m); loamy sand; massive; very friable; very strongly acid.

*acidity determined by pH in water (CANSIS, 1982)

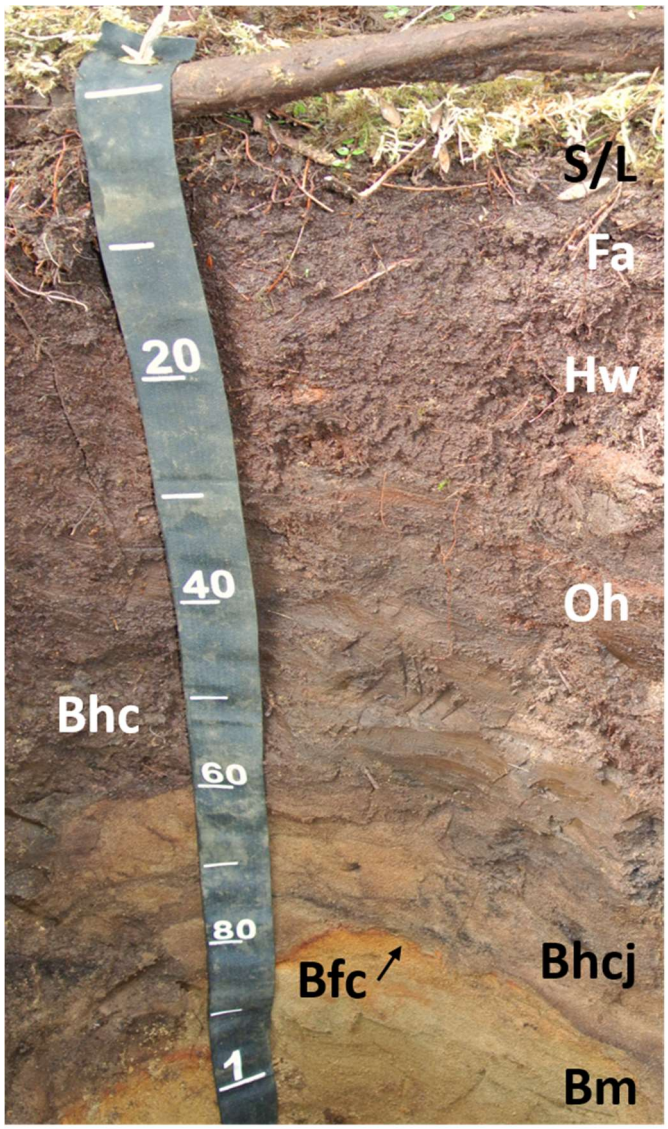

Figure A2- 15. Pedon CIDS16A with horizon designations. Depth is in cm.

***Site No*:** CIDS16B
Soil Classification: HU.FO

Site Description
Latitude: 51˚39.966' N *Longitude*: 128˚07.081' W
Elevation: 13m *Slope Position*: Nearly level
Parent Material: Mesic organic blanket over a sandy eolian ridge
Site Series: 11 CwYc

Humus Form: Lignomoder *Rooting Depth (cm)*: 63
Root Restriction Depth (cm): 63 *Seepage Depth (cm)*: 48

Comments: Re-dug hole used for optical dating. This is a much wetter microsite than CIDS16A. Seepage occurs in Oh.

Table A2- 16. Pedon description of CIDS16B.

Horizon Sample #	**Depth (cm)**	**Description**
S/L CIDS16B-01	0-4	Organic; dark reddish brown (5YR 3/2 m); 2-5 cm thick; very strongly acid.
Fm CIDS16B-02	4-12	Organic; dark brown (7.5YR 3/2 m); moderate, non-compact matted; common mycelia; abundant, very fine to coarse roots; clear, wavy boundary; 4-10 cm thick; strongly acid.
Hw CIDS16B-03	12-45	Organic; very dark brown (10YR 2/2 m); strong, recumbent, massive; few mycelia; abundant, very fine to medium roots; abrupt, wavy boundary; 31-40 cm thick; extremely acid.
Oh CIDS16B-04	45-63	Organic; black (10YR 2/1 m); strong, blocky; few, very fine roots; abrupt, wavy boundary; 14-22 cm thick; extremely acid.
Bhc CIDS16B-05	63-85	Very dark brown (7.5YR 2.5/2 m); loamy sand; massive; firm; few, fine roots; clear, wavy boundary; 14-29 cm thick; extremely acid.
Ae CIDS16B-06	85-86	Dark grayish brown (2.5Y 4/2 m); sand; charcoal; single grain; loose; clear, broken boundary; 0-10 cm thick; extremely acid.
Bmcj CIDS16B-07	86-103	Very dark brown (7.5YR 2.5/3 m), dark yellowish brown (10YR 3/6 m); loamy sand; massive; friable; gradual, broken boundary; 0-37 cm thick; extremely acid.
Bh CIDS16B-08	103-223	Very dark brown (7.5YR 2.5/2 m); loamy sand; charcoal; single grain; friable; extremely acid.
Bm CIDS16B-09	223-234+	N.D.

*acidity determined by pH in water (CANSIS, 1982)

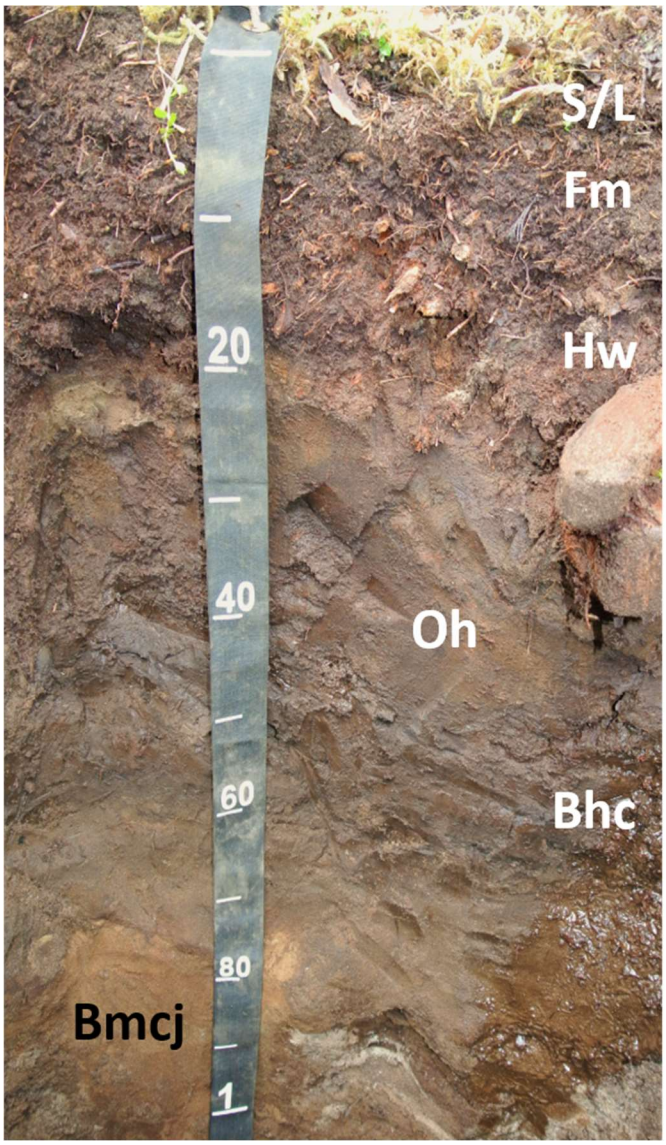

Figure A2- 16. Pedon CIDS16B with horizon designations. Depth is in cm.

APPENDIX 3: ECOLOGICAL DATA

Table A3- 1. Biogeoclimatic (BEC) site series classification for each site and presence and absence data from plant surveys using Latin and common plant names (X indicates presence) (Green and Klinka, 1994).

Common Name	Latin Name	Site and BEC Site Series Classification																	
		CIDS1		CIDS3		CIDS4		CIDS9		CIDS8		CIDS15		CIDS16		CIDS10			
		A	B	A	B	A	B	A	B	A	B	A	B	A	B	A	B		
		N/A		15 - Ss		01 - CwHw		03a - CwYc		14 - Ss		01 - CwHw		11 - CwYc		11 - CwYc			
Yarrow	*Achillea millifolium*	X	X																
Red alder	*Alnus rubra*			X	X			X	X										
Kinniknick	*Arctostaphylos uva-ursi*													X	X				
Deer fern	*Blechnum spicant*			X		X	X	X	X			X	X		X				
Indian paintbrush	*Castilleja miniata*	X	X																
Coastal reindeer lichen	*Cladina portentosa*															X			
Goldthread	*Coptis asplenifolia*													X			X		
Bunchberry	*Cornus canadensis*							X	X			X		X	X		X		
Dune wildrye	*Elymus mollis*	X	X																
Crowberry	*Empetrum nigrum*															X	X		
Red fescue	*Festuca rubra*	X																	
Coastal strawberry	*Fragaria chilonensis*	X	X																
Salal	*Gaultheria shallon*			X	X	X	X	X	X	X	X	X	X	X	X	X	X		
Step moss	*Hylocomium splendens*							X				X	X						
Purple peavine	*Lathyrus japonicus*	X	X																
Labrador tea	*Ledum groendlandicum*													X	X	X	X		
Black Honeysuckle	*Lonicera involucrata*								X										
False azalea	*Menziesia ferruginea*							X	X		X	X	X	X			X		
False lily of the valley	*Mianthemum dilatatum*				X			X			X	X	X	X	X		X		
Sword fern	*Polystichum munitum*			X															
Bracken fern	*Pterdium aquilinum*			X				X	X										
Lanky moss	*Rhytidiadelphus loreus*							X					X						
Salmonberry	*Rubus spectabilis*			X				X	X	X									
False Solomon's seal	*Smilacina racemosa*								X										
Sphagnum	*Sphagnum sp.*													X	X	X			
Red Huckleberry	*Vaccinium parvifolium*					X	X												
	Vaccinium Sp.			X	X			X	X			X	X	X					
Upland moss					X		X			X	X	X		X			X		

Table A3- 2. Percent cover of dominant ground cover classes for each replicate (Rep) on each plot (n=3) and site (n=6).

Plot	Rep	Percent Cover (%)											
		Forbs/ Herbs	Shrubs	Grass	Moss	Lichen	Fungi	Wood	Litter	Bare Ground	Rock	Animal Matter	Trees
CIDS1A	1	5	0	5	5	0	0	0	20	65	0	0	0
CIDS1A	2	10	0	5	10	0	0	0	60	15	0	0	0
CIDS1A	3	5	0	5	10	0	0	0	75	5	0	0	0
CIDS1B	1	15	0	10	<1	0	0	0	75	<1	0	0	0
CIDS1B	2	5	0	5	<1	0	0	0	90	<1	0	0	0
CIDS1B	3	25	0	<1	5	0	0	0	55	15	0	0	0
CIDS3A	1	0	0	0	15	0	0	5	80	0	0	0	0
CIDS3A	2	0	<1	0	10	0	0	20	70	0	0	0	0
CIDS3A	3	0	0	0	25	0	0	15	60	0	0	0	0
CIDS3B	1	0	0	0	60	0	0	15	25	0	0	0	0
CIDS3B	2	0	5	0	10	0	0	10	75	0	0	0	0
CIDS3B	3	0	0	0	5	0	0	10	85	0	0	0	0
CIDS4A	1	5	15	0	10	0	0	0	70	0	0	0	0
CIDS4A	2	<1	10	0	25	0	0	0	65	0	0	0	0
CIDS4A	3	<1	20	0	70	0	0	0	10	0	0	0	0
CIDS4B	1	0	0	0	70	<1	0	15	15	0	0	0	0
CIDS4B	2	5	0	0	30	5	0	0	60	0	0	0	0
CIDS4B	3	<1	25	0	45	0	0	0	30	0	0	0	0
CIDS9A	1	25	5	<1	20	0	0	0	50	0	0	0	0
CIDS9A	2	30	0	0	50	0	0	0	20	0	0	0	0
CIDS9A	3	25	5	0	55	0	0	0	15	0	0	0	0
CIDS9B	1	0	10	0	0	0	0	0	90	0	0	0	0
CIDS9B	2	0	0	0	0	0	0	20	80	0	0	0	0
CIDS9B	3	5	10	0	5	0	0	30	50	0	0	0	0
CIDS8A	1	0	60	0	<1	0	0	0	40	0	0	0	0
CIDS8A	2	0	5	0	10	0	0	0	85	0	0	0	0
CIDS8A	3	0	20	0	25	0	0	10	45	0	0	0	0
CIDS8B	1	0	15	0	<1	0	0	5	80	0	0	0	0
CIDS8B	2	0	15	0	0	0	0	55	30	0	0	0	0
CIDS8B	3	0	0	0	0	0	0	25	75	0	0	0	0
CIDS15A	1	40	0	0	10	0	0	0	50	0	0	0	0
CIDS15A	2	15	10	0	35	0	0	0	40	0	0	0	0
CIDS15A	3	25	0	0	45	0	0	0	30	0	0	0	0
CIDS15B	1	5	5	0	20	0	0	0	70	0	0	0	0
CIDA15B	2	20	0	0	5	0	0	0	75	0	0	0	0

Plot	Rep	Percent Cover (%)											
		Forbs/ Herbs	Shrubs	Grass	Moss	Lichen	Fungi	Wood	Litter	Bare Ground	Rock	Animal Matter	Trees
CIDS15B	3	30	5	0	10	0	0	0	55	0	0	0	0
CIDS16A	1	5	15	0	60	0	0	0	20	0	0	0	0
CIDS16A	2	5	20	<1	35	0	0	15	25	0	0	0	0
CIDS16A	3	0	20	<1	60	0	0	0	20	0	0	0	0
CIDS16B	1	5	25	<1	50	0	0	0	20	0	0	0	0
CIDS16B	2	10	15	0	70	0	0	0	5	0	0	0	0
CIDS16B	3	<1	15	0	20	0	0	35	30	0	0	0	0
CIDS10A	1	<1	25	<1	5	50	0	0	20	0	0	0	0
CIDS10A	2	5	20	0	10	0	0	0	15	0	0	0	50
CIDS10A	3	10	10	0	5	55	0	0	15	0	0	0	5
CIDS10B	1	10	10	<1	20	45	0	0	15	0	0	0	0
CIDS10B	2	15	25	0	25	0	0	10	25	0	0	0	0
CIDS10B	3	10	15	<1	10	<1	0	0	50	0	0	0	15

Table A3- 3. Count of tree species within different size classes on each replicate for each site (n=3) and the sum of all species for one size class for red alder (Dr), western hemlock (Hw), mountain hemlock (Hm), western redcedar (Cw), yellow cedar (Yc), shore pine (Pc) and sitka spruce (Ss).

Site	Replicate	DBH Size class (cm)	Species Count							Sum
			Dr	Hw	Hm	Cw	Yc	Pc	Ss	
CIDS3	1	0-2.9	0	10	0	0	0	0	0	10
CIDS3	1	3.0-5.9	4	17	0	0	0	0	0	21
CIDS3	1	6.0-8.9	2	11	0	0	0	0	0	13
CIDS3	2	0-2.9	0	4	0	0	0	0	0	4
CIDS3	2	3.0-5.9	2	13	0	0	0	0	0	15
CIDS3	2	6.0-8.9	1	8	0	0	0	0	1	10
CIDS3	3	0-2.9	0	7	0	0	0	0	0	7
CIDS3	3	3.0-5.9	1	4	0	0	0	0	0	5
CIDS3	3	6.0-8.9	1	3	0	0	0	0	0	4
CIDS4	1	0-2.9	0	0	0	0	0	0	0	0
CIDS4	1	3.0-5.9	0	5	0	0	0	0	0	5
CIDS4	1	6.0-8.9	0	4	0	0	0	0	0	4
CIDS4	2	0-2.9	0	0	0	0	0	0	0	0
CIDS4	2	3.0-5.9	0	0	0	0	0	0	0	0
CIDS4	2	6.0-8.9	0	1	0	0	0	0	0	1
CIDS4	3	0-2.9	0	3	0	0	0	0	0	3
CIDS4	3	3.0-5.9	0	1	0	0	0	0	0	1
CIDS4	3	6.0-8.9	0	3	0	0	0	0	0	3
CIDS9	1	0-2.9	0	8	0	6	0	0	0	14
CIDS9	1	3.0-5.9	1	7	0	5	0	0	0	13
CIDS9	1	6.0-8.9	2	1	0	3	0	0	0	6
CIDS9	2	0-2.9	8	3	0	20	0	0	0	31
CIDS9	2	3.0-5.9	3	2	0	5	0	0	0	10
CIDS9	2	6.0-8.9	0	3	0	0	0	0	0	3
CIDS9	3	0-2.9	6	0	0	5	0	0	0	11
CIDS9	3	3.0-5.9	0	1	0	0	0	0	0	1
CIDS9	3	6.0-8.9	1	0	0	0	0	0	0	1
CIDS8	1	0-2.9	0	0	0	0	0	0	0	0
CIDS8	1	3.0-5.9	0	0	0	0	0	0	0	0
CIDS8	1	6.0-8.9	0	0	0	0	0	0	0	0
CIDS8	2	0-2.9	0	0	0	0	0	0	0	0
CIDS8	2	3.0-5.9	0	0	0	0	0	0	0	0
CIDS8	2	6.0-8.9	0	0	0	0	0	0	0	0
CIDS8	3	0-2.9	0	0	0	0	0	0	0	0
CIDS8	3	3.0-5.9	0	0	0	0	0	0	0	0
CIDS8	3	6.0-8.9	0	0	0	0	0	0	0	0
CIDS15	1	0-2.9	0	7	0	1	0	0	0	8
CIDS15	1	3.0-5.9	0	0	0	0	1	0	0	1
CIDS15	1	6.0-8.9	0	2	0	0	0	0	0	2
CIDS15	2	0-2.9	0	7	0	3	0	0	0	10
CIDS15	2	3.0-5.9	0	2	0	1	0	0	0	3
CIDS15	2	6.0-8.9	0	0	0	0	0	0	0	0
CIDS15	3	0-2.9	0	9	0	1	0	0	0	10
CIDS15	3	3.0-5.9	0	4	0	1	0	0	0	5
CIDS15	3	6.0-8.9	0	1	0	0	0	0	0	1
CIDS16	1	0-2.9	0	8	1	4	2	0	0	15

Site	Replicate	DBH Size class (cm)	Species Count							Sum
			Dr	Hw	Hm	Cw	Yc	Pc	Ss	
CIDS16	1	3.0-5.9	0	0	0	3	0	0	0	3
CIDS16	1	6.0-8.9	0	0	0	0	1	0	0	1
CIDS16	2	0-2.9	0	2	0	4	0	0	0	6
CIDS16	2	3.0-5.9	0	0	1	1	0	0	0	2
CIDS16	2	6.0-8.9	0	1	0	0	0	0	0	1
CIDS16	3	0-2.9	0	4	0	1	1	0	0	6
CIDS16	3	3.0-5.9	0	0	0	1	2	0	0	3
CIDS16	3	6.0-8.9	0	1	0	0	0	0	0	1
CIDS10	1	0-2.9	0	1	0	8	0	0	0	9
CIDS10	1	3.0-5.9	0	2	0	5	1	1	0	9
CIDS10	1	6.0-8.9	0	0	1	1	1	0	0	3
CIDS10	2	0-2.9	0	1	0	6	0	0	0	7
CIDS10	2	3.0-5.9	0	1	0	5	0	0	0	6
CIDS10	2	6.0-8.9	0	0	0	1	0	0	0	1
CIDS10	3	0-2.9	0	0	0	2	2	2	0	6
CIDS10	3	3.0-5.9	0	0	0	1	2	1	0	4
CIDS10	3	6.0-8.9	0	0	0	0	0	1	0	1

Table A3- 4. Diameter at breast height (DBH) for all trees with a DBH greater than nine cm on each replicate for each site (n=3) including western hemlock (Hw), red alder (Dr), western redcedar (Cw), sitka spruce (Ss), yellow cedar (Yc), and shore pine (Pc).

Plot	Replicate	Species	DBH (cm)
CIDS3	1	Hw	10.0
CIDS3	1	Hw	12.4
CIDS3	1	Hw	14.2
CIDS3	1	Hw	15.7
CIDS3	1	Hw	24.2
CIDS3	2	Hw	9.7
CIDS3	2	Hw	13.4
CIDS3	2	Hw	15.4
CIDS3	2	Dr	10.0
CIDS3	2	Dr	9.9
CIDS3	2	Dr	10.6
CIDS3	2	Dr	17.5
CIDS3	3	Hw	9.8
CIDS3	3	Hw	9.0
CIDS3	3	Hw	11.4
CIDS3	3	Hw	11.0
CIDS3	3	Hw	18.0
CIDS3	3	Dr	36.9
CIDS4	1	Hw	23.4
CIDS4	1	Hw	10.5
CIDS4	1	Hw	18.7
CIDS4	1	Hw	30.5
CIDS4	1	Hw	9.1
CIDS4	1	Cw	56.6
CIDS4	1	Ss	62.1
CIDS4	2	Hw	25.5
CIDS4	2	Hw	11.8
CIDS4	2	Hw	14.1
CIDS4	2	Hw	28.0
CIDS4	2	Hw	29.6
CIDS4	2	Hw	18.8
CIDS4	2	Hw	10.6
CIDS4	2	Ss	61.3
CIDS4	3	Hw	18.9
CIDS4	3	Hw	19.1
CIDS4	3	Hw	24.2
CIDS4	3	Hw	19.5
CIDS4	3	Hw	9.8
CIDS4	3	Hw	11.3
CIDS4	3	Ss	66.8
CIDS4	3	Ss	30.7
CIDS9	1	Hw	15.9
CIDS9	1	Hw	13.1
CIDS9	1	Hw	15.9
CIDS9	1	Hw	9.6
CIDS9	1	Cw	12.9
CIDS9	1	Dr	9.3
CIDS9	2	Dr	15.6
CIDS9	2	Cw	11.9
CIDS9	3	Hw	10.7
CIDS9	3	Cw	11.5
CIDS9	3	Cw	35.4
CIDS8	1	Hw	40.9
CIDS8	1	Cw	60.6
CIDS8	1	Ss	40.6
CIDS8	2	Hw	52.6
CIDS8	2	Hw	32.5
CIDS8	2	Hw	34.0
CIDS8	2	Hw	34.2
CIDS8	3	Hw	54.8
CIDS8	3	Hw	51.3
CIDS8	3	Ss	52.0
CIDS15	1	Hw	14.4
CIDS15	1	Cw	15.1
CIDS15	1	Cw	48.2
CIDS15	1	Yc	31.0
CIDS15	2	Hw	12.0
CIDS15	2	Cw	16.9
CIDS15	2	Cw	32.0
CIDS15	2	Yc	17.7
CIDS15	2	Yc	13.5
CIDS15	2	Yc	13.5
CIDS15	2	Ss	39.1
CIDS15	3	Cw	61.3
CIDS15	3	Yc	19.7
CIDS16	1	Pc	34.9
CIDS16	1	Cw	35.9
CIDS16	1	Cw	25.4
CIDS16	1	Cw	19.8
CIDS16	1	Cw	20.3
CIDS16	2	Yc	29.1
CIDS16	2	Yc	43.5
CIDS16	3	Cw	42.3
CIDS16	3	Yc	19.7
CIDS16	3	Yc	32.8
CIDS16	3	Pc	11.4

Table A3- 4 Cont'd. Diameter at breast height (DBH) for all trees with a DBH greater than nine cm on each replicate for each site (n=3) including western hemlock (Hw), red alder (Dr), western redcedar (Cw), sitka spruce (Ss), yellow cedar (Yc), and shore pine (Pc).

Plot	Replicate	Species	DBH (cm)
CIDS10	1	Pc	16.5
CIDS10	1	Pc	17.7
CIDS10	1	Cw	17.1
CIDS10	1	Cw	11.2
CIDS10	1	Cw	13.3
CIDS10	1	Cw	13.8
CIDS10	1	Cw	11.5
CIDS10	1	Yc	13.2
CIDS10	1	Yc	14.1
CIDS10	1	Hw	13.0
CIDS10	1	Hw	14.6
CIDS10	1	Hw	9.8
CIDS10	1	Hw	10.5
CIDS10	2	Pc	17.3
CIDS10	2	Pc	13.7
CIDS10	2	Hw	31.2
CIDS10	2	Cw	12.0
CIDS10	3	Pc	16.5

Table A3- 5. Location of tree basal area replicate plots for the Calvert Island chronosequence by northing (N) and westing (W).

Plot	Replicate	N	W
CIDS3	1	51˚39.205	128˚08.283
CIDS3	2	51˚39.207	128˚08.284
CIDS3	3	51˚39.215	128˚08.283
CIDS4	1	51˚39.381	128˚08.316
CIDS4	2	51˚39.383	128˚08.318
CIDS4	3	51˚39.383	128˚08.315
CIDS8	1	51˚38.478	128˚09.114
CIDS8	2	51˚38.480	128˚09.110
CIDS8	3	51˚38.484	128˚09.106
CIDS9	1	51˚39.600	128˚08.739
CIDS9	2	51˚39.607	128˚08.735
CIDS9	3	51˚39.608	128˚08.735
CIDS10	1	51˚38.663	128˚08.723
CIDS10	2	51˚38.667	128˚08.736
CIDS10	3	51˚38.663	128˚08.723
CIDS15	1	51˚39.722	128˚08.475
CIDS15	2	51˚39.725	128˚08.471
CIDS15	3	51˚39.728	128˚08.468
CIDS16	1	51˚39.967	128˚07.067
CIDS16	2	51˚39.960	128˚07.063
CIDS16	3	51˚39.966	128˚07.081

APPENDIX 4 : PHYSICAL AND CHEMICAL SOIL ANALYSES

Abbreviations:

Abbreviation	Explanation	Reference
Po	Organic phosphorus determined by combustion	Saunders and Williams, 1955
Al_p	Sodium pyrophosphate extractable aluminum	Courchesne and Turmel, 2008
Fe_p	Sodium pyrophosphate extractable iron	Courchesne and Turmel, 2008
Al_o	Ammonium oxalate extractable aluminum	Courchesne and Turmel, 2008
Fe_o	Ammonium oxalate extractable iron	Courchesne and Turmel, 2008
Si_o	Ammonium oxalate extractable silicon	Courchesne and Turmel, 2008
CEC	Cation exchange capacity determined using barium chloride	Hendershot et al., 2008
BS	Base saturation (not corrected with hydrogen ions)	Hendershot et al., 2008
LOI	Loss on ignition at 950°C pre-fusion	Claisse, 2003
Allophane	Estimated allophane concentration using Si:Al	Parfitt, 1990

Table A4- 1. Select chemical analyses for CIDS1A.

Horizon	Depth (cm)	Total (%)			Po (mg kg^{-1})	pH H2O	pH CaCl2	Al_p (%)	Fe_p (%)	Al_o (%)	Fe_o (%)	Si_o (%)
		C	N	S								
C	0-27	0.41	0.00	-	19.2	8.4	7.8	0.01	0.00	0.01	0.02	0.01
Ahb	27-34	0.53	0.01	-	3.9	8.2	7.6	0.01	0.00	0.02	0.03	0.01
C2	34-62	0.44	0.01	-	31.2	8.8	7.9	0.01	0.01	0.02	0.02	0.01
Ahb2	62-67	0.61	0.01	-	15.5	8.7	7.8	0.01	0.01	0.02	0.02	0.02
BC	67-116	0.51	0.01	-	15.9	8.6	7.9	0.01	0.01	0.02	0.02	0.01
C3	116-122+	0.68	0.00	-	9.5	8.6	7.9	0.01	0.01	0.02	0.03	0.01

Horizon	Depth (cm)	Barium Chloride Exchangeable Cations / CEC (cMol +/Kg)				BS (%)	LOI (%)
		Al	Ca	K	Mg		
C	0-27	0.0	1.0	0.0	0.0	97.8	1.5
Ahb	27-34	0.0	1.9	0.0	0.1	98.5	1.6
C2	34-62	0.0	1.1	0.0	0.0	97.8	1.6
Ahb2	62-67	0.0	1.3	0.0	0.0	98.0	2.3
BC	67-116	0.0	1.3	0.0	0.0	98.1	2.0
C3	116-122+	0.0	1.6	0.0	0.1	98.0	2.4

Horizon	Depth (cm)	Mehlich III Extractable (mg/kg)					Allophane (%)
		Al	Ca	Fe	Mg	P	
C	0-27	-	4186.9	11.2	90.3	3.5	3.2
Ahb	27-34	-	2633.8	15.3	48.2	2.9	3.9
C2	34-62	-	4951.9	12.4	83.7	3.4	3.2
Ahb2	62-67	-	7396.0	12.5	137.7	3.0	3.4
BC	67-116	-	6242.0	11.8	134.8	2.0	3.6
C3	116-122+	-	7509.4	11.4	140.0	2.5	-

Table A4- 2. Select chemical analyses for CIDS1B.

Horizon	Depth (cm)	Total (%)			Po (mg kg^{-1})	pH H2O	pH CaCl2	Al_p (%)	Fe_p (%)	Al_o (%)	Fe_o (%)	Si_o (%)
		C	N	S								
C	0-13	0.25	0.01	-	12.1	8.3	7.5	0.01	0.01	0.02	0.02	0.01
Ahb	13-18	1.11	0.04	-	29.3	7.5	7.0	0.01	0.00	0.00	0.00	0.00
BC	18-92	0.56	0.00	-	4.1	8.6	7.7	0.01	0.00	0.01	0.02	0.01
C2	92-111+	0.54	0.00	-	19.2	8.6	7.7	0.01	0.00	0.01	0.02	0.01

Horizon	Depth (cm)	Barium Chloride Exchangeable Cations (cMol +/Kg)				BS (%)	LOI (%)
		Al	Ca	K	Mg		
C	0-13	0.0	0.9	0.0	0.0	97.8	0.9
Ahb	13-18	0.0	4.4	0.1	0.1	99.0	2.4
BC	18-92	0.0	1.1	0.0	0.0	98.4	2.2
C2	92-111+	0.0	1.1	0.1	0.1	98.0	1.9

Horizon	Depth (cm)	Mehlich III Extractable (mg/kg)					Allophane (%)
		Al	Ca	Fe	Mg	P	
C	0-13	-	1235.4	18.2	31.1	3.4	3.1
Ahb	13-18	0.8	2035.5	24.9	48.0	3.4	0.0
BC	18-92	-	5008.6	11.7	104.6	2.4	3.1
C2	92-111+	-	4560.8	11.9	109.2	2.4	3.3

Table A4- 3. Select chemical analyses for CIDS3A.

Horizon	Depth (cm)	Total (%)			Po (mg kg^{-1})	pH H2O	pH CaCl2	Al_p (%)	Fe_p (%)	Al_o (%)	Fe_o (%)	Si_o (%)
		C	N	S								
S/L	28-26	46.46	1.37	0.13	610.0	4.2	3.7	-	-	-	-	-
Fm	26-22	28.33	0.74	0.09	328.9	3.5	3.1	-	-	-	-	-
Hw	22-0	54.82	1.38	0.18	469.2	3.4	3.0	-	-	-	-	-
Ae	0-3	0.21	0.01	-	5.0	4.2	3.7	0.01	0.01	0.02	0.02	0.01
Bmj	3-58	0.18	0.01	-	25.0	5.1	4.4	0.02	0.03	0.03	0.06	0.01
BC	58-93+	0.19	0.00	-	6.8	5.0	4.4	0.03	0.03	0.04	0.05	0.01

Horizon	Depth (cm)	Barium Chloride Exchangeable Cations (cMol +/Kg)				BS (%)	LOI (%)
		Al	Ca	K	Mg		
S/L	28-26	0.3	16.0	2.9	8.3	93.2	-
Fm	26-22	1.5	7.5	1.2	5.4	85.1	-
Hw	22-0	0.4	15.2	1.2	9.9	94.0	-
Ae	0-3	0.2	0.2	0.0	0.1	47.5	0.7
Bmj	3-58	0.1	0.3	0.0	0.1	66.9	0.7
BC	58-93+	0.1	0.2	0.0	0.0	56.6	0.7

Horizon	Depth (cm)	Mehlich III Extractable (mg/kg)					Allophane (%)
		Al	Ca	Fe	Mg	P	
S/L	28-26	125.2	2076.7	38.9	756.0	275.5	-
Fm	26-22	491.6	1228.0	278.6	590.4	84.7	-
Hw	22-0	203.9	2312.0	94.8	1071.5	85.3	-
Ae	0-3	88.5	34.2	47.3	12.2	3.0	2.6
Bmj	3-58	232.0	59.6	163.8	17.5	13.4	3.1
BC	58-93+	278.7	44.0	182.6	9.4	13.4	4.2

Table A4- 4. Select chemical analyses for CIDS3B.

Horizon	Depth (cm)	Total (%)			Po (mg kg^{-1})	pH H2O	pH CaCl2	Al_p (%)	Fe_p (%)	Al_o (%)	Fe_o (%)	Si_o (%)
		C	N	S								
S/L	37-35	53.11	0.93	0.11	451.6	3.8	3.4	-	-	-	-	-
Fm	35-33	53.65	1.34	0.16	637.0	3.5	3.1	-	-	-	-	-
Hw	33-0	52.60	1.13	0.15	410.1	3.5	3.1	-	-	-	-	-
Ae	0-3	0.16	0.00	-	5.3	4.3	3.7	0.01	0.01	0.02	0.02	0.01
Bhj	3-26	0.33	0.01	-	25.8	4.6	4.0	0.04	0.03	0.04	0.05	0.01
Bm	26-55	0.22	0.01	-	< 1.0	4.9	4.3	0.03	0.02	0.04	0.05	0.01
BC	55-120+	0.12	0.00	-	50.8	5.0	4.4	0.02	0.02	0.04	0.06	0.01

Horizon	Depth (cm)	Barium Chloride Exchangeable Cations (cMol +/Kg)				BS (%)	LOI (%)
		Al	Ca	K	Mg		
S/L	37-35	0.3	15.5	2.5	8.1	93.2	-
Fm	35-33	0.4	21.5	2.0	10.5	95.5	-
Hw	33-0	0.6	23.0	0.7	9.6	95.6	-
Ae	0-3	0.2	0.1	0.0	0.1	45.8	0.5
Bhj	3-26	0.3	0.2	0.0	0.1	40.9	0.9
Bm	26-55	0.2	0.2	0.0	0.1	51.3	0.7
BC	55-120+	0.1	0.1	0.0	0.0	53.6	0.6

Horizon	Depth (cm)	Mehlich III Extractable (mg/kg)					Allophane (%)
		Al	Ca	Fe	Mg	P	
S/L	37-35	85.9	2296.3	27.5	819.2	163.6	-
Fm	35-33	230.6	3297.6	71.2	1171.3	138.9	-
Hw	33-0	353.1	3418.6	144.9	1047.6	62.3	-
Ae	0-3	75.7	24.2	29.2	11.4	2.6	2.7
Bhj	3-26	363.2	42.9	206.6	13.2	24.7	3.3
Bm	26-55	288.4	51.8	151.1	14.8	15.0	4.2
BC	55-120+	229.3	36.1	133.7	10.7	15.5	4.1

Table A4- 5. Select chemical analyses for CIDS4A.

Horizon	Depth (cm)	Total (%)			Po (mg kg^{-1})	pH H2O	pH CaCl2	Al_p (%)	Fe_p (%)	Al_o (%)	Fe_o (%)	Si_o (%)
		C	N	S								
S/L+Fa	9-7	36.30	0.72	0.10	432.1	4.0	3.5	-	-	-	-	-
Hh	7-0	49.05	0.90	0.11	448.9	3.5	3.2	-	-	-	-	-
Ae	0-3	0.92	0.03	-	12.9	3.8	3.3	0.02	0.01	0.02	0.02	0.01
Bhj	3-23	0.25	0.01	-	5.6	4.7	4.2	0.03	0.03	0.04	0.04	0.01
Bm	23-73	0.12	0.00	-	10.5	5.2	4.7	0.02	0.01	0.03	0.03	0.01
BC	73-111+	0.08	0.01	-	30.6	5.3	5.0	0.01	0.01	0.03	0.03	0.01

Horizon	Depth (cm)	Barium Chloride Exchangeable Cations (cMol +/Kg)				BS (%)	LOI (%)
		Al	Ca	K	Mg		
S/L+Fa	9-7	0.6	15.2	2.7	5.4	93.2	-
Hh	7-0	0.7	20.4	3.2	6.0	93.8	-
Ae	0-3	0.4	0.3	0.1	0.1	54.1	1.6
Bhj	3-23	0.3	0.2	0.0	0.1	48.5	0.8
Bm	23-73	0.1	0.1	0.0	0.0	71.7	0.5
BC	73-111+	0.0	0.1	0.0	0.1	84.2	0.3

Horizon	Depth (cm)	Mehlich III Extractable (mg/kg)					Allophane (%)
		Al	Ca	Fe	Mg	P	
S/L+Fa	9-7	254.2	2329.4	110.4	553.7	205.5	-
Hh	7-0	260.2	3347.1	93.6	700.3	302.9	-
Ae	0-3	138.3	75.5	71.0	17.9	10.1	3.7
Bhj	3-23	356.1	59.1	182.3	23.0	27.5	4.8
Bm	23-73	250.8	39.0	92.5	15.9	7.7	6.6
BC	73-111+	123.8	34.9	51.7	12.9	8.3	6.6

Table A4- 6. Select chemical analyses for CIDS4B.

Horizon	Depth (cm)	Total (%)			Po (mg kg^{-1})	pH H2O	pH CaCl2	Al_p (%)	Fe_p (%)	Al_o (%)	Fe_o (%)	Si_o (%)
		C	N	S								
S/L	10-8	50.35	0.71	0.10	464.0	4.3	3.8	-	-	-	-	-
Fm	8-6	50.57	0.85	0.11	433.5	3.8	3.4	-	-	-	-	-
Hh	6-0	48.81	0.88	0.12	429.0	3.4	3.0	-	-	-	-	-
Ae	0-5	1.01	0.03	-	21.1	4.0	3.7	0.03	0.04	0.04	0.05	0.01
Bhj	5-19	0.48	0.02	-	22.9	4.4	4.0	0.06	0.07	0.06	0.07	0.01
Bm	19-64	0.11	0.00	-	16.6	5.0	4.6	0.02	0.01	0.03	0.03	0.01
BC	64-103+	0.07	0.00	-	12.3	5.1	4.9	0.01	0.01	0.03	0.03	0.01

Horizon	Depth (cm)	Barium Chloride Exchangeable Cations (cMol +/Kg)				BS (%)	LOI (%)
		Al	Ca	K	Mg		
S/L	10-8	0.4	17.2	4.8	7.7	94.5	-
Fm	8-6	0.6	18.0	2.4	6.1	94.2	-
Hh	6-0	1.3	16.9	1.6	8.4	91.6	-
Ae	0-5	0.7	0.2	0.0	0.1	31.4	2.0
Bhj	5-19	0.4	0.2	0.0	0.1	43.0	1.0
Bm	19-64	0.1	0.1	0.0	0.0	69.6	0.5
BC	64-103+	0.0	0.2	0.0	0.0	84.9	0.4

Horizon	Depth (cm)	Mehlich III Extractable (mg/kg)				
		Al	Ca	Fe	Mg	P
S/L	10-8	167.5	2350.5	37.4	775.0	314.9
Fm	8-6	257.0	2632.8	49.4	607.9	223.9
Hh	6-0	511.2	2578.8	100.5	920.6	118.6
Ae	0-5	301.8	51.7	217.2	19.9	8.8
Bhj	5-19	602.3	59.0	347.8	15.7	8.0
Bm	19-64	211.1	37.4	98.4	16.7	5.7
BC	64-103+	166.5	43.0	72.2	13.5	6.0

Table A4- 7. Select chemical analyses for CIDS8A.

Horizon	Depth (cm)	Total (%)			Po (mg kg^{-1})	pH H2O	pH CaCl2	Al_p (%)	Fe_p (%)	Al_o (%)	Fe_o (%)	Si_o (%)
		C	N	S								
L	37-34	52.84	0.67	0.14	478.3	5.7	5.4	-	-	-	-	-
Fm	34-15	48.64	0.77	0.16	321.1	4.2	4.0	-	-	-	-	-
Hw	15-0	55.51	0.48	0.13	182.3	3.9	3.6	-	-	-	-	-
Ahe	0-6	10.72	0.07	-	23.5	4.1	3.8	0.04	0.02	0.03	0.01	0.00
Ae	6-25	0.22	0.00	-	4.2	4.1	3.9	0.01	0.00	0.03	0.01	0.02
Bhc	25-43	2.47	0.05	-	55.7	4.6	4.3	0.27	0.02	0.28	0.02	0.01
Bfc1	43-45	2.43	0.05	-	52.7	4.6	4.5	0.44	1.97	0.46	2.11	0.07
Bm1	45-65	0.49	0.01	-	12.1	4.9	4.4	0.17	0.09	0.19	0.07	0.05
Bfc2	65-67	1.37	0.03	-	28.0	4.9	4.5	0.32	1.96	0.40	3.42	0.13
Bm2	67-95	0.26	0.00	-	5.6	5.0	4.6	0.10	0.07	0.20	0.12	0.07
BC	95-163+	0.15	0.01	-	22.1	5.1	4.7	0.05	0.02	0.11	0.06	0.05

Horizon	Depth (cm)	Barium Chloride Exchangeable Cations (cMol +/Kg)				BS (%)	LOI (%)
		Al	Ca	K	Mg		
L	37-34	0.0	37.0	1.9	33.9	83.8	-
Fm	34-15	0.1	20.0	1.1	27.3	77.7	-
Hw	15-0	0.4	12.9	0.7	29.2	71.0	-
Ahe	0-6	0.4	0.7	0.1	1.4	57.1	14.3
Ae	6-25	0.1	0.1	0.0	0.3	50.5	0.5
Bhc	25-43	0.8	0.6	0.0	0.8	48.8	4.2
Bfc1	43-45	0.3	0.1	0.0	0.1	23.9	6.0
Bm	45-65	0.2	0.1	0.0	0.1	37.9	1.2
Bfc2	65-67	0.5	0.4	0.0	0.4	44.3	2.6
Bm	67-95	0.1	0.1	0.0	0.1	42.4	0.9
BC	95-163+	0.0	0.1	0.0	0.1	58.6	0.6

Table A4- 7 cont'd. Select chemical analyses for CIDS8A.

Horizon	Depth (cm)	Mehlich III Extractable (mg/kg)					Allophane (%)
		Al	Ca	Fe	Mg	P	
L	37-34	45.4	4726.0	32.5	3572.3	145.3	-
Fm	34-15	264.0	2805.3	124.2	3274.5	40.9	-
Hw	15-0	531.9	1714.7	114.3	3412.0	29.7	-
Ahe	0-6	204.1	96.0	49.9	124.9	16.4	-
Ae	6-25	69.8	27.9	9.2	29.5	2.5	0.0
Bhc	25-43	1758.8	131.2	99.7	115.7	43.7	8.4
Bfc1	43-45	1458.7	42.9	917.9	23.3	nd	3.3
Bm	45-65	1508.0	30.3	277.6	17.9	41.9	1.5
Bfc2	65-67	1290.6	48.7	595.9	33.8	nd	2.2
Bm	67-95	1517.3	20.9	118.6	12.5	36.5	2.8
BC	95-163+	810.6	23.8	61.3	13.6	31.4	8.8

Table A4- 8. Select chemical analyses for CIDS8B.

Horizon	Depth (cm)	Total (%)			Po (mg kg^{-1})	pH H2O	pH CaCl2	Al_p (%)	Fe_p (%)	Al_o (%)	Fe_o (%)	Si_o (%)
		C	N	S								
L	28-27	54.45	0.58	0.10	385.7	5.1	4.6	-	-	-	-	-
Fa	27-10	53.20	0.77	0.12	316.6	4.0	3.6	-	-	-	-	-
Hw	10-0	54.98	0.44	0.09	193.9	3.9	3.4	-	-	-	-	-
Ae	0-22	1.13	0.01	-	3.8	4.0	3.6	0.02	0.02	0.03	0.03	0.02
Bhc	22-57	2.61	0.07	-	89.5	4.6	4.1	0.33	0.19	0.34	0.19	0.02
Bfcj	57-58	1.61	0.03	-	49.8	5.2	4.7	0.44	1.10	0.54	1.32	0.11
Bh	58-72	1.08	0.02	-	59.3	5.0	4.5	0.22	0.07	0.32	0.08	0.08
Bhcj	72-106	1.45	0.03	-	46.2	4.8	4.4	0.27	0.17	0.29	0.16	0.06

Horizon	Depth (cm)	Barium Chloride Exchangeable Cations (cMol +/Kg)				BS (%)	LOI (%)
		Al	Ca	K	Mg		
L	28-27	0.0	29.8	2.0	21.5	88.1	-
Fa	27-10	0.2	19.1	0.8	22.8	83.5	-
Hw	10-0	0.3	12.5	0.5	18.3	81.7	-
Ae	0-22	0.2	0.1	0.0	0.2	54.0	1.9
Bhc	22-57	1.0	0.6	0.0	0.6	47.4	4.5
Bfcj	57-58	0.2	0.3	0.0	0.3	61.7	3.8
Bh	58-72	0.3	0.4	0.0	0.3	58.5	2.1
Bhcj	72-106	0.2	0.4	0.0	0.3	58.2	2.6

Horizon	Depth (cm)	Mehlich III Extractable (mg/kg)					Allophane (%)
		Al	Ca	Fe	Mg	P	
L	28-27	49.9	4320.1	24.5	2442.8	174.2	-
Fa	27-10	234.4	2849.8	95.6	2730.9	51.1	-
Hw	10-0	210.4	1814.6	65.6	2040.7	60.5	-
Ae	0-22	82.2	36.2	17.4	30.4	3.9	6.2
Bhc	22-57	1847.2	132.3	404.4	86.7	20.8	3.1
Bfcj	57-58	1549.8	108.3	549.5	59.5	4.9	4.3
Bh	58-72	1827.4	98.9	257.6	55.9	22.3	8.3
Bhcj	72-106	1701.3	125.9	576.6	70.3	19.1	2.1

Table A4- 9. Select chemical analyses for CIDS9A.

Horizon	Depth (cm)	Total (%)			Po (mg kg^{-1})	pH H2O	pH CaCl2	Al_p (%)	Fe_p (%)	Al_o (%)	Fe_o (%)	Si_o (%)
		C	N	S								
S/L	25-23	48.29	0.86	0.11	568.5	4.6	4.3	-	-	-	-	-
Fm	23-18	42.27	0.88	0.13	451.0	3.6	3.3	-	-	-	-	-
Hh	18-5	43.31	0.87	0.12	385.2	3.5	3.2	-	-	-	-	-
Hw	5-0	56.62	0.57	0.10	235.5	3.6	3.2	-	-	-	-	-
Ae	0-6	0.19	0.00	-	1.9	4.1	3.7	0.02	0.01	0.04	0.01	0.02
Bhj	6-36	0.68	0.02	-	15.0	4.6	4.1	0.11	0.08	0.11	0.08	0.02
Bhcj	36-39	1.59	0.05	-	73.3	4.4	4.0	0.26	0.14	0.28	0.14	0.02
Bmj	39-90	0.35	0.01	-	< 1.0	4.7	4.3	0.07	0.04	0.09	0.05	0.02
BC	90-112+	0.28	0.01	-	< 1.0	4.8	4.4	0.06	0.03	0.08	0.04	0.02

Horizon	Depth (cm)	Barium Chloride Exchangeable Cations (cMol +/Kg)				BS (%)	LOI (%)
		Al	Ca	K	Mg		
S/L	25-23	0.1	34.8	4.6	14.5	95.3	-
Fm	23-18	0.5	22.7	1.9	10.2	94.8	-
Hh	18-5	1.4	17.0	0.9	12.8	91.2	-
Hw	5-0	0.9	5.6	0.5	17.7	89.4	-
Ae	0-6	0.3	0.1	0.0	0.1	33.1	0.5
Bhj	6-36	0.5	0.2	0.0	0.1	41.3	1.4
Bhcj	36-39	0.8	0.4	0.0	0.2	38.7	2.9
Bmj	39-90	0.2	0.1	0.0	0.0	39.9	0.8
BC	90-112+	0.1	0.1	0.0	0.0	40.6	0.8

Horizon	Depth (cm)	Mehlich III Extractable (mg/kg)					Allophane (%)
		Al	Ca	Fe	Mg	P	
S/L	25-23	129.0	4916.7	83.7	1546.9	178.3	-
Fm	23-18	329.2	3537.7	151.4	1186.0	127.9	-
Hh	18-5	827.2	2463.1	214.6	1408.8	53.4	-
Hw	5-0	383.5	587.9	57.0	1412.0	42.1	-
Ae	0-6	110.6	27.5	17.0	12.4	1.9	6.8
Bhj	6-36	1070.3	56.1	213.4	18.3	13.5	2.1
Bhcj	36-39	1992.4	99.1	300.5	28.5	10.2	2.6
Bmj	39-90	631.7	36.9	129.1	9.5	13.5	3.9
BC	90-112+	627.5	31.7	103.9	6.1	11.0	6.3

Table A4- 10. Select chemical analyses for CIDS9B.

Horizon	Depth (cm)	Total (%)			Po (mg kg^{-1})	pH H2O	pH CaCl2	Al_p (%)	Fe_p (%)	Al_o (%)	Fe_o (%)	Si_o (%)
		C	N	S								
L	4-3	49.52	1.14	0.12	527.5	4.8	4.5	-	-	-	-	-
Fm/Hi	3-1, 1-0	15.88	0.42	-	158.0	3.9	3.5	0.03	0.01	0.04	0.03	0.00
Ahe	0-13	2.05	0.05	-	24.8	4.0	3.4	0.05	0.06	0.07	0.07	0.01
Hwb	13-33	50.34	0.46	0.08	156.0	3.7	3.2	-	-	-	-	-
Bm	33-58	0.24	0.01	-	7.1	4.5	3.9	0.03	0.04	0.04	0.05	0.02
Bhjcj	58-113	0.81	0.02	-	19.1	4.7	4.1	0.08	0.09	0.10	0.10	0.01

Horizon	Depth (cm)	Barium Chloride Exchangeable Cations (cMol +/Kg)				BS (%)	LOI (%)
		Al	Ca	K	Mg		
L	4-3	0.1	43.1	1.8	16.6	97.1	-
Fm/Hi	3-1, 1-0	0.6	11.9	1.1	5.9	94.5	0.0
Ahe	0-13	1.1	0.4	0.0	0.3	39.7	3.7
Hwb	13-33	1.5	16.9	0.3	11.5	92.6	-
Bm	33-58	0.3	0.2	0.0	0.1	49.3	0.7
Bhjcj	58-113	0.6	0.4	0.0	0.2	49.1	1.5

Horizon	Depth (cm)	Mehlich III Extractable (mg/kg)					Allophane (%)
		Al	Ca	Fe	Mg	P	
L	4-3	270.0	5332.2	122.9	1631.1	157.8	-
Fm/Hi	3-1, 1-0	445.4	1557.5	192.2	569.0	55.6	-
Ahe	0-13	354.0	76.3	185.0	36.4	9.1	-
Hwb	13-33	662.6	2393.5	157.5	1195.4	29.6	6.4
Bm	33-58	259.2	49.7	254.1	24.9	18.7	4.6
Bhjcj	58-113	944.3	109.5	686.6	29.8	34.7	7.1

Table A4- 11. Select chemical analyses for CIDS10A.

Horizon	Depth (cm)	Total (%)			Po (mg kg^{-1})	pH H2O	pH CaCl2	Al_p (%)	Fe_p (%)	Al_o (%)	Fe_o (%)	Si_o (%)
		C	N	S								
Lv	28-27	34.20	0.44	0.06	205.3	3.6	3.9	-	-	-	-	-
Fm	27-24	52.15	0.81	0.11	349.4	2.9	3.5	-	-	-	-	-
Hh1	24-10	55.06	0.84	0.10	359.3	2.6	3.1	-	-	-	-	-
Hh2	10-0	60.04	0.59	0.09	173.3	3.5	2.9	-	-	-	-	-
Bhcj	0-10	9.89	0.16	-	56.7	3.6	3.2	0.49	0.02	0.50	0.02	0.02
Ae	10-22	0.38	0.01	-	9.9	4.0	4.9	0.13	0.01	0.47	0.03	0.20
Bfc	22-25	1.75	0.04	-	35.7	4.1	4.6	0.57	1.29	1.59	2.33	0.51
Bmcj	22-80	0.37	0.01	-	14.2	4.0	5.1	0.16	0.03	0.96	0.21	0.44
BCg1	80-148	0.09	0.03	-	11.7	4.2	5.3	0.07	0.01	0.28	0.05	0.14

Horizon	Depth (cm)	Barium Chloride Exchangeable Cations (cMol +/Kg)				BS (%)	LOI (%)
		Al	Ca	K	Mg		
Lv	18-17	2.4	11.7	1.6	4.7	82.2	-
Fm	17-14	1.1	11.2	1.7	9.3	90.1	-
Hh1	14-0	1.2	9.3	1.5	16.6	91.4	-
Hh2	0-10	3.0	0.4	0.2	3.5	53.0	-
Bhcj	10-20	6.5	0.1	0.0	0.2	4.2	17.0
Ae	20-22	0.1	0.0	0.0	0.0	14.7	-
Bfc	22-25	0.4	0.0	0.0	0.0	11.8	-
Bmcj	22-80	0.0	0.0	0.0	0.0	25.0	-
BCg1	80-148	0.2	0.0	0.0	0.0	11.0	-

Horizon	Depth (cm)	Mehlich III Extractable (mg/kg)					Allophane (%)
		Al	Ca	Fe	Mg	P	
Lv	18-17	1699.5	1439.7	143.0	372.0	55.8	-
Fm	17-14	529.6	1764.7	84.8	1055.1	35.9	-
Hh1	14-0	554.2	1372.9	128.5	1840.7	38.5	-
Hh2	0-10	724.3	62.6	83.1	224.0	8.9	-
Bhcj	10-20	1784.0	22.6	37.1	29.7	6.3	2.5
Ae	20-22	1755.9	48.5	11.5	3.5	1.8	12.0
Bfc	22-25	2195.6	12.2	145.6	2.4	0.6	14.1
Bmcj	22-80	2186.3	34.3	58.5	3.4	1.8	12.8
BCg1	80-148	1314.5	37.5	23.1	2.4	23.1	8.8

Table A4- 12. Select chemical analyses for CIDS10B.

Horizon	Depth (cm)	Total (%)			Po (mg kg^{-1})	pH H2O	pH CaCl2	Al_p (%)	Fe_p (%)	Al_o (%)	Fe_o (%)	Si_o (%)
		C	N	S								
S/L	28-25	42.27	0.46	0.06	253.1	4.7	4.5	-	-	-	-	-
Fm	25-20	45.75	0.80	0.10	344.8	4.5	4.0	-	-	-	-	-
Hh1	20-14	54.04	0.99	0.11	409.4	3.9	3.6	-	-	-	-	-
Hh2	14-0	59.72	0.35	0.05	96.7	3.9	3.3	-	-	-	-	-
Bhc	0-7	5.02	0.10	-	22.5	4.1	3.4	0.30	0.02	0.30	0.02	0.01
Ae	7-10	0.71	0.02	-	5.0	4.2	3.8	0.08	0.07	0.12	0.07	0.02
Bfc	10-13	1.20	0.03	-	10.5	4.4	4.6	0.35	0.38	1.29	1.01	0.42
Bmcj	13-33	0.33	0.01	-	15.8	4.5	5.3	0.12	0.01	1.19	0.26	0.48
BC	33-90+	0.09	0.01	-	7.3	4.5	5.5	0.06	0.00	0.38	0.07	0.18
BC2	170-204	-	-	-	-	-	-	0.04	0.00	0.35	0.09	0.17

Horizon	Depth (cm)	Barium Chloride Exchangeable Cations (cMol +/Kg)				BS (%)	LOI (%)
		Al	Ca	K	Mg		
S/L	28-25	0.1	28.9	1.4	10.0	95.0	-
Fm	25-20	0.2	34.5	1.5	13.4	92.9	-
Hh1	20-14	0.2	26.8	1.5	13.4	94.2	-
Hh2	14-0	0.5	2.4	0.3	3.6	84.5	-
Bhc	0-7	5.0	0.3	0.0	0.4	11.7	8.7
Ae	7-10	1.3	0.1	0.0	0.1	14.2	1.5
Bfc	10-13	0.5	0.0	0.0	0.0	10.5	3.2
Bmcj	13-33	0.0	0.0	0.0	0.0	23.3	0.9
BC	33-90+	0.0	0.0	0.0	0.0	28.2	0.4
BC2	170-204	0.0	0.0	0.0	0.0	38.4	0.6

Horizon	Depth (cm)	Mehlich III Extractable (mg/kg)					Allophane (%)
		Al	Ca	Fe	Mg	P	
S/L	28-25	417.6	3941.7	49.0	1038.7	38.8	-
Fm	25-20	610.9	4829.8	99.0	1416.9	80.9	-
Hh1	20-14	268.8	3779.3	81.7	1427.3	59.6	-
Hh2	14-0	222.8	311.4	37.9	307.5	9.2	-
Bhc	0-7	1737.2	43.9	57.0	40.8	9.0	0.0
Ae	7-10	814.0	18.7	185.3	13.6	0.5	12.7
Bfc	10-13	2132.7	9.2	96.1	3.7	0.6	22.4
Bmcj	13-33	2129.1	5.0	23.7	0.9	3.0	22.3
BC	33-90+	1827.0	5.3	17.4	0.7	16.5	12.6

Table A4- 13. Select chemical analyses for CIDS15A.

Horizon	Depth (cm)	Total (%)			Po (mg kg^{-1})	pH H2O	pH CaCl2	Al_p (%)	Fe_p (%)	Al_o (%)	Fe_o (%)	Si_o (%)
		C	N	S								
S/L	20-18	53.94	0.74	0.08	425.0	4.9	4.5	-	-	-	-	-
Fm	18-14	51.15	0.92	0.11	523.2	4.2	3.9	-	-	-	-	-
Hh	14-0	51.86	1.18	0.14	545.2	3.8	3.5	-	-	-	-	-
Ae	0-4	6.03	0.10	-	38.0	3.7	3.2	0.07	0.01	0.08	0.02	0.01
Ahe	4-12	9.88	0.13	-	79.3	3.7	3.2	0.10	0.02	0.11	0.02	0.00
Bhc	12-21	6.14	0.14	-	82.0	4.0	3.4	0.49	0.02	0.52	0.02	0.01
Bfcj	21-23	1.66	0.03	-	38.2	4.4	4.3	0.41	0.47	1.01	0.69	0.27
Bmcj	23-49	0.55	0.02	-	22.7	4.4	4.6	0.19	0.05	0.56	0.11	0.19
BC	49-103+	0.14	0.01	-	41.8	4.6	5.1	0.07	0.01	0.23	0.05	0.09

Horizon	Depth (cm)	Barium Chloride Exchangeable Cations (cMol +/Kg)				BS (%)	LOI (%)
		Al	Ca	K	Mg		
S/L	20-18	0.1	44.3	2.7	11.4	93.8	-
Fm	18-14	0.1	33.3	2.8	9.1	92.7	-
Hh	14-0	0.3	26.6	2.4	9.0	94.4	-
Ae	0-4	1.4	0.4	0.1	0.2	30.7	9.9
Ahe	4-12	2.3	0.4	0.1	0.2	22.7	15.5
Bhc	12-21	6.1	0.6	0.0	0.2	12.6	9.8
Bfcj	21-23	1.0	0.1	0.0	0.0	7.6	3.7
Bmcj	23-49	0.2	0.0	0.0	0.0	9.0	1.2
BC	49-103+	0.0	0.0	0.0	0.0	39.5	0.7

Horizon	Depth (cm)	Mehlich III Extractable (mg/kg)					Allophane (%)
		Al	Ca	Fe	Mg	P	
S/L	20-18	109.2	5091.5	23.1	1006.2	143.0	-
Fm	18-14	301.5	5181.6	76.1	1027.1	106.8	-
Hh	14-0	305.5	3956.9	94.4	982.9	91.8	-
Ae	0-4	450.5	69.1	48.4	26.8	17.7	8.0
Ahe	4-12	783.6	56.6	82.4	24.8	41.0	36.0
Bhc	12-21	2033.5	91.0	50.9	25.3	11.3	32.3
Bfcj	21-23	2483.7	11.7	574.7	1.8	0.5	22.1
Bmcj	23-49	2169.5	6.3	85.9	0.8	16.8	13.8
BC	49-103+	1564.8	6.1	34.5	0.8	81.1	11.8

Table A4- 14. Select chemical analyses for CIDS15B.

Horizon	Depth (cm)	Total (%)			Po (mg kg^{-1})	pH H2O	pH CaCl2	Al_p (%)	Fe_p (%)	Al_o (%)	Fe_o (%)	Si_o (%)
		C	N	S								
S/L	18-16	44.81	0.60	0.07	351.2	4.8	4.4	-	-	-	-	-
Fm	16-13	51.02	0.85	0.12	458.8	4.6	4.2	-	-	-	-	-
Hh	13-0	51.66	1.37	0.16	499.2	3.9	3.6	-	-	-	-	-
Ae	0-9	15.20	0.15	-	78.8	3.9	3.3	0.15	0.02	0.17	0.02	0.01
Ahe	9-14	3.39	0.08	-	49.0	4.2	3.4	0.10	0.00	0.11	0.01	0.01
Bhc	14-28	4.58	0.09	-	47.7	4.2	3.6	0.55	0.04	0.62	0.05	0.04
Bhc2	28-38	1.53	0.03	-	30.2	4.3	4.2	0.44	0.02	0.84	0.03	0.19
Bh	38-43	1.65	0.04	-	32.8	4.4	4.2	0.30	0.01	0.85	0.02	0.23
Bfc	43-45	1.62	0.04	-	49.3	4.6	4.4	0.56	1.50	1.10	2.88	0.36
Bm	45-128+	0.27	0.01	-	17.1	4.4	4.8	0.14	0.12	0.38	0.10	0.14

Horizon	Depth (cm)	Barium Chloride Exchangeable Cations (cMol +/Kg)				BS (%)	LOI (%)
		Al	Ca	K	Mg		
S/L	18-16	0.2	28.2	3.0	11.9	94.1	-
Fm	16-13	0.1	39.1	2.5	15.8	94.7	-
Hh	13-0	0.5	40.0	1.7	17.8	94.3	-
Ae	0-9	3.0	1.0	0.1	0.6	35.4	24.9
Ahe	9-14	2.0	0.5	0.0	0.3	28.6	5.4
Bhc	14-28	4.2	0.5	0.0	0.2	14.9	7.2
Bhc2	28-38	1.0	0.1	0.0	0.0	8.0	2.9
Bh	38-43	1.0	0.1	0.0	0.0	7.2	2.4
Bfc	43-45	0.4	0.1	0.0	0.0	14.8	2.7
Bm	45-128+	0.1	0.0	0.0	0.0	21.5	0.9

Horizon	Depth (cm)	Mehlich III Extractable (mg/kg)					Allophane (%)
		Al	Ca	Fe	Mg	P	
S/L	18-16	831.0	3912.0	64.9	1159.5	113.5	-
Fm	16-13	300.2	5410.4	54.2	1688.9	152.7	-
Hh	13-0	715.0	5437.8	191.9	1958.4	100.2	-
Ae	0-9	917.3	128.5	67.1	53.9	33.8	8.0
Ahe	9-14	792.9	86.2	26.2	32.1	32.7	13.4
Bhc	14-28	2454.9	73.8	152.2	20.4	6.7	13.2
Bhc2	28-38	2496.8	10.5	56.4	1.4	3.3	20.8
Bh	38-43	2339.2	11.0	27.4	1.7	5.2	23.8
Bfc	43-45	2078.8	11.6	277.0	1.6	nd	9.0
Bm	45-128+	1873.4	5.0	46.9	0.7	52.3	11.7

Table A4- 15. Select chemical analyses for CIDS16A.

Horizon	Depth (cm)	Total (%)			Po (mg kg^{-1})	pH H2O	pH CaCl2	Al_p (%)	Fe_p (%)	Al_o (%)	Fe_o (%)	Si_o (%)
		C	N	S								
S/L	0-3	53.30	0.65	0.08	393.9	4.7	4.4	-	-	-	-	-
Fa	3-8	54.15	0.99	0.13	434.9	4.2	3.9	-	-	-	-	-
Hw	8-35	57.62	1.08	0.11	289.7	3.3	2.9	-	-	-	-	-
Oh	35-55	48.83	0.84	0.16	348.3	3.4	3.1	-	-	-	-	-
Bhc	55-64	4.06	0.08	-	38.6	4.1	3.8	0.66	0.02	0.71	0.02	0.04
Bhcj	64-80	1.24	0.03	-	28.7	4.3	4.3	0.46	0.01	0.57	0.02	0.11
Bfc	80-81	1.44	0.03	-	27.5	4.6	4.3	0.42	0.76	0.66	1.19	0.17
Bm	81-136+	0.35	0.01	-	15.2	4.7	4.6	0.14	0.06	0.32	0.09	0.11

Horizon	Depth (cm)	Barium Chloride Exchangeable Cations (cMol +/Kg)				BS (%)	LOI (%)
		Al	Ca	K	Mg		
S/L	0-3	0.1	37.3	4.6	10.8	96.5	-
Fa	3-8	0.1	42.9	2.6	12.5	96.9	-
Hw	8-35	1.6	2.1	0.4	14.0	85.2	-
Oh	35-55	17.0	0.9	0.1	1.1	10.8	-
Bhc	55-64	3.0	0.1	0.0	0.0	2.4	7.3
Bhcj	64-80	0.5	0.0	0.0	0.0	6.7	2.5
Bfc	80-81	0.5	0.1	0.0	0.0	13.1	2.4
Bm	81-136+	0.1	0.0	0.0	0.0	26.7	1.0

Horizon	Depth (cm)	Mehlich III Extractable (mg/kg)					Allophane (%)
		Al	Ca	Fe	Mg	P	
S/L	0-3	93.0	5056.3	25.1	1091.6	67.0	-
Fa	3-8	107.8	6243.3	53.3	1353.4	98.2	-
Hw	8-35	526.7	213.4	69.9	1086.3	13.9	-
Oh	35-55	3919.9	96.3	37.3	100.1	21.7	-
Bhc	55-64	2927.7	10.7	7.1	2.3	4.6	7.1
Bhcj	64-80	2411.6	6.7	21.3	0.8	8.4	4.7
Bfc	80-81	2123.1	13.5	422.1	3.4	nd	8.3
Bm	81-136+	1876.1	7.1	84.3	1.2	41.5	11.7

Table A4- 16. Select chemical analyses for CIDS16B.

Horizon	Depth (cm)	Total (%)			Po (mg kg^{-1})	pH H2O	pH CaCl2	Al_p (%)	Fe_p (%)	Al_o (%)	Fe_o (%)	Si_o (%)
		C	N	S								
S/L	0-4	53.40	0.73	0.09	457.8	5.0	4.7	-	-	-	-	-
Fm	4-12	55.06	1.14	0.14	571.2	5.1	4.8	-	-	-	-	-
Hw	12-45	58.78	1.05	0.15	241.6	3.2	2.9	-	-	-	-	-
Oh	45-63	37.01	0.59	0.15	213.7	3.4	3.1	-	-	-	-	-
Bhc	63-85	3.24	0.07	-	31.1	4.0	3.9	0.54	0.01	0.55	0.01	0.03
Ae	85-86	0.65	0.03	-	18.9	4.1	3.3	0.04	0.01	0.06	0.02	0.02
Bmcj	86-103	0.91	0.02	-	21.7	4.2	3.9	0.17	0.00	0.41	0.01	0.12
Bh	103-223	1.27	0.03	-	19.2	4.1	3.6	0.15	0.03	0.19	0.03	0.05

Horizon	Depth (cm)	Barium Chloride Exchangeable Cations (cMol +/Kg)				BS (%)	LOI (%)
		Al	Ca	K	Mg		
S/L	0-4	0.1	45.7	4.6	10.1	96.8	-
Fm	4-12	0.0	64.6	2.1	9.9	97.8	-
Hw	12-45	2.6	1.3	0.2	9.8	76.1	-
Oh	45-63	13.4	0.5	0.0	0.9	9.6	-
Bhc	63-85	2.8	0.1	0.0	0.0	3.4	6.2
Ae	85-86	0.4	0.1	0.0	0.2	40.9	1.3
Bmcj	86-103	1.0	0.1	0.0	0.0	9.1	1.8
Bh	103-223	1.1	0.1	0.0	0.1	12.8	2.3

Horizon	Depth (cm)	Mehlich III Extractable (mg/kg)					Allophane (%)
		Al	Ca	Fe	Mg	P	
S/L	0-4	32.7	5057.6	17.9	925.5	77.9	-
Fm	4-12	9.8	6943.0	28.5	893.8	57.9	-
Hw	12-45	730.2	157.5	50.2	757.8	10.4	-
Oh	45-63	3675.2	83.0	28.7	88.8	24.0	-
Bhc	63-85	2659.0	11.9	1.9	1.7	9.4	1.8
Ae	85-86	229.4	22.7	54.0	29.4	15.3	6.9
Bmcj	86-103	2190.1	15.0	18.2	3.4	67.7	13.8
Bh	103-223	1448.7	19.7	131.5	8.3	50.7	3.4

Table A4- 17. Total elemental analysis of 2mm fractions for CIDS1A. Lithium metaborate fusion was performed on mineral samples (Claisse, 2003).

Horizon	Depth (cm)	Lithium Metaborate Fusion (mg/Kg)						
		Al	Ca	K	Na	P	Ti	Zr
C	0-27	70362	32192	9219	29462	239	693	41
Ahb	27-34	71150	31868	9355	29594	237	986	45
C2	34-62	71648	36053	9405	29543	199	715	44
Ahb2	62-67	70296	39660	9560	29307	189	724	49
BC	67-116	71783	36025	9302	29548	188	876	43
C3	116-122+	70620	36715	9963	29521	188	664	41

Table A4- 18. Total elemental analysis of 2mm fractions for CIDS1B. Lithium metaborate fusion was performed on mineral samples (Claisse, 2003).

Horizon	Depth (cm)	Lithium Metaborate Fusion (mg/Kg)						
		Al	Ca	K	Na	P	Ti	Zr
C	0-13	69936	25607	8834	29816	208	556	35
Ahb	13-18	70047	30464	8572	28921	230	1077	65
BC	18-92	65754	32649	8605	27658	147	569	47
C2	92-111+	68399	32758	9013	28702	174	588	38

Table A4- 19. Total elemental analysis of 2mm fractions for CIDS3A. Ultrawave acid digestion was performed on organic samples, whereas, lithium metaborate fusion was performed on mineral samples (Kalra and Maynard, 1991; Claisse, 2003).

Horizon	Depth (cm)	Ultrawave Acid Digestion				
		Al (mg/kg)	Ca (%)	K (%)	Na (mg/Kg)	P (%)
S/L	28-26	1508	0.6914	0.1531	432	0.1089
Fm	26-22	4600	0.5618	0.0779	410	0.0461
Hw	22-0	869	0.3884	0.0572	388	0.0699

Horizon	Depth (cm)	Lithium Metaborate Fusion (mg/Kg)						
		Al	Ca	K	Na	P	Ti	Zr
Ae	0-3	71256	28096	8418	29349	50	1990	94
Bmj	3-58	71731	28896	8137	29592	293	2111	64
BC	58-93+	71092	27606	8303	29270	288	1992	133

Table A4- 20. Total elemental analysis of 2mm fractions for CIDS3B. Ultrawave acid digestion was performed on organic samples, whereas, lithium metaborate fusion was performed on mineral samples (Kalra and Maynard, 1991; Claisse, 2003).

Horizon	Depth (cm)	Ultrawave Acid Digestion				
		Al (mg/kg)	Ca (%)	K (%)	Na (mg/Kg)	P (%)
S/L	37-35	534	0.5528	0.1155	356	0.0789
Fm	35-33	799	0.5415	0.1047	362	0.0983
Hw	33-0	1421	0.5673	0.0430	304	0.0564

Horizon	Depth (cm)	Lithium Metaborate Fusion (mg/Kg)						
		Al	Ca	K	Na	P	Ti	Zr
Ae	0-3	69974	29070	7713	28913	< 10.0	2256	136
Bhj	3-26	69753	25478	8397	29957	290	1043	65
Bm	26-55	75611	30676	9080	30279	218	1871	109
BC	55-120+	75558	43522	6908	26819	407	5427	369

Table A4- 21. Total elemental analysis of 2mm fractions for CIDS4A. Ultrawave acid digestion was performed on organic samples, whereas, lithium metaborate fusion was performed on mineral samples (Kalra and Maynard, 1991; Claisse, 2003).

Horizon	Depth (cm)	Ultrawave Acid Digestion				
		Al (mg/kg)	Ca (%)	K (%)	Na (mg/Kg)	P (%)
S/L+Fa	9-7	2767	0.5638	0.1253	411	0.0701
Hh	7-0	1411	0.5718	0.1549	396	0.0972

Horizon	Depth (cm)	Lithium Metaborate Fusion (mg/Kg)						
		Al	Ca	K	Na	P	Ti	Zr
Ae	0-3	69109	23555	8434	30003	< 10.0	878	50
Bhj	3-23	65356	22505	8960	29238	154	732	42
Bm	23-73	71600	24060	9111	30721	188	791	66
BC	73-111+	73318	25416	9075	31523	270	1020	42

Table A4- 22. Total elemental analysis of 2mm fractions for CIDS4B. Ultrawave acid digestion was performed on organic samples, whereas, lithium metaborate fusion was performed on mineral samples (Kalra and Maynard, 1991; Claisse, 2003).

Horizon	Depth (cm)	Ultrawave Acid Digestion				
		Al (mg/kg)	Ca (%)	K (%)	Na (mg/Kg)	P (%)
S/L	10-8	963	0.6791	0.2306	308	0.1083
Fm	8-6	1257	0.4886	0.1101	297	0.0950
Hh	6-0	1543	0.4494	0.0780	389	0.0683

Horizon	Depth (cm)	Lithium Metaborate Fusion (mg/Kg)						
		Al	Ca	K	Na	P	Ti	Zr
Ae	0-5	72119	25051	8735	31487	45	927	60
Bhj	5-19	69855	24227	8690	30477	142	878	54
Bm	19-64	71427	25379	8840	30884	206	1041	49
BC	64-103+	68529	22405	9478	30163	199	607	41

Table A4- 23. Total elemental analysis of 2mm fractions for CIDS8A. Ultrawave acid digestion was performed on organic samples, whereas, lithium metaborate fusion was performed on mineral samples (Kalra and Maynard, 1991; Claisse, 2003).

Horizon	Depth (cm)	Ultrawave Acid Digestion				
		Al (mg/kg)	Ca (%)	K (%)	Na (mg/Kg)	P (%)
L	37-34	348	1.2426	0.0940	3114	0.0717
Fm	34-15	1615	0.5686	0.0681	3402	0.0428
Hw	15-0	1380	0.3491	0.0389	3946	0.0249

Horizon	Depth (cm)	Lithium Metaborate Fusion (mg/Kg)						
		Al	Ca	K	Na	P	Ti	Zr
Ahe	0-6	58610	19102	7583	27480	85	2672	598
Ae	6-25	69068	21775	9101	31049	48	1166	140
Bhc	25-43	72967	25981	7876	30603	254	1921	320
Bfc1	43-45	69845	24538	7194	27945	345	1589	171
Bm	45-65	75099	25335	8921	32426	352	1390	107
Bfc2	65-67	72898	24189	8345	30164	327	1248	71
Bm	67-95	76110	27037	8947	32286	358	1480	80
BC	95-163+	77229	27922	9282	33174	365	1477	156

Table A4- 24. Total elemental analysis of 2mm fractions for CIDS8B. Ultrawave acid digestion was performed on organic samples, whereas, lithium metaborate fusion was performed on mineral samples (Kalra and Maynard, 1991; Claisse, 2003).

Horizon	Depth (cm)	Ultrawave Acid Digestion				
		Al (mg/kg)	Ca (%)	K (%)	Na (mg/Kg)	P (%)
L	28-27	396	1.0348	0.1006	1667	0.0676
Fa	27-10	906	0.4800	0.0497	2006	0.0441
Hw	10-0	843	0.3240	0.0313	1664	0.0276

Horizon	Depth (cm)	Lithium Metaborate Fusion (mg/Kg)						
		Al	Ca	K	Na	P	Ti	Zr
Ae	0-22	68285	22065	8731	30889	98	1618	203
Bhc	22-57	74721	25061	8922	31332	246	1516	95
Bfcj	57-58	71662	23613	8915	30349	318	1239	99
Bh	58-72	75317	25684	9336	32140	333	1325	128
Bhcj	72-106	72584	26841	8217	28242	360	1602	150

Table A4- 25. Total elemental analysis of 2mm fractions for CIDS9A. Ultrawave acid digestion was performed on organic samples, whereas, lithium metaborate fusion was performed on mineral samples (Kalra and Maynard, 1991; Claisse, 2003).

Horizon	Depth (cm)	Ultrawave Acid Digestion				
		Al (mg/kg)	Ca (%)	K (%)	Na (mg/Kg)	P (%)
S/L	25-23	1182	0.9761	0.1885	531	0.0966
Fm	23-18	1872	0.6149	0.0917	402	0.0687
Hh	18-5	2272	0.4583	0.0491	474	0.0527
Hw	5-0	1241	0.1628	0.0227	564	0.0329

Horizon	Depth (cm)	Lithium Metaborate Fusion (mg/Kg)						
		Al	Ca	K	Na	P	Ti	Zr
Ae	0-6	73911	27294	9624	30902	123	1771	153
Bhj	6-36	70525	27091	8947	29321	244	1697	158
Bhcj	36-39	73916	24968	9503	30532	165	964	49
Bmj	39-90	76208	27028	9960	31576	228	1076	103
BC	90-112+	70350	22669	10460	29956	259	732	47

Table A4- 26. Total elemental analysis of 2mm fractions for CIDS9B. Ultrawave acid digestion was performed on organic samples, whereas, lithium metaborate fusion was performed on mineral samples (Kalra and Maynard, 1991; Claisse, 2003).

Horizon	Depth (cm)	Lithium Metaborate Fusion (mg/Kg)						
		Al	Ca	K	Na	P	Ti	Zr
L	4-3	-	-	-	-	-	-	-
Fm/Hi	3-1, 1-0	54615	20026	7761	25088	192	858	59
Ahe	0-13	69632	24289	8776	29472	120	1075	108
Hwb	13-33	-	-	-	-	-	-	-
Bm	33-58	76330	27483	9673	31715	175	1244	132
Bhjcj	58-113	75308	26825	10797	32033	262	1210	60

Table A4- 27. Total elemental analysis of 2mm fractions for CIDS10A. Ultrawave acid digestion was performed on organic samples, whereas, lithium metaborate fusion was performed on mineral samples (Kalra and Maynard, 1991; Claisse, 2003).

Horizon	Depth (cm)	Ultrawave Acid Digestion				
		Al (mg/kg)	Ca (%)	K (%)	Na (mg/Kg)	P (%)
Lv	18-17	4823	0.5272	0.0824	265	0.0312
Fm	17-14	1482	0.3061	0.0758	284	0.0443
Hh1	14-0	1318	0.2320	0.0717	355	0.0437
Hh2	0-10	3974	0.0328	0.0462	266	0.0246

Horizon	Depth (cm)	Lithium Metaborate Fusion (mg/Kg)						
		Al	Ca	K	Na	P	Ti	Zr
Bhcj	10-20	44975	10043	8566	17956	127	1705	165
Ae	20-22	75701	22159	11867	29377	44	1559	120
Bfc	22-25	78878	20658	9959	25371	131	1859	151
Bmcj	22-80	82319	24089	11369	29525	87	1859	149
BCg1	80-148	79407	26733	11369	30861	131	1918	143

Table A4- 28. Total elemental analysis of 2mm fractions for CIDS10B. Ultrawave acid digestion was performed on organic samples, whereas, lithium metaborate fusion was performed on mineral samples (Kalra and Maynard, 1991; Claisse, 2003).

Horizon	Depth (cm)	Ultrawave Acid Digestion				
		Al (mg/kg)	Ca (%)	K (%)	Na (mg/Kg)	P (%)
S/L	28-25	2364	1.2946	0.0754	397	0.0297
Fm	25-20	2254	0.9160	0.0816	531	0.0494
Hh1	20-14	1197	0.6466	0.0779	552	0.0539
Hh2	14-0	1575	0.1020	0.0394	262	0.0128

Horizon	Depth (cm)	Lithium Metaborate Fusion (mg/Kg)						
		Al	Ca	K	Na	P	Ti	Zr
Bhc	0-7	41496	9958	7699	17101	104	1328	112
Ae	7-10	52440	15453	8993	22890	69	1913	127
Bfc	10-13	71000	19075	9342	26521	140	1845	92
Bmcj	13-33	72315	19992	10044	28754	180	1187	54
BC	33-90+	71326	22468	9806	30618	97	1478	90
BC2	170-204	73813	25873	10149	30362	234	2451	197

Table A4- 29. Total elemental analysis of 2mm fractions for CIDS15A. Ultrawave acid digestion was performed on organic samples, whereas, lithium metaborate fusion was performed on mineral samples (Kalra and Maynard, 1991; Claisse, 2003).

Horizon	Depth (cm)	Ultrawave Acid Digestion				
		Al (mg/kg)	Ca (%)	K (%)	Na (mg/Kg)	P (%)
S/L	20-18	630	1.5569	0.1367	351	0.0711
Fm	18-14	835	0.9445	0.1297	311	0.0772
Hh	14-0	1247	0.7161	0.1232	374	0.0817

Horizon	Depth (cm)	Lithium Metaborate Fusion (mg/Kg)						
		Al	Ca	K	Na	P	Ti	Zr
S/L	20-18	-	-	-	-	-	-	-
Fm	18-14	-	-	-	-	-	-	-
Hh	14-0	-	-	-	-	-	-	-
Ae	0-4	45343	11297	8648	19522	155	946	74
Ahe	4-12	42320	10433	8134	18544	122	843	61
Bhc	12-21	56584	14487	9167	22346	157	757	64
Bfcj	21-23	76330	23210	9410	29978	217	943	39
Bmcj	23-49	71767	21433	9255	30259	211	718	35
BC	49-103+	75407	25523	8847	31648	247	981	68

Table A4- 30. Total elemental analysis of 2mm fractions for CIDS15B. Ultrawave acid digestion was performed on organic samples, whereas, lithium metaborate fusion was performed on mineral samples (Kalra and Maynard, 1991; Claisse, 2003).

Horizon	Depth (cm)	Ultrawave Acid Digestion				
		Al (mg/kg)	Ca (%)	K (%)	Na (mg/Kg)	P (%)
S/L	18-16	2057	1.0325	0.1470	592	0.0574
Fm	16-13	1232	1.2101	0.1164	757	0.0749
Hh	13-0	2106	1.0263	0.0825	861	0.0737

Horizon	Depth (cm)	Lithium Metaborate Fusion (mg/Kg)						
		Al	Ca	K	Na	P	Ti	Zr
Ae	0-9	44241	10897	8179	18464	197	874	79
Ahe	9-14	55378	14345	10620	24154	140	582	54
Bhc	14-28	68880	19932	9821	28301	173	887	45
Bhc2	28-38	74047	21881	9955	31737	120	805	39
Bh	38-43	80582	23637	10997	33133	151	1005	39
Bfc	43-45	84518	25235	10510	33530	251	1147	41
Bm	45-128+	73958	23887	9217	31724	273	877	38

Table A4- 31. Total elemental analysis of 2mm fractions for CIDS16A. Ultrawave acid digestion was performed on organic samples, whereas, lithium metaborate fusion was performed on mineral samples (Kalra and Maynard, 1991; Claisse, 2003).

Horizon	Depth (cm)	Ultrawave Acid Digestion				
		Al (mg/kg)	Ca (%)	K (%)	Na (mg/Kg)	P (%)
S/L	0-3	478	1.4650	0.2119	289	0.0507
Fa	3-8	519	1.1732	0.1399	279	0.0676
Hw	8-35	1663	0.0728	0.0297	334	0.0382
Oh	35-55	13364	0.0323	0.0286	199	0.0420

Horizon	Depth (cm)	Lithium Metaborate Fusion (mg/Kg)						
		Al	Ca	K	Na	P	Ti	Zr
Bhc	55-64	69552	19352	9300	28463	180	579	38
Bhcj	64-80	74938	22364	9184	31560	149	642	38
Bfc	80-81	74948	21982	10232	31725	200	686	34
Bm	81-136+	79745	25440	10336	34846	222	743	46

Table A4- 32. Total elemental analysis of 2mm fractions for CIDS16B. Ultrawave acid digestion was performed on organic samples, whereas, lithium metaborate fusion was performed on mineral samples (Kalra and Maynard, 1991; Claisse, 2003).

Horizon	Depth (cm)	Ultrawave Acid Digestion				
		Al (mg/kg)	Ca (%)	K (%)	Na (mg/Kg)	P (%)
S/L	0-4	596	1.6453	0.2278	324	0.0660
Fm	4-12	419	1.8612	0.0906	271	0.0786
Hw	12-45	2238	0.0547	0.0179	310	0.0291
Oh	45-63	10408	0.0465	0.0320	251	0.0242

Horizon	Depth (cm)	Lithium Metaborate Fusion (mg/Kg)						
		Al	Ca	K	Na	P	Ti	Zr
Bhc	63-85	74392	22825	9449	30763	154	896	39
Ae	85-86	73696	23910	10318	34922	108	655	34
Bmcj	86-103	78741	23713	10820	34673	229	657	32
Bh	103-223	73394	23541	9996	33607	156	709	30

APPENDIX 5 : SELECTED P-NMR SPECTRA AND DATA

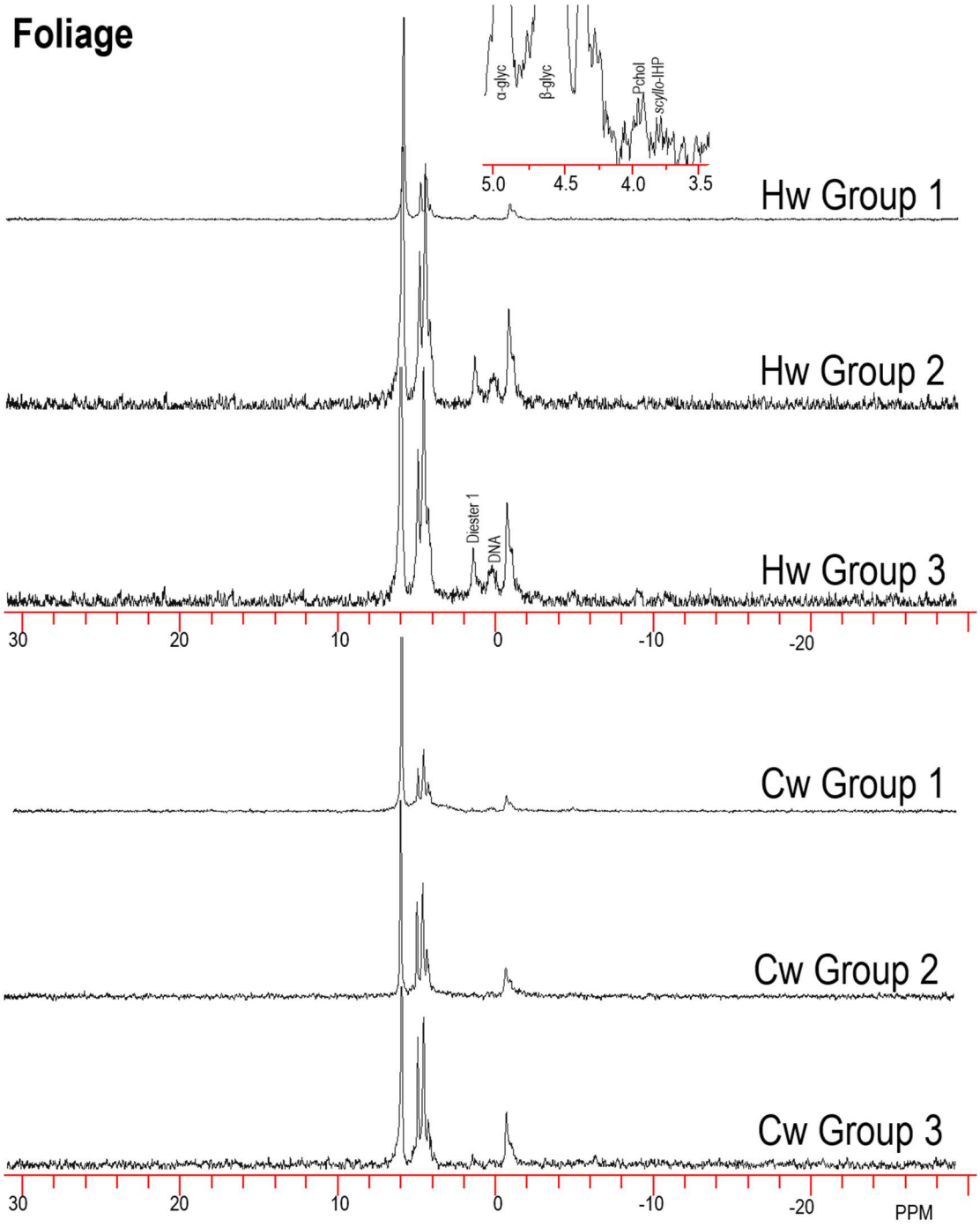

Figure A5- 1. Select ^{31}P-NMR spectra for composited foliage samples, western hemlock (Hw) and western redcedar (Cw), extracted with NaOH-EDTA for group 1 (105 - 139 a BP), group 2 (605 – 4,198 a BP) and group 3 (7,236 – 10,760 a BP). Spectra were generated by B. Cade-Menun on a Bruker Avance 500 MHz spectrometer with a 10-mm broadband probe with a 45˚ pulse, 4.5-s pulse delay, 0.5-s acquisition time, 21˚C, 0.13-µs pulse width and no proton decoupling.

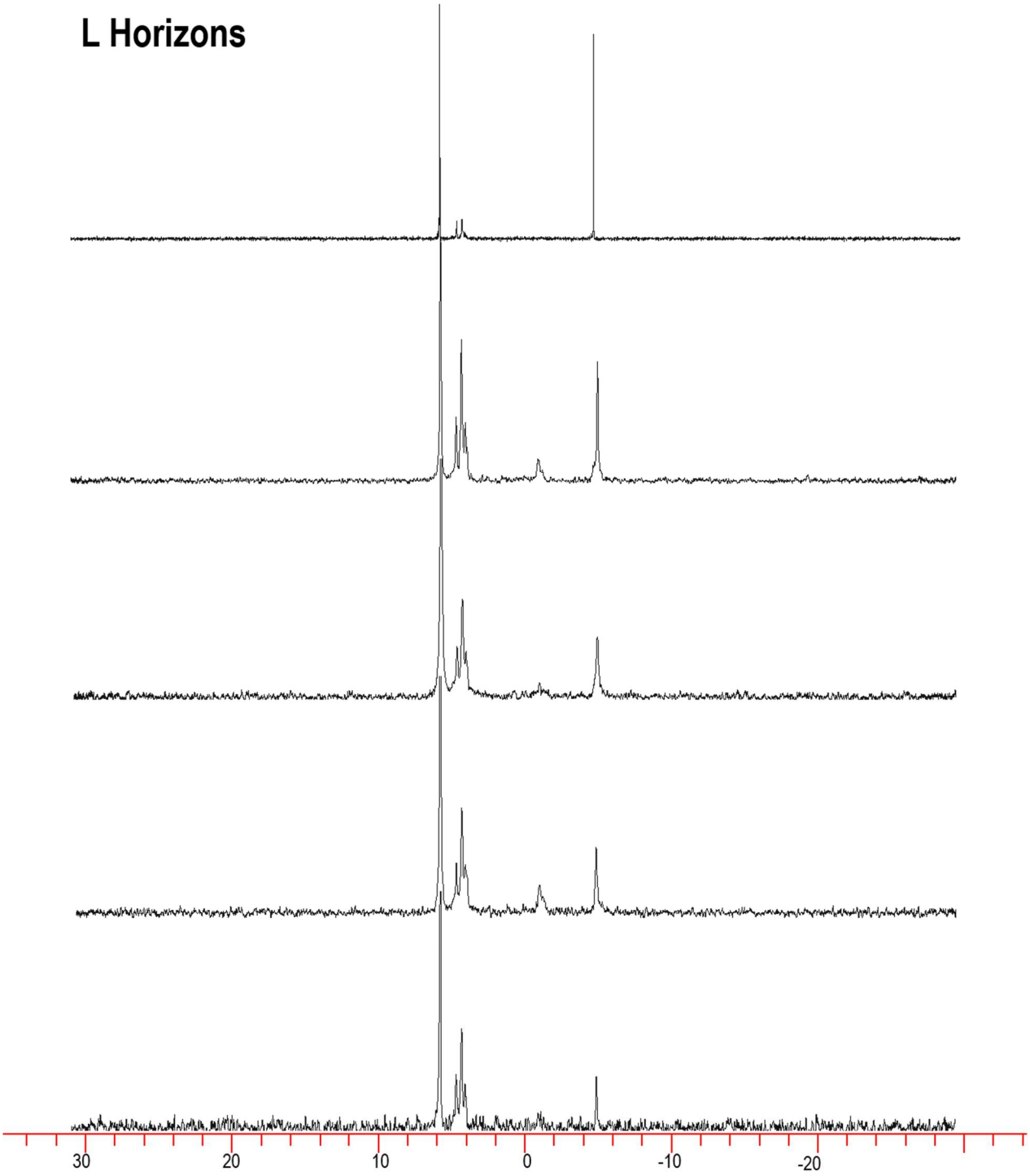

Figure A5- 2. Select ^{31}P-NMR spectra for litter horizon (L) samples along the Calvert Island chronosequence extracted with NaOH-EDTA for sites CIDS1 (0 a BP), CIDS3 (105 a BP), CIDS9 (605 a BP), CIDS15 (4,198 a BP) and CIDS10 (10,760 a BP). Spectra were generated by B. Cade-Menun on a Bruker Avance 500 MHz spectrometer with a 10-mm broadband probe with a 45˚ pulse, 4.5-s pulse delay, 0.5-s acquisition time, 21˚C, 0.13-µs pulse width and no proton decoupling.

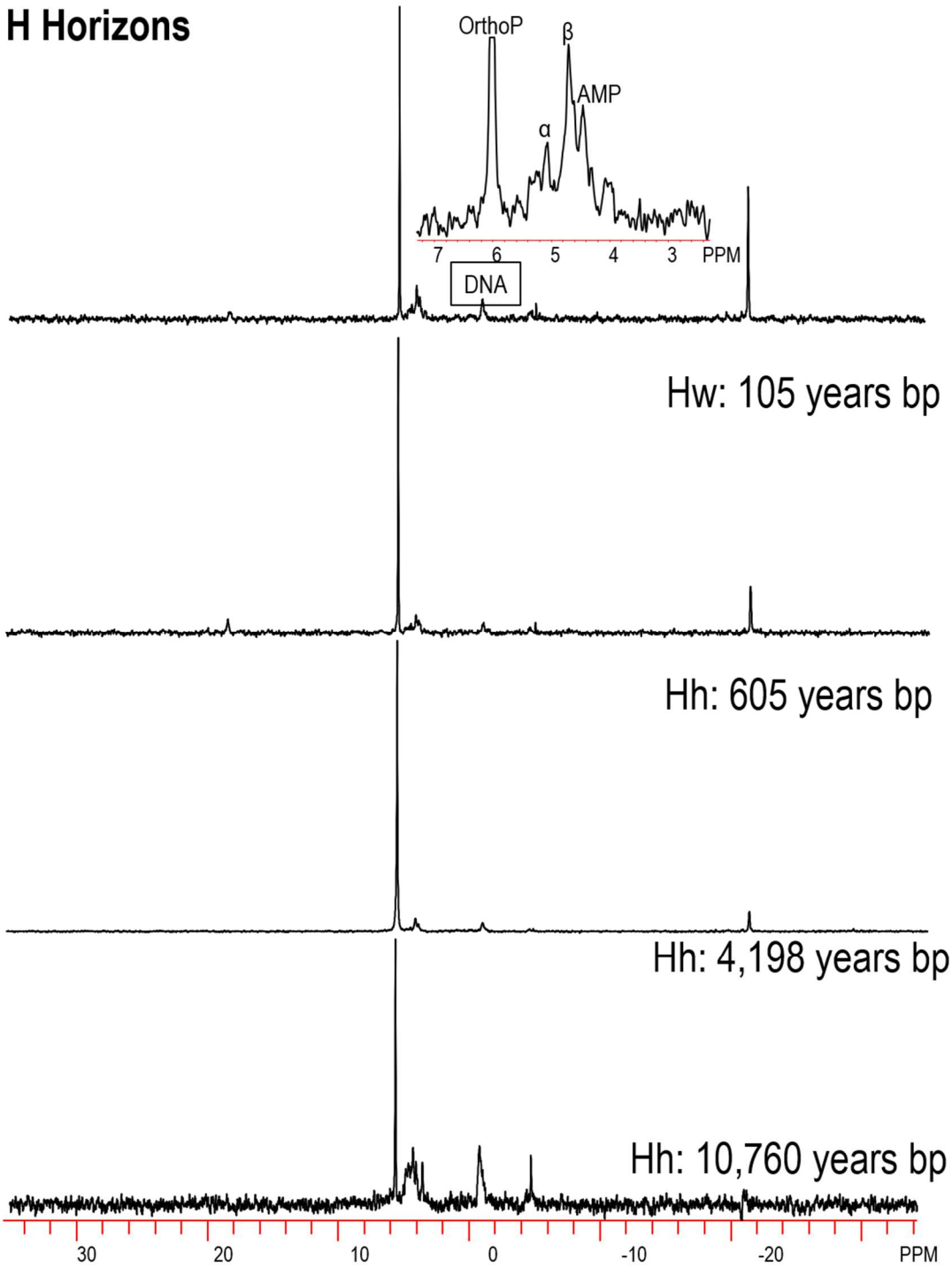

Figure A5- 3. Select ^{31}P-NMR spectra for humic-enriched organic horizon (H) samples along the Calvert Island chronosequence extracted with NaOH-EDTA for sites CIDS1 (0 a BP), CIDS3 (105 a BP), CIDS9 (605 a BP), CIDS15 (4,198 a BP) and CIDS10 (10,760 a BP). Spectra were generated by C. Liu and were obtained on a Varian Inova 600-MHz spectrometer (202.5 MHz for P) with a 10-mm broad band probe with a 45˚ pulse, 4.5-s pulse delay, 0.5-s acquisition time, 20˚C, 0.22-μs pulse width and no proton decoupling

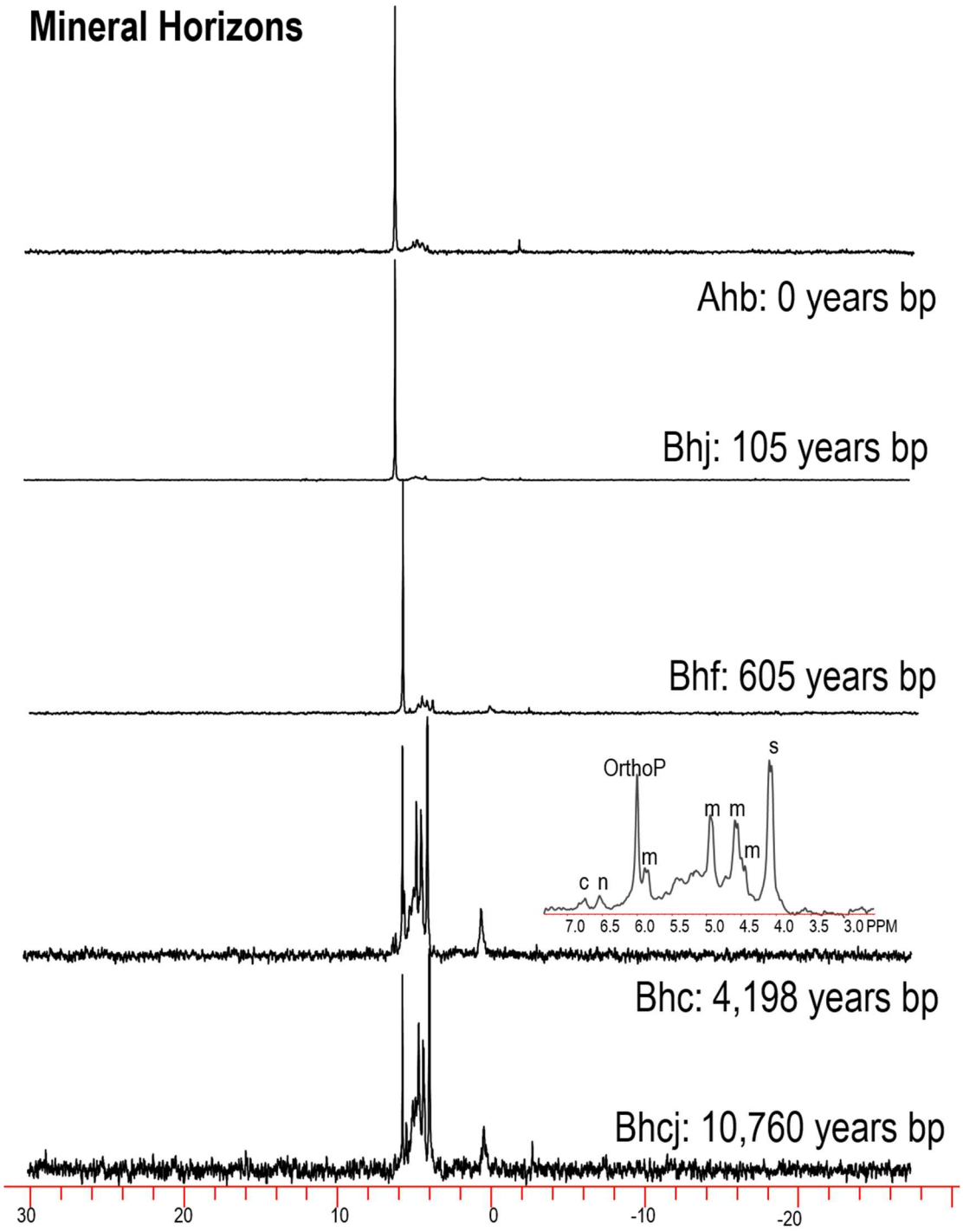

Figure A5- 4. Select ^{31}P-NMR spectra for mineral horizon samples along the Calvert Island chronosequence extracted with NaOH-EDTA for sites CIDS1 (0 a BP), CIDS3 (105 a BP), CIDS9 (605 a BP), CIDS15 (4,198 a BP) and CIDS10 (10,760 a BP). Spectra were generated by C. Liu and were obtained on a Varian Inova 600-MHz spectrometer (202.5 MHz for P) with a 10-mm broad band probe with a 45˚ pulse, 4.5-s pulse delay, 0.5-s acquisition time, 20˚C, 0.22-μs pulse width and no proton decoupling

Table A5- 1. Results from ^{31}P-NMR data analysis for foliage (western hemlock = Hw, western redcedar = Cw) and litter horizon (L) samples including: total extractable P with NaOH-EDTA, total P determined by the Parkinson-Allen (P-A) method, and concentration of orthophosphate (ortho), pyrophosphate (pyro), phosphonates (phos) and *myo*-inositol hexakisphosphate (IHP). Note: n.d. is not determined.

				mg/kg	mg/Kg		mg kg^{-1}				
NMR ID	**Sample Name**	**Age**	**Type**	**Extract P**	**Total P**	**Method**	**Ortho**	**Pyro**	**Poly**	**Phos**	***Myo*-IHP**
LN17	Hw G1	0 - 139	Hw	1227.5	1266.0	P-A	750.0	2.5	7.4	0.0	16.0
LN18	Hw G2	605 - 4,198	Hw	1043.0	1003.2	P-A	247.2	4.2	35.5	8.3	34.4
LN19	Hw G3	7,236 - 10 760	Hw	431.7	515.0	P-A	95.4	3.0	9.9	3.5	13.4
LN20	Cw G1	0 - 139	Cw	1287.2	1405.8	P-A	700.2	3.9	15.4	9.0	34.8
LN21	Cw G2	605 - 4,198	Cw	725.7	916.3	P-A	272.1	1.5	9.4	5.1	25.4
LN22	Cw G3	7,236 - 10 760	Cw	448.7	521.1	P-A	122.0	2.7	14.4	3.1	17.5
LN24	CIDS8A	3,588	Salal	675.7	929.3	P-A	304.8	0.0	10.1	5.4	23.7
LN25	CIDS8B	3,588	Salal	645.6	977.1	P-A	293.1	0.0	5.2	5.2	22.6
LN23	CIDS15B	4,198	Salal	532.2	781.6	P-A	183.6	0.0	8.0	8.0	13.3
LN1	CIDS1A	0	L	465.8	643.1	P-A	178.4	99.2	23.3	3.7	10.2
LN2	CIDS1B	0	L	393.3	529.1	P-A	86.9	74.7	41.7	3.1	21.6
LN3	CIDS3A	105	L	815.2	896.7	P-A	277.2	42.4	79.1	5.7	14.7
LN4	CIDS3B	105	L	690.1	816.4	P-A	213.2	94.5	41.4	4.8	15.9
LN5	CIDS4A	139	L	413.1	496.4	P-A	116.9	33.9	46.7	3.3	9.5
LN6	CIDS4B	139	L	494.4	625.7	P-A	186.4	42.5	35.1	3.5	16.8
LN9	CIDS9A	605	L	613.2	720.8	P-A	262.5	52.1	34.3	4.3	11.7
LN10	CIDS9B	605	L	777.2	950.9	P-A	240.2	101.8	44.3	6.2	17.9
LN7	CIDS8A	3,588	L	377.5	467.8	P-A	141.9	64.6	18.9	2.6	8.7
LN8	CIDS8B	3,588	L	346.8	493.8	P-A	102.0	58.3	26.0	2.4	7.6
LN11	CIDS15A	4,198	L	372.7	469.9	P-A	145.0	28.7	21.6	3.0	8.6
LN12	CIDS15B	4,198	L	325.6	427.3	P-A	111.7	25.7	14.0	2.6	12.0
LN13	CIDS16A	7,236	L	194.6	237.0	P-A	32.7	24.7	21.8	1.6	6.2
LN14	CIDS16B	7,236	L	187.4	266.9	P-A	28.1	22.5	13.9	1.5	6.0
LN15	CIDS10A	10,760	L	116.3	147.9	P-A	47.6	4.4	5.0	0.9	4.7
LN16	CIDS10B	10,760	L	155.2	209.4	P-A	28.6	20.3	11.3	1.2	7.0

Table A5- 2. Results from ^{31}P-NMR data analysis for humic-enriched organic (H) and mineral (M) horizon samples including: total extractable P with NaOH-EDTA, total P determined by microwave acid digestion (DIG) or lithium metaborate fusion (FUS), and concentration of orthophosphate (ortho), pyrophosphate (pyro), phosphonates (phos) and *myo*-inositol phosphate (IHP).

NMR ID	Sample Name	Age	Type	mg/kg	mg/Kg		mg kg^{-1}				
				Extract P	Total P	Method	Ortho	Pyro	Poly	Phos	*Myo*-IHP
LAN 3	CIDS3A	105	H	172.4	699.5	DIG	45.5	5.7	35.0	6.0	7.1
LAN 5	CIDS3B	105	H	188.3	563.8	DIG	41.2	3.4	61.9	3.8	4.0
LAN 7	CIDS4A	139	H	531.3	971.9	DIG	339.0	7.4	37.2	14.9	6.4
LAN 9	CIDS4B	139	H	296.9	682.8	DIG	172.5	6.5	22.0	6.5	3.3
LAN 15	CIDS9A	605	H	208.5	527.0	DIG	64.4	2.9	40.4	16.1	4.2
LAN18	CIDS9B	605	H	176.5	191.9	DIG	49.1	11.1	24.4	2.5	4.6
LAN 11	CIDS8A	3,588	H	56.5	249.2	DIG	13.6	1.1	17.2	2.3	0.7
LAN 13	CIDS8B	3,588	H	106.8	276.1	DIG	55.2	2.0	12.1	4.7	2.2
LAN 23	CIDS15A	4,198	H	338.3	816.8	DIG	202.3	3.4	40.6	4.7	3.7
LAN25	CIDS15B	4,198	H	307.3	737.3	DIG	156.4	2.2	43.9	8.9	4.9
LAN27	CIDS16A	7,236	H	113.3	419.7	DIG	13.0	0.6	5.8	2.7	13.8
LAN29	CIDS16B	7,236	H	164.8	241.7	DIG	11.2	1.0	8.4	5.9	20.4
BC 14-05-04	CIDS10A	10,760	H	106.3	246.0	DIG	14.6	5.0	13.4	2.4	5.6
LAN21	CIDS10B	10,760	H	53.0	128.3	DIG	16.3	0.3	9.9	2.9	1.0
LAN 1	CIDS1A	0	M	14.6	237.5	FUS	8.1	0.6	0.5	0.4	0.6
LAN 2	CIDS1B	0	M	31.8	230.0	FUS	14.1	2.1	0.7	0.4	1.2
LAN 4	CIDS3A	105	M	27.6	293.0	FUS	18.0	0.2	0.4	0.4	1.1
LAN 6	CIDS3B	105	M	41.8	289.8	FUS	30.0	0.3	0.8	0.6	1.6
LAN 8	CIDS4A	139	M	44.3	153.5	FUS	28.4	0.5	1.0	0.9	2.0
LAN 10	CIDS4B	139	M	34.2	142.4	FUS	14.2	0.4	1.0	0.5	2.5
LAN 17	CIDS9A	605	M	29.9	244.4	FUS	12.6	0.4	0.7	1.3	3.1
LAN19A	CIDS9B	605	M	62.1	119.9	FUS	10.3	3.0	2.2	3.0	12.4
LAN 12	CIDS8A	3,588	M	74.8	254.2	FUS	18.9	0.7	1.4	3.7	13.9
LAN 14	CIDS8B	3,588	M	90.1	246.3	FUS	19.7	0.0	1.3	5.1	10.5
LAN 24	CIDS15A	4,198	M	71.9	156.5	FUS	6.5	0.1	1.8	1.5	17.8
LAN 26	CIDS15B	4,198	M	66.4	173.4	FUS	8.9	0.3	2.1	1.4	13.3
LAN 28	CIDS16A	7,236	M	60.3	179.6	FUS	7.8	0.0	1.3	3.0	12.8
LAN 30	CIDS16B	7,236	M	54.5	154.1	FUS	15.9	0.0	1.5	2.3	5.9
BC 6	CIDS10A	10,760	M	95.0	127.0	FUS	5.5	0.5	3.9	2.8	20.1
LAN 22	CIDS10B	10,760	M	32.0	104.0	FUS	2.0	0.2	1.0	1.0	7.9

Table A5- 3. Results from ^{31}P-NMR data analysis for foliage (western hemlock = Hw, western redcedar = Cw) and litter horizon (L) samples including: *chiro*-, *neo*-, and *scyllo*- inositol hexakisphosphate (IHP), glucose-6-phosphate (G6P), an unknown peak near 5 ppm, α- and β-glycerophosphate (glyc), nucleotides (nucl) and choline phosphate (Pchol).

				mg kg^{-1}								
NMR ID	**Sample Name**	**Age**	**Type**	***Chiro*-IHP**	***Neo*-IHP**	***Scyllo*-IHP**	**g6P**	**5 ppm**	**α-glyc**	**β-glyc**	**Nucl**	**Pchol**
LN17	Hw G1	0 - 139	Hw	17.2	8.6	8.6	8.6	8.6	57.7	106.8	24.6	8.6
LN18	Hw G2	605 - 4,198	Hw	33.4	6.3	6.3	6.3	6.3	63.6	121.0	97.0	6.3
LN19	Hw G3	7,236 - 10 760	Hw	11.7	2.6	2.6	2.6	4.7	24.6	49.6	34.1	2.6
LN20	Cw G1	0 - 139	Cw	25.7	0.0	0.0	9.0	9.0	52.8	104.3	78.5	9.0
LN21	Cw G2	605 - 4,198	Cw	8.0	4.4	0.0	4.4	4.4	58.8	116.8	29.0	4.4
LN22	Cw G3	7,236 - 10 760	Cw	17.1	2.7	0.0	2.7	2.7	34.5	69.5	26.0	2.7
LN24	Salal CIDS8A	3,588	Salal	23.0	4.1	4.1	4.1	4.1	23.7	47.3	47.3	11.5
LN25	Salal CIDS8B	3,588	Salal	19.4	3.9	3.9	3.9	3.9	22.6	45.2	49.7	11.6
LN23	Salal CIDS15B	4,198	Salal	13.8	3.2	3.2	3.2	3.2	30.3	63.9	53.2	3.2
LN1	CIDS1A	0	FF	14.9	2.8	2.8	2.8	2.8	18.2	30.7	30.7	2.8
LN2	CIDS1B	0	FF	12.6	2.4	4.3	2.4	2.4	19.7	38.9	26.0	2.4
LN3	CIDS3A	105	FF	19.6	4.9	4.9	4.9	9.8	38.3	82.3	58.7	4.9
LN4	CIDS3B	105	FF	19.3	4.1	4.1	4.1	4.1	39.3	78.7	59.3	4.1
LN5	CIDS4A	139	FF	12.4	2.5	2.5	2.5	5.0	26.9	53.3	28.9	2.5
LN6	CIDS4B	139	FF	14.3	3.0	3.0	3.0	3.0	19.8	43.0	40.0	3.0
LN9	CIDS9A	605	FF	23.3	3.7	3.7	3.7	3.7	27.0	50.3	38.6	3.7
LN10	CIDS9B	605	FF	21.8	4.7	4.7	4.7	4.7	48.2	95.6	48.2	4.7
LN7	CIDS8A	3,588	FF	10.6	2.3	2.3	2.3	2.3	21.9	43.8	17.4	2.3
LN8	CIDS8B	3,588	FF	9.4	2.1	2.1	2.1	2.1	18.7	36.1	24.6	2.1
LN11	CIDS15A	4,198	FF	10.4	2.2	2.2	2.2	2.2	17.1	33.9	27.6	2.2
LN12	CIDS15B	4,198	FF	9.8	2.0	2.0	2.0	3.9	16.0	31.9	23.8	2.0
LN13	CIDS16A	7,236	FF	6.2	1.0	1.0	1.0	2.1	12.3	24.5	18.3	1.0
LN14	CIDS16B	7,236	FF	6.0	0.9	0.9	0.9	2.1	12.9	26.0	17.1	0.9
LN15	CIDS10A	10,760	FF	3.8	0.8	0.8	0.8	1.5	6.3	12.4	7.0	0.8
LN16	CIDS10B	10,760	FF	2.6	0.9	0.9	0.9	1.7	13.8	27.6	13.8	0.9

Table A5- 4. Results from ^{31}P-NMR data analysis for humic-enriched organic (H) and mineral (M) horizon samples including: *chiro*-, *neo*-, and *scyllo*- inositol hexakisphosphate (IHP), glucose-6-phosphate (G6P), an unknown peak near 5 ppm, α- and β-glycerophosphate (glyc), nucleotides (nucl) and choline phosphate (Pchol).

				mg kg^{-1}								
NMR ID	**Sample Name**	**Age**	**Type**	**ChirIHP**	**neoIHP**	**ScyIHP**	**g6P**	**5 ppm**	**α-glyc**	**β-glyc**	**Nucl**	**Pchol**
LAN 3	CIDS3A	105	H	2.4	0.9	1.6	0.9	1.6	2.4	4.7	10.2	2.4
LAN 5	CIDS3B	105	H	3.2	0.6	1.3	0.6	1.3	3.2	6.4	13.7	1.9
LAN 7	CIDS4A	139	H	16.5	3.2	6.4	3.2	3.2	6.4	13.3	10.1	3.2
LAN 9	CIDS4B	139	H	6.5	1.5	3.3	1.5	1.5	4.8	9.5	9.5	1.5
LAN 15	CIDS9A	605	H	4.2	1.0	1.0	1.0	2.1	3.1	6.3	12.5	2.1
LAN18	CIDS9B	605	H	3.9	0.9	3.2	0.9	0.9	6.2	12.5	10.1	1.6
LAN 11	CIDS8A	3,588	H	1.5	0.2	0.2	0.5	0.5	0.7	1.7	1.5	0.2
LAN 13	CIDS8B	3,588	H	3.7	0.7	1.5	1.5	0.7	1.5	3.0	4.5	0.7
LAN 23	CIDS15A	4,198	H	9.1	1.7	1.7	1.7	1.7	3.7	7.8	13.2	1.7
LAN25	CIDS15B	4,198	H	8.3	1.5	1.5	1.5	3.4	3.4	6.5	11.1	1.5
LAN27	CIDS16A	7,236	H	6.8	1.5	7.6	1.5	3.9	2.3	4.5	9.2	1.5
LAN29	CIDS16B	7,236	H	6.3	1.0	18.5	2.0	8.2	4.1	7.1	9.2	2.0
BC 14-05-04	CIDS10A	10,760	H	2.8	0.4	3.7	1.0	2.8	1.9	3.7	6.1	1.0
LAN21	CIDS10B	10,760	H	1.2	0.3	0.3	0.3	0.5	1.3	2.5	2.3	0.3
LAN 1	CIDS1A	0	M	0.6	0.1	0.3	0.1	0.2	0.4	0.8	0.4	0.2
LAN 2	CIDS1B	0	M	1.3	0.2	0.6	0.2	0.2	1.5	2.5	2.3	0.4
LAN 4	CIDS3A	105	M	0.9	0.2	0.7	0.2	0.4	0.2	0.4	0.9	0.4
LAN 6	CIDS3B	105	M	1.4	0.5	0.8	0.3	0.3	0.3	0.5	0.5	0.5
LAN 8	CIDS4A	139	M	2.0	0.3	0.7	0.3	0.3	0.7	1.0	1.0	0.3
LAN 10	CIDS4B	139	M	1.2	0.2	2.1	0.2	0.2	0.6	1.0	1.5	0.4
LAN 17	CIDS9A	605	M	1.1	0.4	1.2	0.2	0.2	0.5	0.9	1.0	0.5
LAN19A	CIDS9B	605	M	2.1	0.4	5.2	0.4	0.7	1.1	2.0	1.7	0.4
LAN 12	CIDS8A	3,588	M	2.7	1.3	9.7	0.4	0.9	1.3	2.3	1.9	0.9
LAN 14	CIDS8B	3,588	M	3.4	0.5	10.5	1.2	1.2	1.7	2.9	8.1	1.7
LAN 24	CIDS15A	4,198	M	2.9	1.0	11.4	1.0	1.0	1.0	1.4	4.0	1.4
LAN 26	CIDS15B	4,198	M	2.7	0.9	8.0	0.9	0.9	1.3	2.2	3.5	1.8
LAN 28	CIDS16A	7,236	M	2.2	0.7	8.6	0.4	0.7	0.7	1.1	2.5	0.7
LAN 30	CIDS16B	7,236	M	2.0	0.7	5.3	0.7	0.3	0.7	1.3	2.9	0.7
BC 6	CIDS10A	10,760	M	3.4	1.7	12.8	1.1	0.6	1.1	1.7	4.5	1.7
LAN 22	CIDS10B	10,760	M	1.3	0.2	4.6	0.2	0.7	0.4	0.7	0.7	0.2

Table A5- 5. Results from ^{31}P-NMR data analysis for foliage (western hemlock = Hw, western redcedar = Cw) and litter horizon (L) samples including: orthophosphate monoesters (mono) 1, 2 and 3, orthophosphate diesters (OthDi) 1 and 2, DNA, and total inorganic (Pi) and organic phosphorus (Po) within the NaOH-EDTA extract.

				mg kg^{-1}							
NMR ID	**Sample Name**	**Age**	**Type**	**Mono1**	**Mono2**	**Mono3**	**OthDi1**	**DNA**	**OthDi2**	**Pi**	**Po**
LN17	Hw G1	0 - 139	Hw	16.0	31.9	8.6	55.2	78.6	12.3	759.9	467.7
LN18	Hw G2	605 - 4,198	Hw	11.5	57.4	11.5	143.9	128.3	14.6	286.8	756.2
LN19	Hw G3	7,236 - 10 760	Hw	4.7	26.8	4.7	67.3	61.3	6.5	108.4	323.3
LN20	Cw G1	0 - 139	Cw	9.0	52.8	9.0	68.2	75.9	20.6	719.5	567.6
LN21	Cw G2	605 - 4,198	Cw	4.4	24.7	8.0	29.0	101.6	14.5	283.0	442.7
LN22	Cw G3	7,236 - 10 760	Cw	5.8	29.2	5.8	24.7	61.5	4.0	139.1	309.6
LN24	Salal CIDS8A	3,588	Salal	4.1	27.7	4.1	96.6	20.3	10.1	314.9	360.8
LN25	Salal CIDS8B	3,588	Salal	3.9	22.6	7.7	98.1	17.4	5.8	298.3	347.3
LN23	Salal CIDS15B	4,198	Salal	3.2	23.4	3.2	69.7	31.9	10.6	191.6	340.6
LN1	CIDS1A	0	L	5.1	12.6	2.8	5.6	10.7	5.6	300.9	164.9
LN2	CIDS1B	0	L	4.3	21.6	4.3	7.9	8.3	7.9	203.3	190.0
LN3	CIDS3A	105	L	9.8	58.7	14.7	25.3	44.8	14.7	398.6	416.6
LN4	CIDS3B	105	L	7.6	20.0	11.7	22.8	26.2	14.5	349.2	340.9
LN5	CIDS4A	139	L	5.0	16.9	7.4	17.3	12.0	7.8	197.5	215.6
LN6	CIDS4B	139	L	5.9	25.7	5.9	14.8	16.8	8.9	264.0	230.4
LN9	CIDS9A	605	L	7.4	35.0	7.4	12.9	20.8	7.4	348.9	264.3
LN10	CIDS9B	605	L	8.5	35.0	4.7	21.0	49.7	10.9	386.3	390.9
LN7	CIDS8A	3,588	L	2.3	15.5	4.2	9.4	2.6	1.9	225.4	152.1
LN8	CIDS8B	3,588	L	3.8	22.5	5.5	10.8	5.9	2.8	186.2	160.6
LN11	CIDS15A	4,198	L	2.2	19.0	2.2	11.6	23.5	7.1	195.3	177.4
LN12	CIDS15B	4,198	L	3.9	23.8	3.9	6.8	22.5	5.5	151.4	174.2
LN13	CIDS16A	7,236	L	2.1	10.1	2.1	9.0	14.2	2.7	79.2	115.4
LN14	CIDS16B	7,236	L	2.1	15.0	3.0	4.7	18.2	4.7	64.5	122.9
LN15	CIDS10A	10,760	L	0.8	4.7	1.5	3.8	5.6	3.0	57.0	59.3
LN16	CIDS10B	10,760	L	1.7	8.5	2.6	3.3	5.7	1.6	60.2	95.0

Table A5- 6. Results from ^{31}P-NMR data analysis for humic-enriched organic (H) and mineral (M) horizon samples including: orthophosphate monoesters (mono) 1, 2 and 3, orthophosphate diesters (OthDi) 1 and 2, DNA, and total inorganic (Pi) and organic phosphorus (Po) within the NaOH-EDTA extract.

NMR ID	Sample Name	Age	Type	mg kg^{-1}							
				Mono1	Mono2	Mono3	OthDi1	DNA	OthDi2	Pi	Po
LAN 3	CIDS3A	105	H	1.6	7.8	4.7	15.0	15.0	2.2	86.2	86.2
LAN 5	CIDS3B	105	H	1.3	9.2	1.9	9.2	16.6	3.6	106.6	81.7
LAN 7	CIDS4A	139	H	3.2	10.1	3.2	13.3	26.0	5.3	383.6	147.7
LAN 9	CIDS4B	139	H	1.5	4.8	3.3	16.3	16.3	4.5	201.0	95.9
LAN 15	CIDS9A	605	H	2.1	8.3	6.3	5.8	19.8	4.8	107.8	100.7
LAN18	CIDS9B	605	H	1.6	7.8	2.3	10.9	18.9	3.4	84.5	91.9
LAN 11	CIDS8A	3,588	H	0.5	2.4	1.0	3.9	3.9	2.8	31.9	24.6
LAN 13	CIDS8B	3,588	H	1.5	6.1	2.2	1.3	1.1	0.4	69.3	37.5
LAN 23	CIDS15A	4,198	H	1.7	7.8	1.7	9.5	18.3	2.4	246.3	92.0
LAN25	CIDS15B	4,198	H	3.4	11.1	4.9	17.8	9.5	5.5	202.5	104.8
LAN27	CIDS16A	7,236	H	2.3	19.0	3.9	7.0	4.6	1.9	19.4	94.0
LAN29	CIDS16B	7,236	H	2.0	24.6	7.1	14.5	6.4	4.9	20.6	144.2
BC 14-05-04	CIDS10A	10,760	H	1.0	10.3	2.8	8.5	16.0	3.4	32.9	73.3
LAN21	CIDS10B	10,760	H	0.5	2.3	1.3	2.9	5.3	1.5	26.5	26.4
LAN 1	CIDS1A	0	M	0.2	0.7	0.1	0.1	0.1	0.1	9.2	5.4
LAN 2	CIDS1B	0	M	0.4	1.7	0.4	0.7	0.7	0.1	17.0	14.8
LAN 4	CIDS3A	105	M	0.6	0.9	0.4	0.9	0.3	0.2	18.6	9.1
LAN 6	CIDS3B	105	M	0.3	0.8	0.3	0.5	1.3	0.3	31.1	10.7
LAN 8	CIDS4A	139	M	0.7	1.3	0.7	0.9	0.8	0.5	30.0	14.4
LAN 10	CIDS4B	139	M	0.2	2.1	0.8	1.3	2.8	1.0	15.6	18.6
LAN 17	CIDS9A	605	M	0.4	1.4	0.5	0.9	1.9	0.6	13.7	16.1
LAN19A	CIDS9B	605	M	0.4	5.2	1.7	2.6	6.3	1.1	15.6	46.5
LAN 12	CIDS8A	3,588	M	0.9	5.6	1.3	1.9	4.3	0.7	20.9	53.9
LAN 14	CIDS8B	3,588	M	1.2	8.1	2.9	3.0	5.6	1.6	21.0	69.1
LAN 24	CIDS15A	4,198	M	1.4	5.9	1.9	4.0	5.3	0.5	8.4	63.5
LAN 26	CIDS15B	4,198	M	0.9	6.2	2.2	1.4	6.9	0.9	11.2	55.2
LAN 28	CIDS16A	7,236	M	0.7	6.1	1.4	2.6	6.3	0.5	9.1	51.2
LAN 30	CIDS16B	7,236	M	0.7	4.3	2.0	2.2	4.2	1.1	17.4	37.1
BC 6	CIDS10A	10,760	M	2.3	14.5	5.0	4.7	4.7	2.1	9.9	85.1
LAN 22	CIDS10B	10,760	M	0.7	2.9	1.3	1.6	3.3	1.3	3.1	28.9

Table A5- 7. Results from ^{31}P-NMR data analysis for foliage (western hemlock = Hw, western redcedar = Cw) and litter horizon (L) samples including: total polyphosphates (totpoly), total inositol hexakisphosphates (IHP), total uncorrected and corrected orthophosphate monoesters (mono; Cmono, respectively) and diesters (di; Cdi, respectively), degradation rate (deg) and monoester to diester ratios for uncorrected (M:D) and corrected (cM:D) values.

				mg kg^{-1}								
NMR ID	**Sample Name**	**Age**	**Type**	**TotPoly**	**IHP**	**Mono**	**Di**	**M:D**	**Cmono**	**Cdiest**	**Deg**	**cM:D**
LN17	Hw G1	0 - 139	Hw	9.8	50.3	321.6	146.1	2.2	132.6	343.7	189.0	0.4
LN18	Hw G2	605 - 4,198	Hw	39.6	80.3	461.0	286.8	1.6	179.4	574.7	281.6	0.3
LN19	Hw G3	7,236 - 10 760	Hw	13.0	30.2	184.8	135.1	1.4	76.4	246.1	108.4	0.3
LN20	Cw G1	0 - 139	Cw	19.3	60.5	393.9	164.8	2.4	158.3	409.3	235.6	0.4
LN21	Cw G2	605 - 4,198	Cw	10.9	37.7	292.5	145.1	2.0	87.8	354.1	204.7	0.2
LN22	Cw G3	7,236 - 10 760	Cw	17.1	37.2	216.3	90.2	2.4	86.2	223.0	130.1	0.4
LN24	Salal CIDS8A	3,588	Salal	10.1	54.7	228.4	127.0	1.8	110.1	256.8	118.3	0.4
LN25	Salal CIDS8B	3,588	Salal	5.2	49.7	220.8	121.4	1.8	103.3	250.5	117.5	0.4
LN23	Salal CIDS15B	4,198	Salal	8.0	33.5	220.3	112.3	2.0	72.9	262.9	147.4	0.3
LN1	CIDS1A	0	L	122.5	30.7	139.3	21.9	6.4	59.6	104.3	79.6	0.6
LN2	CIDS1B	0	L	116.4	40.9	162.8	24.0	6.8	78.3	110.9	84.6	0.7
LN3	CIDS3A	105	L	121.5	44.0	326.1	84.8	3.8	146.7	269.0	179.3	0.5
LN4	CIDS3B	105	L	135.9	43.5	272.6	63.5	4.3	95.2	245.0	177.3	0.4
LN5	CIDS4A	139	L	80.6	26.9	175.2	37.2	4.7	66.1	148.7	109.1	0.4
LN6	CIDS4B	139	L	77.6	37.1	186.4	40.5	4.6	83.6	146.3	102.8	0.6
LN9	CIDS9A	605	L	86.5	42.3	218.9	41.1	5.3	103.0	160.7	115.9	0.6
LN10	CIDS9B	605	L	146.1	49.0	303.1	81.6	3.7	111.1	278.2	192.0	0.4
LN7	CIDS8A	3,588	L	83.4	23.8	135.5	14.0	9.7	52.5	99.3	83.1	0.5
LN8	CIDS8B	3,588	L	84.3	21.2	138.7	19.4	7.1	59.3	100.9	79.4	0.6
LN11	CIDS15A	4,198	L	50.3	23.5	132.3	42.1	3.1	53.7	123.0	78.6	0.4
LN12	CIDS15B	4,198	L	39.7	25.7	136.8	34.8	3.9	65.1	108.4	71.6	0.6
LN13	CIDS16A	7,236	L	46.5	14.4	88.0	25.9	3.4	32.9	81.9	55.1	0.4
LN14	CIDS16B	7,236	L	36.4	13.9	93.9	27.5	3.4	37.9	84.5	56.0	0.4
LN15	CIDS10A	10,760	L	9.4	10.1	45.9	12.4	3.7	20.2	38.9	25.7	0.5
LN16	CIDS10B	10,760	L	31.7	11.5	83.2	10.6	7.9	27.9	66.7	55.3	0.4

Table A5- 8. Results from ^{31}P-NMR data analysis for humic-enriched organic (H) and mineral (M) horizon samples including: total polyphosphates (totpoly), total inositol phosphates (IHP), total uncorrected and corrected orthophosphate monoesters (mono; Cmono) and diesters (di; Cdi), degradation rate (deg) and uncorrected (M:D) and corrected (cM:D)monoester to diester ratios.

				mg kg^{-1}								
NMR ID	**Sample Name**	**Age**	**Type**	**TotPoly**	**IHP**	**Mono**	**Di**	**M:D**	**Cmono**	**Cdiest**	**Deg**	**cM:D**
LAN 3	CIDS3A	105	H	40.7	11.9	47.9	32.2	1.5	30.7	49.5	17.2	0.6
LAN 5	CIDS3B	105	H	65.3	9.0	48.6	29.4	1.7	25.2	52.7	23.3	0.5
LAN 7	CIDS4A	139	H	44.6	32.4	88.2	44.6	2.0	58.4	74.4	29.8	0.8
LAN 9	CIDS4B	139	H	28.5	14.5	52.3	37.1	1.4	28.5	60.9	23.8	0.5
LAN 15	CIDS9A	605	H	43.4	10.4	54.2	30.4	1.8	32.3	52.3	21.9	0.6
LAN18	CIDS9B	605	H	35.5	12.5	56.3	33.2	1.7	27.5	61.9	28.8	0.4
LAN 11	CIDS8A	3,588	H	18.3	2.7	11.7	10.6	1.1	7.8	14.5	3.9	0.5
LAN 13	CIDS8B	3,588	H	14.1	8.2	30.0	2.8	10.8	21.0	11.7	9.0	1.8
LAN 23	CIDS15A	4,198	H	44.0	16.2	57.2	30.1	1.9	32.5	54.8	24.7	0.6
LAN25	CIDS15B	4,198	H	46.1	16.3	63.0	32.9	1.9	42.1	53.8	20.9	0.8
LAN27	CIDS16A	7,236	H	6.3	29.7	77.6	13.6	5.7	61.7	29.6	16.0	2.1
LAN29	CIDS16B	7,236	H	9.4	46.1	112.4	25.9	4.3	91.9	46.3	20.4	2.0
BC 14-05-04	CIDS10A	10,760	H	18.4	12.5	42.9	27.9	1.5	31.2	39.6	11.7	0.8
LAN21	CIDS10B	10,760	H	10.2	2.8	13.8	9.7	1.4	7.8	15.7	6.0	0.5
LAN 1	CIDS1A	0	M	1.1	1.6	4.8	0.2	23.4	3.2	2.0	1.6	1.5
LAN 2	CIDS1B	0	M	2.9	3.3	12.8	1.5	8.4	6.6	8.2	6.2	0.8
LAN 4	CIDS3A	105	M	0.6	3.0	7.3	1.3	5.5	5.8	3.2	1.5	1.8
LAN 6	CIDS3B	105	M	1.1	4.4	8.1	2.0	4.0	6.8	3.9	1.3	1.7
LAN 8	CIDS4A	139	M	1.6	5.0	11.3	2.1	5.3	8.6	5.1	2.7	1.7
LAN 10	CIDS4B	139	M	1.4	6.0	13.1	5.0	2.6	10.0	8.6	3.1	1.2
LAN 17	CIDS9A	605	M	1.1	5.8	11.4	3.3	3.4	9.0	6.3	2.4	1.4
LAN19A	CIDS9B	605	M	5.3	20.0	33.4	10.1	3.3	28.6	15.2	4.8	1.9
LAN 12	CIDS8A	3,588	M	2.1	27.7	43.3	6.9	6.3	37.8	13.3	5.5	2.8
LAN 14	CIDS8B	3,588	M	1.3	24.9	53.8	10.2	5.3	41.1	24.6	12.7	1.7
LAN 24	CIDS15A	4,198	M	1.9	33.0	52.1	9.8	5.3	45.7	17.7	6.4	2.6
LAN 26	CIDS15B	4,198	M	2.3	24.8	44.6	9.2	4.8	37.5	18.1	7.0	2.1
LAN 28	CIDS16A	7,236	M	1.3	24.3	38.7	9.5	4.1	34.4	14.5	4.3	2.4
LAN 30	CIDS16B	7,236	M	1.5	13.8	27.3	7.5	3.6	22.4	13.1	4.9	1.7
BC 6	CIDS10A	10,760	M	4.4	38.1	70.7	11.6	6.1	63.3	20.6	7.3	3.1
LAN 22	CIDS10B	10,760	M	1.2	14.0	21.7	6.2	3.5	19.9	8.2	1.8	2.4